19th INTERNATIONAL CONFERENCE on spectral line shapes

15-20 june 2008 / valladolid (spain)

Local Organizing Committee:

Marco Antonio Gigosos (co-chairman)
Manuel Ángel González (co-chairman)
Dionisio Bermejo — Patrick Sauvan — Bernardo Zurro

Universidad de Valladolid

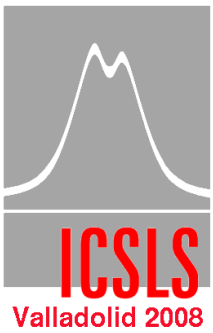

International Scientific Committee:

Dionisio Bermejo (Spain)
Elisabeth Dalimier (France)
Alexander Devdariani (Russia)
Milan S. Dimitrijević (Serbia)
Robert Gamache (USA)
Marco A. Gigosos (Spain)
Jean-Michel Hartmann (France)
Volkmar Helbig (Germany)
Carlos Iglesias (USA)
John Kielkopf (USA)
John C. Lewis (Canada)
Valery Lisitsa (Russia)
Massimo Moraldi (Italy)
Kenji Ohmori (Japan)
Eugene Oks (USA)
Gillian Peach (U.K.)
Roland Stamm (France)
Chantal Stehle (France)
Willian Stwalley (USA)
Josef Szudy (Poland)

Sponsors:

Junta de Castilla y León
Ministerio de Educación y Ciencia
Consejo Superior de Investigaciones Científicas
Ministerio de Asuntos Exteriores
Centro de Investigaciones Energéticas, Medioambientales y Tecnológicas
Fundación Universidades de Castilla y León
Universidad de Valladolid
Ayuntamiento de Valladolid
Oficina de Congresos de Valladolid

Program

10:35 **Coffee break**

12:35 **Lunch break**

15:45 **Coffee break**

16:00 **Poster session 1**

17:15 **Business Meeting**

18:30 **Concert at the Conference Site**

FRIDAY, 20 JUNE 195

10:35 **Coffee break**

12:35 **The next Conference**

12:50 **Closure**

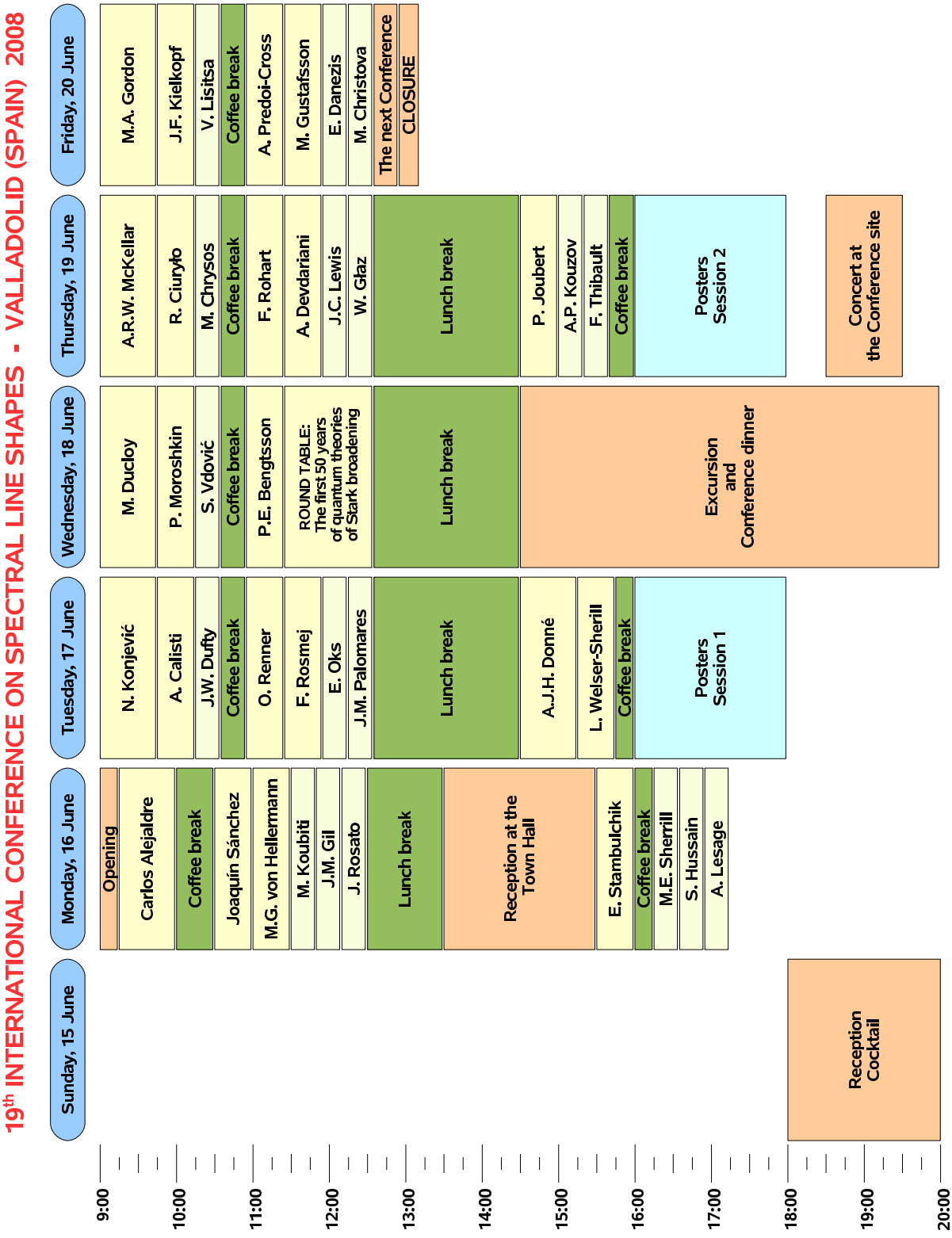
19th INTERNATIONAL CONFERENCE ON SPECTRAL LINE SHAPES - VALLADOLID (SPAIN) 2008
Sunday, 15 June
Monday, 16 June
Tuesday, 17 June
Wednesday, 18 June
Thursday, 19 June
Friday, 20 June
Opening
Carlos Alejaldre
Coffee break
Joaquín Sánchez
M.G. von Hellermann
M. Koubiti
J.M. Gil
J. Rosato
Lunch break
Reception at the Town Hall
E. Stambulchik
Coffee break
M.E. Sherrill
S. Hussain
A. Lesage
Reception Cocktail
N. Konjević
A. Calisti
J.W. Dufty
Coffee break
O. Renner
F. Rosmej
E. Oks
J.M. Palomares
Lunch break
A.J.H. Donné
L. Welser-Sherill
Coffee break
Posters Session 1
M. Ducloy
P. Moroshkin
S. Vdović
Coffee break
P.E. Bengtsson
ROUND TABLE: The first 50 years of quantum theories of Stark broadening
Lunch break
Excursion and Conference dinner
A.R.W. McKellar
R. Ciuryło
M. Chrysos
Coffee break
F. Rohart
A. Devdariani
J.C. Lewis
W. Glaz
Lunch break
P. Joubert
A.P. Kouzov
F. Thibault
Coffee break
Posters Session 2
Concert at the Conference site
M.A. Gordon
J.F. Kielkopf
V. Lisitsa
Coffee break
A. Predoi-Cross
M. Gustafsson
E. Danezis
M. Christova
The next Conference
CLOSURE
9:00
10:00
11:00
12:00
13:00
14:00
15:00
16:00
17:00
18:00
19:00
20:00

MONDAY, 16 JUNE

Overview of ITER Project

Lina Rodriguez-Rodrigo and Carlos Alejaldre

ITER Organization
13108 St Paul lez Durance. FRANCE

ITER is the most important step on the path to developing fusion energy using magnetic confinement. For the first time, reactor-grade plasma will be brought together with current technology to see whether a viable power source can be built with the ultimate goal of demonstrating the scientific and technological feasibility of fusion energy for peaceful purposes. The device is designed to generate 500 megawatts of fusion power for periods of 300 to 500 seconds with a fusion power multiplication factor, Q, of at least 10 ($Q \geq 10$). The device is also intended to demonstrate non-inductive steady-state operation with a fusion power multiplication factor of 5 and, ultimately, pulse lengths of up to several thousand seconds. In addition, the design does not exclude the possibility that controlled ignition can be achieved.

ITER is based on the "tokamak" concept of plasma magnetic confinement, in which the fusion fuel is contained in a doughnut-shaped vessel. The fuel —a mixture of deuterium and tritium, two isotopes of hydrogen— is heated to temperatures in excess of 100 million degrees, forming a hot plasma. The plasma is kept away from the walls by strong magnetic fields produced by superconducting coils surrounding the vessel and an electrical current driven in the plasma.

The main engineering challenge of ITER is therefore to build the device on time and within budget to have a timely decision on possible future energy sources and show the economic possibilities. Since the ITER design was completed some years ago, to the extent that a cost estimate could be agreed on by the then Participants, there have been a number of design modifications with a view to making the design and the cost estimates more realistic in practice, or actually to cut costs. Naturally there have also been some research and technical developments during that period, which now might allow better design solutions to be implemented. Thus, before ITER construction went ahead, and before the licensing documents were finalized, a detailed design review was carried out to assess whether the solutions now proposed still were valid, and could be accomplished in the planned timescale.

The collaboration formed by China, Europe, India, Japan, Russia, South Korea and United States to build the ITER project is a powerful mix of many countries, cultures and institutions, with their different strengths and specialties, and with a common interests to develop the key technologies for fusion but the procurement process for many components will as a consequence highly interdependent, and its integration a true challenge. Experience in the large particle accelerator construction, other areas of science as well as in industry, however, shows that with a cooperative atmosphere between different suppliers of similar components there are great benefits when problems inevitably arise. Certainly the design of ITER has inherited the experience from a lot of fusion machines in the world, although only two installations based on magnetic confinement have used up to now deuterium and tritium as fuel: the Tokamak Fusion Test Reactor, TFTR in Princeton, USA and the Joint European Torus, JET, in Europe and only occasionally. ITER will be the first fully nuclear fusion machine.

Actually on the 31st of January, the Director General of ITER Organization (IO) sent out the request for Authorization of Creation (DAC files) of the ITER Nuclear Basic Installation (INB) and following French law, became formally a Nuclear Operator. Consequently French Nuclear regulation applies to all the aspects of design, construction, operation and dismantling.

From the physics point of view ITER will follow a progressive start-up through HH, DD and DT phases covering all the plasma and fusion physics research. One of the main support for this research are the diagnostics (and spectroscopic techniques particularly) that will allow to control, optimize and evaluate the long pulse plasmas of ITER. It will be necessary to measure accurately and reliably a wide range of key plasma parameters as well as those that describe the condition of the first wall and the divertor which is the component that exhausts the flow of energy from charged particles produced in the fusion reactions and removes helium and other impurities resulting from the reactions, and from interaction of plasma particles with the material walls. In addition to plasma and fusion parameters the overall installation will be monitored by different networks that include radioprotection monitoring, chemical and electromagnetic risks detection and sampling systems. Although ITER will not reach a very high neutron fluence, diagnostics will work under radiation-hard environment and remote handling will be use for maintenance, conditions very important for their design.

ITER must be viewed in the context that is the intermediate stage between the existing machines and those future reactors, DEMO, to which it will provide input on plasma performances, tritium breeding, blanket/divertor designs and solution of engineering issues, as well as bounding accidents or classification of waste and general safety approach but it must be fully understood that ITER is still a purely experimental installation that will allow full exploration of the science relevant to fusion power, as well as testing key technologies for future power plants.

The EU, China, Japan, India, Russian Federation, Republic of Korea and United States signed on 21 November 2006, at the Palais d'Elysée in a ceremony presided over by President Chirac, the Joint Implementation Agreement for constructing, operating and decommissioning the fusion project ITER. That moment ended a process that started in 1985 and that, even from its conception as an idea, was conceived as a truly global project where, finally, more than 50% of human population are represented by the ITER Partners. In this paper, the status, challenges, difficulties and opportunities associated to the project will be presented.

STELLARATORS AS FUSION REACTORS: THE TJ-II EXPERIMENT

Joaquín Sanchez
Asociacion EURATOM-CIEMAT 28040 Madrid, Spain

ABSTRACT

Magnetic confinement of hot plasmas in toroidal geometry cannot be achieved with the simple configuration based on magnetic lines parallel along the torus. The radial gradient of magnetic field, intrinsic to the toroidal geometry, leads to an outward drift of ions and electrons which would escape in microseconds. In order to keep the confinement, the magnetic field lines must have a helical twist as they progress along the torus, the so called "rotational transform". The two main lines of development in toroidal magnetic confinement: the "tokamak" and the "stellarator" differ basically on they way they achieve this rotational transform.

Whereas the stellarator uses coils with complex tridimensional geometry in order to provide the twisted magnetic field configuration, the tokamak, a later development, uses a simpler coil system and generates a toroidal electrical current in the hot plasma itself in order to complete the required twisted magnetic field. Due to its relative simplicity of design and construction, the tokamak has developed faster than the stellarator and the largest devices, those which are closer to ignition parameters, are tokamaks. ITER is the evident example.

Nevertheless, the coupling between the plasma and its confinement generates limitations in the flexibility and stability of tokamak operation. The main limitation comes from the fact that the basic mechanism for current generation in the plasma is magnetic induction, which leads to pulsed operation. On the contrary, the stellarator, though less developed, offers the potential for stable steady state operation. In a simplifying view, we could say that the tokamak is more suited as prototype, easy to build more difficult to operate, whereas the stellarator would be advantageous for commercial operation: the difficulty of construction, which decreases with the number of units produced, would be counterbalanced by the stability during operation.

The world stellarator programme is presently being carried out by three main devices, two of them are located in Japan: LHD a large device with superconducting coils and Heliotron J, a smaller size system. The third one is the TJ-II experiment, slightly larger than Heliotron J, located in Madrid and currently the only stellarator in operation in Europe. There are stellarators under development in the US (the NCSX in Princeton), and Germany, where the largest stellarator in the world, W7X, is being constructed. W7X will start operation by 2014 and will follow the long tradition of German stellarator research, whose last device was the W7AS device, closed down in 2003.

TJ-II is a helical axis system, with a major radius of 1.5m, a minor radius of 0.2m and able to operate with a magnetic field of up to 1.1 Tesla. The plasma is generated by 600 kW of radiofrequency at 53 GHz and high density scenarios are achieved by 1 MW neutral beam injection (H_2) at 40 keV, being currently upgraded to 2 MW.

The main capabilities of TJ-II are the flexibility of changes in the configuration, that can be achieved by just varying currents in the different coils, and the potential for stability at high plasma pressure, derived from its helical axis. Based on those properties, two of the main physics objectives of TJ-II are the dependence of the confinement with the degree of rotational transform and the exploration of the stability limits of the plasma.

In order to achieve its objectives TJ-II is equipped with an extensive system of plasma diagnostics. Amongst those we could mention the high resolution Thomson Scattering, based on a ruby laser, the dual color CO_2/He-Ne interferometer, the charge exchange recombination spectroscopy, passive spectroscopy in the visible and UV-VUV for impurity survey and Doppler measurements, laser induced fluorescence, global radiation detectors and beam based spectroscopy systems with lithium and helium.

MODELLING AND EVALUATION OF SPECTRA IN BEAM AIDED SPECTROSCOPY

M.G. von Hellermann[a], E.Delabie[a], R.Jaspers[a], P.Lotte[b], H.P.Summers[c]
[a] FOM-Institute for Plasma Physics Rijnhuizen, Association Euratom-FOM, www.rijnhuizen.nl
Partner in ITER-NL, PO Box 1207, 3430 BE Nieuwegein, The Netherlands
[b] Association Euratom-CEA Cadarache, F-13108 St. Paul-lez-Durance, France
[c] Strathclyde University, Dept. Appl. Physics, 107 Rottenrow, G4 0NG Glasgow,UK

Abstract. The evaluation of active beam induced spectra requires advanced modelling of both active and passive features. Three types of line shapes are addressed in this paper: Thermal spectra representing Maxwellian distribution functions described by Gaussian-like line shapes, secondly broad-band fast ion spectra with energies well above local ion temperatures, and, finally, the narrow lines shapes of the equi-spaced Motion Stark multiplet (MSE) of excited neutral beam particles travelling through the magnetic field confining the plasma. In each case additional line shape broadening caused by Gaussian-like instrument functions is taken into account. Further broadening effects are induced by collision velocity dependent effective atomic rates where the observed spectral shape is the result of a convolution of emission rate function and velocity distribution function projected into the direction of observation. In the case of Beam Emission Spectroscopy which encompasses the Motional Stark features, line broadening is also caused by the finite angular spread of injected neutrals and secondly by a ripple in the acceleration voltage associated with high energy neutral beams.
Keywords: Active beam spectroscopy, diagnostics of hot fusion plasmas, CXRS, MSE, BES.

INTRODUCTION

The need for quantitative evaluation of complex line emission spectra as observed in hot fusion plasmas initiated a challenging development of sophisticated interpretation tools based on integrating advanced atomic modelling with detailed treatment of the plasma environment. The successful merging of the two worlds has led to routine diagnostic procedures which have contributed enormously to the understanding of underlying plasma processes and also to a wide acceptance of spectroscopy as a reliable diagnostic method [1].

The present paper addresses spectra linked to active beam spectroscopy, that is, charge exchange recombination spectroscopy (CXRS) and beam emission spectroscopy (BES). In this case, a spectrum is composed of a (usually) dominating active spectrum and an underlying passive emission spectrum. Its analysis requires modelling of both active and passive features. Examples used here are from the CXRS diagnostic at JET and TEXTOR and more recently, predicted spectra for ITER CXRS diagnostic. They display characteristic features of the main light impurity ions (C^{+6}, He^{+2}, N^{+7}, Ne^{+10} and Ar^{+18}), as well as that of the bulk plasma ions, H^+, D^+ and T^+.

In the case of ion temperatures comparable, or in the same order of magnitude as the collision energy between probing neutral beam and fully stripped plasma ion, the effective atomic emission rates [2] may change noticeably over the Maxwellian velocity distribution function. As a result the observed spectral shape may deviate from a simple Gaussian shape.

Synthetic line shapes need to be reconstructed from a convolution of emission rate function and the original particle velocity distribution function projected into the direction of observation. This requires a 3-dimensional integration in velocity space. However, for the case $v_{thermal} << v_{beam}$, the resultant synthetic spectrum retains in a first order approximation [3] its Gaussian-like shape and the observed spectra may described in terms of apparent Doppler-width (ion temperature), apparent Doppler shift (-plasma rotation) and apparent amplitude (ion density).

A second class of non-Gaussian synthetic line shape arises in the case of passive CX line emission [4], which represent the non-local, line-of-sight integrated, measurement of spectra induced by the interaction of neutral hydrogen and fully stripped impurity ions. The neutral hydrogen density profile may adequately described by an exponential decay as characterized by the mean free path. Typically, and that is the good news, the peak of the passive CX layer is localized close to the separatrix and has a width of the order of a/10, where **a** is the minor plasma radius. At JET and TEXTOR the passive CX component may therefore adequately represented by a single Gaussian with an ion temperature and a Doppler-shift corresponding to $T_i(r/a=0.9)$ and $v_{rot}(r/a=0.9)$ respectively. The biggest uncertainty in the passive CX modelling efforts is the actual neutral hydrogen density at the plasma wall. So absolute intensities are difficult to assess, and hence amplitudes of PCX features have to remain free parameters.

Another type of synthetic active spectra is that of fast-ion-spectra, i.e. slowing-down fusion alpha particles, fast beam ions [6] or minority ions accelerated by Ion Cyclotron Resonance Heating (ICRH). In all three examples, the range of energies of the fast ions exceeds by far the width of the CX emission rate function which typically peaks at about 50keV/amu, and contributes at most to measurable signals for relative velocities less than 100 keV/amu. As a result the broad slowing-down distribution function is convolved by a comparatively narrow emission rate function and the observed spectral shape is no longer a direct mapping of the original distribution function. As an example, we show here fast beam ion spectra as measured on TEXTOR and predicted spectra for slowing-down fusion alpha

particles with energies in the MeV range as expected for ITER and making use of the 1 MeV D^0 ITER heating neutral injector as probe beam [6].

BULK ION CXRS AND BEAM EMISSION SPECTROSCOPY

In spite of the pre-dominant application of active beam spectroscopy to the measurement of low-Z impurity ion spectra such as the CVI line at 590nm, for routine data on radial profiles of ion temperature, plasma rotation and ion density, the most challenging ions in a fusion plasma are the bulk ions proper, that is, deuterons, or in a burning plasma deuterons and tritons. Historically, in fact, the complex features in the case of the active Balmer-Alpha spectrum which encompasses both the bulk ion CX feature as well as the Doppler shifted beam emission spectrum (cf. Figs.1 and 2), have started a long chain of advanced modelling on the combined use of CXRS and BES [7], [8],[9]. Probably the main reason which excludes the routine use of Balmer-Alpha as a tool for ion temperature diagnostics, is on the one hand the co-existence of a very bright edge line (Ti<5eV), the occurrence of a significant passive CX feature (Ti<1keV) and the main CX feature whose line shape is already significantly affected even at moderately hot plasmas of 10 keV. For ITER we expect temperatures around 20 keV. On the other hand, there is clear evidence of a unique link between the local deuteron density and the intensity of the observed active Balmer-Alpha spectrum [10] and potentially the active bulk ion feature can be extracted from a composite spectrum.

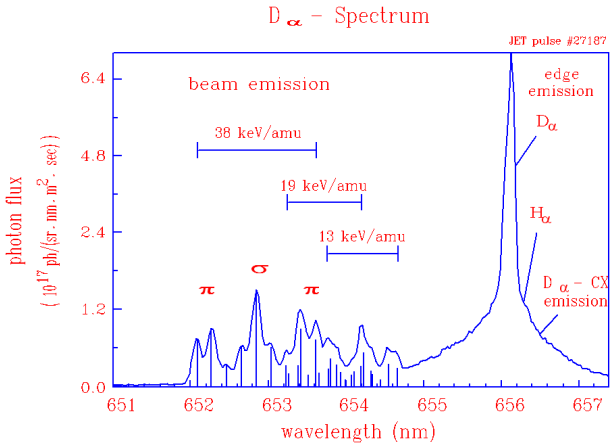

Figure 1. JET example of active and passive features in the Balmer-Alpha spectrum. The edge lines contain H and D, where D is the dominant isotope. The Zeeman splitting of the edge lines is not resolved. The complex beam spectrum encompasses 27 components representing full, half and third energy each containing 9 Motional Stark Effekt (MSE) multiplet components (cf. **Fig.2**).

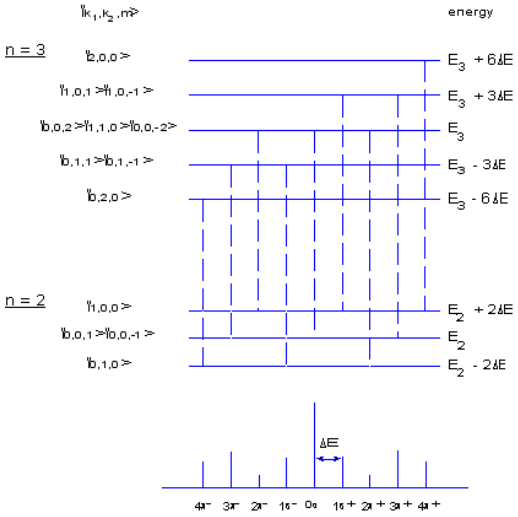

Figure 2 Energy levels of beam induced Stark multiplet. The Lorentz field $\mathbf{E}_L=\mathbf{v}_{beam}\mathrm{x}\mathbf{B}_{total}$ leads to a line splitting of :

$$\Delta\lambda_s(0)=\frac{3}{2}e\cdot a_0\cdot\frac{\lambda_0^2}{h\cdot c}\cdot E_{Lorentz}$$

LINE SHAPE MODELLING OF MOTIONAL STARK FEATURES

The MSE feature, which is induced by the Lorentz field $\mathbf{E}_{Lorentz}=\mathbf{v}_{beam}$ x $\mathbf{B}$ experienced by a neutral beam travelling through a magnetically confined plasma, is modified by the finite angular spread of the neutral beam direction cone, which is typically of the order of 10 to 20 mrad. For each velocity direction we get a different Doppler-shift:

$$\Delta\lambda_d=\Delta\lambda_d(0)\cdot(1-\delta\tan(\beta)) \qquad (1)$$

and also a line shift for MSE component k representing the local Lorentz-field:

$$\Delta\lambda_s=k\cdot\Delta\lambda_s(0)\cdot(1+\delta\cot(\alpha)-\frac{1}{2}\delta^2) \qquad (2)$$

Where: α is the angle between velocity vector and magnetic field direction, β the angle between line of sight, and finally δ the angular deviation from the beam axis. The central values for Doppler shift and Stark split are given by:

$$\Delta\lambda_d(0)=\lambda_0\cdot\cos(\beta)\cdot v_{beam}/c \qquad (3)$$

$$\Delta\lambda_s(0)=\frac{3}{2}e\cdot a_0\cdot\frac{\lambda_0^2}{h\cdot c}\cdot E_{Lorentz} \qquad (4)$$

Integrating over the angles δ, assuming a Gaussian-like beam shape, with a beam divergence 1/e-angle "w", and a spectral line width d composed of instrument function and voltage ripple of the DNB energy we get finally for the line shape of each Stark component:

$$f_k(\lambda)=\frac{1}{\sqrt{\pi}\cdot\sqrt{A_k^2 w^2+d^2}}\,e^{-(u_k^2)/(A_k^2\cdot w^2+d^2)} \tag{5}$$

with: $A_k=k\cdot\Delta\lambda_s^0\cdot\cot(\alpha)-\Delta\lambda_d^0\cdot\tan(\beta)$ and $d=\sqrt{\Delta\lambda_{ripple}^2+\Delta\lambda_{instr}^2}$ (6)

Where indices k represent the 9 MSE components: π_{-4}, π_{-3}, π_{-2}, σ_{-1}, σ_0, σ_{+1}, π_{+2}, π_{+3}, π_{+4} .

Applying this model of individual line widths and amplitudes to MSE spectra as observed, for example, on Tore Supra (Fig.3), we get clearly asymmetric multiplet features. Conveniently we introduce also a factor R representing the intensity of pi over sigma components, which is a measure of the angle , between line-of-sight and Lorentz vector which allows therefore the deduction of the local pitch-angle, i.e. the ratio of $B_{poloidal}/B_{toroidal}$.

$$R=\frac{I_\pi}{I_\sigma}=\frac{\sin^2}{1+\cos^2}=\frac{2\cdot I_{\pi\pm2}+2\cdot I_{\pi\pm3}+2\cdot I_{\pi\pm4}}{I_{\sigma0}+2\cdot I_{\sigma\pm1}} \tag{7}$$

Note, the empirically observed deviations from inner shell populations as described in ref.[8] indicates the need for an atomic revision of level populations in the case of strongly anisotropic collision between beam and plasma ions.

$$I_{\sigma1}/I_{\sigma0}=0.412\pm0.027 \qquad I_{\pi2}/I_{\pi3}=0.325\pm0.047 \qquad I_{\pi4}/I_{\pi3}=0.811\pm0.052 \tag{8}$$

Current investigations address the role of alignment [12].

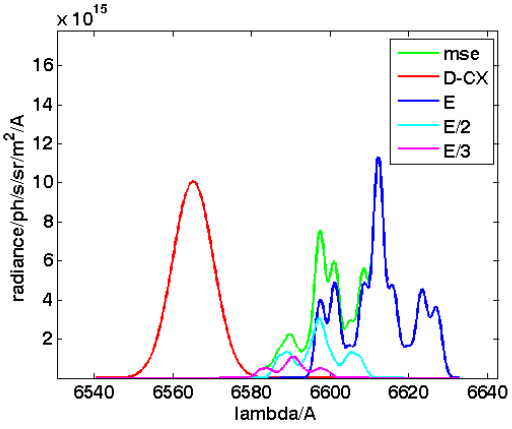

Figure 3 Predicted MSE spectrum on Tore Supra. The total spectrum (green) encompasses the 3 energy components of the neutral beam (E, E/2 and E/3). The π_- group (left) is about 9% higher and narrower than the π_+ group. On the left the active Balmer alpha CX feature representing bulk ion deuterons.

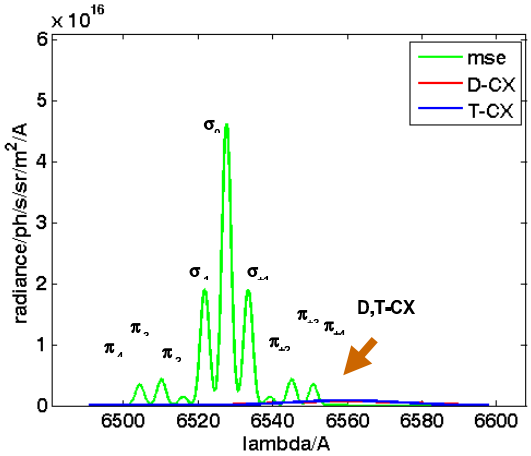

Figure 4 Predicted MSE spectrum for ITER using a 100keV/amu Diagnostic Neutral beam which is injected approximately radially into ITER. The magnetic field is 5.2T.

FAST ION SPECTRA

Fast ion transport, fast ion energy contents and fast ion loss mechanisms play an important role for present and future fusion experiments. Active spectra associated with fast ion physics include on the one hand anisotropic slowing-down features, as in the case of a fast ion population following the injection of high energy neutrals, or, on the other hand, isotropic slowing-down features as expected for a thermo-nuclear plasma. The first case is linked to spectra of beam ions or minority ions (e.g. DI, HeII) and the second case is linked to HeII spectra representing alpha particles in the energy range between 20 keV and the birth energy of 3.5MeV. In each case we need a neutral probe beam for the CXRS interaction and the excitation of observable spectra. The common factor of fast ion CX spectra is the spread of energies which exceeds by far the half-width energy range of the emission rate function (c.f. [2]) .

The resulting spectrum is a convolution of emission rate function and slowing-down function (c.f. [13])

$$f_{obs}(v_z)=\int_0^\infty v'^2 dv'\int_0^\pi d\theta'\sin\theta'\int_0^{2\pi} d'g\ _{slow}(v',\theta',')\,Q_{cx}(v_r)\,\delta(v_z-v'\cos\theta') \tag{9}$$

where the slowing-down velocity distribution function g_{slow} is for the fast beam ion case:

$$g_{slow}(v,\xi)=\frac{S\tau_s}{v^3+v_c^3}\frac{1}{\sqrt{4\pi\alpha}}\exp\left\{-(\xi-\xi_0)^2/4\alpha\right\} \quad (10)$$

$$\alpha(v)=\frac{\beta}{3}(1-\xi_0^2)\log\frac{[1+(v_c/v)^3]}{[1+(v_c/v_b)^3]} \quad (11)$$

Where we have used, τ_s slowing-down time, v_c the critical velocity, v_b the birth velocity, beam energy and finally ξ_0 the initial pitch angle between beam ion and magnetic field. The neutral beam source-rate S is derived from the local beam attenuation factor ζ along the entire beam trajectory:

$$S=\frac{P_{beam}}{e\cdot E_{beam}}\cdot\frac{\partial\zeta}{\partial V} \qquad \tau_s=\frac{3v_e^3 m_e m}{16\sqrt{\pi}e^4 Z^2 n_e \ln\Lambda} \qquad v_c^3=\frac{3}{4}\sqrt{\pi}\left(\frac{2T_e}{m_e}\right)^{3/2}\sum_j\frac{n_j}{n_e}Z_j^2\frac{m_e}{m_j} \quad (12)$$

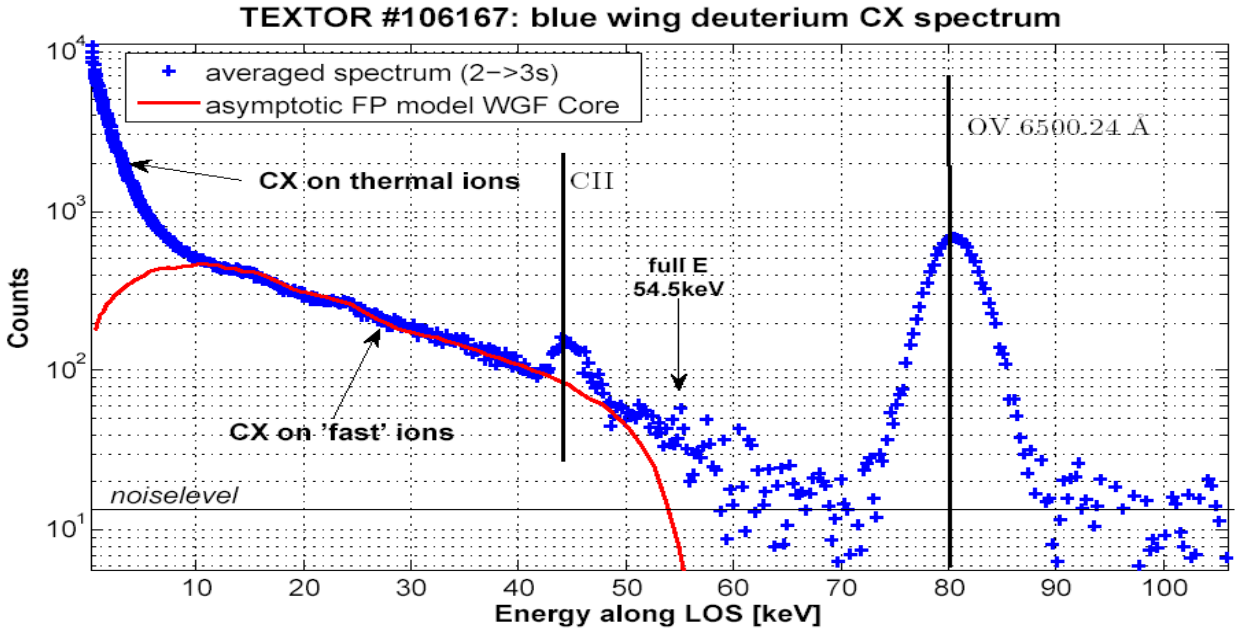

Figure 5 Measured and predicted fast ion beam spectrum on TEXTOR. The energy scale is proportional to ρ^2. Note : TEXTOR uses 2 NB injectors, one in co- and one in counter-direction. In the example above the 54.5 keV ,1.3 MW D^0 co-beam is the fast ion source and the MW D^0 counter-beam is the probe beam . The experimental data (blue) include thermal and non-thermal features. The solid line (red) is the anisotropic fast ion beam spectrum (cf. [5,13,14]).

REFERENCES

[1] M.G.von Hellermann, W.Biel, G.Bertschinger, C.Jupen, M.O'Mullane, H.Summers, A.Whiteford, Physica Scripta, T120, 2005

[2] https://adas.phys.strath.ac.uk

[3] M.G. von Hellermann, P.Breger, J.G.Frieling, R.W.T.König, W.Mandl, A.Maas, H.P.Summers, Plasma Phys. & Contr. Fusion, **37**, 71 (1995)

[4] M.Tunklev, P. Breger, K. Günther, M.G. von Hellermann, R.W. König, M. O'Mullane , K-D. Zastrow, Pl. Phys. &Contr.Fus. **41**,985(1999)

[5] W.Heidbrink, Y Luo, K H Burrell, R W Harvey, R I Pinsker and E Ruskov, Plasma Phys. Control. Fusion 49 No 9 (September 2007) 1457

[6] M.G von Hellermann, W.G.F.Core, J.Frieling, L.D.Horton, R.W.T. König, W.Mandl, H.P.Summers, Plasma Phys. Contr. Fus., **35**,799, 1993

[7] A. Boileau, M.G. von Hellermann, L.D. Horton, J. Spence, H.P. Summers, Plasma Phys. Contr. Fusion, **31**, 779 (1989)

[8] W.Mandl, R.Wolf, M.G. von Hellermann, H.P Summers, Plasma Phys. Contr. Fusion, **35**,1373, 1993

[9] M.G. von Hellermann, E.Delabie, R.J.E.Jaspers, W.Biel, O.Marchuk, H.P.Summers, A.Whiteford, C.Giroud, N.C.Hawkes, K.D.Zastrow , Int. Workshop on Burning Plasma Diagnostics, Varenna, Italy, September 2007, Melville N.Y. ,IOP Conf. Proc. Vol. 988, p165(2008)

[10] H.Anderson, M.G.von Hellermann, R.Hoekstra. L.D.Horton, A.C.Howman, R.W.T. Koenig, R.Martin, R.E.Olson, H.P.Summers, Plasma Physics and Contr. Fusion **42**,781-806(2000)

[11] J.Svensson, M.G. von Hellermann, R.W.T.König, Plasma Physics and Controlled Fusion **43**, 389(2001)

[12] A.Sakaue, M. Atake, M. Goto, S.Morita, A. Iwamae, "Motional Stark Effect Spectra of H_α on LHD", to be submitted to PPCF (2008)

[13] M von Hellermann, W.G.F.Core, J.Frieling, L.D.Horton, R.W.T. König, W.Mandl, H.P.Summers, Plasma Phys. Contr. Fusion, **35**,799, 1993,

[14] E.Delabie, R.J.E. Jaspers, M.G. von Hellermann, S.K. Nielsen, O. Marchuk and the TEXTOR team, 17th Topical Conference on High Temperature Plasma Diagnostics, Albuquerque, May, 2008, to appear in Rev. Sci. Instr. (2008)

On the use of spectral lines emitted by carbon ions for plasma diagnostics in magnetic fusion devices

M. Koubiti[*], S. Ferri[*], L. Godbert-Mouret[*], Y. Marandet[*], T. Nakano[§], J. Rosato[*] and R. Stamm[*]

[*] *Laboratoire de Physique des Interactions Ioniques et Moléculaires, UMR 6633 CNRS/Université de Provence, Campus Scientifique de Saint-Jérôme, service 232, F-13397 Marseille Cedex 20, France*
[§] *NFRE, Japan Energy Research Institute, Naka, Ibaraki 311-0193, Japan*

ABSTRACT

Spectroscopy is a common and powerful method to characterize plasmas such as those confined magnetically in thermonuclear fusion-oriented devices (both tokamaks and stellarators). This technique, based on the use of spectral line emission (line intensities, line shapes or both), allows the deduction of one or several plasma parameters like the ion, electron or/and neutral densities and temperatures. Recently measured lithium-like carbon lines have been used to obtain the electron density and temperature of the emissive plasma region in the tokamak where high-electron densities up to 10^{22} m^{-3} have been deduced near the X-point region for detached plasmas [1]. Such a high electron density has to be confirmed by other independent methods. For that purpose, we propose to use line broadening to diagnose the same emissive plasma. In this paper, profiles of C IV n=5-6 (λ = 4658 Å) and n=6-7 (λ = 7726 Å) lines are computed for plasma conditions of tokamak divertors (Ne=10^{19}-10^{22} m^{-3}, Te=1-10 eV) in order to be compared to the measured spectra. Comparisons between experiments and calculations are promising [2] and encourage fitting of various experimental data from JT-60U and other magnetic fusion devices. A study of the broadening mechanisms affecting lines emitted by carbon at different ionization stages and a discussion concerning their use for diagnostics purposes will be presented. Our results are based on calculations made with a modified version of the PPP line shape code [3] using an atomic data basis built with the most accurate available data for carbon [4-5] in addition to the Cowan's code [6]

REFERENCES

1. .T. Nakano et al, J. Plasma Fusion Res. **80**, 500 (2004); Nucl. Fusion **47**, 1458 (2007)
2. M. Koubiti et al, Proc. 34th EPS Conf. Plasma Physics (Warsaw) P2-128 (2007)
3. B. Talin *et al*, Phys. Rev. **A51**, 1918-1928 (1995)
4. P. Quinet, *Astron. Astrophys. Suppl. Ser.* **129**, 603-608 (1998)
5. Yu. Ralchenko *et al*, NIST Atomic Spectra Database (version 3.1.2), [Online]. Available: http://physics.nist.gov/asd3
6. Cowan code package for atomic physics (http://das101.isan.troitsk.ru/cowan.htm)

ABAKO/RAPCAL: A flexible computational package to perform radiative properties calculations and diagnostics in a wide range of plasma conditions

R. Florido[#] , R.Rodríguez[#], J.M.Gil[#], J.G.Rubiano[#], P.Martel[#], E.Mínguez*, P.Sauvan and R.Mancini[§]

[#] *Departamento de Física, Universidad de Las Palmas de Gran Canaria, 35017 Las Palmas de Gran Canaria, Spain*
** Instituto de Fusión Nuclear, E.T.S. de Ingeniros Industriales, U.P.M., 28006 Madrid, Spain*
Departamento de Ingeniería Energética, UNED, Madrid, Spain
[§] *Physics Department University of Nevada, Reno, NV 89557, USA*

ABSTRACT

Radiative properties of hot dense plasmas remain a subject of current interest [1, 2] since they play an important role in the inertial fusion confinement (ICF) research as well as studies in stellar physics. In particular, the understanding of ICF plasmas requires emissivities and opacities both for hydro-simulations and diagnostics [3]. The first step on the calculation of plasma radiative properties is the computation of the required atomic data. However, this is a complex task since the number of the atomic levels involved, and therefore the amount of atomic data to obtain is huge and approximations must be made in order to include. Due to this fact, the calculation of plasma ion populations and radiative properties is still an open question and continuous efforts are made to develop new models and numerical codes that improve the currently available ones.

Recently, it has been developed at the University of Las Palmas de Gran Canaria a computation package composed by two codes called ABAKO [4] and RAPCAL [5] that calculate atomic data and plasma level populations (ABAKO) and radiative properties such as opacities, emisivities, intensities or radiative power losses (RAPCAL) for optically thin and thick plasmas, both under LTE and NLTE conditions. In particular, plasmas of elements such as carbon, aluminum, argon, iron, krypton, xenon and gold have been studied in several plasma situations (Corona, NLTE or LTE, optically thin and thick,…) and density and temperature conditions, obtaining accurate results. In this work ABAKO/RAPCAL code is described and some applications of this code to analyse experimental spectra are showed.

REFERENCES

1. S. Alexiou, et al. *JQSRT*, **58**, 399 (1997).
2. G. Csanak, and W. Daughton *JQSRT,* **83**, 83, (2004).
3. O. Peyrusse, *Nucl. Fus.,* **44**, S202, (2004).
4. J.M. Gil, et al. *Laser Part. Beams* **26,** (2008).
5. R. Rodríguez, et al. *J. Phys. IV* **133**, 981, (2006).

Line shapes and opacity studies in divertor plasmas

J. Rosato*,†, V. Kotov* and D. Reiter*

*IEF - Plasma Physics, Forschungszentrum Jülich GmbH, Euratom Association, Trilateral Euregio Cluster, D-52425 Jülich, Germany
†PIIM, UMR 6633 Université de Provence - CNRS, Centre de St Jérôme, Case 232, F-13397 Marseille Cedex 20, France

Some recent investigations have been made on radiative transfer in magnetized fusion devices. In the edge of several tokamaks, the so-called divertor region contains a cold and dense plasma in recombining regime (typically $T_e < 5$ eV and $N_e > 10^{14}$ cm^{-3}) which is affected by important radiation trapping at frequencies near the Lyman lines of the hydrogen isotopes. Opacity effects have been experimentally measured, in particular in Alcator C-Mod [1] where the high gas density (up to 10^{15} cm^{-3}) leads to very efficient photon absorption. Such effects are also expected in the plasma of the ITER divertor because of its large size $\times$ density values [2]. The main consequence of the opacity is that the plasma ionization-recombination equilibrium is modified. The photon absorption provides an additional source of excited atoms and thus contributes to ionization, whereas the produced additional electrons entail a significant additional source for recombination. The effects of opacity on the ionization-recombination equilibrium are currently studied by solving collisional-radiative models coupled to the radiative transfer equation [3]. This requires the knowledge of detailed expressions for the line shapes, which are as accurate as possible to increase the reliability of simulations. In this work, we consider the line shape models which are used in the transport code EIRENE [4, 5] and we discuss the role of the main broadening mechanisms on the absorption efficiency: Doppler, Zeeman and Stark effects. The influence of these broadening mechanisms is investigated in term of the photon transmission factor [6], defined as $T(a,\vec{\Omega}) = \int d\omega \phi(\omega,\vec{\Omega}) \exp(-\chi(\omega,\vec{\Omega})a)$. This quantity gives a measure of the efficiency of the absorption process in an optically thick medium, for a pencil of radiation covering the distance a in the direction $\vec{\Omega}$: one has $T(a,\vec{\Omega}) = 1$ in case of no absorption, 0 in case of a purely opaque medium. The integral is made over the frequencies ω, $\phi(\omega,\vec{\Omega})$ is the normalized line shape, and $\chi(\omega,\vec{\Omega}) \propto N_g \phi(\omega,\vec{\Omega})$ is the extinction coefficient, proportional to the line shape and to the density N_g of the absorbers in the considered energy level g. We consider the first lines of Lyman series since those are the most opaque in fusion plasmas. Stark broadening is described within the impact assumption for both electrons and ions. Non-impact effects, which are expected for the ions at high density [7], are retained by using effective widths obtained with the numerical simulation method. We discuss the influence of Stark effect on the opacity. Progress on the calculations of the photo-excitation rate in realistic cases with the code EIRENE will be reported.

ACKNOWLEDGMENTS

This work is partially supported by a Euratom mobility contract, and by the project "Radiation absorption effects" of the fédération de recherche sur la fusion par confinement magnétique in the frame of the LRC DSM 99-14 (Laboratoire PIIM / CEA Cadarache).

REFERENCES

1. J. L. Terry *et al.*, *Phys. Plasmas* **5**, 1759–1766 (1998).
2. A. Loarte *et al.*, *Nucl. Fusion* **47**, S203–S263 (2007).
3. V. Kotov *et al.*, *Contrib. Plasma Phys.* **46**, 635–642 (2006).
4. D. Reiter *et al.*, *J. Nucl. Mater.* **363-365**, 649–657 (2007).
5. J. Rosato *et al.*, *J. Nucl. Mater.* **363-365**, 421–425 (2007).
6. F. E. Irons, *J. Quant. Spectrosc. Radiat. Transfer* **22**, 1–20 (1979).
7. J. Rosato *et al.*, these proceedings.

Measurements of magnetic and electric fields in turbulent plasmas

Evgeny Stambulchik*, Konstantin Tsigutkin*,†, Rami Doron*, Vladimir Bernshtam* and Yitzhak Maron*

*Faculty of Physics, Weizmann Institute of Science, Rehovot 76100, Israel
†(Present address: Department of Physics, University of California, Berkeley, CA 94720-7300, USA)

A fundamental problem common to many studies in the field of plasma physics, both in laboratory and in space, is the interaction of pulsed magnetic fields with plasmas. The physics of laser-matter interaction, z-pinches, wire explosions, plasma switches, tokamaks, sunspots and flares, supernova remnants, and collisionless shocks are examples where magnetic fields play an important role in the plasma dynamics and in the energy balance of the system.

A major difficulty in analyzing the interaction of plasmas with intense, pulsed magnetic fields results from the fact that the system usually becomes unstable (e.g., Rayleigh-Taylor instabilities) and a dynamic, turbulent state develops, encompassing a wide range of scale lengths. Plasmas admit several scale lengths, which can each support a different type of turbulence. There are also various gradients, which are the source of free energy of the turbulence. A very common energy source is the density gradient in the presence of an effective gravity, which could occur due to plasma acceleration or magnetic-field-line curvature. These instabilities often affect both the plasma motion and the magnetic field, and themselves become a source of fluctuating electric fields.

The electric fields play a crucial role in the interaction of the magnetic field with the plasma. The electric field transfers energy to the current-carrying plasma (the Joule heating), the electric field that is generated by the space-charge separation due to the magnetic field accelerates the ions, and the Hall electric field may induce the magnetic field penetration into the plasma.

While the macroscopic interaction scale, as described by MHD is generally observable, short wavelength MHD turbulence or Hall-MHD turbulence (see for example, [1]), which typically occurs on the ion skin-depth scale, are most difficult to investigate experimentally. Indeed, while numerous theories and numerical simulations on this subject were published, the experimental work is usually limited to phenomenological description by imaging, without obtaining the plasma or the magnetic field properties that are essential for understanding the turbulence and testing the various theories. Thus, the influence of the small-scale turbulence on the macroscopic evolution of the system is an unresolved issue (e.g., [2]). Yet, it is thought to play a crucial role in the conversion of the magnetic energy into plasma kinetic energy, heat and radiation (e.g., in z-pinch [3] and in space [4, 5]), as well as in the magnetic field penetration into the plasma (e.g, [6]). Any significant progress in the field would require attacking the problem of the lack of detailed experimental data on turbulence, and in particular on small-scale turbulence.

Evidently, if the space or time scales of the turbulence are beyond the resolving capabilities, the electromagnetic fields may have various directions and amplitudes in the region viewed, or the field direction and amplitude may vary significantly during the time of observation.

Consequently, magnetic-field diagnostic methods that are based on detecting an anisotropy in either the emitted radiation (the Zeeman effect) or in the dispersion properties of the medium (the Faraday rotation) are either inapplicable or provide ambiguous results for such [quasi-]isotropic magnetic fields. Instead, an approach for measurements of magnetic fields, based on the comparison of the magnetic-field-induced contributions to the line shapes of different fine-structure components of an atomic multiplet, was proposed and experimentally demonstrated [7]. Contrary to the methods based on detecting an anisotropy in either the emitted radiation or in the dispersion properties of the medium, the present method is applicable when the field direction or amplitude vary significantly in the region viewed or during the time of observation. The technique can be used even when the line shapes are Stark- or Doppler-dominated.

Similarly, the electric fields associated with the turbulent or turbulent-like plasma motion tend to be difficult to measure unambiguously, since they may have no preferred direction and have a distribution of magnitudes and a wide frequency spectrum. Indeed, these properties make it difficult to distinguish the Stark effect of such fields from that of the plasma microfields (produced by the thermal motion of plasma particles). We will describe a method based on laser spectroscopy combined with plasma doping, which allows for such electric-field measurements using a dipole-forbidden emission-line shape. It was applied to a 3D-resolved investigation of the time evolution of electric fields in plasmas under high-current pulses [8].

REFERENCES

1. J. D. Huba, J. G. Lyon, and A. B. Hassam. Theory and simulation of the Rayleigh-Taylor instability in the limit of large Larmor radius. *Phys. Rev. Lett.*, 59(26):2971–2974, 1987.
2. D. D. Ryutov, M. S. Derzon, and M. K. Matzen. The physics of fast Z pinches. *Rev. Mod. Phys.*, 72:167–223, 2000.
3. M. G. Haines, P. D. LePell, C. A. Coverdale, B. Jones, C. Deeney, and J. P. Apruzese. Ion viscous heating in a magnetohydrodynamically unstable Z pinch at over 2×10^9 Kelvin. *Phys. Rev. Lett.*, 96:075003, 2006.
4. M. Balikhin, M. Gedalin, and M. Petrukovich. A new mechanism for electron heating in shocks. *Phys. Rev. Lett.*, 70:1259, 1993.
5. B. Lembege, J. Giacalone, M. Scholer, T. Hada, M. Hoshino, V. Krasnoselkikh, H. Kucharek, P. Savoini, and T. Terasawa. Selected problems in collisionless-shock physics. *Space Science Reviews*, 110:161–226, 2004.
6. R. Arad, K. Tsigutkin, Y. Maron, A. Fruchtman, and J. D. Huba. Observation of faster-than-diffusion magnetic field penetration into a plasma. *Phys. Plasmas*, 10:112–125, 2003.
7. E. Stambulchik, K. Tsigutkin, and Y. Maron. Spectroscopic method for measuring plasma magnetic fields having arbitrary distributions of direction and amplitude. *Phys. Rev. Lett.*, 98(22):225001, 2007.
8. K. Tsigutkin, R. Doron, E. Stambulchik, V. Bernshtam, Y. Maron, A. Fruchtman, and R. J. Commisso. Electric fields in plasmas under pulsed currents. *Phys. Rev. E*, 76(4):046401, 2007.

Spectroscopic Modeling and Characterization of a Collisionally Confined Laser-ablated Plasma Plume

M.E. Sherrill[*,†], R.C. Mancini[*], J.E. Bailey[**], A. Filuk[**], B. Clark[**], P. Lake[**] and J. Abdallah, Jr.[†]

[*]*Department of Physics, University of Nevada, Reno, Nevada 89557, USA*
[†]*Theoretical Division, Los Alamos National Laboratory, Los Alamos, New Mexico 87545, USA*
[**]*Sandia National Laboratories, Albuquerque, New Mexico 87185, USA*

Plasma plumes produced by laser ablation are an established method for manufacturing the high quality stoichiometrically complex thin films used for a variety of optical, photoelectric and superconducting applications. The state and reproducibility of the plasma close to the surface of the irradiated target play a critical role in producing high quality thin films. Unfortunately, this dense plasma has historically eluded quantifiable characterization. The difficulty in modeling the plume formation arises in accounting for the small amount of energy deposited into the target when physical properties of these exotic target materials are not known. In this work we obtain the high density state of the plasma plume through the use of a novel experimental spectroscopic technique and a custom spectroscopic model[1]. Besides obtaining detailed temperature and density profiles, issues regarding line broadening and opacity for spectroscopic characterization will be addressed for this unique environment.

ACKNOWLEDGMENTS

This work was supported by NSF Grant OSR-9353227, and the UCCSN.

REFERENCES

1. M. E. Sherrill, R. C. Mancini, J. E. Bailey, A. Filuk, B. Clark, P. Lake, and J. Abdallah, Jr., *Phys. Rev. E.* **76**, 056401 (2007).

Measurement of oscillator strength distribution in the discrete and continuous spectrum of lithium

Shahid Hussain, M. Saleem*, and M. A. Baig*

National Tokamak Fusion Program P.O.Box 3329 Islamabad Pakistan
**Atomic and Molecular Physics Laboratory, Department of Physics, Quaid-i-Azam University, Islamabad 45320, Pakistan*

(Hussain S, Saleem M and Baig M A 2007, *Phy. Rev. A* 75 022710)

Abstract

Oscillator strength is a very important atomic parameter but its experimental measurement is usually difficult. There are only fewer experimental efforts that have been devoted to determine the oscillator strength of lithium[1]. The oscillator strength distribution in the discrete and continuous regions of the spectrum of lithium has been determined by employing the saturation technique[2,3] in conjunction with a thermionic diode ion detector. The photoionization cross section from the 3s ^{2}S excited state at the ionization threshold has been determined by the direct absorption of the 614 nm laser and also from extrapolating the photoabsorption cross sections measured for eight transitions of the 3s ^{2}S → *n*p ^{2}P (*n* = 14, 16, 18, 20, 22, 24, 26, 28) Rydberg series. The average value of the photoionization cross section measured at the ionization threshold has been used to extract the *f*-values for the 3s ^{2}S → *n*p ^{2}P Rydberg series of lithium from *n* = 14 to *n* = 56. The discrete *f*-values also depend on the line width and the relative intensity of the observed spectral lines. The Rydberg series was carefully recorded to avoid stark and power broadening of the lines. The measured *f*-values of the observed Rydberg series decrease smoothly with an increase of the principal quantum number. The oscillator strength densities in the continuum region have also been determined from the measured values of the photoionization cross section from the 3s ^{2}S excited state at four ionizing laser wavelengths above the first ionization threshold. Continuity has been found between the discrete and the continuous spectrum across the ionization threshold. This technique has been employed to determine the oscillator strength distribution in helium[4].

Energy level diagram and Experimental arrangement

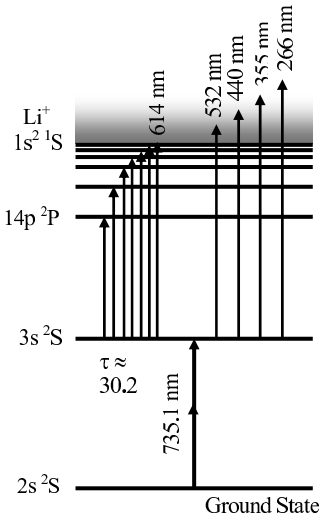

Figure 1

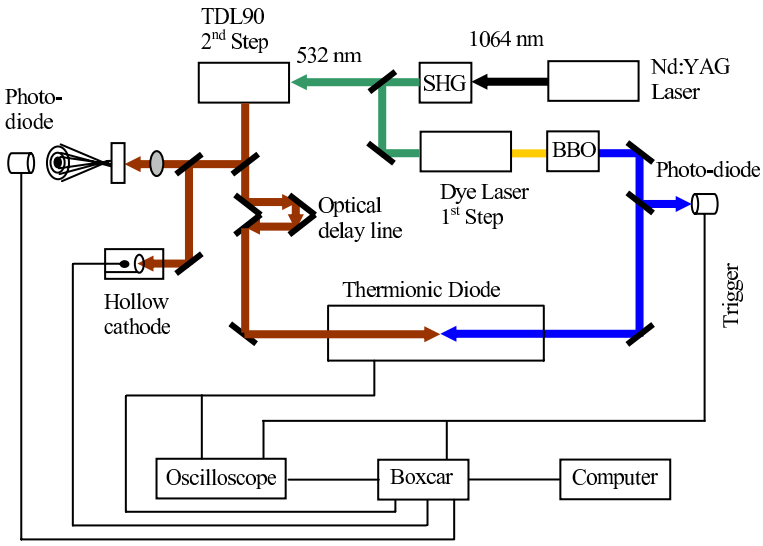

Figure 2

A portion of the 3s ^{2}S → *n*p ^{2}P ($24 \le n \le 56$) Rydberg series of lithium

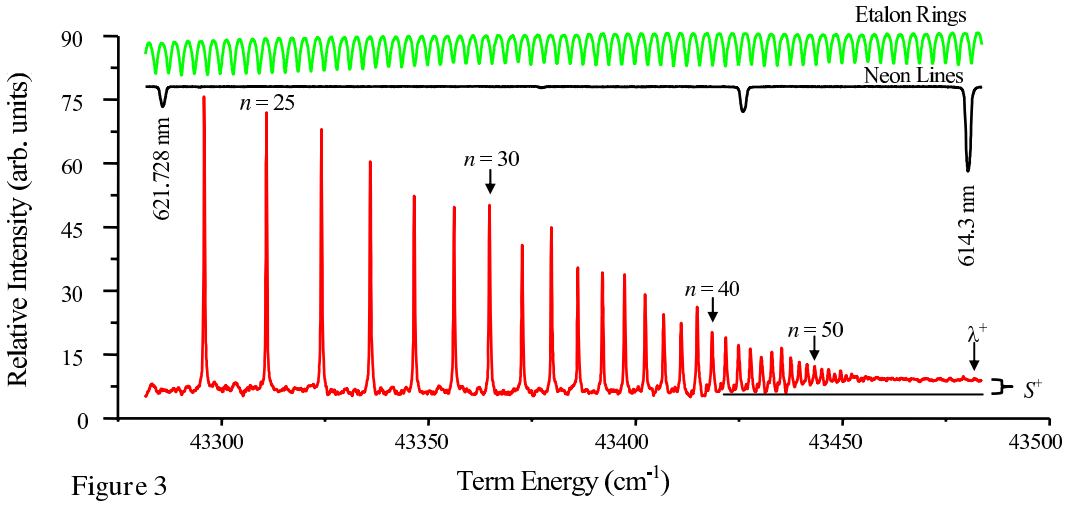

Figure 3

Mathematical expression for oscillator strength measurement[3]

$$f_n = \frac{4\varepsilon_o mc S^n \lambda^+}{e^2 S^+ \lambda_n}\sigma(\lambda^+)$$

$$\frac{df}{dE} \cong \frac{n^3 f_n}{2R}$$

$$\frac{df}{dE} = 9.11\times10^{15}\,\sigma(E) \quad \text{cm}^{-2}.(\text{eV})^{-1}$$

f_n - oscillator strength for Rydberg transitions

$\sigma(\lambda^+)$ - photoionization cross section at the threshold

λ^+ - wavelength of ionizing laser corresponding to threshold

λ_n - wavelength corresponding to *n*th transition of a Rydberg series

S^n - integrated ion signal intensity for the *n*th transition

Measured oscillator strength of lithium

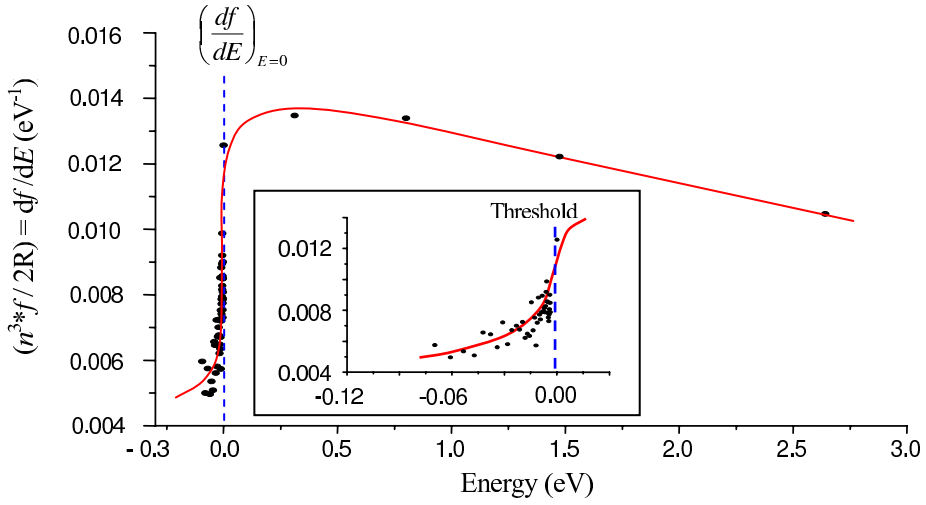

Figure 4

References

1. Marr G V and Creek D M 1968 *Proc. Roy. Soc. A* 304 245
2. Burkhardt C E, Libbert J L, Xu J, Leventhal J J and Kelley J D 1988 *Phys. Rev. A* 38 5949
3. Mende W and Kock M 1996 *J. Phys. B* 29 655
4. Hussain S, Saleem M and Baig M A 2007 *Phy. Rev. A* 76 012701

Experimental Stark Widths and Shifts for Spectral Lines of Neutral and Ionized Atoms

(A Critical Review of Selected Data for the Period 2001 through 2007)

A. Lesage
GEPI/UMR 8111, Observatoire de Paris, 92195 Meudon Cedex, France

SUMMARY

A critical review of the available experimental data on Stark widths and shifts for spectral lines of non-hydrogenic neutral atoms and positive ions has been carried out. The review covers the period from 2001 through the end of 2007 and represents a continuation of earlier critical reviews up to 2000. Data tables containing the selected experimental Stark broadening parameters are presented with estimated accuracy. Guidelines for the accuracy estimates, developed during the previous reviews, are summarized again. The data are arranged according to elements and spectra, and these are presented in alphabetical and numerical order, respectively. A total of 41 spectra are covered. Comparisons with comprehensive calculations based on semi-classical theory or on semi-empirical method are made whenever possible, since the comparison with theory has often been a principal motivation for the experiments.
The 2008 edition of "A Critical Review of Selected Data" continues the material already published in the Journal of Physical and Chemical Reference Data in 2002[1]. The data collected for the period from 2001 through end of 2007, has been evaluated and included in the present edition
The source of literature references has been the *Atomic Spectral Line Broadening Bibliographic Database*[2] and the data bases "BiblioPlanet ERLWebspir" of "l'Institut de l'Information Scientifique et Technique" (INIST).
This tabulation is a continuation of a series of critical reviews and tables on experimental Stark broadening data for spectral lines of non-hydrogenic atoms and ions which started in 1976[3,4] and continued in 1984[5,6], 1990[7] and 2002[1]
Generally, we have adhered to the format of the previous reviews, and we have subjected the data again to the same evaluation criteria as established earlier.
Our main source of literature references has been the master file[2] of the Data Center on Atomic Line Shapes and Shifts at the National Institute of Standards and Technology (formerly the National Bureau of Standards), the "Bibliography on Atomic Line Shapes and Shifts[8]" and the Digital Library for Physics and Astronomy[9] (ADS).
That issue of the critical review has been accepted in "New Astronomy Review". Improvements in the experimental methods will be underlined in the present contribution, as the astrophysical interest[10,11] of such Stark parameters measurements.

REFERENCES

[1]N. Konjević, A. Lesage, J. R. Fuhr, and W. L. Wiese, J. Phys. Chem. Ref. Data **31**, 819 (2002).
[2]J. R. Fuhr and H. R. Felrice, *Atomic Spectral Line Broadening Bibliographic Database*, http://physics.nist.gov/linebrbib. And J. R. Fuhr, A. Lesage, http://balss.obspm.fr/
[3]N. Konjević and J. R. Roberts, J. Phys. Chem. Ref. Data **5**, 209 (1976).
[4]N. Konjević and W. L. Wiese, J. Phys. Chem. Ref. Data **5**, 259 (1976).
[5]N. Konjević, M. S. Dimitrijević, and W. L. Wiese, J. Phys. Chem. Ref. Data **13**, 619 (1984).
[6]N. Konjević, M. S. Dimitrijević, and W. L. Wiese, J. Phys. Chem. Ref. Data **13**, 649 (1984).
[7]N. Konjević and W. L. Wiese, J. Phys. Chem. Ref. Data **19**, 1307 (1990).
[8]J. R. Fuhr, W. L. Wiese, and L. J. Roszman, *Bibliography on Atomic Line Shapes and Shifts*, Spec. Publ. 366 (1972); Suppl. 1 (1974); Suppl. 2 (1975) (with G. A. Martin and B. J. Specht); Suppl. 3 (1978) (with B. J. Miller and G. A. Martin); Suppl. 4 (1993) (with A. Lesage).
[9]Digital Library for Physics and Astronomy (ADS): http://adsabs.harvard.edu/
[10]A. Lesage, in Astrophysical Applications of Powerful New Databases, S. J. Adelman and W. L. Wiese, Editors. Astron. Soc. Pacific Conf. Ser., Vol. 78 (1994).
[11]M. S. Dimitrijević, T. Ryabchikova, Z. Simić, L. Č. Popović, and M. Dač, A & A **469**,681 (2007).

TUESDAY, 17 JUNE

Anomalous broadening of hydrogen Balmer lines in electrical gas discharges

N. Konjević and N. M. Šišović

Faculty of Physics, University of Belgrade, 11001 Belgrade, P.O. Box 368, Serbia

ABSTRACT

It is well known that in a low pressure gas discharges the electron temperature T_e is much larger than temperature of heavy particles T_{hp}, like molecules, atoms and their ions, i.e. $T_e >> T_{hp}$. This is the consequence of a small mass of the electron and its electric charge. It was shown in 1984, however, that excited hydrogen atoms with Doppler temperatures exceeding T_e more than two orders of magnitude exist in a low-pressure hollow cathode (HC) glow discharge (GD) operated with a hydrogen or with noble gas-hydrogen mixtures [1]. For the studies of this phenomenon, apart from various types HCGD, other low-pressure electric discharges were used as well. Fast excited hydrogen atoms moving towards and from the cathode are detected also in a plan- parallel electrode GD, Townsend discharge with plane parallel electrodes, plane cathode-hollow anode GD with different cathode materials in hydrogen and in hydrogen containing gas mixtures. The discharge was run with direct current or in radio frequency mode. In all these experiments high-energy excited hydrogen atoms with energies ranging from several tens up to several hundreds eV were detected by means of Doppler spectroscopy of the Balmer lines. Due to exceedingly large line broadening the name anomalous, excessive or excess Doppler broadening is used in relation to this phenomenon. Recently, group of authors detected anomalous broadening of the hydrogen H_α line in a microwave induced discharge but the findings of another experiment did not confirm this result. Comprehensive bibliography of anomalous broadening studies of hydrogen Balmer lines in gas discharges is reported in [2].

Similar hydrogen Balmer line shapes were detected in the edge region of plasma fusion devices. The reason for the similarities between discharge and fusion edge plasma indicates that the sheath potential at the edge close to limiter surface of fusion plasma plays the role of cathode sheath in some gas discharges, enabling similar collision processes of molecular ions in matrix gas. In spite of apparent similarities with tokamak or stelerator spectra, there are also important and significant differences between gas discharges and fusion plasmas where strong magnetic fields are present and therefore, In addition to Doppler broadening, the Zeeman splitting is superimposed as well.

According to so called "plasma sheath-collision model" [3-5] the explanation of an anomalously broadened part of hydrogen line profile is related to the hydrogen atomic and molecular ions (H^+, H_2^+ and H_3^+) present in discharge under the typical discharge conditions. In the cathode sheath region the accelerated ions exchange electric charge with hydrogen molecules and, as a result, fast neutrals and slow ions appear:

$$(H^+)_f + (H_2)_s \rightarrow H_f^* + (H_2^+)_s$$

$$(H_2^+)_f + (H_2)_s \rightarrow H_f^* + H_f + (H_2^+)_s$$

$$(H_3^+)_f + (H_2)_s \rightarrow H_f^* + (H_2)_f + (H_2^+)_s$$

where f and s denote fast and slow particles, respectively. It is shown that the particles (H^+, H_2^+ and H_3^+, H_2 and H) having energies of the order of magnitude of 10^2 eV are back scattered from cathode in the form of fast hydrogen atoms H [6]. The number and the energy of back-scattered atoms depends upon the cathode material, while their spatial distribution is proportional to $\cos\theta$, where θ is the angle in respect to the axis perpendicular to the cathode surface.

The main sources of fast excited hydrogen atoms are H^+ and H_3^+ ions (exhibit an asymmetrical charge-exchange reaction in collisions with H_2), which are, as a consequence of relatively low cross-sections for collisions, efficiently accelerated towards cathode. On their way to cathode, some of these ions collide with the matrix gas H_2, producing fast exited neutrals H^*. The rest of accelerated ions reach the cathode where they neutralize, or neutralize and fragmentize. The back-reflected particles from the cathode are fast H atoms directed back to discharge. After collisions of these fast H atoms with H_2 and/or with other discharge constituents, fast excited hydrogen atoms H^*, are produced also. Thus, the fast excited hydrogen atoms moving towards and from the cathode are detected in different discharges by means of Doppler spectroscopy of Balmer lines.

It should be pointed out that, apart from the anomalous broadening other broadening mechanisms exist and the shape of hydrogen Balmer line emitted from low pressure gas discharge exhibits multi-component behavior. The origin of

the narrowest and medium width part of line profile is related to the dissociative excitation and dissociative ionization with excitation, respectively. Both processes are induced by electron collision with hydrogen molecule.

This paper reviews research activity in the field of anomalous broadening of hydrogen Balmer lines in gas discharges operated with hydrogen isotopes and their mixtures with inert gases. The emphasis will be on recent studies of anomalous broadening and its potential for application.

REFERENCES

1. M. W. Benesh and E. Li, *Opt.Lett.* **9**, 338-340 (1984).
2. G. Lj. Majstorović, N. M. Šišović, N. Konjević, *Phys.Plasmas* **14**, 043504-9 (2007).
3. Z. Lj. Petrović, B. M. Jelenković and A. V. Phelps, *Phys.Rev.Lett.* **68**, 325-328 (1992).
4. S. B. Radovanov, K. Dzierzega, J. R. Roberts and J. K. Olthoff, *Appl.Phys.Lett.* **66**, 2637-2639 (1995).
5. M.R. Gemišić-Adamov, B. M. Obradović, M. M. Kuraica and N. Konjević, *IEEE Trans.Plasma Sci.* **31**, 444-454 (2003).
6. W. Eckstein, F. E. P. Matschke and H. Verbeek, *J.Nucl.Mater.* **63**, 199-204 (1976).

Slow and fast micro-field components in warm and dense hydrogen plasmas

A. Calisti*, S. Ferri*, C. Mossé*, B. Talin*, V. Lisitsa†, L. Bureyeva**, M.A. Gigosos‡, M.A. González‡, T. del Río Gaztelurrutia§ and J.W. Dufty¶

*PIIM, Université de Provence, CNRS, Centre Saint Jérôme, 13397 Marseille Cedex 20, France.
†Russian Research Center "Kurchatov Institute", Moscow, 123182, Russia.
**Institute of Spectroscopy, Troitsk, Moscow region 142190, Russia.
‡Departamento de Óptica y Física Aplicada, Facultad de Ciencias, Universidad de Valladolid, 47071 Valladolid, Spain.
§Escuela Superior de Ingenieros, Ald. Urquijo s/n 48013, Bilbao, Spain.
¶Department of Physics University of Florida, Gainesville, FL 32611

The study of the local stochastic electric fields at neutral or charged points in an homogeneous infinite plasma is of interest for several domains. For instance they can be used as external perturbations within semiclassical models designed to synthesize line spectra for diagnostic purposes [1, 2, 3, 4]. This work addresses the simpler problem of an hydrogen plasma and the analysis of the local field at neutral points.

The mass ratio between electrons and protons results in fields involving both fast and slow fluctuations characteristics. In order to analyze the statistical properties of these fields, a couple of components, a slow-fluctuation component (S) and a fast-fluctuation component (F) is introduced,

$$\mathbf{E}(t) = \mathbf{E}_e(t) + \mathbf{E}_i(t) = \mathbf{E}_{slow}(t) + \mathbf{E}_{fast}(t), \tag{1}$$

where $\mathbf{E}_e$ and $\mathbf{E}_i$ are the fields due to the electrons and ions, respectively, at an arbitrary neutral point. Our objective is to suggest a natural definition of the slow and fast components subject to the constraints 1) their sum must be the total field, 2) they must be statistically independent and then determine their statistical properties.

Years ago, S and F components have been defined in well known articles [5, 6] (BMHH). The present work exploits two component plasma molecular dynamics simulations (MD), [7], of a partially ionized hydrogen plasma.

Different plasma conditions have been considered corresponding to $\alpha = 0.8$, $\alpha = 0.6$ and $\alpha = 0.4$, where $\alpha = r_0/\lambda_D$ is the parameter introduced in BMHH. MD simulation provides a means of direct access to the local ion, electron and total fields at neutral hydrogen atoms. An example is shown on figure 1.

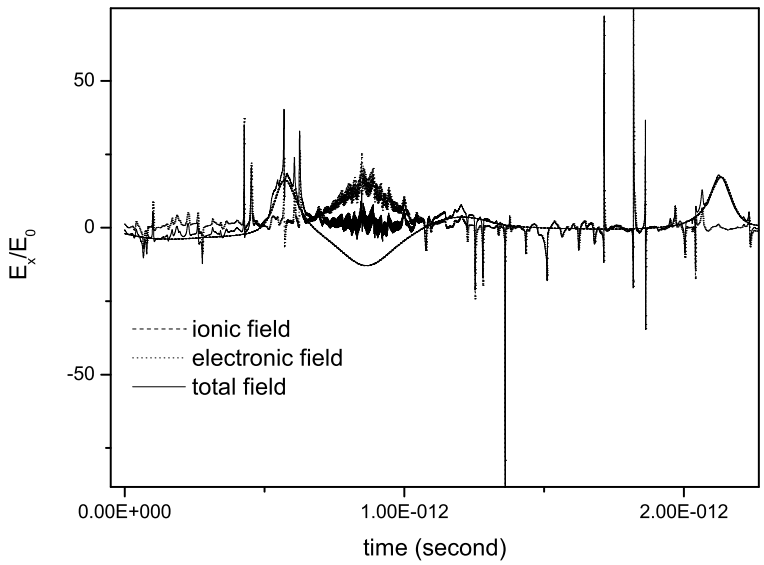

FIGURE 1. Example of electric field obtained by MD simulation for $\alpha = 0.8$

The results presented in this work, are based on the analysis of the stochastic fluctuations of sums and differences of the ionic and electronic local fields, $\mathbf{E}_i(t)$, $\mathbf{E}_e(t)$ and the time averaged electron field

$$\overline{\mathbf{E}_e(t)}_{\Delta t} = \frac{1}{\Delta t}\int_{-\Delta t/2}^{\Delta t/2} \mathbf{E}_e(t-t')dt'. \tag{2}$$

The mean electronic field, $\overline{\mathbf{E}_e(t)}_{\Delta t}$, calculated on variable periods of time, Δt, can be considered also as a simple measurement device, with variable response time, averaging out on the fast fluctuation of the total field due to the electrons. Accordingly, the slow component is defined as the slowly varying ion field plus the residual slowly varying mean electron field $\mathbf{E}_{S,\Delta t}(t) = \mathbf{E}_i(t) + \overline{\mathbf{E}_e(t)}_{\Delta t}$. The fast component is the remainder $\mathbf{E}_{F,\Delta t}(t) = \mathbf{E}(t) - \mathbf{E}_{S,\Delta t}(t) = \mathbf{E}_e(t) - \overline{\mathbf{E}_e(t)}_{\Delta t}$.
In Fig.2 three field correlation functions have been plotted on the same graph in units of τ_e (electronic characteristic time), for the case $\alpha = 0.8$.

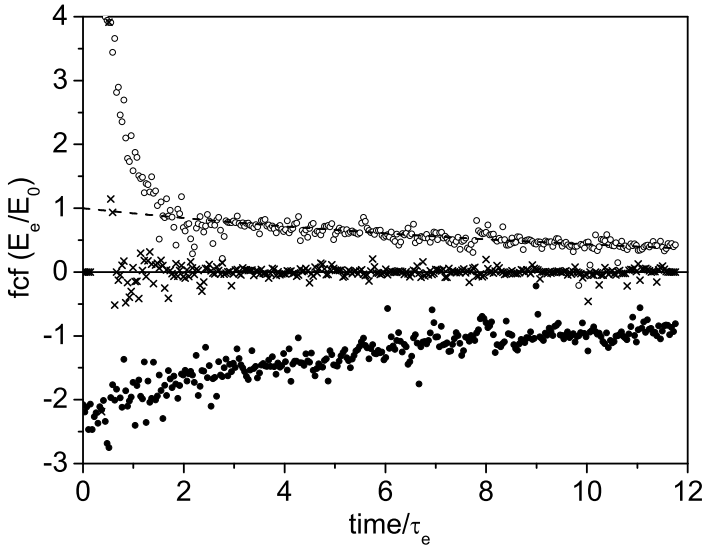

FIGURE 2. Field correlation functions for $\alpha = 0.8$: $\langle \mathbf{E}_e(0).\mathbf{E}_e(t)\rangle$, (circles); $\langle \mathbf{E}_{F,\Delta t}(0).\mathbf{E}_{F,\Delta t}(t)\rangle$ for $\Delta t = 0.4\tau_e$ (crosses); exponential fit (dash line); $\langle \mathbf{E}_i(0).\mathbf{E}_e(t)\rangle$, (black circles).

Clearly, in the framework of two component plasmas, the electron field appears inappropriate to represent the F component as the corresponding field correlation function manifestly shows a slow de-correlation due to electron-ion coupling mechanisms [8, 9], implying a statistical dependency between ion and electron fields. In contrast, the correlation of $\mathbf{E}_{F,\Delta t}(t)$ with $\Delta t = 0.4\tau_e$ is lost over a time $< \tau_e$. The definitions for the S and F components depend on Δt. It will be understood that the fast and slow characteristics of fields can get a more precise meaning by comparison to an additional time τ connected to some physical process, e.g., the relaxation of a plasma density fluctuation or the relaxation of an atomic radiation due to atom emitters imbedded in the plasma.

REFERENCES

1. H.R. Griem, *Spectral Line Broadening by Plasmas* (Academic Press, New York, 1974); H.R. Griem, *Principles of Plasma Spectroscopy*, (Cambridge University Press, 1997).
2. A. Brissaud and U. Frisch, *J. Quant. Spectroscp. Radiat. Transfer* **11**, 1767 (1971).
3. D.B. Boercker, C.A. Iglesias and J.W. Dufty, *Phys. Rev. A* **36**, 2254 (1987).
4. B. Talin, A. Calisti, L. Godbert, R. Stamm, R.W. Lee and L. Klein, *Phys. Rev. A* **51**, 1918 (1995).
5. M. Baranger and B. Mozer, *Phys. Rev.* **115**, 521 (1959); B. Mozer and M. Baranger, *Phys. Rev.* **118**, 626 (1960).
6. C.F. Hooper, Jr., *Phys. Rev.* **149**, 77 (1966); C.F. Hooper, Jr., *Phys. Rev.* **165**, 215 (1968).
7. A. Calisti, T. del Río Gaztelurrutia and B. Talin, *HEDP* **36**, (2007) 52.
8. B. Talin, et al. *J.Phys A: Math. Gen.* **36**, 6049(2003).
9. E. Stambulchick, D.V. Fisher, Y. Maron, H.R. Griem and S. Alexiou, *HEDP* **36**, (2007) 272.

Kinetic Theory for Electron Dynamics Near a Positive Ion

James W. Dufty and Jeffrey Wrighton

Department of Physics, University of Florida, Gainesville, FL 32611

The structure and dynamics of electrons near a positive ion of charge number Z is important for both center of mass motion (transport, stopping power) and spectroscopy (line broadening). A semi-classical description is considered using regularized electron - ion interactions. A formally exact kinetic theory for electron correlations near the ion is approximated by its exact form in the short time limit. The resulting Markov kinetic equation is solved in terms of an effective mean field single particle dynamics and dynamical screening by in an inhomogeneous electron gas random phase approximation with "local field corrections". Practical applications are illustrated by calculating the Z dependence of the electric field autocorrelation function, and showing its dependence on bound and free electron configurations. The results here generalize recent studies [1, 2] to strong electron coupling and a wide range of correlation functions.

REFERENCES

1. J. W. Dufty, I. Pogorelov, B. Talin, and A. Calisti, *J. Phys. A* **36**, 6057-6062 (2003).
2. B. Talin, A. Calisti, J. Dufty, and I. Pogorelov, *Phys. Rev. E (in press)*; cond-mat/0402023.

Advanced X-ray Spectroscopy of Hot Dense Plasmas: Signature of Laser-Induced Electric Fields

O. Renner[*], E. Dalimier[†], C. Riconda[†], F.B. Rosmej[†], S. Weber[†‡], O. Peyrusse[‡], P. Sauvan[§], I. Uschmann[||], S. Höfer[||], T. Kämpfer[||], R. Lötzsch[||], U. Zastrau[||], E. Förster[||] and E. Oks[¶]

[*]*Institute of Physics, Academy of Sciences CR, Na Slovance 2, 18221 Prague, Czech Republic*

[†]*Physique Atomique dans les Plasmas Denses, LULI, UMR 7605, CNRS-CEA-École Polytechnique-Université Paris 6, 4 Place Jussieu, 75252 Paris Cedex 05, France*

[‡]*CELIA Université Bordeaux - CEA, 33405 Talence, France*

[§]*Dept. de Ingeniería Energética – UNED, 28040 Madrid, Spain*

[||]*Institut für Optik und Quantenelektronik, Friedrich-Schiller-Universität, 07743 Jena, Germany*

[¶]*Physics Department, 206 Allison Laboratory, Auburn University, Auburn, AL 36849, USA*

High-resolution x-ray spectroscopy is capable of providing complex information on environmental conditions in hot dense plasmas. Benefiting from application of modern spectroscopic methods, we report experiments aiming at identification of different phenomena occurring in laser-produced plasma. Fine features observed in broadened profiles of the emitted x-ray lines and their satellite structures are interpreted using two-dimensional simulations of the plasma evolution and theoretical models predicting spectra modification under diverse experimental situations.

DIAGNOSTIC POTENTIAL OF HIGH-RESOLUTION X-RAY SPECTRA

Diagnostic applications of x-ray spectroscopy [1] provide comprehensive information on environmental conditions and processes accompanying creation and evolution of moderately or strongly coupled plasmas. The standard diagnostic methods profit from relatively simple atomic models describing the spectra that arise from transitions into K-shells [2]. In addition to the widespread investigation of the macroscopic plasma parameters (density, temperature, ion velocity and charge state distribution) based on intensity ratios and widths of the emitted resonance lines, a diagnostic potential contained in precisely measured spectral line profiles (their frequency shifts, detailed shapes, and accompanying satellite structure) provides complementary information on phenomena occurring in hot dense plasma.

The role of dielectronic satellites in spectroscopic diagnosis of laser produced plasmas has been analyzed, e.g., in a review paper [3] where various plasma processes were correlated with different channels for the satellite excitation and decay. Here we report three different experiments in which the high-resolution investigation of the satellite-rich emission spectra was of paramount importance. To elucidate the used experimental approaches, first we provide a brief survey of advanced spectroscopic methods and define their limits. Then we interpret precise spectroscopic data in terms of exchange energy shifts in dense plasmas, ion collisions and trapping at laser-irradiated double-foil targets, and appearance of electric-field-induced satellites in the x-ray line profiles.

SPECTROSCOPIC PRINCIPLES AND EXPERIMENTAL LIMITS

High-resolution x-ray spectroscopic methods of the plasma diagnosis are mostly based on crystal analyzers. We briefly discuss the basic principles applied in a design of advanced spectroscopic schemes [4] and derive the main characteristics of the instruments used in the reported experiments (the vertical-geometry Johann spectrometer with the cylindrically bent crystal, the spherically bent crystal spectrometer with the out-of-Rowland circle position providing 2D images of the plasma sources, and the toroidally bent crystal spectrometer). In the same time, we present practical conclusions concerning the attainable spectral ($\lambda/\Delta\lambda \sim 10^3$-$10^4$) and spatial (<10 μm) resolution, collection efficiency, precision of the intensity measurements, reliability and reproducibility of the spectral records.

SELECTED APPLICATIONS

The first reported experiment concerns identification of the density- and temperature-dependent spectral line shifts in emission of Al Heα group from constrained-flow laser produced plasma [5]. The high-dispersion time-integrated spectra covering the resonance and intercombination lines were collected at the LULI ns-laser. The complex spectral profiles modified by the satellite formation, line broadening, and frequency shifts were decomposed into individual pseudo–Voigt components by using a problem–dependent genetic algorithm. We have demonstrated that the rigorous spectra fitting must be based on anticipatory theoretical knowledge of the dielectronic satellite structure. Assuming the aggregate plasma–induced shift of the parent lines and their satellites, the analysis of the spectral profiles

revealed systematic red shifts of the resonance and the intercombination lines comparable with predictions of the atomic data and spectral line shape codes. Differential shifts of these lines result in small variations of the exchange energy (EE), i.e. the separation between the singlet and triplet energy levels. The trends in the observed density-dependent decline of the EE agree with theoretical predictions, its magnitude is, however, by one order of magnitude larger than predicted. Conclusive verification of this effect requires further experiments with higher-density plasmas.

The second experiment performed at the PALS laser was dedicated to the investigation of plasma clouds collisions and ion trapping at laser-irradiated double-foil targets [6]. Colliding plasmas produced at single–side irradiated Al/Mg targets represent a well–defined model environment for studying the plasma wall interactions. The front Al foil burns through before the laser pulse maximum, thus the forward–accelerated Al ions are not trapped by the cold Mg foil but collide with the Mg plasma. The complex dielectronic satellite–rich structure observed in emission spectra of the Al Lyα group is discussed in terms of interaction of counter–propagating plasmas, in particular trapping, deceleration and thermalization of the Al ions close to the Mg foil. The qualitative analysis of the observed spectra is supported by the 2D hydrodynamic modelling of the expanding plasma. Prospective use of the J–satellite line shifts in diagnosis of colliding plasmas is envisaged.

The last reported experiment bears on rather controversial topics, namely demonstration of the presence and unambiguous interpretation of electric-field-induced satellites in x-ray lines emitted from hot dense plasmas. The single-frequency electric fields associated with electron plasma waves (Langmuir oscillations) or externally introduced (laser) fields may substantially modify the energy level population and result in an appearance of local extremes (dips and peaks, so-called plasma or laser satellites) in spectral line profiles [7]. Recent experiments [8, 9] performed with the single laser beam irradiated gas-jet and solid targets revealed line shapes with regular intensity modulations ascribed to different parametric driven instabilities. In experiments realized at the IOQ Ti:sapphire laser JETI (1.2 J, 800 nm, 12.5 ps), the laser beam was split into two beams: the first beam introduced to the interaction chamber (5×10^{15} W/cm^2) was focused to a flat tip of the roof-shaped Al target thus creating the expanding plasma, the second temporally synchronized beam (1.1×10^{16} W/cm^2) was hitting the plasma transversally. The plasma emission was observed using the toroidally bent crystal spectrometer combined with the CCD camera. The spectra were taken in single shots, the spectral range covered was sufficient to study the full profile of the Al Heβ emission. The perturbing external electric fields modifying the plasma environment in the vicinity of radiators were varied by changing the time delay between both beams (30-80 ps) and the distance above the target where the transversal beam hit the plasma. The recorded spectra display distinct modulations due to the action of the perturbing beam; the line profiles vary with the delay of both laser beams and with the distance above the irradiated target. The interpretation of these modulations was based on extensive plasma and atomic simulations. The temporal distribution of the plasma parameters was modeled by 1D and 2D hydrodynamic codes. The transverse electric field strength distribution was derived from kinetic simulations using the 1D PIC code. Finally the detailed spectral line profiles were synthesized using the nonperturbative Floquet treatment of the external oscillating field previously suggested for hydrogenic ions [10]. Using this approach, a very good fit between the experimental results and synthetic spectra has been achieved. Practical conclusions following from these experiments and their theoretic interpretation are discussed.

ACKNOWLEDGEMENTS

A substantial part of this research was performed within the Access to Research Infrastructures Activity, 6th Framework Programme of the EU (contract RII3-CT-2003-506350, LASERLAB Europe), and partially funded by the Czech Science Foundation under grant No. 202/06/0801. The authors gratefully acknowledge the assistance of scientific and technical staffs from LULI, IOP and IOQ (in particular, B. Beleites and F. Ronneberger) in performing the experiments. The primary author acknowledges a support provided within the frame of his Visiting Scientist position at the École Polytechnique and his Invited Professor position at the Université Pierre et Marie Curie.

REFERENCES

1. H.R. Griem, *Principles of plasma spectroscopy*, Cambridge University Press, Cambridge, 1997.
2. H.-K. Chung et al, *High Energy Density Physics* **1**, 3-12 (2005).
3. F.B. Rosmej et al, *Proc. SPIE* **5196**, 163-176 (2004).
4. O. Renner, I. Uschmann and E. Förster, *Laser Part. Beams* **22**, 25-28 (2004).
5. O. Renner et al, *J. Quant. Spectr. Rad. Transfer* **99**, 523-536 (2006).
6. O. Renner et al, *High Energy Density Physics* **3**, 211-217 (2007).
7. E. Oks, *Plasma Spectroscopy: The Influence of Microwave and Laser Fields*, Springer, Berlin, 1995.
8. V.P. Gavrilenko et al, *Phys. Rev. A* **73**, 013203 (2006).
9. N.C. Woolsey et al, *High Energy Density Physics* **3**, 292-296 (2007).
10. O. Peyrusse, *Physica Scripta* **56**, 371-380 (1997).

Contour shape analysis of hollow ion x-ray emission

F. Rosmej[*,†], P. Angelo[*,†] and Y. Aoaud[*]

[*]*Université Pierre et Marie Curie, LULI-PAPD, UMR 7605, case 128, 4 Place Jussieu, 75252 Paris Cedex 05, France*
[†]*Ecole Polytechnique, Laboratoire pour l'Utilisation des Lasers Intenses, "Physique Atomique dans les Plasmas Denses", 91128 Palaiseau Cedex, France*

Hollow ion emission (e.g. $K^0L^N \rightarrow K^1L^{N-1} + h\nu_x$) has been of great interest for atomic physics research and interaction experiments of ion beams with surfaces and clusters have been performed to provoke their x-ray emission under low density conditions [1, 2, 3]. More than about 2 decades later, HI emission has been observed in a Mega-Ampère Z-pinch [4] and also in a few visible and IR laser produced plasmas [5, 6].
Although at present HI emission in dense plasmas is still a rare observation, their emission is of fundamental interest because of their outstanding properties: low opacity even in super-dense plasmas, extremely short emission (some 10 fs) to probe high density signatures only [7, 8]. However, their large intensities as observed in dense laser produced plasmas are still not explained in a satisfactory manner and ab initio simulations show order of magnitudes discrepancies. We begin the study of hollow ions with the analysis of their line width and line intensities. Under real experimental conditions, the contour shape of a certain configuration (e.g. $K^0L^3 \rightarrow K^1L^2 + h\nu_x$) depends not only on the Stark effect but also on the precision of the line center position and the number of levels incorporated in the simulations. First simulations of the hollow ion x-ray contour shapes are presented. The implications for atomic physics research, atomic kinetics, diagnostics and dense laser produced plasma experiments with free electron x-ray lasers will be given.

REFERENCES

1. I. A. Armour et al., *J. Phys. B: At. Mol. Opt. Phys.* **13**, 2701 (1980).
2. J.-P. Briand et al., *Phys. Rev. Lett.* **65**, 159 (1990).
3. S. Martin et al., *Phys. Rev. A* **57**, 4518 (1998).
4. F. Rosmej et al., *Nuc. Instrum. Methods A* **464**, 257 (2001).
5. A. Ya. Faenov et al., *Physica Scripta* **T80**, 536 (1999).
6. J. Abdallah et al., *Quantum Electronics* **30**, 694 (2000).
7. F. B. Rosmej and R .W. Lee, *Europhys. Lett.* **77**, 24001 (2007).
8. F. B. Rosmej, R .W. Lee and D. H. G. Schneider, *High Energy Density Phys.* **3**, 218 (2007).

Laser Satellites: a New Method for Diagnosing both the Laser Fields and Opacities

Eugene Oks

Physics Dept., 206 Allison Lab., Auburn University, Auburn AL 36849, USA

The topic "Laser-induced satellites" is currently experiencing a surge of interest because new, more precise experiments are ongoing in several experimental groups. The primary challenge in the theoretical interpretation of these experimental results is the following. There is an interplay of the laser field and of the opacity in such a way that one and the same experimental spectrum could correspond to different pairs of the laser field and of the opacity.

We present a method to uniquely determine both the laser field and the opacity from the experimental spectrum.

Experimental characterization of the asymmetry and the dip form of the H_β-line profiles in microwave-produced plasmas at atmospheric pressure

J M Palomares[1], J Torres[1], M A Gigosos[2], J J A M van der Mullen[3], A Gamero[1] and A Sola[1(*)]

[1]*Departamento de Física, Universidad de Córdoba. 14071 Córdoba, Spain.*
[2]*Departamento de Óptica, Universidad de Valladolid. 47071 Valladolid, Spain.*
[3]*Department of Applied Physics, Eindhoven University of Technology. P.O. Box 513. 5600 MD Eindhoven, The Netherlands.*

(*)*fa1sodia@uco.es*

An experimental study on the asymmetry of the Balmer H_β profile in plasmas produced by microwaves at atmospheric pressure is presented. The study is based on the definition of several functions that quantify the asymmetry aspects of the profile. The study shows the experimental dependence of these characteristics on the electron density and control parameters such as the gas flow and the hydrogen admixture ratio. The possible use of these newly introduced profile characteristics to plasma diagnosis is discussed.

The broadening, shifts and deformations of spectral lines emitted by plasmas have been widely studied in the past [1-4], but since many aspects of this field of plasma spectroscopy are still not fully understood, many investigators continue with performing experiments and/or developing computer models of line shapes. The spectral line studied most extensively in the past is the H_β line of the hydrogen Balmer series especially in relation with its function in plasma diagnosis. The width of the H_β line is a rather well-known function of the electron density and only weakly depends on the electron temperature. However, apart from the line width H_β has several other features that can globally be divided in its asymmetry and the presence of a central dip. These features have been and continue to be studied and measured by various groups [3-5]. Most of the experimental and theoretical studies on the asymmetry of the hydrogen spectral lines has been made up for plasmas with electron densities equal or higher than 10^{23} m^{-3} [6-8] for which one expects this asymmetry to be appreciable. The objective of this work is the study and characterization of the Stark asymmetry and dip formation of the line H_β at lower electron densities, *i.e.* in the order of 10^{21} m^{-3}, and to investigate whether the behaviour of the asymmetry and dip-formation follows a tendency that is consistent with the plasma characteristics. This could point towards new possibilities for plasma diagnosis and might give guidelines for the future theory formation.

The reasons behind the asymmetry and dip formation are not well studied yet. Up to date, the most efficient Stark-broadening models in plasmas have been developed with the help of micro-field theories (or micro-field model methods, *MMM*), either by means of theoretical calculations or by means of computer simulations. But, from the first broadening theories of spectral lines until the modern models that include the effect of the ion dynamics, only the terms of first order in the perturbing electric field have been taken into account. As a result the linear Stark effect, - with or without ion dynamics -, only generates symmetric profiles without shift. Therefore, to be able to generate profiles that include the aforementioned asymmetry as well as the central-wavelength shift, it is necessary to include terms of higher orders in the calculations.

The mechanisms that might be capable to explain the appearance of the asymmetry and shift of spectral lines are: the quadrupolar effect in the ion-emitter interaction that generates in-homogeneities or gradients in the field, the quadratic Stark effect that produces the mixture or quenching of atomic levels with different principal quantum numbers, the inclusion in the calculations of the fine structure and the correlation effects among ions. But not all these effects have the same importance: they depend differently on the plasma conditions and seem not to have the same influence on the shift of the line and its asymmetry. Different measurements and theoretical calculations on the H_β line shift can be found in J Halenka *et al* [9] and Z Mijatovic *et al* [10].

At present, there is no complete model available that fully describes the asymmetry in the profiles as a function of the electron density and temperature. But it is possible to find some studies in which calculations and partial corrections on the current theories of the Stark broadening are carried out,

where the asymmetry for some concrete profiles is obtained. We can highlight in this sense the works of S Djurovic *et al* [5], S Sörge *et al* [8], C Stehle *et al* [11] and Halenka *et al* [12]. The improvement of these models is going on at the moment and new detailed experimental data might contribute to the further development of broadening models.

This experimental study is intended to get more detailed information on the asymmetry on the *H*-beta profile and the dip formation. In that way we might give support to future theory formation. The study will be guided by the introduction and the study of seven functions that quantify the asymmetry and the dip-form. Three of these functions are used to study the flanks of the profile, including the wings; the other four are constructed to study the inner part of the profile, *i.e.* the central valley or the upper region where the dip is situated in between two peaks (it is normal to term the whole central valley as *dip* as well). The performance of these functions will be investigated by employing them to various profiles as obtained in several experimental conditions. These are obtained by changing the gas flux and the hydrogen admixture ratio. It will be shown that five of the seven spectral form-functions vary smoothly with the electron density. The two functions that describe the asymmetry of the dip show much scattering in their dependence on the electron densities. This points to the effect of the small fluctuations caused by the plasma turbulences and instabilities.

The asymmetry of the H_β line has been described in several studies (a good and early example is that of Wiese [3]) in a qualitative way, and most of the studies report that the *blue peak is higher than the red one*, while *the red wing is higher than the blue one*. Moreover, it is generally accepted that the asymmetry of the profile becomes higher when the electron density is increased. To make the asymmetry in the profile quantitative, relevant definitions of line aspects have to be introduced. The *FWHM* is used in this study to determine the average electron density of the observed plasma part, which is widely accepted in plasma diagnosis.

As conclusions, this asymmetry shows a dependence on the electron density and the flux of gases in the discharge that in general follows clear tendencies, and it has been studied with the help of some asymmetry functions for the flanks of the profile, including the wings. It has been shown how the asymmetry of the profiles increases with the electron density in the discharge, which is coherent with the known behavior for the studied line. With respect to the gas flux influence, a decreasing of the asymmetry is detected in the central part of the profile when the gas flux is lowered. At gas flux low enough, strange or anomalous values of the asymmetry have been detected for which the red side of the profile is more intense than the blue one, contrary to that happens habitually. For the central part of the profile, the so-called central valley or dip, specific functions charactering its shape have been used. The spectral distance between peaks, *FWPP*, and the dip depth, *DD*, exhibit a clear and bare increasing (quasi-linear) dependence on the electron density, less pronounced at a higher flux of gas, which is valued as a coherent tendency. The other two functions comparing the red and blue sides of the profile, *i.e.* the difference of intensity between peaks, *PID*, and the spectral position of the dip, *DP*, are seriously affected by the fluctuations in the plasma, although they follow some kind of decreasing dependence on the electron density at values slightly lower when the gas flux decreases. In some cases, when the gas flux drops enough, it can end up inverting the normal tendency of the profile asymmetry, giving rise to the so-called anomalous asymmetry in which the blue peak of the H_β is less intense than the red one.

1. HR Griem 1974 *"Spectral line broadening by plasmas"* Academic Press Inc. (New York, US); Griem HR 1997 *"Principles of plasma spectroscopy"* Cambridge University Press (Cambridge, UK).
2. M Miller 1987 "*Inductively Coupled Plasmas in Analytical Spectrometry*" VCH (New York, US).
3. WL Wiese, DR Paquette and DE Kelleher 1972 *Phys. Rev. A* **6**, 1132.
4. WL Wiese, DE Kelleher, V Helbig 1975 *Phys. Rev. A* **11**, 1854.
5. S Djurovic, D Nikolic, I Savic, S Sörge, A Demura. 2005 *Physical Review E* **71**, 036407.
6. K Grutzmacher 1978 *Phys. Rev. A* **18**, 2140
7. Olchawa W, 2002 *J. Quant. Spectros. Rad. Transfer* **74**, 417.
8. S Sörge and S Gunter 2000 *Eur. Phys. Journal D* **12**, 369.
9. J Halenka, B Vujicic and S Djurovic 1989 *J. Quant. Spectros. Rad. Transfer* **42**, 571.
10. Z Mijatovic, M Pavlov and S Djurovic 1991 *Phys. Rev. A* **43**, 6095.
11. C Stehle, D Gilles and A Demura 2000 *Eur. Phys. Journal D* **12**, 355.
12. J Halenka, 1990 *Zeitschrift Fur Physik D - Atoms Molecules And Clusters* **16**, 1.

Diagnostics for ITER

A.J.H. Donné[a], R. Barnsley[b] and M.G. von Hellermann[a]

[a] *FOM-Institute for Plasma Physics Rijnhuizen, Association Euratom-FOM, www.rijnhuizen.nl*
Partner in ITER-NL, PO Box 1207, 3430 BE Nieuwegein, The Netherlands

[b] *ITER International Organization, Cadarache Centre, 13108 St Paul-Les-Durance, France*

Abstract. After an introduction into the specific challenges in the field of diagnostics for ITER (specifically high level of nuclear radiation, long pulses, high fluxes of particles to plasma facing components, need for reliability and robustness), an overview will be given of the spectroscopic diagnostics foreseen for ITER. The paper will describe both active neutral-beam based diagnostics as well as passive spectroscopic diagnostics operating in the visible, ultra-violet and x-ray spectral regions.

Keywords: Plasma diagnostics, spectroscopy, fusion, ITER
PACS: 52.70.-m, 52.70.Kz, 52.55.Fa, 28.52.-s

INTRODUCTION

The development of diagnostics for ITER is a major challenge. This is because the measurement requirements are in general the same or more stringent than on present day devices while the environment in which the diagnostics have to be implemented is much harsher. Moreover, in view of the key role of many measurements in the real-time control of the plasma, a high level of reliability and robustness is required.

Implementation of existing diagnostic techniques requires substantial design and in some cases dedicated R&D. Moreover, some plasma parameters cannot be measured by existing techniques under ITER conditions and new techniques are required. The starting point in the development of the diagnostics for ITER is to identify and develop the requirements and their justifications for the large range of measurements. After this, the appropriate diagnostic techniques can be selected, and their implementation on ITER can be developed, including integration with other machine and/or diagnostic components.[1]

In this paper a brief overview of the diagnostic challenges for ITER will be given, followed by an overview of the spectroscopic techniques. Firstly, the use of diagnostics for machine protection and basic plasma control, advanced plasma control and for physics evaluation will be illustrated along with the associated measurement requirements. Secondly, the specific environmental effects in ITER will be introduced. These are amongst others related to:

- the high neutron- and gamma flux and fluences which lead to radiation induced effects in electrical and optical components as well as to nuclear heating;
- the high particle fluxes (e.g. from recombination) on front-end diagnostic components (in particular mirrors) which lead to erosion and re-deposition;
- the long pulse lengths, which demands high reliability of the diagnostics;
- the specific properties of ITER being a nuclear device, which complicates maintenance. Diagnostics should be robust and designed to survive the full ITER life cycle;
- the limited number of diagnostic ports, which necessitates integration of multiple diagnostics in a single port plug.

Most spectroscopic systems have the technical advantage that signals from a large number of optical observation lines can be fed to high resolution spectrometers placed outside the biological wall by means of only a limited number of optical components. The critical element in every optical diagnostic is the plasma facing mirror – i.e. the mirror close to the plasma. The survival of this “first mirror” is a common critical concern for all optical diagnostics.[2] The situation is most severe for diagnostics having channels viewing up from the divertor cassettes. Intensive studies on reflectivity changes due to coating effects by deposition, sputtering of layers by erosion and also active schemes including shutters and on-line calibration techniques are currently being explored.

ACTIVE SPECTROSCOPY

ITER will be equipped with two active beam spectroscopic diagnostic.[3] The first of these: *Charge Exchange Recombination Spectroscopy* (CXRS) is based on a powerful diagnostic neutral beam (H^0 or D^0), that is sufficiently energetic to allow penetration into the plasma centre. The diagnostic neutral beam (DNB) of 100 keV/amu and with a power of 3.6 MW will be injected radially into the plasma.[4] Charge capture between neutral particles from the beam and fully stripped plasma ions such as He^{2+}, C^{6+} or Be^{4+} will lead to excitation of charge exchange emission lines in the visible spectral range. In ITER two observation ports are envisaged, incorporating in total three periscope systems viewing the DNB. Each periscope features a fan of observation lines for highly localized measurements along the outer minor radius of the ITER plasma, that will be imaged onto multi-species spectrometers tuned to characteristic wavelength regimes covering the main ion species in the plasma.

Modeling studies (c.f. ref. [5]) have demonstrated that the CXRS diagnostic will provide a feasible solution for ITER, promising adequate radial resolution and the means of measuring ion temperatures, plasma rotation, and the densities of the main intrinsic impurity ions as well as the density of the bulk ions. The top priority for the CXRS diagnostic is the direct measurement of thermal helium ash densities. Ion temperatures measured by CXRS in ITER will rely on the evaluation of the CVI charge exchange spectrum,[6] where carbon is an intrinsic impurity with concentrations of the order of 1% of the electron density. Spectral signal-to-noise numbers in excess of 30 are expected even close to the magnetic axis with a local electron density of 10^{20} m^{-3}. Feasibility and conceptual design studies for ITER have shown that the use of high throughput optics, "vertical" observation of the beam and optimisation of the detection system will result in typical signal to noise ratios of the order of 10 or higher for helium, beryllium, carbon (as well as deuterium or tritium).[7]

Beam Emission Spectroscopy (BES) will be used in combination with CXRS on the DNB and enables the deduction of absolute ion densities of the main low-Z contaminants (He, Be, C) in their fully ionized states, from measured line-intensity ratios.[8] The measurement is based on determining the intensity ratio between lines emitted by the plasma impurities as a result of charge exchange processes and lines emitted by the beam atoms as a result of electron impact excitation. BES and CXRS use exactly the same in-port front-end optics, but different spectrometers to focus on different parts of the spectrum. The ITER geometry and the concept of the combined BES/CXRS system is presently being tested in a pilot experiment at TEXTOR. [9]

Another active spectroscopy diagnostic is the *Motional Stark Effect* (MSE) system, based on a measurement of the orientation of one of the Stark components in the Balmer-alpha spectrum emitted by high-velocity neutral beam particles passing transversely through the magnetic field. Two schemes for MSE are currently used. One is the 'conventional' active polarization measurement of the linearly polarised σ or π components, and the other is a spectroscopy measurement of the full D_α spectrum. Active polarization methods make use of photo-elastic modulators followed by high étendue interference filters and fiber links. The signal evaluation at the modulation frequency and its harmonics yields the local pitch angle of the magnetic field. In ITER, in principle both the proposed heating neutral beams (HNB) and also the dedicated diagnostic neutral beam (DNB) can be exploited as source for a MSE diagnostic. MSE on the HNB has the advantage of a good plasma core penetration, of passing very close to the magnetic axis, and to be continuous, but it will only work in neutral beam heated plasmas. MSE on the DNB is limited by a maximum duty cycle of the order 25% but is available in all plasma scenarios.

To minimize the neutron flux escaping from the ITER device via the MSE viewing periscope, it is necessary to use at least four mirrors. Because reflections on mirrors are known to alter the initial polarization, it is necessary to prove that MSE measurements can still be done with a high accuracy.[10]This problem is further amplified by the presence of layers of deposits on especially the first mirror. To cope with these effects, in-situ calibrations have to be integrated in the design of the diagnostic, and real time check-up techniques (as the simultaneous measurement of σ and π lines) are envisaged.[11]

Active spectroscopy for the divertor, in the form of *Laser-induced fluorescence*, has also been proposed for ITER to measure concentrations (and temperatures) of impurities in the divertor.[12] Based on a tuneable, narrow band laser, the system would primarily be devoted to measurement of neutral helium (but other populations such as Ar^{1+} are also being suggested). The approach considered in more detail so far is based on a 4-level scheme in the He I triplet system, which would certainly be representative of the population of the metastable state $2\ ^3S$. Uncertainties remain however about the ability to make firm deductions about the total helium population in a medium where several local parameters will remain unknown or poorly known (e.g. densities of some neutral populations) and where transit times of neutral atoms across a narrow plasma layer might be comparable to their lifetimes in some metastable states.

PASSIVE SPECTROSCOPIC TECHNIQUES

Impurities are intrinsically produced in the plasma as fusion reaction (helium) ash, they can be generated by plasma wall interaction on the solid surfaces surrounding the discharge, or they can be injected or puffed into the plasma for performance optimisation or diagnostic purposes. Expected impurities include a wide range of elements with nuclear charge, Z, ranging from above 70 (as tungsten will probably be used as a constituent material of plasma facing components) and down to 1 (as the mass-1 isotope of hydrogen is a fusion product that cannot be considered as "fuel"). Impurities play an important role in all regions of the tokamak from the core plasma to the scrape-off layer and the divertor plasma. Measurements of their concentration, ionisation and kinetic state in the discharge can be performed by spectroscopy of the continuum and line radiation, in a wavelength domain ranging approximately from 0.05 to 1000 nm.

The ratio of the Z=1 contaminant, ^{1}H, to that of deuterium and tritium in ITER will be measured at the plasma periphery by *H_α spectroscopy*. This diagnostic will supply local values of the influxes of the three hydrogenic isotopes. Because these sources are asymmetric, the ITER monitoring system is proposed to have several viewing fans with multiple lines of sight aiming at different positions at the periphery of the main plasma.[13]

The effective ion charge, Z_{eff}, is usually derived from *observations of visible continuum emission* by filter arrays observing in a narrow spectral range (about $\lambda = 523$ nm)[14] that is free from spectroscopic line emission. Additionally, it is proposed to use a few other spectral intervals and also at least a limited number of spatial channels featuring a good spectral resolution to confirm that the wavelength intervals used are indeed free of line emission.

Much design effort is focused on two classes of vacuum-coupled systems: *vacuum ultraviolet (VUV) spectroscopic diagnostics*, mainly using gratings as dispersing elements, and arrays of *X-ray crystal spectrometers*. The detection and monitoring of core impurities requires medium-resolution spectroscopy over a broad band between about 0.1 nm and 160 nm.[15] In the VUV wavelength region, the use of vacuum windows is not practical. Therefore, these systems will need to be themselves extensions of the plasma main chamber vacuum and be included in the ITER tritium circuit. Shielding of detectors and matching of the spectrometer apertures with the divergence of the light beams can be incorporated by employing focusing mirrors under a grazing angle. Beam partitioning and multiplexing between VUV instruments in a tritium-compatible vacuum system covering different ranges and/or with different spectral resolving power will be achieved with various kinds of reflectors, as demonstrated during recent trace tritium experiments in JET.[16] A 6-channel system covering the spectrum between 2.3 nm and 160 nm is proposed for impurity monitoring in the main plasma of ITER. Additionally an imaging VUV spectrometer has been designed, to view the outer plasma from an upper port for profile reconstruction in the edge and scrape-off layer (SOL).

X-ray crystal spectrometers, with high sensitivity and stable calibration, are used to monitor lines and the associated continuum of the soft X-ray spectrum between 0.1 nm and 10 nm, which contains strong $\Delta n=1$ transitions of all impurities with $Z \geq 4$ (Be). Photon-counting, energy-resolving detectors can provide excellent signal-to-noise ratios. Multi-channel systems exploring the plasma with several neighboring lines of sight[17] and/or imaging systems[18,19] employing position-sensitive detectors are proposed to deliver spatially and spectrally resolved information on line radiation from He- and/or H-like states of the various impurities. This information can be tomographically processed to reconstruct the one-dimensionally space-resolved emission (as well as ion temperature and toroidal velocity) profiles and hence the concentration of the emitting impurities.

The observation of the divertor with its complex geometry with absolutely calibrated spectrally resolving instruments is a particularly challenging task. An *ITER divertor impurity monitor*[20] is proposed featuring many sight lines from the upper and equatorial ports as well as from a divertor port. Filter spectrometers (with about 300 spatial channels each) are foreseen to monitor 12 emission lines, while low- and high-resolution spectrometers will supply information on influxes, localisation (e.g. ionisation fronts) radiation, ionisation state and temperature of impurities and of fuel components.

High-resolution x-ray crystal spectroscopy of impurities is foreseen in ITER for Doppler measurements of T_i, v_{tor} and v_{pol}, and the line-ratio measurement of T_e. Thanks to recent advances in fast, 2D x-ray solid-state[21] and gas-filled[22] detectors, it is possible to develop space-resolving high-resolution x-ray crystal spectrometers (cf. ref. [23]), such that radially-resolved Doppler measurements from such instruments can be expected to become routine. The present design for ITER is based on this recent progress.[24] The plasma radial profile is viewed by several imaging crystal spectrometers shared between an equatorial and an upper port. The plasma between $\sim 0.75 < r/a < 0.9$ cannot be viewed directly with the present ITER port design, and is accessed via graphite reflectors. To maximize reliability, maintainability and upgradeability, the incorporation of any components inside the port-plugs has been as much as possible avoided. Detector background measurements obtained during D-T experiments at JET

indicate that solid-state gas-filled and micro-channel plate detectors can be adequately shielded from the background radiation expected behind the port plug.[25] Detailed modeling calculations have pointed to helium-like Krypton as the prime candidate for core Doppler spectroscopy on ITER, due to its almost ideal ionization balance and ease of injection. The ITER system will be designed primarily for Kr, but is also able to observe Fe with better signal-to-noise ratio. The He-like Kr and H-like Fe ionization stages are suitable for Doppler spectroscopy in the core, while He-like Fe and H-like Ar are more suited for observing the outer plasma. The ITER measurement requirements can broadly be met with impurity concentrations of $\sim 10^{-5} n_e$, corresponding to an incremental radiated powers $\Delta P_{rad} \sim$ 500 kW.

Measurement of the ion temperature in the divertor plasma is challenging. One idea that is explored is to use a technique similar to that on JT-60U, where ion temperatures in the divertor plasma are deduced from the Doppler broadening of the (n=6-7) visible CIV line.[26]

ACKNWOLEDGEMENTS

The work described in this paper is largely based on years of detailed work and discussions within the Diagnostics Topical Group of the International Tokamak Physics Activity (ITPA). This work, supported by the European Communities under the Contract of Association between EURATOM-FOM, was carried out within the framework of the European Fusion Programme. The views and opinions expressed herein do not necessarily reflect those of the European Commission.

REFERENCES

1. A.J.H. Donné et al, Nucl. Fusion **47**, S337 (2007).
2. A. Litnovsky *et al, Nucl. Fusion* **47**, 833 (2007).
3. M.G. von Hellermann, *these Proceedings*.
4. E. Di Pietro *et al Fusion Eng. and Design* **56-7,** 929 (2001).
5. M.G. von Hellermann. *et al* 2001 Proc. Int. Conf. on Advanced Diagnostics for Magnetic and Inertial Fusion, Varenna, Italy, (New York, Plenum Press) Eds. P.Stott et al p. 205.
6. M. von Hellermann *et al* 2006 in Fusion Energy 2006 (Proc. 21st Int. Conf. Chengdu, 2006) (Vienna: IAEA) paper IT/P1-26.
7. S. Tugarinov *et al Rev. Sci. Instrum.* **74**, 2075 (2003).
8. M. von Hellermann *et al Rev. Sci. Instrum.* **75**, 3458 (2004).
9. M. von Hellermann *et al Rev. Sci. Instrum.* **77**, 10F516 (2006).
10. M. Kuldkepp *et al Rev. Sci. Instrum.* **75**, 3446 (2004).
11. N.C. Hawkes and M. Brix *Rev. Sci. Instrum.* **77**, 10E509 (2006).
12. I. Moskalenko *et al Plasma Phys. Rep.* **30**, 432 (2004).
13. ITER EDA documentation series No.24 2002 *2.6 Plasma Diagnostic System in ITER Technical Basis* (Vienna, IAEA).
14. K. Kadota *et al Nucl. Fusion* **20**, 209 (1980).
15. ITER Design Description Document, 1998 in Final Design Report, ITER EDA Documentation Series, (IAEA, Vienna).
16. R. Barnsley *et al Rev. Sci. Instrum.* **74**, 1969 (2003).
17. M. Bitter *et al Rev. Sci. Instrum.* **57**, 2145 (1986).
18. M. Bitter *et al Rev. Sci. Instrum.* **70**, 292 (1999).
19. M. Bitter *et al., to be submitted to Rev. Sci. Instrum.* (2008).
20. T. Sugie *et al* 2003 *Proc. 30th EPS Conf. on Controlled Fusion and Plasma Physics* (St. Petersburg, Russia) Europhys. Conf. Abstr. **27A**, paper P-4.63. http://epsppd.epfl.ch/StPetersburg/PDF/P4_063.PDF.
21. B. Mikulec *et al Nucl. Instrum. Meth.* **A511**, 282 (2003).
22. F. Sauli *Nucl. Instrum. Meth.* **A477**, 1 (2002).
23. S.G. Lee *et al Rev. Sci. Instrum.* **75**, 3693 (2004).
24. R. Barnsley (UKAEA, Culham) 2002 *private communication*.
25. R. Barnsley *et al Rev. Sci. Instrum.* **75**, 3743 (2004).
26. T. Nakano *et al J. Plasma Fusion Res.* **80**, 500 (2004).

Spectroscopic Determination of Temperature, Density, and Mix Spatial Profiles in Inertial Confinement Fusion Implosion Cores

L. Welser-Sherrill[*], R.C. Mancini[†], J.A. Koch[**], N. Izumi[**], R. Tommasini[**], S.W. Haan[**], D.A. Haynes[*], I.E. Golovkin[‡], J.J. MacFarlane[‡], J.A. Delettrez[§], F.J. Marshall[§], S.P. Regan[§], J.H. Cooley[*], M.E. Sherrill[*], V.A. Smalyuk[§] and G. Kyrala[*]

[*]*Los Alamos National Laboratory*
[†]*University of Nevada, Reno*
[**]*Lawrence Livermore National Laboratory*
[‡]*Prism Computational Sciences*
[§]*Laboratory for Laser Energetics, University of Rochester*

ABSTRACT

In the field of Inertial Confinement Fusion (ICF), work has been consistently progressing in the past decade toward a more fundamental understanding of the plasma conditions in ICF implosion cores. The research presented in this talk represents a substantial evolution in the ability to diagnose plasma temperatures and densities, along with characteristics of mixing between fuel and ablator materials. Mixing is an important property to study and quantify, since it can significantly affect implosion quality. We employ a number of new spectroscopic techniques that allow us to probe these important quantities in a series of indirect drive ICF implosions of Ar-doped and D_2-filled plastic capsules [1]. The first technique is an emissivity analysis, which uses the emissivity ratio of the optically thin Ar Lyβ and Ar Heβ lines to spectroscopically extract temperature profiles, followed by the solution of emissivity equations to infer density profiles. The second technique, an intensity analysis, models the radiation transport through the implosion core and allows us to extract spatial density and mixing profiles. We compare the resulting mix profiles to two independent theoretical mix models, Youngs' model [2] and the Haan saturation model [3], which were used to estimate the level of Rayleigh-Taylor mixing in the experiments [4].

We have recently extended our modeling efforts to design ICF experiments which have varying levels of mix, and subsequently to extract information on mixing directly from the experimental data using spectroscopic techniques. The experimental design was accomplished using hydrodynamic simulations in conjunction with Haan's saturation model, which was used to predict the mix levels of candidate experimental configurations [5]. These theoretical predictions were then compared to the mixing information which was extracted from the experimental data, and it was found that Haan's mix model performed well in predicting the percentage of the core radius that comprises the mixing layer. With these results, we have assessed the range of validity and predictive capability of the Haan saturation model, as well as increased our confidence in the methods used to extract mixing information from experimental data.

SPECTROSCOPIC MODELING TECHNIQUES

Spectroscopy has been used extensively in the field of Inertial Confinement Fusion (ICF) as a powerful non-intrusive diagnostic tool. It provides a method for the characterization of plasma conditions such as temperature and density, as well as mixing between ablator and fuel material.

Spectroscopic methods have evolved with the goal of determining the structure of implosion cores using Ar emission as a diagnostic tool. These techniques initially focused on interpreting the line spectrum comprising the Ar Heβ and Li-like satellites, along with the associated Heβ narrow-band image [6, 7]. More recent advances in diagnostic equipment and analysis methods have made it possible to unfold the spatial information contained in spatially-resolved Ar Lyβ and Heβ narrow-band images [8, 9].

This work focuses on indirect drive Ar-doped implosions in which Ar Lyβ ($1s-3p$), Ar Heβ ($1s^2-1s3p$), and Ar Lyα ($1s-2p$) narrow-band images were recorded. Using special geometric considerations, it is possible to construct intensity and emissivity maps which can be translated into temperature and density maps of the core.

This talk will focus on the determination of temperature and density spatial profiles using several novel techniques of spectroscopic modeling [1], as shown graphically in Fig. 1. The first method, an emissivity analysis, enables the extraction of a temperature profile using the emissivity ratio of the Lyβ and Heβ lines. The second spectroscopic

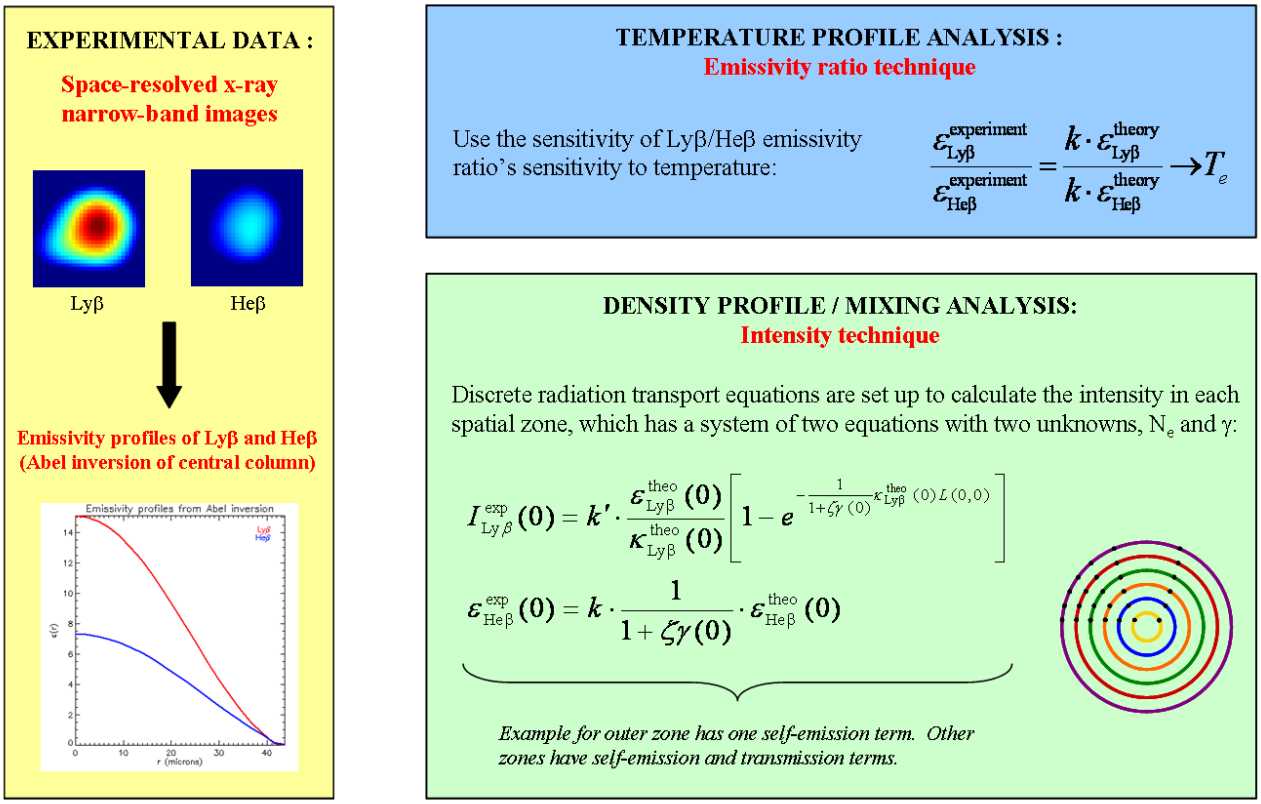

FIGURE 1. Experimental data, in the form of Lyβ and Heβ narrow-band images, are Abel-inverted one column at a time to produce emissivity profiles. These emissivities are then used in an emissivity analysis to extract the temperature profile, T_e(r). The experimental emissivity and intensity, along with the temperature profile, are used to calculate the density, N_e(r), and mixing, $\gamma(r)$, profiles through a set of two equations with two unknowns.

technique, an intensity analysis, involves calculating the density profiles by solving a set of nonlinear discrete transport equations which represent radiation transport through the core. The equations can be solved either in the optically thin approximation or including the effect of opacity. In addition, a mixing term can be included in the transport equations and can be used to extract spatial profiles of mixing between fuel and ablator materials.

EXPERIMENTAL DESIGN

The ultimate goal of our recent experimental design effort was to facilitate a more complete understanding of the mixing process by validating both experimentally- and theoretically-based mix diagnostic tools. An important outcome of the work is an assessment of our ability to predict the extent of mix in ICF experiments by using a combination of hydrodynamic simulation post-processing and off-line mix modeling.

Theoretical mix modeling was used *a priori* to design direct drive experiments with measurably different levels of mix. First a number of hydro simulations were post-processed with Haan's saturation model to study the parameter space, in order to determine which physical characteristics of the lasers and targets are most sensitive to mix. Next, detailed hydro simulations of the most appealing cases were performed to settle on a series of experimental conditions. The chosen designs consisted of three experimental configurations that were nominally identical except for the varying shell thickness of the plastic capsules.

The experiments were conducted based on these designs, and information on the mixing region was directly extracted from the experimental data using the narrow-band image intensity analysis. The data-derived spatial mixing profiles, shown in Fig. 2, were evaluated to determine the corresponding width of the mixing region, for direct comparison to the mix modeling results. Table 1 compares theoretically- and experimentally-derived mix widths,

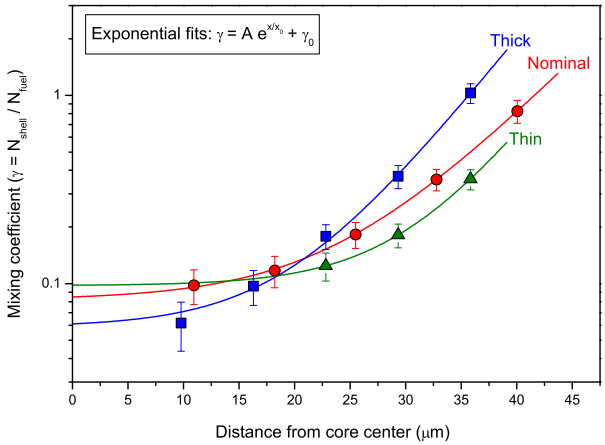

FIGURE 2. Spatial mix profiles for the nominal, thin, and thick shells were directly extracted from experimental data using spectroscopic arguments.

TABLE 1. Comparison between mix information calculated by post-processing simulations with Haan's saturation model and mix data extracted from the experiments.

Shot	Simulation			Experiment		
	Core size	Mix width	% of core mixed	Core size	Mix width	% of core mixed
Thin (47484)	34.4 μm	18.0 μm	52 %	39.1 μm	11.1 μm	28 %
Nominal (47477)	26.3 μm	6.8 μm	26 %	43.7 μm	10.0 μm	23 %
Thick (47485)	26.7 μm	3.5 μm	13 %	39.1 μm	7.1 μm	18 %

and demonstrates that the trends match for the percentage of the core that is mixed. These results indicate that Haan's saturation model provides a reasonable predictive tool for designing direct drive experiments with different amounts of mix.

ACKNOWLEDGMENTS

The development of the spectroscopic techniques was supported by DOE-NLUF grants DE-FG52-2005NA26012 and DE-FG03-03SF22696 and LLNL. The experimental design work was performed under the auspices of the U.S. DOE/NNSA Campaign 10 at LANL. The authors wish to acknowledge the support of DOE-NLUF grant DE-FG52-2005NA26012, which provided the direct drive experimental campaign.

REFERENCES

1. L. Welser-Sherrill, R. Mancini, J. Koch, N. Izumi, R. Tommasini, S. Haan, I. Golovkin, J. MacFarlane, J. Delettrez, F. Marshall, et al., Phys. Rev. E **76**, 056403 (2007).
2. D. Youngs, Physica D **12**, 32 (1984).
3. S. Haan, Phys. Rev. A **39**, 5812 (1989).
4. L. Welser-Sherrill, R. Mancini, D. Haynes, S. Haan, J. Koch, N. Izumi, R. Tommasini, I. Golovkin, J. MacFarlane, J. Delettrez, et al., Phys. Plasmas **14**, 072705 (2007).
5. L. Welser-Sherrill, D. Haynes, R. Mancini, J. Cooley, S. Haan, I. Golovkin, AIP Conf. Proc. **CP926**, 238 (2007).
6. I. Golovkin and R. Mancini, J. Quant. Spectrosc. Radiat. Transfer **65**, 273 (2000).
7. I. Golovkin, R. Mancini, S. Louis, R. Lee, and L. Klein, J. Quant. Spectrosc. Radiat. Transfer **75**, 625 (2002).
8. J. Koch, T. Barbee, N. Izumi, R. Tommasini, R. Mancini, L. Welser, and F. Marshall, Rev. Sci. Instrum. **76**, 073708 (2005).
9. L. Welser, R. Mancini, J. Koch, N. Izumi, S. Louis, I. Golovkin, T. Barbee, S. Haan, J. Delettrez, F. Marshall, et al., J. Quant. Spectrosc. Radiat. Transfer **99**, 649 (2006).

Using line broadening to determine the electron density in an argon surface-wave discharge at atmospheric pressure

M. Christova*, L. Christov†, E. Castaños-Martinez**, M. S. Dimitrijević‡ and M. Moisan**

*Department of Applied Physics, Technical University- Sofia, BG-1000 Sofia, Bulgaria
†Faculty of Chemistry, Sofia University, BG-1164 Sofia, Bulgaria
**Groupe de Physique des Plasmas, Université de Montréal, Montréal H3C 3J7, Québec
‡Astronomical Observatory, Volgina 7, 11060 Belgrade, Serbia

INTRODUCTION

Pressure broadening of spectral lines is important for the diagnostics and modeling of laboratory plasmas, and for many purposes in astrophysics, as for example opacity calculations, abundance determination and analysis and synthesis of stellar spectra. Neutral atom broadening is more important for cooler stars like our Sun and Stark broadening for hot stars like A-type stars and in particular for DO and DB white dwarfs..

It is well known that argon is one of the most widely used gases in various fields of science and technology. On the other hand, with the development of space-borne spectroscopy, the importance of atomic data, including line broadening parameters for trace elements like argon [1], is increasing. Spectral lines within the optical spectral range are of particular interest.

In this work, different line broadening models are applied to three Ar I spectral lines to evaluate the electron density in a surface-wave discharge at atmospheric pressure. This method is useful in cases where the classical methods using hydrogen lines for electron density diagnostic cannot be applied.

THEORETICAL CALCULATIONS

Under atmospheric pressure conditions, the broadening mechanisms of spectral lines are: Stark broadening (due to collisions with charged particles), neutral atom collision broadening (due to collisions with neutral atoms), Doppler broadening and natural broadening. Natural broadening is negligible in comparison with other broadenings and broadening due to self-absorption can be avoided by a proper choice of the spectral lines. For both pressure-induced mechanisms of line broadening (Stark broadening and neutral atom broadening), the impact approximation theory has been applied.

Stark broadening

In this work, the Stark broadening has been calculated using Sahal-Bréchot theory [2, 3]. Within the semi-classical perturbation formalism, used in this theory, the full half width (W) of an isolated line originating from the transition between the initial level i and the final level f is expressed as:

$$W = 2n_e \int_0^\infty v f(v) dv [\Sigma_{i' \neq i} \sigma_{ii'}(v) + \Sigma_{f' \neq f} \sigma_{ff'}(v) + \sigma_{el}] \quad (1)$$

where i' and f' are perturbing levels, n_e and v are the electron density and the velocity of perturbers respectively, and $f(v)$ is the Maxwellian distribution of electron velocities. The inelastic collisional cross sections $\sigma_{ii'}(v)$ (respectively $\sigma_{ff'}(v)$) and the corresponding elastic collision contribution σ_{el} to the W are described in detail in [2, 3].

Neutral atom collision broadening

The line broadening by the neutral atoms has been treated using the semi-classical theory calling for the impact approximation where the full width at half intensity maximum γ is given by:

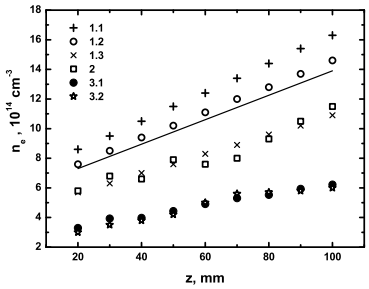

FIGURE 1. Axial variation (z - the position on the axis) of the electron density (n_e) obtained from different Ar I lines. Results obtained using the theory of Sahal-Bréchot for Stark broadening [2, 3] and the potential of Kaulakys [4] for neutral atom impact broadening: 1.1 - Ar I 522 nm; 1.2 - Ar I 549 nm; 1.3 - Ar I 603 nm. Results obtained with Stark broadening data of Griem [6] and van der Waals potential: 2 - Ar I 549 nm. Results obtained with data for Stark broadening of Hβ line from Griem [6] and Gigosos [7]: 3.1 - Hβ (Griem); 3.2 - Hβ (Gigosos).

$$\gamma = 2N < \sigma' v >= \beta N \tag{2}$$

where N is the perturber density, σ' is the effective cross section for the impact broadening of the line and β is the broadening coefficient. Here the symbols <...> denote the (thermal) average over a Maxwellian distribution of the relative velocities of the interacting atoms. Kaulakys potential [4] for the interaction between an emitting atom and rare-gas atoms has been used. This potential accounts for the polarization attractions between the emitter and perturber and for the short-range interactions between excited electrons of the emitter and perturber. The contributions from the polarization attraction of this potential are given by:

$$V\left(\vec{R},\vec{r}\right) = V_c\left(\vec{R}\right) + V_{ce}\left(\vec{R},\vec{r}\right) + V_e\left(\vec{r}-\vec{R}\right), |\vec{R}-\vec{r}| > r_0 \tag{3}$$

where $\vec{R}$ is the distance between the interacting atoms, $\vec{r}$ is the location of the excited electron and r_0 is the distance of the short-range interaction. The short-range interaction is approximated by the Fermi pseudo-potential:

$$V_e\left(\vec{r}-\vec{R}\right) = 2\pi L\delta\left(\vec{r}-\vec{R}\right) \tag{4}$$

where L is the scattering length.

RESULTS

Results for the axial variation of the electron density of surface-wave tubular discharges from the line broadening of three argon neutral lines are presented on the same figure. The examined argon lines Ar I 522.1, 549.6 and 603.2 nm are from the spectral series $3p^5nd$-$3p^54p$. The results are compared with those obtained in [5] from Ar I 549.6 nm and with the electron density values from the Stark broadening of hydrogen line H_β, using Griem's theory [6] and using Gigosos et al. model [7]. The calculations presented are of interest for determining the electron density of, for example, surface-wave discharges at atmospheric pressure using the line broadening of the carrier gas itself, therefore avoiding the use of hydrogenic spectral lines that imply perturbing the discharge to be diagnosed.

REFERENCES

1. K. Werner, T. Rauch, J. W. Kruk, *Astron. Astrophys.* **466**, 317 (2007).
2. S. Sahal-Bréchot, *Astron. Astrophys.* **1**, 91 (1969).
3. S. Sahal-Bréchot, *Astron. Astrophys.* **2**, 322 (1969).
4. B. Kaulakys, *J. Phys. B: At. Mol. Phys.* **17**, 4485 (1984).
5. M. Christova, E. Castaños-Martinez, M. D. Calzada, Y. Kabouzi, J. M. Luque and M. Moisan, *Appl. Spectroscopy* **58**, 1032 (2004).
6. H. R. Griem, *Plasma Spectroscopy*, New York, McGraw Hill (1964).
7. M Gigosos, V. Cardeñoso and M. Gonzáles, *Spectrochim. Acta Part: B* **58**, 1489 (2003).

Calculation of the shifts of argon spectral lines

M. Christova*, L. Christov†, M. S. Dimitrijević** and N. Andreev*

*Department of Applied Physics, Technical University- Sofia, BG-1000 Sofia, Bulgaria
†Faculty of Chemistry, Sofia University, BG-1164 Sofia, Bulgaria
**Astronomical Observatory, Volgina 7, 11060 Belgrade, Serbia

INTRODUCTION

In the previous works [1-3] the broadening of argon spectral lines emitted from surface wave plasma at atmospheric pressure have been studied. The purpose was to obtain the electron density in this type of discharge using the widths of spectral lines of the working gas, without any impurities and contaminations of the plasma.

In this work we look for the shift values of the same argon spectral lines. If their values are significant enough to be measured, it is possible to use them for plasma diagnostic too.

THEORETICAL CALCULATIONS

The theoretical calculations of the shifts of argon spectral lines have been made using semi-classical impact theory. Under atmospheric pressure the shifts of the spectral lines are due to: (i) the interactions between the emitters and the charged particles (Stark shift) and (ii) the interactions emitters - neutral atoms in a ground state.

Stark shifts

In this work, the Stark shifts have been calculated using Sahal-Bréchot theory [4, 5]. Within the semi-classical perturbation formalism, the Stark shift (d) of an isolated line originating from the transition between the initial level i and the final level f is expressed as:

$$d_{St} = n_e \int_0^\infty v f(v) dv \int_{\rho_3}^{\rho_d} 2\pi\rho d\rho \sin 2\phi_p \tag{1}$$

where n_e and v are the electron density and the velocity of perturbers respectively, $f(v)$ is the Maxwellian distribution of electron velocities, and ρ is the impact parameter. The phase shift ϕ_p is due to the polarization potential The cut-off parameter ρ_3, the Debye cut-off ρ_d and the symmetrization procedure are described in [4, 5].

Shift due to collisions with neutral atoms

The shift by the neutral atoms has been treated using semi-classical theory in impact approximation where the shift value d_K is given by:

$$d_K = N < \sigma" v > = N\delta \tag{2}$$

where N is the perturber density, σ" is the effective cross section for the impact line shift, δ is the shift coefficient, v is the relative velocity between the radiator and the perturber. Here the symbols <...> denote the thermal average over a Maxwellian distribution of the relative velocities of the interacting atoms. The interactions between the emitter and the rare-gas atoms are described using Kaulakys potential [6]. It is approximated by a superposition of polarization potentials and the Fermi pseudopotential. The polarization potentials describe the long range interactions: (i) excited electron - perturber interaction; (ii) three body interaction between the excited electron and perturber in the presence of emitter core and (iii) emitter core - perturber interaction.

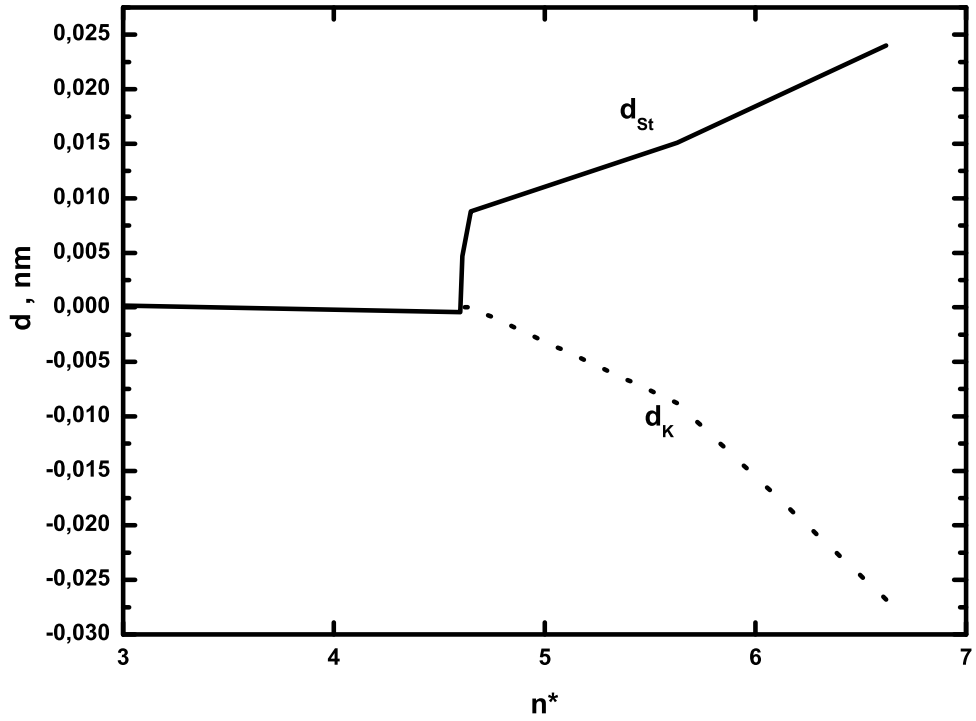

FIGURE 1. Stark shift (d_{St}) and neutral shift (d_K) of the argon spectral lines versus effective quantum number (n^*).

RESULTS

Results for the shifts of nine argon spectral lines corresponding to the transitions $3p^5nd$ - $3p^54p$ for n = 4 - 7, $3p^56s$ - $3p^54d$ and $3p^54p'$ - $3p^54s$ have been obtained. Comparison of our semi-classical Stark shift [2] and the theoretical shift caused by the neutral atom impacts, have been presented, as well as the dependence of the shift of spectral lines versus the effective quantum number.

REFERENCES

1. M. Christova, E. Castaños-Martinez, M. D. Calzada, Y. Kabouzi, J. M. Luque and M. Moisan, *Appl. Spectroscopy* **58**, 1032 (2004).
2. M. S. Dimitrijević, M. Christova and S. Sahal-Bréchot, *Phys. Scripta* **75**, 809 (2007).
3. M. Christova, *J. Phys.: Conf. Series* **63** 012012 (2007).
4. S. Sahal-Bréchot, *Astron. Astrophys.* **1**, 91 (1969).
5. S. Sahal-Bréchot, *Astron. Astrophys.* **2**, 322 (1969).
6. B. Kaulakys, *J. Phys. B: At. Mol. Phys.* **17**, 4485 (1984).

SPECTROSCOPIC DIAGNOSTICS OF SIX ELECTRODES PLASMA ARC AS AN EXCITATION SOURCE FOR SPECTROCHEMICAL ANALYSIS

Z. F. Ghatass and G. D. Roston*

Institute of Graduate Studies and Research, Alexandria University, Egypt
** Department of Physics, Faculty of Science, Alexandria University, Egypt*
(gamal_daniel@yahoo.com)

Abstract

A six electrodes direct current plasma arc has been developed for atomic emission spectrochemical analysis. The background emission spectrum is recorded over wavelength range (200 – 700) nm. The effects of the argon flow rates and different applied currents have been studied on the emission spectra lines of MgI and MgII. Emission spectroscopy has been used to determine the plasma temperature by using the line-to-continuum intensity ratio method. The electron density has been calculated. The plasma temperatures ranged from about 5500 to 6350 K, and the electron number density varied from 9×10^{13} cm^{-3} to 3×10^{14} cm^{-3}. Vertical profiles of the Ca(I) 422.67 nm emission along the central vertical axis of the plasma with and without the presence of an easy ionized element are studied. The detection limits of elements Ca, Cr, Fe, Mg and Mn have been carried out. The present technique is capable to determine the trace element concentration in the environmental samples. Advantages of this system are simple, low cost, stable and the ability to operate for several hours.

REFERENCES

1. Rippetoe W.E, Johnson E.R, Vickers T.J; Anal. Chem, 47, 436, 1975.
2. Rastiaans G.J, Mangold R. A; Spectrochim. Acta; 40B, 885, 1985.
3. Mohamed M.M, Shalaby E.A, Ghatass Z.F, Naim M.A, El-Raey M.A; Indian J. Pure Appl. Phys., 36, 719, 1998.
4. Mohamed M.M, Ghatass Z.F, Shalaby E.A, Kotb M.M, El-Raey M.A; Freseniu J Anal Chem , 368, 809, 2000.
5. Ghatass Z. F; 16th International Conference on Spectral Line Shape, Edit. C. A. Back, Berkeley, California, USA, 434, 2002.
6. Ghatass Z. F, Roston G. D, Mohamed M. M; Anal. Bioanal. Chem., 376, 549 2003.
7. Laux C.O, Spence T.G, Hruger C.H, Zare R.N; Plasma Sources Sci. Technol. 12, 125, 2003.

The effect of time ordering on line profiles revisited

J. Rosato, D. Boland, H. Capes, Y. Marandet and R. Stamm

PIIM, CNRS-Université de Provence, centre de Saint Jérôme, F13397 Marseille

A consequence of the advent, half a century ago, of comprehensive quantum line broadening theories [1, 2, 3], was that the problem of an accurate calculation of Stark broadened line shapes suddenly became more severe. Obtaining the time evolution operator of the emitter in a fluctuating microfield asks for the solution of a general problem of quantum dynamics which even today has no general solution. Retaining the time dependence of the electric microfield is indeed essential for many plasma conditions for both its electronic and ionic contributions. This requirement is even stronger today with the attempt of developing spectroscopic diagnostics of plasmas affected by plasma wave fields or turbulent fluctuations [4, 5]. The dynamics of quantum systems with a time dependent interaction potential between the emitter and the perturbers is formally solved by the following Dyson expansion for the evolution operator U(t,0) written in the interaction representation :

$$U(t,0) = 1 + \sum_{n=1}^{\infty} \frac{1}{(i\hbar)^n} \int ... \int_{0<\tau_1<...<\tau_n<t} V(\tau_n)...V(\tau_1) = T \exp\left(\frac{1}{i\hbar}\int_0^t d\tau V(\tau)\right) \quad (1)$$

where for example $V(\tau_n)$ is the interaction potential at time τ_n, and T is the time ordering operator ensuring that the potentials are arranged from left to right in order of decreasing times. For an arbitrary atomic system with many interacting sublevels, an exact analytic solution of the Schrödinger's equation is generally not available. A noteworthy exception is the case of hydrogen lines using a non relativistic approximation. This case has been used in the past for a calculation of Balmer lines retaining time ordering for the binary electronic contribution, demonstrating that this effect significantly broadens the line in arc plasma conditions [6]. Our purpose here is to revisit the effect of time ordering on benchmark cases. We will first try to illustrate how the quantum atom responds through its dipole autocorrelation function to a well characterized microfield. Numerical integrations of the Schrödinger's equation will be performed with and without the effect of time ordering for a comparison. We will also present a study of time ordering effects on Lyman α in presence of an external magnetic field $\vec{B}$, treating the Zeeman effect in the strong field regime. We will again compare the numerically obtained exact solution of Schrödinger's equation to an expression which neglects time ordering effects. A discussion will be made in term of the ratio ω_S/ω_Z between the characteristic Stark and Zeeman frequencies, $\omega_S = 3ea_0E/\hbar$ and $\omega_Z = eB/2m_e$ where E denotes the Holtsmark field .

ACKNOWLEDGMENTS

This work is supported by the grant ANR-07-BLAN-0187 of the Agence Nationale de la Recherche, and by the project "Radiation absorption effects" of the fédération de recherche sur la fusion par confinement magnétique.

REFERENCES

1. A. C. Kolb, H. R. Griem, *Phys. Rev.* **111**, 514–521 (1958).
2. M. Baranger, *Phys. Rev.* **111**, 481–504 (1958), *ibid*. 494–504.
3. M. Baranger, *Phys. Rev.* **112**, 855–865 (1958).
4. H. R. Griem, Principles of Plasma Spectroscopy, Cambridge university press (1997).
5. J. Rosato et al., Contrib. Plasma Phys. **46**, 667–671 (2006).
6. L. J. Roszman, *Phys. Rev. Lett*. **34**, 785–788 (1975).

Local Electric Field Strength in a Hollow Cathode determined by Stark Splitting of the 2S Level of Hydrogen Isotopes by Optogalvanic Spectroscopy

C. Pérez*, M. I. de la Rosa*, K. Grützmacher*, A.B. Gonzalo† and L.M. Fuentes*

* *Departamento de Física Teórica, Atómica y Óptica*
Facultad de Ciencias, Universidad de Valladolid
47071 Valladolid (Spain)
† *Departamento de Ingeniería Cartográfica y del Terreno*
Escuela Politécnica Superior de Ávila, Universidad de Salamanca
05003 Ávila (Spain)

Electric field (E-field) is an important parameter to be known in low pressure plasmas such as glow, RF and microwave discharges, plasma boundaries in tokamaks etc. Until now, many techniques have been developed for E-field determination, among them non intrusive methods, like laser spectroscopy are preferred [1-5]. One of the advantages of using laser spectroscopy is to perform measurements of high temporal and spatial resolution.

The principle of determining E-field is based on the well known Stark effect that produces shifting and mixing of spectral components and variations in their intensities. Comparisons of the measured spectra with theoretical values or with calibrated ones give the E-field. We use Doppler-free two photon excitation of the 1S - 2S transition provided by two counter propagating circularly polarized laser beams of opposite directions, at 243 nm, in accordance with the selection rule for the angular momentum $\Delta L = 0$. And we determine the E-field via Doppler-free spectra of the Stark splitting of the 2S level [6].

We started with the discharge in deuterium in order to simplify the spectra, i.e. the hyperfine structure of deuterium does not show up in the Stark splitting under our laser spectroscopic conditions. In this work we propose optogalvanic detection, the optogalvanic spectra are obtained by measuring the change of plasma impedance caused by the two photon absorption as a function of the laser frequency. Even though optogalvanic effect is well known since 1928, it was not until the introduction of the dye laser that optogalvanic spectroscopy became a practical tool; a very exhaustive review can be found in reference [7]. However, the optogalvanic signal created in our case is somehow different compared to optogalvanic signals measured in saturation spectroscopy. The irradiance of about 1 GW/cm^2 present in the excitation region of the laser beams, causes not only two-photon excitation but results although in subsequent photo ionization due to the absorption of a third laser photon. Hence, the charged particles created in the overlap volume of the laser beams are accelerated by the present electric field and the corresponding variation of the discharge impedance can be measured.

The most suitable parameters for determining the E-field from the Stark splitting in hydrogen (or isotopes) are the frequency shifts of the red ($2P^{1/2}$) and blue ($2P^{3/2}$) Stark components. On the other hand, the two-photon optogalvanic spectroscopic technique is fairly easy to handle, and works well in nearly all discharge regimes (without sparking) and it could be applied therefore in a certain range of discharge parameters.

The full potential provided by the spectroscopic technique is accessible, if a pulsed UV laser radiation of sufficient peak power and SLM spectral quality is available. In brief, the scheme for the generation of 243 nm radiation, as required for the two photon excitation of the 1S - 2S transition, consists of a 10 Hz injection-seeded Q-switched Nd:YAG laser and a substantially modified OPO-OPA system. This concept provides up to 10 mJ pulse energy in 2.5 ns and 300 MHz bandwidth.

This study has been performed in a HCD, made of stainless steel with an inner cathode diameter of 10 mm, for currents from 50 to 200 mA and pressures from 400 to 1350 Pa. The measurements exhibit clearly the variation of the cathode fall characteristics depending on discharge pressure and current, covering the range from a linear to a pronounced parabolic E-field dependence versus distance from the cathode. As an example of the results that we have obtained through this experiment, in figure 1 the variation of the E-field in the cathode fall region is plotted versus the radial distance from the cathode surface, for a fixed current (100 mA), and several pressures: 400, 600, 900 and 1350 Pa. For the 1350 Pa pressure a linear dependence is observed, while with decreasing pressure the dependence is more parabolic, this convex shape has been observed in previous experiments [8]. At the same time with decreasing pressure the maximum field decreases, while the cathode fall region increases. However, this pronounced tendency nearly disappears when the pressure reduces from 600 Pa to 400 Pa. In all

cases we have also calculated the cathode fall voltage drop from the local E-field distribution, which is compared with the discharge voltage (measured between cathode and anode); this ratio (%) appears also in figure 1. Obviously this ratio increases for decreasing pressure, i.e. from: 81 % for 1350 Pa to 94 % for 400 Pa. This fact does not confirm the common understanding that the cathode fall represents nearly the entire voltage drop of the discharge, we may suggest that the differences are probably related to the special characteristic of pure deuterium plasma, which is known to suffer an extremely high electronic recombination due to the dominant molecular density, and this phenomenon depends on the pressure and current of the discharge. This effect is being investigated with hydrogen and different cathode materials. At the Conference we will show comparative results and possible conclusions about new dependencies.

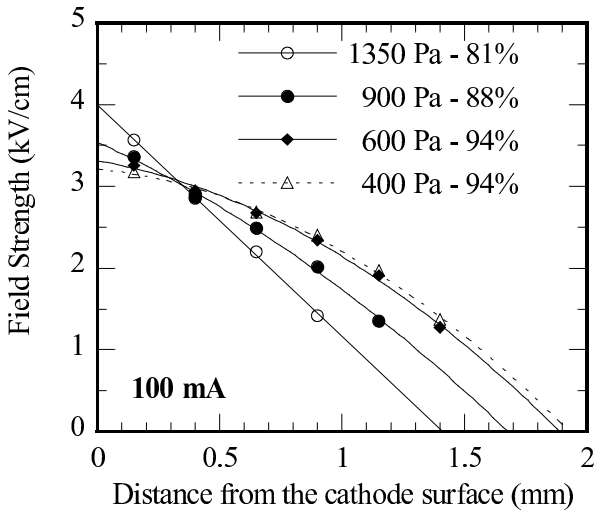

FIGURE 1. Variation of the E-field in the cathode fall region versus the radial distance from the cathode surface determined for a fixed current (100 mA) and various pressures: 400, 600, 900 and 1350 Pa. For each pressure is indicated the ratio (in %) of the cathode fall voltage drop (calculated from the local E-field distribution) with respect to the discharge voltage

ACKNOWLEDGMENTS

Authors will thank DGICYT (Project Nº FIS2007/62604) and the Junta de Castilla y León (Project Nº VA003A06) for financial support.

REFERENCES

1. I.R.Videnovic, N. Konjevic and M.K.Kuraica, *Spectrochim. Acta B* **51**, 1707 (1996)
2. Z. Donkó, K. Rózsa, R.C. Tobin and K.A. Peard, *Phys. Rev. E* **49**, 3283 (1994)
3. J.E. Lawler and D.A.Doughty *Adv. At. Mol. Opt. Phys.* **34**, 171 (1994)
4. J.P.Booth , M.Fadlallah , J. Derouard and N. Sadeghi *Appl. Phys. Lett* **65**, 819 (1994)
5. M.I. de la Rosa, C. Pérez, K. Grützmacher, A.B. Gonzalo and A. Steiger, *Plasma Sources Sci. Technol.* **15**, 105 (2006)
6. J.Seidel, Theoretical calculation of the Stark effect of the 2S level (Private Communication)
7. B. Barbieri and N. Bevrini, *Optogalvanic Spectroscopy, Reviews of Modern Physics*, **62**, 3 (1990)
8. J.E. Lawler and D.A. Dougthy, *Adv. At. Mol. Opt. Phys*. **34**, 171 (1994)

Determination of Two-Photon Absorption Cross-Section of Noble Gases for Calibration of Laser Spectroscopic Techniques

M.I. de la Rosa, C. Pérez, K. Grützmacher and L.M. Fuentes

Departamento de Física Teórica, Atómica y Óptica
Facultad de Ciencias, Universidad de Valladolid
47071 Valladolid (Spain)

INTRODUCTION

The diagnosis of plasmas far off thermodynamic equilibrium is of great importance for the understanding of plasmas for technological application and combustion systems. In particular, diagnostics tools are demanded for quantitative measurements of atomic ground state density for species like hydrogen, carbon, nitrogen and oxygen. Among the different laser-diagnostic techniques, which have been applied to the study of plasmas, Laser-Induced Fluorescence (LIF) or, in general, Multi-photon Laser-Induced Fluorescence (MP-LIF) is one of the most extended methods in order to determine the absolute concentration of ground state atoms. At low pressure, it is a sensitive and quantitative technique. However, with increasing pressure ($p > 1$ kPa) and temperature, the quantitative analysis is only possible if the thermodynamical state of the plasma and all interaction mechanisms are well known. At atmospheric conditions, collisions can be dominant and obtaining quantitative measurements is almost impossible. Nevertheless, several strategies have been described in the literature in order to obtain a quantitative interpretation of the LIF signal: calibration methods based on reference sources, for example titration methods in flow-tube reactors [1-2], use of calibrates two-photon LIF signal in noble gases [3-4], or consistency checks based on combination of LIF with several diagnostic and modeling techniques. The use of noble gases with two-photon resonance spectrally close to the investigated atomic transition requires nearly no modification of the LIF set-up. Nevertheless, this kind of comparisons need a precise knowledge of several atomic parameters like radiative lifetimes of the excited states, their quenching coefficients for different collisions, and the relevant ratios of two-photon excitation cross sections. However, in general, these are not known with the required precision in order to reduce the uncertainty of the density measurements.

We have established in our laboratory a different laser spectroscopic technique, i.e. high precision two-photon polarization spectroscopy, which is not affected by quenching and allows us to measure directly the two-photon absorption. It has been used e.g. to determine absolute atomic hydrogen density in quite different environments with an uncertainty as low as 10% [5-7]. This precision can be by achieved by relative measurements with respect to a standard of atomic hydrogen density. The standard was established [7] at the Physikalisch-Technische Bundesanstalt (PTB), and it is based on the plasma generated in a stationary wall-stabilized cascade arc operated with pure hydrogen, which was demonstrated to generate an ideal gas of atomic hydrogen for the experimental conditions. However, such a hydrogen density standard is quite complicated to be used in other laboratories, because it needs sophisticated technical equipment and requires some special operational experience. In order to overcome these difficulties we have established at the same time a new reliable and easy calibration method using xenon gas at room temperature as a transfer standard calibrated with respect to standard of atomic hydrogen density: i.e. calibrating the two-photon polarization spectroscopic signal of xenon at the wavelength of the hydrogen 1S - 2S transition, mainly caused by the dispersion wing of the nearby two-photon Xe transition $5p^6\ ^1S_0$ - $5p^5\ 6p[1/2]_0$. As the comparison is done in the same wavelength the experimental conditions i.e. overlap volume and laser irradiance are kept constant, and allow therefore high precision measurements.

EXPERIMENT

The objective of our present work is to use two-photon polarization spectroscopy as a new calibration method for the determination of two-photon excitation cross-sections of noble gases, like Xe and Kr, which are commonly used for calibrations of MP-LIF techniques in other laboratories, i.e. to calibrate the two-photon excitation cross-sections with respect to the standard of atomic hydrogen density via the xenon transfer standard. This approach is totally independent and different with respect to all other calibration techniques used so far.

This work requires pulsed UV laser radiation of sufficient peak power and SLM spectral quality. The laser spectrometer used so far for the generation of 243 mm radiation, as required for the two photon excitation of the 1S - 2S transition in hydrogen, consists of a 10 Hz injection-seeded Q-switched Nd:YAG laser and a substantially modified OPO-OPA system. This concept provides up to 10 mJ pulse energy in 2.5 ns and 300 MHz bandwidth. With

slight modifications this system can provide tuneable UV-radiation necessary for other noble gas two-photon transitions.

Two-photon polarization spectroscopy is based on the detection of the small polarization change of a linear polarized signal beam, due to two-photon excitation while interacting with a circularly polarized beam of high irradiance. Taking into account the functional dependency of the polarization signal with respect to the irradiances of the pump and signal beam, the highest precision for comparing or calibrating two-photon excitation cross-sections with quite different frequencies, will be achieved with a fixed frequency pump beam while tuning the signal beam from one two photon transition to another one.

To start our study we have chosen the Xe transition $5p^6\,{}^1S_0$ - $5p^5\,7p[3/2]_2$ at 112.72 nm (2x225.44 nm) very close to the two-photon resonant transition of atomic oxygen at 2x225.58 nm, frequently used therefore for calibration of atomic oxygen densities in LIF experiments. At present, we are involved in preparing the experimental set-up for doing the first measurements. Concerning pump and signal beam the following concept will be applied: the fifth harmonic of the Nd:YAG is used as pump beam, and for the signal beam we have to tune the OPO-OPA system from 239.42 nm for the Xe transition to 283.19 m for the hydrogen 1S-2S resonance (non-resonance Xe calibrated signal). More details will be explained at the Conference.

ACKNOWLEDGMENTS

Authors will thank to DGICYT (Project Nº FIS2007/62604) and to the Junta de Castilla y León (Project Nº VA003A06) for financial support.

REFERENCES

1. U. Meier, K. Kohse-Höinghaus and T. Just, 1986 Chem. Phys. Lett. 126 567
2. J. Bittner, K. Kohse-Höinghaus, U. Meier and S. Kelm, 1988 Combust. Flame 71 41
3. K. Niemi, V. Chulz-von der Gathen and F. Döbele F., 2001 J. Phys. D: Appl. Phys. 34, 2330
4. M.G.H. Boogaarts, S. Mazouffre, G. J. Brinkman, H.W.P.van der Heijden, P. Kankan, J.A.M. van der Mullen and D. C. Schram, 2002 Rev. Sci. Instr. 72 73
5. K. Grützmacher, M.I. de la Rosa, A.B. Gonzalo, M. Steiger and A. Steiger, 2003 Appl. Phys. B00 1
6. A.B. Gonzalo, M.I. de la Rosa, C. Pérez, S. Mar and K. Grützmacher, 2003 Plasma Sources Sci. Technol. 12 150
7. R. Dux, K. Grützmacher, M.I. de la Rosa, and B. Wende, 1995 Phys. Rev. E 51 1416

Charge Correlation Effects in Plasma Line Broadening

Jeffrey Wrighton and James W. Dufty

Department of Physics, University of Florida, Gainesville, FL 32611

The spectral line shape theory for a multi-electron charged radiator in a two component plasma is reconsidered for the special case of quasi-static ions [1]. All charge-charge correlations in the two component plasma are treated exactly. The coupling of the radiator monopole to the plasma electrons and ions is treated exactly, as is the coupling of the radiator dipole to the ions. Width and shift operators are calculated to second order in the weak coupling to the residual bound electron distribution. With no approximations made in the treatment of the charge-charge correlations, the results provide the formal basis for exploring the importance of such correlations for high Z radiators in hot, dense matter.

REFERENCES

1. J. Wrighton, Ph. D. thesis, University of Florida, 2006.

Asymmetry of the H_β-Balmer line in atmospheric pressure microwave plasma

J M Palomares[1], J Torres[1], M A Gigosos[2], J J A M van der Mullen[3], A Gamero[1] and A Sola[1(*)]

[1]*Departamento de Física, Universidad de Córdoba.14071 Córdoba, Spain.*
[2]*Departamento de Óptica, Universidad de Valladolid. 47071 Valladolid, Spain.*
[3]*Department of Applied Physics, Eindhoven University of Technology. P.O. Box 513. 5600 MD Eindhoven, The Netherlands.*
[(*)]*fa1sodia@uco.es*

In this paper we present an experimental study of the spectral profile asymmetry and dip shape of the H_β line in a microwave plasma generated with an axial injection torch (*Torche à Injection Axiale* or *TIA*). This device provides a stable discharge to obtain a two temperature (*2-T*) plasma at atmospheric pressure. The study has been carried out on an Ar plasma introducing impurities of H_2. The microwave power was kept constant at 1000W, while the gas flow of Ar was varied between 1L/min and 5 L/min, also the percentage of hydrogen impurities was varied in the range 2%-20%. The study shows the experimental dependence of these profile features (asymmetry and dip form) on the plasma parameters, mainly the electron density and the gas flux.

The Stark width of the H_β line is a rather well-known function of the electron density and only weakly depends on the electron temperature. Up to date, the most efficient Stark-broadening models developed with the help of micro-field theories only include the terms of first order in the perturbing electric field, and as a result only generates symmetric profiles without shift [1]. Although there is no complete model that fully describes the asymmetry in the profiles, it is possible to find some studies in which calculations and partial corrections on the current theories of the Stark broadening are carried out and the asymmetry for some concrete lines is obtained [2,3]. These features have been and continue to be measured [3,4,5], but most of the experimental and theoretical studies on the asymmetry of the H_β line have been made in plasmas with electron densities equal or higher than 10^{23} m^{-3}. The objective of this work is the characterization of the Stark asymmetry and dip form of the line H_β at lower electron densities, *i.e.* in the order of 10^{21} m^{-3}. To characterize the line shape asymmetry the following three functions that quantify this asymmetry for the entire line profile have been used [3]:

$$A_1(\Delta\lambda)=\frac{I_r(\Delta\lambda)-I_b(\Delta\lambda)}{I_r(\Delta\lambda)+I_b(\Delta\lambda)} \quad (1)$$

$$A_2(I)=\frac{\Delta\lambda_r(I)-\Delta\lambda_b(I)}{\Delta\lambda_r(I)+\Delta\lambda_b(I)} \quad (2)$$

$$A_3(I)=\frac{\Delta\lambda_r(I)-\Delta\lambda_b(I)}{2} \quad (3)$$

where $I_r(\Delta\lambda)$ and $I_b(\Delta\lambda)$ are respectively the intensities of the red and blue sides of the profile at a certain displacement $\Delta\lambda$ with respect to the central wavelength, while $\Delta\lambda_r(I)$ and $\Delta\lambda_b(I)$ represent the spectral position of these red and blue sides at a given intensity I. In general, the profile follows the tendency of the normal asymmetry, which means that the peak intensity is higher whereas the wing intensity is lower at the blue side, and the contrary at the red side. When the average electron density is higher, the asymmetry should grow, which would be translated to a more pronounced slopes of the functions previously defined.

The central zone of the H_β profile has been studied introducing four specific parameters characterizing the dip shape. These parameters will provide additional information concerning the internal structure of the dip and its peaks as functions of the averaged electron density in the observed zone of the discharge. These parameters have the following expressions:

FWPP (full-width peak-to-peak) $\lambda_{rp}-\lambda_{bp}$ (1)

$$DD\ (dip\text{-}depth)\ (I_{max}-I_{dip})\cdot 100/I_{max} \quad (2)$$

$$PID\ (peak\text{-}intensity\text{-}difference)\ (I_{bp}-I_{rp})\cdot 100/I_{max} \quad (3)$$

$$DP\ (dip\text{-}position)\ (\lambda_{dip}-\lambda_{bp})\cdot 100/(\lambda_{rp}-\lambda_{bp}) \quad (4)$$

where λ_{bp}, λ_{rp} and λ_{dip} stand respectively for the spectral positions of the blue peak, red peak and dip, while I_{bp}, I_{rp} and I_{dip} represent the intensity of the same points (the maximum intensity, I_{max}, has been taken as the average of the peaks). The first two parameters are well-know as the spectral separation between peaks (*FWPP*) and the dip depth (*DD*). The third parameter measures the relative difference of the two peak intensities (*PID*), and finally the forth parameter measure the spectral dip position relative to the peaks (*DD*).

In this work the electron density has been experimentally measured by the Stark broadening of the line with the help of the computational results provided by Gigosos *et al* [1]. The different values of the electron density were achieved with 1000 W of *HF* power by changing the concentration of hydrogen introduced in the discharge, from 17% (lower electron density) to 2 % (higher electron density) in plasmas generated with an Ar flow of 5L/min and 2.5L/min.

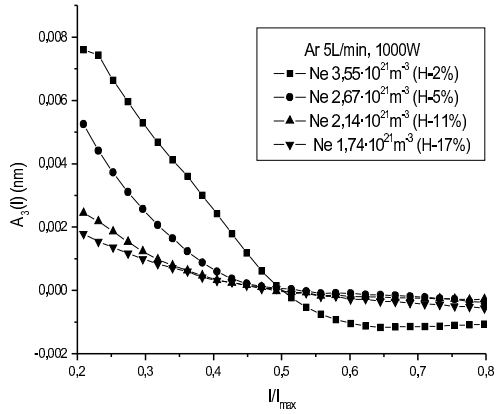

Figure 1: $A_3(I)$ function for 5 L/min of Ar

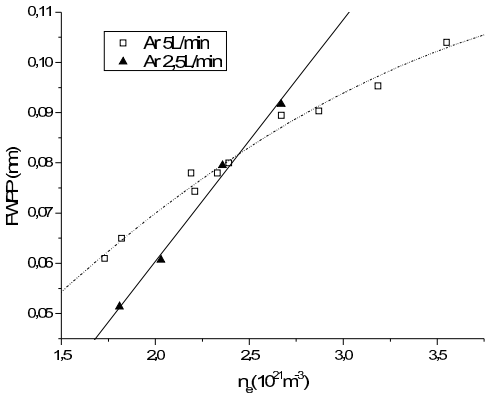

Figure 2: *FWPP* for 2,5L/min and 5L/min of Ar

As an example, the asymmetry function $A_3(I)$ it is shown in Figure 1 for different values of the electron density and an Ar flow of 5 L/min. It can be appreciated how the function of asymmetry is sensitively affected by fluctuations close to the line centre ($I > 0.5I_{max}$). A similar behaviour has been appreciated in the asymmetry functions $A_1(\Delta\lambda)$ and $A_2(I)$, but with a bigger effect of the fluctuations and smaller sensitivity with the electron density.

In Figure 2 the dependence of the parameters characterizing the dip form, *FWPP*, on the electron density for two values of the Ar flow is shown. It can be seen how this parameter follows an increasing dependence on the electron density, which indicates how the internal components of H_β separate each other when the electron density increases. This increasing dependence its owned not only to the increase of the electron density but also to the increase of reduced mass, although in the present experiment is not possible to separate these two effects. It can be seen how the effect of the fluctuations does not seem to disperse the points, and the results fallow a tendency with a small deviation. A similar behaviour has been observed for the *DD*. On the other hand, the third and forth parameters, *PID* and *DP*, have a great dispersion and do not follow a clear tendency with the electron density.

1. MA Gigosos, M González and V Cardeñoso, *Spectrochim. Acta B* **58**, 1489 (2003).
2. C Stehle, D Gilles and A Demura, *Eur. Phys. Journal D* **12**, 355 (2000).
3. S Djurovic, D Nikolic, I Savic, S Sörge, A Demura, *Phys Rev E* **71**, 036407 (2005).
4. WL Wiese, DR Paquette and DE Kelleher, *Phys. Rev. A* **6**, 1132 (1972).
5. WL Wiese, DE Kelleher, V Helbig, *Phys. Rev. A* **11**, 1854 (1975).

Experimental and Theoretical Analysis of Central H_β Asymmetry

A. V. Demura*, G. V. Demchenko*, S. Djurović†, M.Ćirišan†, D. Nikolić**, M. A. Gigosos‡ and M.Á. González§

*HEPTI, RRC "Kurchatov institute", Kurchatov Square 1, Moscow 123182, Russia
†Department of Physics, Faculty of Sciences, 21000 Novi Sad, Serbia
**Department of Physics, Western Michigan University, Kalamazoo MI-49008, USA
‡Departamento de Óptica, Universidad de Valladolid, 47071 Valladolid, Spain
§Departamento de Física Aplicada, Universidad de Valladolid, 47071 Valladolid, Spain

INTRODUCTION

The hydrogen Balmer beta line is used as a plasma diagnostics tool for a long time. It is well known that the experimental profiles of H_β line exhibit an asymmetry while some of most commonly used theoretical models, due to the employed approximations, give unshifted and symmetrical profiles [1, 2]. In the present work the central part of H_β profile is reanalyzed experimentally and in terms of two theoretical approaches based correspondingly on the Standard Theory (ST) assumptions [3] and on the electric field computer simulation method [4, 5]. The present experimental and theoretical results are compared with the obtained earlier experimental [6–12] and theoretical data [13].

EXPERIMENTAL

The experimental measurements were performed using two different experimental arrangements in order to span relatively wide ranges for electron density and temperature. The first experimental plasma source was electromagnetically driven T-tube. The detail about experiment is given in [14]. The plasma electron densities, ranging from $9.6\ 10^{22}$ m^{-3} to $8.9\ 10^{23}$ m^{-3}, were determined from the Stark widths of H_β line. The electron temperatures, ranging from 17000 K to 45000 K were inferred from the line-to-continuum ratio for H_β line [15]. In the second experiment a pulsed discharge lamp was used [16]. The electron densities in this case, ranging from $1.5\ 10^{22}$ m^{-3} to $7.0\ 10^{22}$ m^{-3}, were obtained as in the previous case. The temperature about 10000 K was deduced from the plasma LTE relations.

THEORY

The ST approach assumes the quasistatic broadening by ions and impact broadening by electrons [3]. It includes consideration of many-body quadrupole interaction, linear and quadratic Stark effects. The formalism of joint distribution functions allows to reduce the statistical problem to the calculation of constrained first moments of microfield nonuniformity tensor and thus close the set of equations [3]. This approach was used for the interpretation of multifarious asymmetry parameters in [14]. In the computer simulation the movement of plasma perturbers is modeled numerically. This permits to calculate the electric microfield undergone by the emitter. The electric microfield obtained in this way is incorporated into differential equations that give the emitter evolution. Details of the simulation technique can be found in [4, 17]. For this calculation, the Hamiltonian of the emitter includes all the transitions among the states with principal quantum number from n = 1 to n = 5. Then, the main contributions to quadratic Stark effect are included in a natural way.

RESULTS AND DISCUSSION

We further consider peaks asymmetry as an example of the local conventional characteristics of the central part of H_β profile. The comparison of the relative difference of the blue and red peaks of H_β line according to [13], the ST calculations [3], and computer simulations done for this work with the present and other experimental data [6–12] is given in the Fig. 1.

The experimental results of all experiments show agreement and some general trend. There is, obviously a disagreement between measured and calculated data from [13]. The ST theoretical results [3] and computer simulation,

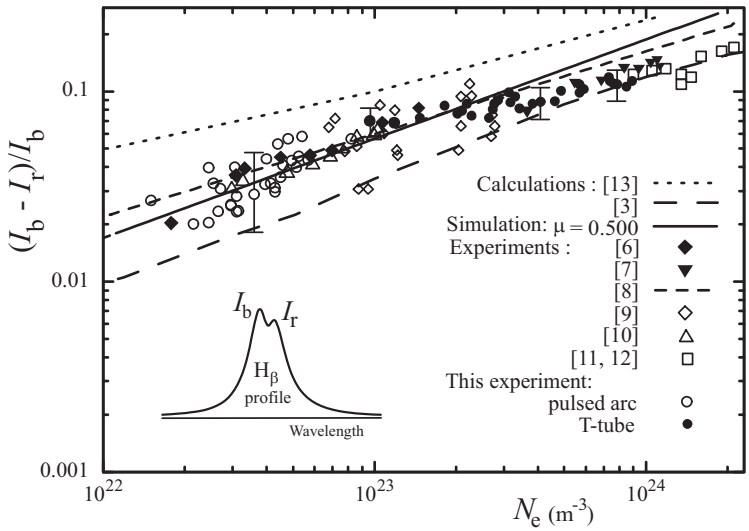

FIGURE 1. Relative difference between blue and red peaks

presented in the Fig. 1 by the dashed and solid lines, describe rather well the general trend of experimental points. For the higher electron densities the agreement of experimental data is a little better with the ST approach, while for the lower electron densities it is definitely better with computer simulation method.

ACKNOWLEDGMENTS

The work of A. V. Demura has been supported by the RRC "Kurchatov institute" grants for fundamental research. The work of S. Djurović is partially supported by Ministry of Science, Republic of Serbia under project 141024. The contribution of D. N. Nikolić was elaborated under the support of Stockholm University during a period from September/2001 to February/2005. The work of M. A. Gigosos and M. Á. González has been partially financed by Spanish Ministerio de Educación y Ciencia through grants ENE2004-05038/FTN and ENE2007-63386/FTN and by the Junta de Castilla y León through grant VA032A06.

REFERENCES

1. H. R. Griem, *Spectral Line Broadening by Plasmas*, Academic Press, New York, 1974.
2. C. R. Vidal, J. Cooper, E. W. Smith, *Astrophys. J. Suppl. Ser.* **25**, 37–136 (1973).
3. A.V. Demura and D. Nikolić, Hb.nb - program for H_β asymmetry investigation (2001): `http://tesla.physics.wmich.edu/dn/programs.html`; A. V. Demura and G. V. Sholin, *J. Quant. Spectrosc. Radiat. Transfer* **15**, 881–899 (1975).
4. M. A. Gigosos, V. Cardenoso, *J. Phys. B* **29**, 4795–4838 (1996).
5. M. A. Gigosos, M. Á. González, V. Cardenoso, *Spectrochim. Acta B* **58**, 1489–1504 (2003).
6. V. Helbig and K. P. Nick, *J. Phys B: At. Mol. Phys.* **14**, 3573–3583 (1981).
7. C. Carlhoff, E. Karametz, J. H. Schäfer and J. Uhlenbusch, *J. Phys B* **19**, 2629–2637 (1986).
8. J. L. Chotin, J. L. Lemaire, J. P. Marque and F. Rostas, *J. Phys B* **11**, 2629–2637 (1986).
9. Z. Mijatović, M. Pavlov and S. Djurović, *J. Quant. Spectrosc. Radiat. Transfer* **38**, 209–210 (1987).
10. J. Halenka, *J. Quant. Spectrosc. Radiat. Transfer* **39**, 347–351 (1988).
11. J. Uhlenbusch and W. Viöl, *Contrib. Plasma Phys.* **29**, 459-467 (1989)
12. J. Uhlenbusch and W. Viöl, *J. Quant. Spectrosc. Radiat. Transfer* **44**, 47-56 (1990).
13. L. P. Kudrin and G. V. Sholin, *Doklady USSR* **7**, 1015–1019 (1963).
14. S. Djurović, D. Nikolić, I. Savić, S. Sörge, A. Demura, *Phys. Rev. E* **71**, 036407-1-036407-15 (2005).
15. H. R. Griem, *Plasma Spectroscopy*, McGraw-Hill, New York, 1964.
16. M. A. Gigisos, S. Mar, C. Perez, and M. I. de la Rosa, *Phys. Rev. E* **49**, 1575–1585 (1994).
17. M.A. Gigosos, M. Á. González and N. Konjević, *Eur. Phys. Journal D* **40**, 57–63 (2006).

On Asymmetry of Hydrogen Spectral Lines in Nonequlibrium Plasmas

A.V. Demura*, G.V. Demchenko* and D. Nikolić†

*HEPTI, RRC "Kurchatov institute". Kurchatov Square 1. Moscow 123182, Russia
†Department of Physics, Western Michigan University, Kalamazoo MI-49008, USA

The Standard Theory (ST) for hydrogen spectral lines asymmetry in dense plasmas is developed on the basis of many-body approach with the simultaneous account of the quadrupole interaction and the quadratic Stark effect. Conventionally for ST the plasma ions are considered as quasistatic and the plasma electrons as impact. The complex multiparametric scaling and similarity dependencies of the conventional asymmetry parameter for each separate Stark component and the H_β line contour as a whole is revealed and studied in detail under the influence of: ionic microfield inhomogeneity and quadratic Stark effect in ionic microfield, electronic collision shifts and impact widths, trivial asymmetry sources, the Boltzmann factor and the dipole intensity scaling factor of frequency to the fourth power for the case of emission line. The consistent inclusion of the latter two factors forced the redefinition of the line contour with limiting the value of negative detunings from the line center. The formation of asymmetry and its evolution under the influence of each of factors and their consecutive inclusion is followed in detail for the first time. The comparison with the precision experiment on stabilized arc data for H_β line, important for diagnostics and obtained in the group of Professor V. Helbig at Kiel University, is performed and analyzed from the line center up to the far line wings. It is demonstrated that the asymmetry of hydrogen spectral lines is the many-parametric sensitive function of broadening mechanisms [1]. In particular it is shown for the first time that this summary asymmetry also is the sensitive function of plasma equilibrium [1].

REFERENCES

1. A.V. Demura, G.V. Demchenko, D. Nikolić, *Eur. Phys. J. D* **46**, 111–127 (2008).

Kinetic Approach for Laser-Induced Plasmas

B. Omar and B. Rethfeld

Technical University of Kaiserslautern, Department of Physics, Erwin Schroedinger Str. 46, D-67663 Kaiserslautern, Germany.

Non-equilibrium distribution functions of electron gas and phonon gas are calculated for laser-induced plasmas occurring solids, excited with ultrashort intense laser pulses. The excitation during femtosecond irradiation and the subsequent thermalization of the free electrons, as well as the dynamics of phonons are described by kinetic equations. The microscopic collision processes, such as absorption by inverse bremsstrahlung, electron-electron, and electron-phonon interaction are considered by complete Boltzmann collision integrals. We apply our kinetic approach to the case of gold by taking the electron density of states into account, and compare with the case of excitation of aluminum.

The interaction of ultrashort laser pulse with material is an interesting topic for a broad field of both theoretical and experimental researches. Here, strongly coupled plasma is produced when a metal surface is irradiated with an intense fs-laser pulse. Ultrafast dynamical processes are influenced by the laser pulse properties, such as intensity and duration of radiation.

Microscopic processes in ultrashort laser pulse-induced plasmas have been investigated theoretically. In this presentation the inverse bremsstrahlung absorption, electron-electron collision and electron-phonon interaction are considered. The transient non-equilibrium evolution of electron distribution function due to excitation and the subsequent thermalization of the free electrons is studied by solving the complete collision terms of Boltzmann equation during and after irradiation, which describes the time resolved dynamical processes. The evolution of the energy distribution for both electrons and phonons are given by the coupled, nonlinear integro-differential equations:

$$\frac{\partial f(\mathbf{k})}{\partial t} = \left.\frac{\partial f(\mathbf{k})}{\partial t}\right|_{\mathrm{e-e}} + \left.\frac{\partial f(\mathbf{k})}{\partial t}\right|_{\mathrm{e-ph}} + \left.\frac{\partial f(\mathbf{k})}{\partial t}\right|_{\mathrm{Laser}}, \tag{1}$$

$$\frac{\partial g(\mathbf{q})}{\partial t} = \left.\frac{\partial g(\mathbf{q})}{\partial t}\right|_{\mathrm{ph-e}}, \tag{2}$$

where each terms on the right hand side denotes a complete Boltzmann collision integral. Starting with initial condition, at room temperature $T = 300\,\mathrm{K}$ and at time $t = 0$, the distribution of the electron gas $f(\mathbf{k})$ is given by Fermi-Dirac distribution function, while the phonon gas $g(\mathbf{q})$ is described by Bose-Einstein distribution functions. Here, $\mathbf{q}$ and $\mathbf{k}$ are the electron and phonon wave vectors, respectively.

This system has been investigated for aluminum by Rethfeld et al. [1], here we apply it for s-band of gold. The kinetic approach yields both temporal evolutions of the free-electron and phonon distributions. The electron distribution function is converted into a logarithmic function $\Phi(\mathbf{k},t) = -\ln[f(\mathbf{k},t)^{-1} - 1]$. This function is a straight line in an equilibrium system, where electrons are described by Fermi-Dirac distribution function. A deviation from equilibrium appears immediately with starting the laser pulse, which perturbs the regular distribution of the electron gas. In Fig. 1 the distribution is shown for gold at different times during and after irradiation. Electrons below Fermi level absorb one photon of energy $h\nu$ lead to increase the occupation number above Fermi level, at the same time the occupied states decreases below Fermi edge in the same rate. The occupation number is increased for energies up to $2h\nu$ if an excited electron absorb a further photon, consequently the Fermi edge appears in steps of photon energy. The excited electrons thermalize due to electron-electron collisions, which smoothes the steps toward thermal equilibrium. Furthermore, after irradiation electron-phonon interactions induce cooling of the electron gas by transferring energy to phonons via collisions. After thermalization and relaxation the equilibrium restored and the linear behavior of Φ can be observed again.

The electron transition probability is proportional to the quasistatically screened Coulomb potential. In this case the time-dependent screening wave number κ is calculated consistently at the current electron distribution function [2]

$$\kappa^2 = \frac{e^2 m_e}{\pi^2 \hbar^2 \varepsilon_0} \int_0^\infty f(k)\, dk\,, \tag{3}$$

where m_e is the effective mass of free electron in the conduction band.

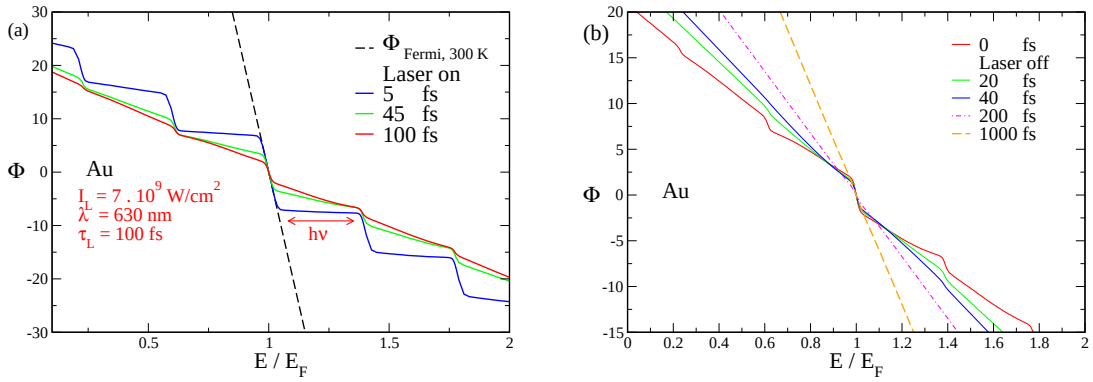

FIGURE 1. Temporal evolution of electron distribution in the conduction band of Au during (a) and after (b) irradiation with 100 fs rectangular-shape laser pulse with intensity 7×10^9 W/cm^2.

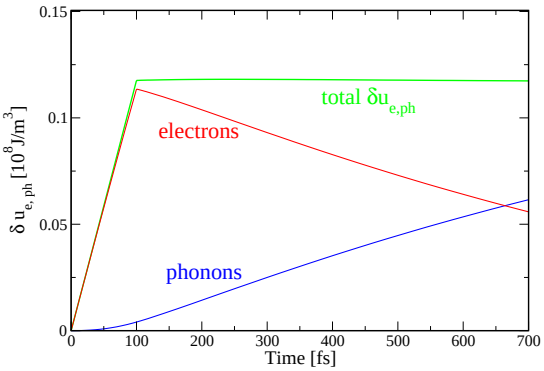

FIGURE 2. Transient energy density of the electron gas δu_e, the phonon gas δu_{ph}, and the total energy density $(\delta u_e + \delta u_{ph})$ for Au, irradiated with 100 fs laser pulse.

The transient energy density within electron gas is performed by

$$u_{\mathrm{e}} \quad = \quad \int_0^\infty E\, D(E)\, f(E,t)\, dE = u_{\mathrm{e}(T=300\,\mathrm{K},t=0)} + \delta u_{\mathrm{e}}\,, \tag{4}$$

where $D(E)$ is the electron density of states. The internal energy of phonons δu_{ph} is treated in analogy to the Eq. (4). The sum of both δu_e and δu_{ph} gives the total absorbed energy by the system, see Fig. 2. The constant energy absorbed during irradiation by electrons increased linearly due to small electron heat capacity, while the phonons remain cold. After irradiation, the system relaxes due to energy exchange between electrons and phonons, where the electrons are cooling down and the phonons are heating up.

In contrast to Al, the d-band electrons in Au lies within the conduction band at about 2.5 eV below the Fermi surface of free electrons in s-band. Therefore, secondary electrons may be excited strongly from the d-band even for a laser pulse with energy lower than 2.5 eV. Our kinetic approach for Au by considering intraband absorption is in progress.

REFERENCES

1. B. Rethfeld, A. Kaiser, M. Vicanek, and G. Simon, *Phys. Rev. B* **65**, 214303–214311 (2002).
2. R. Binder, H. S. Köhler, M. Bonitz, and N. Kwong, *Phys. Rev. B* **55**, 5110–5116 (1997).

QED theory of radiation emission and absorption lines for atoms and ions in a strong laser field

A.V.Glushkov

Odessa University, P.O.Box 24, Odessa-9, South-East, 65009, Ukraine
Institute for Spectroscopy of Russian Academy of Sciences, Troitsk, Moscow reg., 142090, Russia

The interaction of atomic systems with the external alternating fields, in particular, laser fields has been the subject of intensive experimental and theoretical investigation. The appearance of the powerful laser sources allowing to obtain the radiation field amplitude of the order of atomic field in the wide range of wavelengths results to the systematic investigation of the nonlinear interaction of radiation with atoms and molecules. Calculation of the deformation and shifts of the atomic emission and absorption lines in a strong laser field, definition of the k-photon emission and absorption probabilities and atomic levels shifts, study of laser emission quality effect on characteristics of atomic line, dynamical stabilization and field ionization etc are the most actual problems to be solved. Naturally, it is of the great interest to study a phenomenon of the multiphoton ionization. In this paper we present a consistent method for studying the interaction of atom with a realistic laser field, based on QED and S-matrix adiabatic formalism Gell-Mann and Low [1],[2], [3], [4]. In relativistic case the Gell-Mann and Low formula expressed an energy shift δE through the QED scattering matrix including the interaction with as the laser field as the photon vacuum field. It is more natural to describe the interaction of atom with the realistic laser field by means of the radiation emission and absorption lines. Their position and shape fully determine the spectroscopy of atom in a laser field. The radiation atomic lines can be described by moments of different orders $\mu_{\rm n}$. The first order moment is directly connected with the field shift and width of the corresponding resonances. The main contribution into $\mu_{\rm n}$ is given by the resonant range. The values $\mu_{\rm n}$ can be expanded into perturbation theory (PT) series [5], though in resonant range the PT can't be used for the transition probabilities. The effective Ivanov-Ivanova approach [2] is used for calculating the corresponding PT second order sums. As examples we present the results of numerical calculating the multi-photon resonance shift and width for transition 6S-6F in the atom of Cs (wavelength 1059nm) in a laser pulse of the Gaussian and soliton-like shapes. We present other numerical results regarding the Ne-like plasma multicharged ions radiation spectral lines too.

QED APPROACH TO SPECTROSCOPY OF ATOM IN A LASER FIELD

We describe the interaction of atom with laser radiation by means the Ivanov potential:

$$V(r,t) = V(r) \int {\rm d}\omega f(\omega - \omega_0) \sum_{n=-\infty}^{\infty} \cos[\omega_0 t + \omega_0 n\tau], \tag{1}$$

where n is the whole number. The potential V represents the infinite duration of laser pulses with known frequency τ. Here we consider the effects of interaction of an atom with the single pulse. The representation $V(rt)$ as the infinite sequence of pulses is a formal moment connected with the application of the stationary PT formalism. The function $f(\omega)$ is a Fourier component of the laser pulse. The condition $\int d\omega f^2(\omega)$=1 normalizes potential $V(rt)$ on the definite energy in a laser pulse. Let us consider the pulse with Lorentzian shape (coherent 1-mode pulse): $f(\omega) = N/(\omega^2 + \Delta^2)$, Gaussian shape (multi-mode chaotic laser pulse): $f(\omega)$ = Nexp[ln2(ω^2/Δ^2)], and soliton-like pulse of the following shape: f(t) = $N\, ch^{-1}[t/D]$.Further we will be interested by a cases of the Gaussian and soliton-like pulses. A case of the Lorentzian shape has been considered by us earlier [1].

The further program results in the calculating an imaginary part of the energy shift Im $E_\alpha(\omega_0)$ for any atomic level as a function of the laser pulse central frequency. The corresponding function has the shape of resonant curve. Each resonance is connected with the transition $\alpha - p$,in which the definite number of photons is absorbed or radiated. Let us consider following situation: $\alpha - p$ transition with the absorption of k photons(α, p-discrete levels). For the resonance which corresponds to this transition , we calculate the following values:

$$\delta\omega(p\alpha|k) = \int \prime {\rm d}\omega Im E_\alpha(\omega)(\omega - \omega_{p\alpha}/k)/N, \tag{2}$$

$$\mu_{\rm m} = \int \prime {\rm d}\omega Im E_\alpha(\omega)(\omega - \omega_{p\alpha}/k)^{\rm m}/N, \tag{3}$$

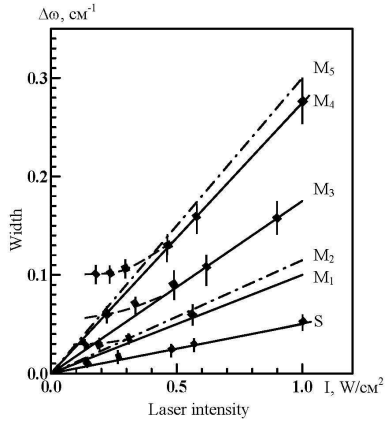

FIGURE 1. The multi-photon resonance width for transition 6S-6F in the atom of Cs (wavelength 1059nm) in dependence upon the laser intensity I: S- for single-mode Lorentz laser pulse; M_1, M_3, M_4- for multi-mode Gauss laser pulse respectively with line band 0.03cm^{-1}, 0.08cm^{-1} and 0.15cm^{-1}; M_2, M_5- for multi-mode soliton-type with line band 0.03 cm^{-1}and 0.15cm^{-1}; marker - experiment

where $\int \imath d\omega$ Im E_α is the normalizing multiplier; $\omega_{p\alpha}$ is a position of the non-shifted line for atomic transition $\alpha - p, \delta\omega(pa|k)$ is the line shift under k-photon absorption and $\omega_{p\alpha} = \omega_{p\alpha} + k \times \delta\omega(p\alpha|k)$. The first moments μ_1, μ_2 and $\mu_3$determine the atomic line center shift, its dispersion and coefficient of the asymmetry. To calculate μ_m, we need to get an expansion of E_α to PT series: $E_\alpha = \sum E_\alpha^{(2k)}$ (ω_0). To get this expansion, we use method, based on the Gell-Mann and Low adiabatic formula for δE_α [1], [2].

SOME RESULTS AND DISCUSSION

As example, in figure 1 we present the results of calculation for the multi-photon resonance width for transition 6S-6F in the atom of Cs (wavelength 1059nm) in dependence upon the laser intensity. In general there is a physically reasonable agreement between our theory and high-qualitative experiment [6]. Analysis shows that the shift and width of the multi-photon resonance line in a case of interaction of an atom with the multimode laser pulse is greater than the corresponding resonance shift and width in a case of interaction of an atom with the single-mode laser pulse. It is corresponding to the experimental data. From physical point of view it is provided by action of the photon-correlation effects and influence of the multimodity of the laser pulse.

ACKNOWLEDGMENTS

Author is very much thankful to Profs. Ivanov L.N., Ivanova E.P., Brandas E., Kohn W., Wilson S. for useful comments

REFERENCES

1. A. V. Glushkov, and L. N. Ivanov, *Phys. Letters* **A170**, 33–38 (1992).
2. L.-N. Ivanov et al., *Phys. Rev. A* **48**, 4365–4380 (1993).
3. A. V. Glushkov et al., *Int. Journ. Quant. Chem.* **99**, 889–938 (2004).
4. Á. Glushkov, 'Energy Approach to Resonance states of compound super-heavy nucleus and EPPP in heavy nucleus collisions," in *LEAP'05*, edited by D. Grzonka et al., AIP Series Vol.796, American Institute of Physics, New York, 2005, pp. 206–210.
5. A. Glushkov et al., "QED calculation of heavy multicharged ions with account for the correlation, radiative and nuclear effects," in *Recent Advances in Theor. Phys. and Chem. Systems*, edited by J. Maruani et al., Springer, Paris, 2006, Vol.15, pp. 285–320.
6. L.-A. Lompre et al., *J.Phys. B.* **14**, 4307–4322 (1981).

Experimental Stark Shift of Some Xe II UV Lines

S. Djurović*, R. J. Peláez†, M. Ćirišan*, J. A. Aparicio† and S. Mar†

*Faculty of Sciences, Department of Physics, Trg Dositeja Obradovića 4, 21000 Novi Sad, Serbia
†Departamento de Fisica Teórica y Óptica, Facultad de Ciencias, Universidad de Valladolid, 47071 Valladolid, Spain

INTRODUCTION

Stark broadening and shift of Xe II lines have been the subject of many experimental [1 -3 and References therein] and theoretical studies [4, 5].

Here, the results of Stark shift measurements for six Xe II lines are presented. All given results are here reported for the first time. Two lines belong to 5d – 6p, two to 5d – 7p and one to 5d – 4f transition. In this experiment pulsed arc plasma made of mixture of 95% helium and 5% xenon was used. Measured electron densities and temperatures were in the range of $(0.2 – 1.8) \cdot 10^{23}$ m^{-3} and 18300 – 25500 K respectively.

EXPERIMENTAL

Experimental apparatus and diagnostic methods are described elsewhere [6, 7]. Excitation unit contains a capacitor bank of 20 μF, charged up to 9.2 kV approximately. The mixture of He-Xe at a pressure of $3.0 \cdot 10^3$ Pa continuously flows through the discharge lamp. Plasma electron density was determined by two-wavelength interferometry, with an error band lower than 10%. The excitation temperature was determined by Boltzmann-plot technique. Estimated error for temperature determination is lower than 15%.

RESULTS

Measured Stark shifts are shown in table 1. In the first two columns, configurations and Terms are given. Next two columns present the line wavelengths and the measured shifts. The wavelengths are taken from [8]. The measurements given in table 1 correspond to temperature of 22000 K and are normalized to electron density of 10^{23} m^{-3}.

TABLE 1. Experimental Stark shift of some Xe II lines

Configurations	Terms	Wavelength (nm)	d_m (pm)
$5p^4$ (^{3}P$_2$) $5d$ – $5p^4$ (^{3}P$_1$) $6p$	$[3]_{7/2}$ - $[2]^\circ_{5/2}$	361.237	|d| < 1
	$[4]_{7/2}$ - $[3]^\circ_{5/2}$	365.774	-2.0
$5p^4$ (^{3}P$_2$) $5d$ – $5p^4$ (^{1}D$_2$) $6p$	$[0]_{1/2}$ - $[1]^\circ_{1/2}$	373.118	|d| < 1
$5p^4$ (^{3}P$_0$) $5d$ – $5p^4$ (^{3}P$_2$) $7p$	$[2]_{3/2}$ - $[2]^\circ_{5/2}$	314.899	-11.7
$5p^4$ (^{3}P$_1$) $5d$ – $5p^4$ (^{3}P$_2$) 4f	$[3]_{7/2}$ - $[2]^\circ_{5/2}$	314.502	|d| < 1
$5p^4$ (^{3}P$_1$) $5d$ – $5p^4$ (^{3}P$_2$) $7p$	$[2]_{5/2}$ - $[2]^\circ_{5/2}$	378.323	-9.1

All measured lines have low intensities. Most of the measured lines have a very small shift, close to zero and at the same time close to the limit of the measurement precision (± 1 pm). This is illustrated in figure 1. Only for two lines, 314.899 nm and 378.323 nm, shift direction is clearly determined (see fig. 2).

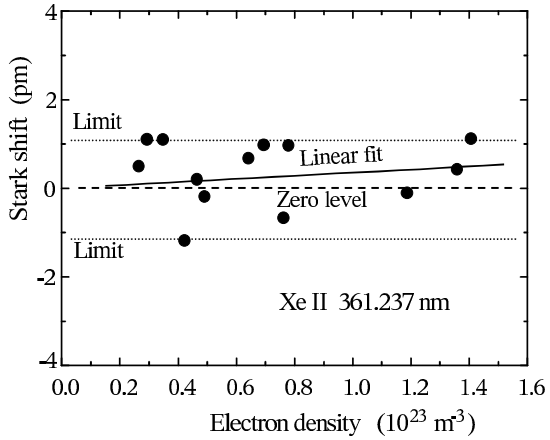

FIGURE 1. Stark shift of Xe II 361.237 nm line

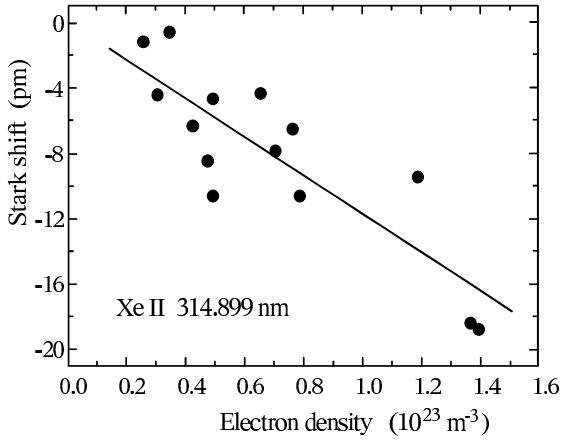

FIGURE 2. Stark shift of Xe II 314.899 nm line

For measuring the line position Lorentzian function was used. The procedure for line shift determination is described in [9].

ACKNOWLEDGMENTS

The authors thank S. González for his collaboration in the experimental arrangement, and the Spanish Dirección General de Investigación Científica y Técnica (Ministerio de Educatión y Ciencia) and the Consejería de Educatión y Cultura de Castilla y León for their financial support Ander contract No. FIS2005-03155 and VA015A05 respectively. Dr. J. Aparicio wonts to express his personal acknowledgment to the Organización Nacional de Ciegos de España (ONCE) for help. Dr. S. Djurović thanks to Ministry of Science, Republic of Serbia for partial support (Project 141024).

REFERENCES

1. N. Konjević, M. S. Dimitrijević, and W. L. Wiese, *J. Phys. Chem. Data* **13**, 649-686 (1984).
2. N. Konjević, and W. L. Wiese, *J. Phys. Chem. Data* **19**, 1307-1385 (1990).
3. N. Konjević, A. Lesage, J. R. Fuhr, and W. L. Wiese, *J. Phys. Chem. Data* **31**, 819-927 (2002).
4. L. Č. Popović, and M. S. Dimitrijević, *Astron. Astrophys. Suppl. Ser.* **116**, 359-365 (1996).
5. H. O. Di Rocco, *Nuovo Cimento* **12** *D*, 1485-1490 (1990).
6. S. Mar, J. Aparicio, M. I. de la Rosa, J. A. del Val, M. A. Gigosos, and C. Perez, *J. Phys. B* **33**, 1169-1184 (2000).
7. M. A. Gigosos, S. Mar, C. Perez, and M. I. de la Rosa, *Phys. Rev. E* **49**, 1575-1585 (1994).
8. A. R. Striganov and N. S. Sventickij, *Tables of Spectral lines of Neutral and Ionized Atoms*, New York – Washington, Plenum, 1968, pp. 581-597.
9. M. Ćirišan, R. J. Peláez, S. Djurović, J. A. Aparicio and S. Mar, *J. Phys. B* **40**, 3477-3490 (2007).

Stark Shift Measurement of Some Xe III Lines

S. Djurović*, R. J. Peláez†, M. Ćirišan*, J. A. Aparicio† and S. Mar†

*Faculty of Sciences, Department of Physics, Trg Dositeja Obradovića 4, 21000 Novi Sad, Serbia
†Departamento de Fisica Teórica y Óptica, Facultad de Ciencias, Universidad de Valladolid, 47071 Valladolid, Spain

INTRODUCTION

Examination of ionized xenon spectrum is of a great interest for plasma diagnostic purposes, theory testing and different applications. In this paper, we present Stark shift data for one blue and five UV Xe III lines. One line belongs to the 5d – 6p transition, while all other lines belong to 6s – 6p transition. Most of the existing papers are devoted to Stark width measurements and only one paper [1] deals with shift data of the lines studied herein.

A low-pressure pulsed arc with 95% of helium and 5% of xenon was used as a plasma source. All measurements were performed under following plasma conditions: electron density $(0.2 – 1.4) \cdot 10^{23}$ m^{-3} and electron temperature 18000 – 23000 K.

EXPERIMENTAL

The experimental apparatus was described in detail in [2]. Plasma was created by discharging a capacitor bank of 20 μF, charged up to 9 kV through the glass tube. Plasma electron density was determined by two-wavelength interferometry, with an error band lower than 10%. The electron temperature was determined by Boltzmann-plot technique using Xe II lines. Estimated error for temperature determination is lower than 15%.

RESULTS AND DISCUSSION

Measured Xe III line Stark shifts are given in table 1. In the first two columns, configurations and Terms are given. Next two columns present the line wavelengths and the measured shifts. The wavelengths are taken from [3]. The measurements given in table 1 correspond to temperature of 21000 K and are normalized to electron density of 10^{23} m^{-3}. The measured shifts are very small and experimental error was estimated to up to 40%. Some points can even deviate from the fitted linear trend for up to 100%. This is illustrated in figure 1.

TABLE 1. Experimental Stark shift of Xe III lines

Configuration	Term	Wavelength (nm)	d_m (pm)	$\frac{d_m}{d_{th}}$	d [1] (pm)
$(^2D^o)6s$-$(^2D^o)6p$	$^1D_2^o - {}^1P_1$	465.778	-2.2	0.18	4.4
	$^3S_1^o - {}^3P_1$	330.680	-6.4		3.3
$(^2P^o)6s$-$(^2P^o)6p$	$^3P_1^o - {}^3D_2$	377.632	-3.6		-17.1
	$^3P_0^o - {}^3P_1$	363.214	-4.2		4.0
$(^2P^o)5d$-$(^2P^o)6p$	$^3D_2^o - {}^3S_1$	353.994	-2.2		22.6
$(^2P^o)6s$-$(^2P^o)6p$	$^1P_1^o - {}^1P_1$	377.253	-7.9		4.3

The procedure for line shift determination is described in [4]. For measuring the line position, Lorentzian function was used.

Only one shift result is compared with modified semi-empirical calculation [5], d_{th} (column five in table 1). This is the only case for which the complete set of perturbing levels necessary for the calculations was available. Concerning the experimental error, it is only the sign of the shift that is in agreement with semi-empirical calculation.

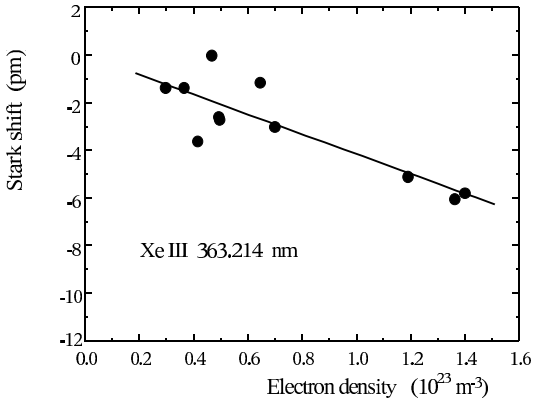

FIGURE 1. Stark shift of Xe III 363.214 nm line

In the last column of the table 1 shift results from [1] are given. These data are also normalized to electron density of 10^{23} m^{-3}, but are given for the temperature of 10000 K, as is given in [1]. The disagreement of present results with the results from [1] is obvious, even in the shift sign. The explanation of this disagreement is similar to the one given in [6] for Xe III line halfwidths.

So, conclusion is that more additional measurements would be useful to clarifying these disagreements.

ACKNOWLEDGMENTS

The authors thank S. González for his collaboration in the experimental arrangement, and the Spanish Dirección General de Investigación Científica y Técnica (Ministerio de Educatión y Ciencia) and the Consejería de Educatión y Cultura de Castilla y León for their financial support Ander contract No. FIS2005-03155 and VA015A05 respectively. Dr. J. Aparicio wonts to express his personal acknowledgment to the Organización Nacional de Ciegos de España (ONCE) for help. Dr. S. Djurović thanks to Ministry of Science, Republic of Serbia for partial support (Project 141024).

REFERENCES

1. H. O. Di Rocco, *Spectrosc. Lett.* **23**, 283-292 (1990).
2. S. Djurović, R. J. Peláez, M. Ćirišan, J. A. Aparicio, and S. Mar, *J. Phys. B: At. Mol. Opt. Phys.* **39**, 2901-2916 (2006).
3. A. R. Striganov and N. S. Sventickij, *Tables of Spectral lines of Neutral and Ionized Atoms*, New York – Washington, Plenum, 1968, pp. 581-597.
4. M. Ćirišan, R. J. Peláez, S. Djurović, J. A. Aparicio, and S. Mar, *J. Phys. B: At. Mol. Opt. Phys.* **40**, 3477-3490 (2007).
5. M. S. Dimitrijević, and V. Kršljanin, *Astron. Astrophys.* **165**, 269-274 (1986).
6. R. J. Peláez, M. Ćirišan, S. Djurović, J. A. Aparicio, and S. Mar, *J. Phys. B: At. Mol. Opt. Phys.* **39**, 5013-5022 (2006).

Stark parameters irregularities of Xe II lines obtained by transitions from $(^3P_1)6p$ levels.

S. Mar*, R. J. Peláez*, S. Djurović†, M. Ćirisan†, F. Rodríguez* and J. A. Aparicio*

*Departamento de Física Teórica Atómica y Óptica, Facultad de Ciencias, Universidad de Valladolid, 47071 Valladolid, Spain.
†Department of Physics, Faculty of Sciences, Trg Dositeja Obradovića 4, 21000 Novi Sad, Serbia.

INTRODUCTION

Stark widths and shifts of some Xe II lines belonging to the supermultiplets with upper levels $(^3P_1)6p$ were measured using a pulsed discharge lamp. Plasma parameters, i.e. electron density and temperature, in this experiment were in the range from 0.2 to $1.4\times10^{23}m^{-3}$ and from 18000 to 23000 K, respectively. Lines obtained by transitions from levels $(^3P_1)6p$ show some strong intra-supermultiplet irregularities in their Stark widths and shifts. These results and the measurements obtained in previous works were used here to analyse the main irregularities that can appear in the case of Xe II. This study may be very useful for obtaining Stark parameters of non-measured lines, using the known parameters of other lines belonging to similar transitions [1, 2].

MEASUREMENTS AND RESULTS

The measurements were performed in an arc pulsed plasma. The most important details concerning the experimental apparatus, plasma generation and synchronization were previously published in [3, 4]. The pulse was created by discharging a capacitor bank of 20 μF charged up to 9000 V in a gas mixture of 5% of Xe and 95% of He. The maximal electron density was $1.4\times10^{23}m^{-3}$. Electron temperature was determined by a Boltzmann-plot of Xe II lines and it was maximal at 40 μs (T_e = 23000 K).

Fifteen instants of the plasma life, at which spectroscopic measurements were performed, were considered for obtaining the Stark width and shift for each line. Fourteen widths (w_S) and eighteen shifts (d_S) were measured for Xe II lines obtained by transitions from levels $(^3P_1)6p$. A good agreement with the most relevant works has been obtained.

DISCUSSION

In Table 1 Stark data belonging to the lines obtained by transitions from levels $(^3P_1)6p$ are shown. The measurements correspond to temperature of 22000 K and are normalized to electron density of $1.0\times10^{23}m^{-3}$. It can be clearly seen that all Stark widths and shifts are very similar, with exception of those lines whose upper level is $(^3P_1)6p[1]^o_{3/2}$. Although in contradiction with the theory, some explanation could be given by the closeness of $(^1D_2)5d[2]_{5/2}$ level (12.5 cm^{-1} above it). According to this assumption, this perturbation effect would strongly affect these transitions by producing an additional broadening and additional shift to the red (due to the relative position of the perturbing level), as can be seen in all four supermultiplets in Table 1.

Some irregularities in Stark shifts of Xe II have been found, as well. This is not usual for other elements. It may be due to the complex structure of Xe II energy scheme. LS coupling and jK coupling do not describe correctly some levels themselves, and for multielectronic atoms like this one, it is usual that strong perturbations exist. All these factors must be considered for obtaining the Xe II Stark parameters using the known parameters' values of the lines from similar transitions.

ACKNOWLEDGMENTS

The authors thank S. González for his collaboration in the experimental arrangement, and the Spanish Dirección General de Investigación Científica y Técnica (Ministerio de Educación y Ciencia) and the Consejería de Educación y

TABLE 1. Stark widths and shifts of four supermultiplets involving $(^3P_1)6p[1]^o_{3/2}$ level

Upper level	**J**	**Lower level**	**J**	**λ (nm)**	**w_S(pm)**	**Acc.**	**d_S(pm)**	**Acc.**
$(^3P_1)6p[2]^o$	5/2	$(^3P_2)6s[2]$	5/2	332.746	21.53	<30%	-5.62	<20%
	3/2			356.430			-4.30	<30%
$(^3\mathbf{P_1})\mathbf{6p}[\mathbf{1}]^\mathbf{o}$	**3/2**	$(^3P_2)6s[2]$	3/2	342.073	33.67	<30%	3.87	<20%
$(^3P_1)6p[2]^o$	5/2	$(^3P_1)6s[1]$	3/2	492.148	46.47	<20%	-4.75	<20%
	3/2			488.730	47.86	<20%	>-1.5	
$(^3\mathbf{P_1})\mathbf{6p}[\mathbf{1}]^\mathbf{o}$	**3/2**		1/2	575.103	105.0	<10%	22.42	
	1/2			565.938	66.66	<20%	-7.6	
$(^3P_1)6p[0]^o$	1/2		3/2	543.896	44.8	<20%	-5.35	<15%
$(^3P_1)6p[2]^o$	3/2	$(^3P_0)6s[0]$	1/2	452.421	39.1	<30%	>-1.5	
$(^3\mathbf{P_1})\mathbf{6p}[\mathbf{1}]^\mathbf{o}$	**3/2**			432.182	72.1	<30%	7.87	
	1/2			426.984	36.75	<20%	-6.09	<20%
$(^3P_1)6p[0]^o$	1/2			499.303			-10.96	<30%
$(^3P_1)6p[2]^o$	5/2	$(^3P_2)5d[3]$	7/2	361.237	27.04	<30%	<1.0	
	3/2	$(^3P_2)5d[2]$	3/2	367.257			3.07	<30%
		$(^3P_2)5d[0]$	1/2	577.639	57.56	<20%	4.69	<20%
$(^3\mathbf{P_1})\mathbf{6p}[\mathbf{1}]^\mathbf{o}$	**3/2**	$(^3P_2)5d[1]$	3/2	526.831	115.1	<30%	3.24	<30%
	1/2	$(^3P_2)5d[0]$	1/2	536.807	55.57	<30%	-7.91	<20%
$(^3P_1)6p[0]^o$	1/2	$(^3P_2)5d[2]$	3/2	397.559			>-1.5	

Cultura de Castilla y León for their financial support under contracts No. FIS2005-03155 and VA015A05 respectively. Dr. J. A. Aparicio wants to express his personal acknowledgement to the Organización Nacional de Ciegos de España (ONCE) for help. Dr. S. Djurović thanks to Ministry of Science, Republic of Serbia for partial support (Project 141024).

REFERENCES

1. W. L. Wiese and N. Konjević, *J. Quant. Spectrosc. Radiat. Transfer* **28**, 185, (1982).
2. W. L. Wiese and N. Konjević, *J. Quant. Spectrosc. Radiat. Transfer* **47**, 185, (1992).
3. J. A. del Val, S. Mar, M. A. Gigosos, I. de la Rosa, C. Pérez and V. R. González, *Jpn. J. Appl. Phys.* **37**, 4177, (1998).
4. J. A. Aparicio, M. A. Gigosos, V. R. González, C. Pérez, M. I. de la Rosa and S. Mar, *J. Phys. B* **31**, 1029, (1998).

Stark regularities in the multiplet $(^3\mathrm{P})3\mathrm{p}(^4\mathrm{P^o}) - (^3\mathrm{P})3\mathrm{d}(^4\mathrm{D})$ of Ne II

R. J. Peláez*, S. Djurović†, M. Cirisan†, F. Rodríguez*, J. A. Aparicio* and S. Mar*

*Departamento de Física Teórica Atómica y Óptica, Facultad de Ciencias, Universidad de Valladolid, 47071 Valladolid, Spain.
†Department of Physics, Faculty of Sciences, Trg Dositeja Obradovića 4, 21000 Novi Sad, Serbia.

INTRODUCTION

In the last few years, different trends and regularities of Stark parameters (width and shifts of spectral lines) have been studied. According to the semi-empirical approximation, the maximal differences between the values of Stark parameters of the lines belonging to the same multiplet are supposed to be lower than 1% for Stark widths and lower than 10% for Stark shifts [1, 2]. The conditions related with atomic structure of the element are responsible for regular or irregular behaviours of the Stark parameters. The absence of very close perturbing levels make Ne II as a good candidate for analyse the regularities. In this work Ne II Stark parameters have been measured and the regularities are analyzed in the $^4\mathrm{P^o} - ^4\mathrm{D}$ multiplet of the transitions $(^3\mathrm{P})3\mathrm{p} - (^3\mathrm{P})3\mathrm{d}$.

MEASUREMENTS AND RESULTS

The measurements were performed using a pulsed arc as a plasma source. All details concerning the experimental apparatus, plasma generation and synchronization are previously published in [3, 4]. Herein, we will only mention the most important details of the present experiment. The pulse was created by discharging a capacitor bank of 20 μF charged up to 8000 V, through a cylindrical tube filled with gas under a low pressure. Under these conditions Ne II spectral lines had a lifetime of about 70 μs. The gas (30% Ne and 70% He) was preionized in order to assure a good reproducibility of the discharges. Spectroscopic measurements were performed in the second order of diffraction. The dispersion of our spectrometer was 2.2 pm/channel at 300 nm.

Two wavelength interferometric method was used for electron density determination. Two laser beams of 543.0 nm and 632.8 nm wavelengths, were passing through the plasma source in the axial direction. The maximal electron density was $2\times10^{23}\mathrm{m}^{-3}$. Electron temperature, determined by a Botzmann-plot of Ne II lines, was maximal at 30μs (T_e=43000 K).

For these plasma conditions, the Stark effect is the most relevant broadening mechanism. A deconvolution procedure was used in order to exclude other broadening mechanisms, like Doppler effect and instrumental function. For obtaining the Stark widths of spectral lines, only the instants of the plasma life with higher values of N_e were considered.

In order to obtain the relative Stark shifts, centre positions of Ne II lines for different instants during the plasma life were plotted versus the corresponding N_e values and a linear fit was made. To get the absolute shift values, the displacement was performed with assumption that shift should be zero at null electron density. Spectroscopic measurements performed at six different instants of the plasma life have been considered for obtaining the Stark shift of each spectral line. Altogether seven widths and seven shifts have been measured for the lines belonging to the multiplet $^4\mathrm{P^o} - ^4\mathrm{D}$. The final results of Stark parameters and their accuracies are shown in the table 1.

DISCUSSION

In the figure 1 the profiles of seven lines belonging to the Ne II multiplet $(^3\mathrm{P})3\mathrm{p}(^4\mathrm{P^o}) - (^3\mathrm{P})3\mathrm{d}(^4\mathrm{D})$ are shown. They were previously normalized by the area. A clear coinciding between these profiles can be seen. The Stark parameters measured for these lines show also clear regularities. Maximal difference between the Stark widths of these lines is lower than 10 %, and in case of Stark shifts is lower than 1 pm. These values are very close to the uncertainties of our experiment.

The regularities obtained within this multiplet are due to the atomic energy structure of Ne II. Levels of this element are determined with high precision in LS coupling scheme and there is an absence of nearby perturbing levels in

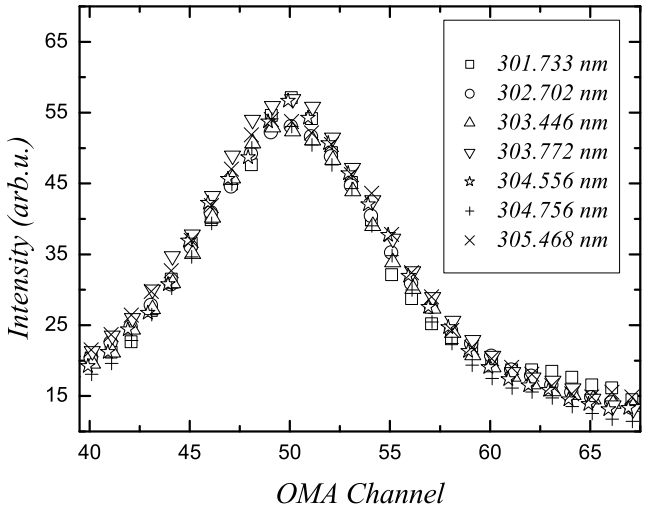

FIGURE 1. Shape of the lines in the multiplet $(^3\mathrm{P})3\mathrm{p}(^4\mathrm{P^o}) - (^3\mathrm{P})3\mathrm{d}(^4\mathrm{D})$. All lines have been normalized by the area.

TABLE 1. Stark parameters of the lines in the multiplet $(^3\mathrm{P})3\mathrm{p}(^4\mathrm{P^o}) - (^3\mathrm{P})3\mathrm{d}(^4\mathrm{D})$ normalized at $N_e=10^{23}\mathrm{m}^{-3}$.

Transition	λ(nm)	w_S(pm)	Acc.(%)	d_S(pm)	Acc.(pm)
$(^3\mathrm{P})3\mathrm{p}(^4\mathrm{P^o}) - (^3\mathrm{P})3\mathrm{d}(^4\mathrm{D})$	301.733	13.36	30	2.92	1.5
	302.702	14.34	20	3.18	1.5
	303.446	14.74	30	3.51	1.5
	303.772	14.01	30	3.66	2.0
	304.556	13.68	20	3.01	2.0
	304.756	14.21	20	3.77	2.0
	305.468	14.33	20	3.09	2.0

the case of analyzed transitions. Therefore, clear regularities obtained in this work can be used for predicting Stark parameters of non-measured lines in the same multiplet, supermultiplet or transition.

ACKNOWLEDGMENTS

The authors thank S. González for his collaboration in the experimental arrangement, and the Spanish Dirección General de Investigación Científica y Técnica (Ministerio de Educación y Ciencia) and the Consejería de Educación y Cultura de Castilla y León for their financial support under contracts No. FIS2005-03155 and VA015A05 respectively. Dr. J. A. Aparicio wants to express his personal acknowledgement to the Organización Nacional de Ciegos de España (ONCE) for help. Dr. S. Djurović thanks to Ministry of Science, Republic of Serbia for partial support (Project 141024).

REFERENCES

1. W. L. Wiese and N. Konjević, *J. Quant. Spectrosc. Radiat. Transfer* **28**, 185, (1982).
2. W. L. Wiese and N. Konjević, *J. Quant. Spectrosc. Radiat. Transfer* **47**, 185, (1992).
3. J. A. del Val, S. Mar, M. A. Gigosos, I. de la Rosa, C. Pérez and V. R. González, *Jpn. J. Appl. Phys.* **37**, 4177, (1998).
4. J. A. Aparicio, M. A. Gigosos, V. R. González, C. Pérez, M. I. de la Rosa and S. Mar, *J. Phys. B* **31**, 1029, (1998).

Zeeman-Stark profiles of low-n hydrogen lines in near impact regime

J. Rosato, H. Capes, S. Ferri, L. Godbert-Mouret, M. Koubiti, Y. Marandet and R. Stamm

PIIM, UMR 6633 Université de Provence - CNRS, Centre de St Jérôme, Case 232, F-13397 Marseille Cedex 20, France

Zeeman-Stark profiles of hydrogen lines with low principal quantum number n are investigated when the impact theory is almost applicable for the ions. This is, for example, the case of the first Lyman and Balmer lines in tokamak edge plasmas, where typically one has τ_{coll}/τ_{int}, $\rho_W/r_0 \leq 0.5$ (here ρ_W, r_0, τ_{int}, and τ_{coll} respectively denote the ion Weisskopf radius, the average atom-perturber distance, the time of interest and the collision time). If the magnetic field is sufficiently high, the Stark broadening of the Zeeman components can be strongly sensitive to the magnetic field intensity. This is related to the nature of Stark effect mechanism, which is linear on the degenerate Zeeman sublevels and quadratic on the nondegenerate ones. A direct consequence of this result is that significant errors could be made in the interpretation of measurements if the Zeeman sublevel structure is not properly taken into account in Stark broadening description. In this work, we investigate the first lines of Lyman and Balmer series using both the impact theory and the numerical simulation method with Zeeman effect. In the impact theory approach, we use a model for the collision operator which is founded on the Griem-Baranger-Kolb-Oertel formalism [1]. The latter is able to retain the quadratic Stark effect acting on the nondegenerate Zeeman sublevels, and yields the same separation of the collision operator into adiabatic and non-adiabatic parts as such reported in the generalized theory of Derevianko-Oks [2]. In the numerical approach, we use a recently developed computer simulation method which is specialized for low coupled magnetized plasmas such as found in the edge of tokamaks [3]. The electric microfield is calculated from a quasi-particle model similar to such presented in [4], using a cubic box with periodic boundary conditions. The Schrödinger's equation is solved for the evolution operator by a first order Euler method with variable time steps. In the case of low density values, the impact theory is found to be in a quite good agreement with the results of the simulation method. An important narrowing of the lateral Zeeman components is predicted by both the numerical simulation method and the impact theory. We give here an interpretation of this result in the frame of the impact theory. In the case of higher density, significant differences appear between the impact and simulation results on the central Zeeman component. Discussions of these non-impacts effects are tentatively made in term of the ratios τ_{coll}/τ_{int} and ρ_W/r_0. Comparisons to experiments carried out at FOM on the Pilot-PSI device are discussed in [5]. Applications to opacity calculations in divertor plasmas are presented in [6].

ACKNOWLEDGMENTS

This work is partially supported by the project "Radiation absorption effects in edge plasmas" of the fédération de recherche sur la fusion par confinement magnétique, in the frame of the LRC DSM 99-14 (Laboratoire PIIM / CEA Cadarache).

REFERENCES

1. H. R. Griem *et al.*, *Phys. Rev.* **125**, 177–195 (1962).
2. A. Derevianko and E. Oks, *Phys. Rev. Lett.* **73**, 2059–2062 (1994).
3. J. Rosato *et al.*, *Contrib. Plasma Phys.* **48**, 153–157 (2008).
4. R. Stamm and D. Voslamber, *J. Quant. Spectrosc. Radiat. Transfer* **22**, 599–609 (1979).
5. S. Ferri *et al.*, these proceedings.
6. J. Rosato, V. Kotov, and D. Reiter, these proceedings.

Emission spectroscopy of Hydrogen lines in magnetized plasmas: Application to PSI studies under ITER relevant conditions.

S. Ferri, J. Rosato, Y. Marandet, L. Godbert-Mouret, M. Koubiti, C. Mossé, and R. Stamm* and A.E. Shumack, J.Westerhout, J. Rapp and G. van Rooij†

*Laboratoire de Physique des Interactions Ioniques et Moléculaires, UMR6633, Case 232, St Jérôme, Université de Provence, 13397 Marseille cedex 20
†FOM Institute for Plasma Physics Rijnhuizen, The Netherlands

ABSTRACT

Modelling of Hydrogen line profiles in ITER divertor plasma entails several challenges. Because of the high density ($N_e > 10^{20} m^{-3}$) and low temperature ($kT_e < 2eV$) expected in the magnetized plasma close to the wall, both Stark broadening and Zeeman splitting have to be taken into account in the line shape calculations [1]. Moreover, the conditions are such that the ion dynamics has to be retained in Stark broadening calculations, and the presence of a high magnetic field ($B \sim 5T$) introduces couplings between Stark and Zeeman effects, which can significantly alter the profile [2, 3]. We present here Balmer lines obtained by numerical simulations based on Molecular Dynamics technique of the plasma in an external magnetic field. Direct integration of the semi-classical evolution equation of the emitter, [4, 5] is performed retaining both electric microfields and magnetic field perturbations. The simulated profiles are compared to experimental ones obtained in Plasma Surface Interaction (PSI) experiments which are carried out on Pilot-PSI of FOM [6, 7]. This linear plasma generator provides an interesting setting for checking line profile models because its plasma conditions (N_e, T_e) are relevant to the ITER divertor, and an Optical Emission Spectroscopy (OES) setup coupled to a Thomson scattering diagnostic is available [8, 9]. The magnetic field on Pilot-PSI is typically 1.6 T. The currently being build Magnum-PSI will have a stationary magnetic field of 3 T. Perspectives in terms of Stark-Zeeman spectroscopy are discussed. Comparison between simulations and Hγ profiles obtained in Pilot-PSI in experiments carried out with increasing densities is presented.

ACKNOWLEDGMENTS

This work is supported by the project "Radiation absorption effects in edge plasmas" of the fédération de recherche sur la fusion magnétique, in the frame of the LRC DSM 99-14 (Laboratoire PIIM/CEA Cadarache)

REFERENCES

1. Y. Marandet *et al.*, *Nucl. fusion* **44**, S118 (2004).
2. A. Derevianko and E. Oks, *Phys. Rev. Lett.* **73**, 2059 (1994).
3. J. Rosato, this conference.
4. B. Talin *et al.*, *J. Phys. A: Math. Gen.* **36**, 6049 (2003).
5. E. Dufour *et al.*, *Phys. Rev. E* **71**, 066409 (2005).
6. A.W. Kleyn , *Vacuum* **80**, 1098 (2006).
7. J. Westerhout *et al.*, *Phys. Scr* **T128**, 18 (2007).
8. G. J. van Rooij *et al.*, *Appl. Phys. Lett.* **90**, 121501 (2007).
9. J. van der Meiden *et al.*, *Rev. Sci. Instr.* **79**, 013505 (2008).

Line shape calculations based on slow and fast micro-field components separation in moderately coupled hydrogen plasmas.

S. Ferri, A.Calisti, C. Mossé and B.Talin *, M.A. Gigosos and M.A. González† and V. Lisitsa**

*Laboratoire PIIM, Université de Provence, CNRS, Case 232 Centre St Jérôme, 13397 Marseille cedex 20
†Departemento de Óptica y Física Aplicada, Facultad de Ciencias, Universidad de Valladolid, 47071 Valladolid, Spain
**Russian Research Center, Kurchatov Institute, Moscow, 123182, Russia

ABSTRACT

Taking advantage of well controlled molecular dynamics (MD) simulations of partially ionized hydrogen plasmas, the concept of microfield partition is revisited, [1, 2]. Statistically independent fast and slow fluctuation components of the electric microfield are redefined in the following way: averaging the electronic field out on time, $\overline{\vec{E}_e(t)}_{\Delta t}$, the field $\vec{E}_{F,\Delta t}(t) = \vec{E}_e(t) - \overline{\vec{E}_e(t)}_{\Delta t}$ is defined as a fast component of the total local field. The definition of the slow component that conserves the total field, follows: $\vec{E}_{S,\Delta t}(t) = \vec{E}_i(t) + \overline{\vec{E}_e(t)}_{\Delta t}$. These definitions depend on a variable periods of time $\Delta t \ll \tau_i$, where τ_i is the characteristic time of the ionic field. Fast and slow characteristics of the field can get a more precise meaning by comparison to a time τ_d which is the typical relaxation time of the dipole autocorrelation function of the line under study. The relation with neutral hydrogen lines radiated by coupled plasmas of proton and electron is considered here. The implication of such separation on a few Lyman and Balmer lines is presented for moderately coupled plasma conditions ($N_e > 10^{17} cm^{-3}, kT_e \sim 1eV$) and discussion on impact limit is proposed.

REFERENCES

1. "Slow and fast micro-field components in warm and dense hydrogen", A. Calisti *et al.*, plasmashttp://arXiv.org/abs/0710.2091v1
2. A. Calisti *et al.*, this conference

Universal FFM hydrogen spectral line shapes applied to ions and electrons

C. Mossé, A. Calisti, S. Ferri, B. Talin*, L.A. Bureyeva† and V.S. Lisitsa**

*Laboratoire PIIM, Université de Provence, Centre St Jérôme,Case 232, 13397 Marseille cedex 20, France
†Institute of Spectroscopy of the RAs, Troitsk, Moscow Reg.142190, Russia
**NFI RRC "Kurchatov Institute", Kurchatov Sq. Moscow 123182, Russia

ABSTRACT

Hydrogen lines shapes calculations are important for plasma diagnostics for laboratory and astrophysical plasmas.

We present a method for the calculation of hydrogen spectral line shapes based on two combined approaches: universal model [1, 2] and FFM procedure [3, 4]. We start with the analytical functions for the intensities of the Stark components of radiative transitions n - n' between highly excited atomic states with large values of principal quantum numbers $n, n' \gg 1$, with $\Delta n = n - n' \ll n$ for the specific cases of $H_{n-\alpha}$ line ($\Delta n = 1$) and $H_{n-\beta}$line ($\Delta n = 2$). The FFM line shape is obtained by averaging on the electric field of the Hooper's field distribution for ion and electron perturber dynamics and by mixing the Stark components with a jumping frequency rate ν_e (ν_i) where $\nu = N^{1/3}u$ (N is electron density and u is the ion or electron thermal velocity) . Finally, the total line shape is given by convolution of ion and electron line shapes.

Hydrogen line shape calculations for Balmer H_α and H_β lines are compared to experimental results [5, 6] in low density plasma ($N_e \sim 10^{16} - 10^{17} cm^{-3}$) and low electron temperature in order of 10 000K. Although the method is developed for transitions with $\Delta n \ll n$, the comparison shows a good agreement between the universal approach and experimental results.

This method relying on analytic expressions permits fast calculation of $H_{n-\alpha}$ and $H_{n-\beta}$ lines of hydrogen and could be used in the study of the Stark broadening of radio recombination lines for high principal quantum number.

REFERENCES

1. L.A. Bureyeva, V.S. Lisitsa, *A Perturbated Atom*,London/New York : Gordon and Breach/Harwood academic (2000)
2. L.A. Bureyeva, V.S. Lisitsa, D.A. Shuvaev, *Sov. Phys. JETP*,**95**,662 (2002)
3. B.Talin, A. Calisti, R.Stamm, R.W. Lee, and L. Klein, Phys. Rev. A 51, 1918 (1995)
4. C.Mossé, A. Calisti,R. Stamm, B.Talin, L.A. Bureyeva, V.S. Lisitsa, *J.Phys. B*, **37**,1343-1352 (2004)
5. W.L. Wiese, D.E. Kelleher, D.R. Paquette, *Phys. Rev. A* **6**, 1132 (1972).
6. C.G. Parigger, D.H. Plemmons, E. Oks, *Applied optics*, **42**,5992 (2003)

A Study of Impurity Spectral Lines in Plasmas Created During the Neutral Beam Injection Heating Phase in the TJ-II stellarator

Kieran J. McCarthy*, J. M. Carmona* and R. Balbín*

Laboratory Nacional de Fusión, CIEMAT, 28040 Madrid, Spain

INTRODUCTION

The TJ-II is a low magnetic shear stellarator of the heliac type with an average major radius of 1.5 m and an average minor radius of ≤ 0.22 m [1]. Its magnetic field ($B_0 \leq 1$ T) is generated by a system of poloidal, toroidal and vertical field coils and the resultant plasma cross-section is bean shaped. Plasmas created with hydrogen are heated ($\Delta t \leq 250$ ms) using one or two gyrotrons, operated at 53.2 GHz the 2nd harmonic of the electron cyclotron resonance frequency, which can provide up to 600 kW. For such operational regimes, central electron densities and temperatures up to1.7 $\times 10^{19}$ m^{-3} and 2 keV respectively are typically achieved. Recently, additional plasma heating by the injection of accelerated neutral hydrogen atoms (up to 35 keV) from one of two neutral beam injectors being commissioned on TJ-II has become available. Each NBI injector can provide up to 300 ms long pulses with ≤1 MW of heating. As a result plasmas densities above 4 $\times 10^{19}$ m^{-3} have been attained.

The TJ-II vacuum vessel, which is constructed of stainless steel SS-304-LN, has a total internal volume of 6 m^3 and a total inner surface area of about 75 m^2. The chamber is pumped by four turbomolecular pumps with a total effective pumping speed of about 4000 l/s. One of the characteristics of TJ-II plasmas is their strong interaction with the region of the chamber (groove) surrounding the hard-core. See Figure 1. In fact, the last closed flux surface (LCFS) can be defined by either the inner side of the vacuum vessel or by its two mobile graphite poloidal limiters. Moreover, numerous diagnostics are located inside the vacuum chamber [2]. Originally, an overnight (~12 hours) glow discharge cleaning (GDC) with helium followed by a short (~30 minutes) glow discharge with argon was performed to remove hydrogen implanted in the walls by previous discharges and to reduce impurities in the plasmas. Later, wall conditioning was performed using boronized walls. At present, wall conditioning is performed with lithium coating on the inner vacuum vessel walls and a short helium glow discharge prior to operation [3]. As a result the level of impurities in TJ-II plasmas has been reduced considerably during its operational lifetime. This has required the identification of spectral lines suitable for performing spectroscopy studies, in particular Doppler based spectroscopy, using both passive and active methods, for obtaining impurity ion temperatures and velocities.

Normal incidence spectrometer

A 1 m normal-incidence spectrometer, operating in the extreme-ultraviolet and ultraviolet wavelength regions (20 to 200 nm), is operated continuously in the TJ-II [4]. The instrument was custom built by McPherson, Chelmsford, MA, and has several unique features and accessories that are described here. It is equipped with three gratings (1200 and 3600 grooves mm^{-1}) and a back-illuminated CCD camera located at the focal plane. It is used for performing surveys and for obtaining impurity temperatures. Indeed, this diagnostic is particularly suited to studying highly ionized impurities emitting from the TJ-II plasma centre during NBI heating.

Impurity spectral lines

In this paper, we first compare impurity line spectra obtained under ECRH and NBI heating conditions in the TJ-II. For this we identify the spectral lines present across a broad wavelength range (20 – 100 nm) during both operating modes. Indeed, the main impurities identified to-date in TJ-II plasmas include lithium, boron, carbon, nitrogen, oxygen, fluorine as well as metals such as iron and chromium. Other impurities, such as chlorine, remain tentatively identified. However, numerous spectral lines that arise during NBI heating remain unidentified in this wavelength range. Next, we identify suitable spectral lines for probing the hot plasma centre, *e.g.* in particular emissions from He- and H-like impurity ions as well as from highly ionized metallic ions, in particular lines that appear during the high-density, reduced electron temperature, NBI heating phase. Also, we search for spectral lines arising from forbidden (M1) emissions as such lines are easier to study with normal incidence spectrometers due to their longer wavelengths, i.e. compared to shorter wavelength that require grazing incidence spectrometers. Next, having determined the instrument function using spectral lines emitted by impurity ions residing in the cooler plasma edge, we study the evolution of the impurity ion temperature (as determined from the Doppler line width), from the

ECRH to NBI phases. These are compared with temperatures obtained using other non-spectroscopic methods such as neutral particle analysis. For this it is necessary to evaluate all non-thermal broadening contributions to the spectral line shape, e.g. *l*-level mixing, Doppler shifts due to poloidal velocities, or possible tails due to charge exchange processes.

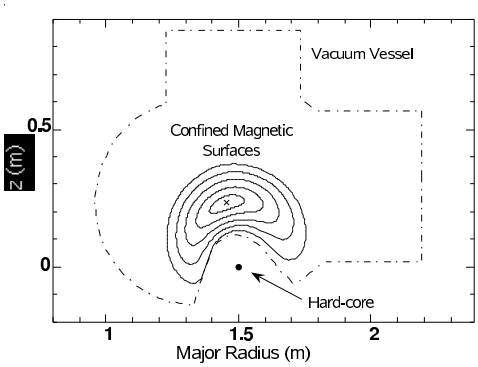

FIGURE 1. Cross-section of the TJ-II showing the vacuum vessel walls, the hard-core and surrounding groove, and nested magnetic surfaces of the standard TJ-II configuration (100_40_63).

ACKNWOLEDGEMENTS

This work was partially funded by the Spanish *Ministerio de Educación y Ciencia* under Project FTN2007-64159.

REFERENCES

1. C. Alejaldre et al., *Plasma Phys. Control. Fusion,* 41, A539 (1999).
2. J. Sánchez et al., *J. Plasma Fusion Res. SERIES* 1, 338 (1998).
3. F. L. Tabarés et al., "Impact of lithium-coated walls on plasma performance in the TJ-II stellarator" to be published in Proceedings of 16th International Stellarator/Heliotron Workshop, Toki, Japan, (2007).
4. K. J. McCarthy, B. Zurro, R. Balbín, A. Baciero, J. Herranz, and I. Pastor, *Europhys. Lett.* 63, 49 (2003).

An Overview of Rotation and Ion Temperature Measurements of Impurities and Hydrogen by Passive Emission Spectroscopy in the TJ-II Stellarator

A. Baciero[*], B. Zurro[*], D. Rapisarda[*], V. Tribaldos[*], D. Jiménez-Rey[*] and the TJ-II team[*]

[*] *Laboratorio Nacional de Fusión por Confinamiento Magnético. Asociación EURATOM - CIEMAT. Madrid. Spain*

An overview of the spectroscopic methods and the numerical techniques to deduce plasma rotation and impurity temperatures in the TJ-II stellarator by means of passive spectroscopy is summarized. The final goals of these experiments are to understand the impurity and main ions rotation [1], and to estimate whether the electric field is the main driving term for these rotations.

The poloidal measurements have been carried out using a multichannel system. The analysis method [2] and the impurity poloidal rotation behavior with plasma density have previously been reported [3]. Toroidal measurements were carried out by an absolutely calibrated system which scans the toroidal view by a shot to shot procedure [4]. The studied TJ-II scenarios are plasmas with different ECRH powers and electron densities, as well as NBI-heated discharges

We will compare for selected discharges, apart from poloidal rotation between species, the kinetic profiles of electrons, the ion temperatures and the spatial distribution of line impurity emissions. This analysis allows us to draw a more complete picture capable of aiding in the interpretation. We plan to get physical conclusions by discussing our observations in the context of different mechanisms which influence poloidal rotation [5].

REFERENCES

1. B. Zurro et al., "A comparative study of impurity and proton poloidal rotation in the TJ-II stellarator", in *34th EPS Conference on Plasma Phys.*, Europhysics Conference Abstracts, Warsaw, 2007, Vol. 31F, P-5.117.
2. A. Baciero et al., *Rev. Sci. Instrum.* **72**, 971 (2001).
3. B. Zurro et al., *Fusion Science and Technology* **50**, 41 (2006).
4. D. Rapisarda et al, *Rev. Sci. Instrum.* **77**, 033506 (2006).
5. W.M. Stacey, *Phys. Plasmas* **15**, 012501 (2008).

The Reaction of Dissociative Recombination in a Strong Light Field

Golubkov M.G.[1,2], Adamson S.O.[3], Apukhtina N.V.[4],
Golubkov G.V.[1,2], Dementiev A.I.[4], Ryabinkin I.G.[3]

[1]*Semenov Institute of Chemical Physics, Moscow, Russia*
[2]*RSUTS, Moscow region, Russia*
[3]*Lomonosov Moscow State University, Moscow, Russia*
[4]*Moscow State Pedagogical University, Moscow, Russia*

The effect of intensive laser radiation on the dynamics of elementary atomic and molecular processes is the fundamental problem of modern chemical physics. The principal place among such processes takes the dissociative recombination (DR) reaction of slow electrons with positively charged molecular ions. This reaction is responsible for the charge disappearance kinetics in the Earth's ionosphere and upper atmosphere, in low-temperature plasma and gas-discharge lasers. The study of this reaction in the presence of electromagnetic field is interesting for both the theory of radiative collisions and experimentalists, who develop new laser methods of elementary chemical process initiation and control. Because of different reaction mechanism competition the cross sections in some spectrum regions should have the sharp dependence on the frequency of external radiation. It can be key factor for the relative reaction product yield.

It is well known, that the cross section of low-temperature DR reaction of electrons and molecular oxygen ions with the transition to Schumann-Runge continuum can increase for several orders of magnitude for the certain external radiation parameter choice [1,2]. Such behaviour points out the direct possibility of laser stimulation of this reaction. In the absence of the external field the main contribution here give only the dissociative states with potential energy curves lying close to minimum of molecular ion potential. When the external electromagnetic field is turned on the additional field induced states, which are populated due to absorption or radiation of photons, are involved into the process. Since the amplitudes of population are proportional to external field strength (which may vary from 10^{-4} to 10^{-1} a.u.), the problem can be reduced to the search of optimal conditions for laser control for low-temperature DR reaction and preparing the recommendations for future experiments. The different regimes of external field influence depend on incident electron energy, the field strength and frequency and also the angle between electron and light beams.

The DR theory of slow electrons with molecular ions in strong monochromatic light field was developed. It takes into account the interference among different reaction channels and is constructed in the rotationally strict adiabatic basis (the approximation of fixed molecular axis). Note, that the problem of electromagnetic field influence on the intermediate complex differs from traditional nonstationary problems on the theory of laser radiation interaction with atoms and molecules [3]. The main difference is due to impossibility at quantum conditions to fix the moment of intermediate complex appearance. It is difficult also to carry out the investigation taking into account the interaction of closed channels with continua (including coupling of autoionization with predissociation). If the laser impulse duration significantly exceeds the intrinsic times of intermolecular complex transitions, one can use the stationary variant of the theory for DR description. Than in the case of monochromatic radiation the energy spectrum of the compound system "excited molecule+external field" will contain the set of "quasienergetic states" distorted by field, which are shifted relative to each other on the values with field frequency whole multiple factor.

The mathematical apparatus of the presented theory is based on utilization of stationary formalism of radiation collision matrix, the poles of which correspond to quasienergetic states of compound system [2]. For this purpose the detailed information about the potential energy curves of the states is needed with taking into account the external electromagnetic field. The main interest represents the situation when the initial molecular ions are in the ground vibronic states. The total number of the potential energy curves which should be taken into account could be maintained after the detailed analysis of the all possible mechanisms of the field influence (in the wide spectrum region from IR to UV light). These mechanisms can be proposed rely on the developed theoretical approach and the results of ab initio calculations of molecular ion potential energy curves including the characteristics of configuration coupling. For example, the case of oxygen molecular ion was considered. The classification of all transitions in the presence of external electric field was done. The adiabatic potential energy curves were calculated for both singlet and triplet states which correlate with three low-lying dissociative limits.

This investigation was supported by Russian Foundation for Basic Researches (grant #07-03-00592).

References:

1. Golubkov G.V., Golubkov M.G., Romanov A.N. Sov.Phys.JETP. V.94. P.489. 2002.
2. Golubkov G.V., Golubkov M.G., Romanov A.N., and Buenker R.J. PCCP. V.5. P.3174. 2003.
3. Delone N.B., Krainov V.P. Atoms in Strong Light Fields. Springer-Verlag, New York. 1985.
4. Golubkov G.V., Ivanov G.K. Sov.Phys.JETP. V.77. P.574. 1993.

Rydberg atom A** in a field of neutral atom B

Golubkov G.V.[1,2], Golubkov M.G.[1,2], Ivanov G.K.[1]

[1] *Semenov Institute of Chemical Physics, RAS, Moscow, Russia*
[2] *RSUTS, Moscow region, Russia*

Recently the upper atmosphere electromagnetic radiation effect on living organisms became the subject of intensive investigations. This radiation is a result of solar activity and the following magnetic storms. The microwave radiation (MR) plays the most important role here. In accordance with aerospace measurements MR is formed at a height of one hundred kilometres from the ground surface due to excitation of Rydberg atoms and molecules [1]. The MR spectrum differs noticeably from the spectrum calculated by Bates and Damgaart [2] in the case of isolated highly excited particles. It can be explained by the presence of exterior neutral particles of atmosphere. For example, the perturbation of excited atom A** states by one neutral atom B is the principal cause of MR at a height of 100 km, where the surrounding environment density is 10^{13} cm^{-3}. As a result of difference in masses among electron, A^+ and B particles, the processes of energy exchange during A^{**} - B collisions are improbable here. Therefore the potential energy surface (PES) calculations of combined system should be done before the dynamic collision investigations. It is necessary to determine such regions of the particle positional relationship, where the PES quasicrossings or convergings take place.

A great number of publications devoted to describing of PES features and the collision process dynamics were reviewed in [3]. The approaches, which utilize the information about independent free-electron scattering on the ion core or atom B, are widely used in the most publications. The asymptotic approach is the most popular and well developed. It is correct when the internuclear distances are quite large (order to size of an excited atom), where the general results may be represented in the simple analytical form. It is owing to the fact that the basic wave functions and Green's function of electron movement in the field of ion A^+ are known [4].

In the present report the regular construction method of PES and the corresponding electron wave functions for perturbed system "Rydberg atom-neutral atom" in the wide internuclear distance range including intermediate ones (order to the weakly bound electron wave-length), where the asymptotic approaches and quasiclassical approximations are not valid [5]. The sequential procedure for determination of one-center operators is developed for the description of the electron scattering on isolated atoms. It permits to consider P- and higher angular momenta of weakly bounded electron relate to perturbing atom B, that differs from the well-known zero-radius potential (ZRP) model.

This procedure is based on the finite radius potential (FRP) approach and takes into account the short-range and long-range interaction of Rydberg electron with perturbing particles at intermediate internuclear distances for arbitrary principle quantum numbers in a self-consistent way [6]. The detailed investigation of one-center scattering operator structure and PES features is carried out for the $A^{**} - B$ system. It is shown, that taking into account P-scattering leads to splitting of the degenerate covalent states on interaction state groups classified by the projection of electron angular momentum on the quasi-molecular axis. The wave functions of perturbed Rydberg and covalent states are constructed and their properties are investigated. The calculations are carried out for Na^{**} - He system and the comparison with ZRP model and asymptotic theory is fulfilled. It is shown, that the well-known result of Firsov-Smirnov [7] is valid at vicinity of perturbing atom only. The approach proposed in present work can be applied also for the solution of the problem of highly exited atom perturbing by the system of random located medium atoms. It is necessary for describing the radiative processes taking place in more dense atmosphere at lower heights.

References

1. Avakyan S.V. Journal of Optical Technology, V. 72, Issue 8, P. 577. 2005.
2. Bates D.R., Damgaart A. Phil. Trans. Roy. Soc. London. A. V.242. P.101. 1949.

3. Golubkov G.V., Ivanov G.K. Rydberg states of atoms and molecules and elementary processes with their participation. Editorial URSS, Moscow. 2001.
4. Golubkov G.V., Ivanov G.K., Golubkov M.G. Khim. Fizika. V.24. N. 6. P.3. 2005.
5. Golubkov G.V., Ivanov G.K., Golubkov M.G., Khim. Fizika. V.24, N.9. P.3. 2005.
6. Smirnov B.M. Asymptotical methods in the theory of atomic collisions. Atomizdat, Moscow. 1973.

SPECTROSCOPIC PROBLEMS IN A PLASMA DIAGNOSTICS OF ELECTRIC ARC DISCHARGES BETWEEN COPPER ELECTRODES

Babich I.L., Boretskij V.F. and Veklich A.N.

Radio Physics Faculty, Taras Shevchenko Kyiv National University, Volodymyrs'ka Str. 64, Kyiv 01033, Ukraine, E-mail: boretskij@univ.kiev.ua

The radial distribution of the temperature and the electron density in the plasma of free burning electric arc in air and in air flow as well as in carbon dioxide flow between copper electrodes are studied by optical emission spectroscopy techniques. The spectroscopic problems of such diagnostics are widely discussed.

INTRODUCTION

As well known, a gas shielded arc is often used in electric arc technology. A welding or an arc cutting processes are usually realized in argon, carbon dioxide, nitrogen, oxygen and air or mixtures of different gases. From one hand the spatial distribution of plasma parameters are depended from flow rate or kind of surround gas. And from another hand the metal vapour content in arc discharge significantly determine these parameters too [1]. Therefore the investigations of electric arc plasma with metal vapour in different shielding gases are interesting for industry applications as well as for fundamental science.

EXPERIMENTAL SETUP

The arc was ignited in air between the end surfaces of the non-cooled copper electrodes. The diameter of the rod electrodes was of 6 mm. The discharge gap was 8 mm and the arc current was 3.5 and 30 A. Because of the discharge spatial and temporal instability the method of the single tomographic recording of the spectral line emission was used [1]. The statistical averaging of recorded spatial distributions of radiation intensities was carried out. The program interface on the base of the Operation System Windows 9.x./NT/XP is developed. The data acquisitions, data approximations, statistical treatments of these data and Abel inversions are realized in this interface. In such way we obtain the local spectral line intensity values. Also the non-uniformity of spectral sensitivity of the experimental set-up is taken into account. Finally, calculations of temperature, electron density and plasma composition are realized in this interface too. The measurements of plasma parameters were carried out in the average cross section of discharge gap.

RESULTS AND DISCUSSIONS

Measurements of radial profiles of the electron density $N_e(r)$

To determine the radial profile of electron density we investigated the shape of spectral line CuI 515.3 nm broadened by the dominating quadratic Stark effect [2]. The measurements were carried out by techniques based on a Fabri-Perot interferometer (FPI) [3]. Such approach realized the simultaneous registration of spatial and spectral distribution of radiation intensities. So, we measured contours of spectral lines in different spatial points of plasma volume (see figure 1, left and center). We calculated in such way the radial profile of electron density (see curve 1 in figure 1, right).

Unfortunately the width of this spectral line at arc current 3.5 A is practically comparable with instrument function of FPI (see figure 1, left). Therefore, to extend the measuring range of the electron density we studied the radial distribution of absolute intensity of a spectral line CuI 465.1 nm [3]:

$$I \sim N_e^2 T^{-3/2} exp[(E_i - E_s)/kT] \sim N_e^2 T^{-3/2}, \quad (1)$$

where E_i is the ionization potential, E_s is the excitation energy of upper level of considered spectral transition. The curve 2 in figure 1 (right) is obtained by this techniques.

According to eq. (1) it is necessary to measure the plasma temperature for determination of the electron density.

Measurements of radial profiles of the plasma temperature $T(r)$

The radial temperature profiles $T(r)$ can be determined from the ratio of local intensities of the CuI spectral lines 465.1, 510.5, 515.3, 521.8 and 578.2 nm.

The next problem in the temperature determination is the choosing of appropriate spectroscopic data of these lines.

For example, in figure 2 the radial profiles of the plasma temperature of free burning electric arc (left) and electric arc discharge in air flow (center) as well as in carbon dioxide flow (right) are shown. We used spectroscopic data derived by [4], [5] and [6]. One can see that the discrepancy of the plasma temperature determination is about 2000 K. Therefore, spectroscopic data must be carefully analyzed and chosen.

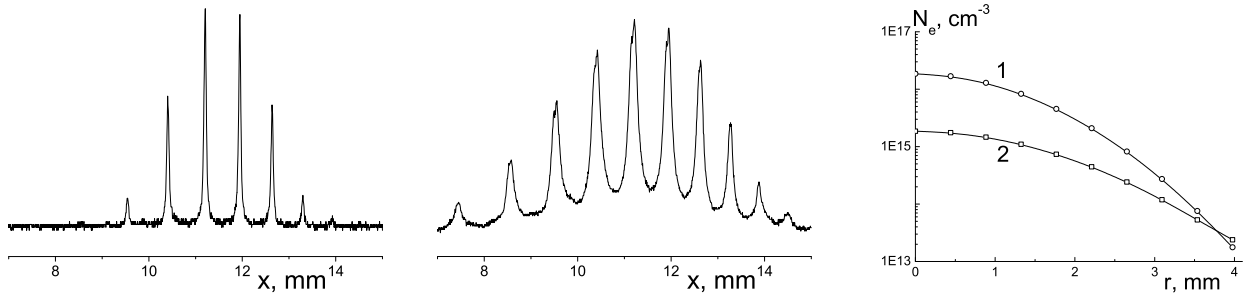

FIGURE 1. Contours of spectral line CuI 515.3 nm in different spatial points of plasma volume of electric discharge at arc current 3.5 A (left) and 30 A (center). Radial profiles of the electron density (right) at arc current 30 A (curve 1) and 3.5 A (curve 2).

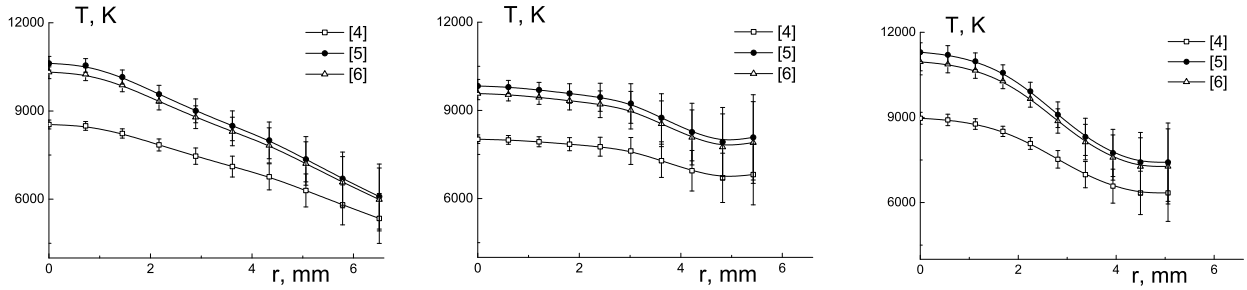

FIGURE 2. Radial profiles of the temperature of free burning electric arc (left), electric discharge in air flow (center) and carbon dioxide flow (right) obtained by the ratio of local intensities of CuI spectral lines 465.1 and 510.5 nm. Spectroscopic data were used from [4], [5] and [6].

In conclusion, the extension of the measuring range of the electron density is realized. The spectroscopic data in the plasma temperature measurements must be carefully chosen and improved.

REFERENCES

1. I. L. Babich, V. Ye. Osidach, V. I. Sobovoy and A. N. Veklich, *Czechoslovak J. of Phys.* **52**, Suppl. D, D731-D735 (2002).
2. R. Konjevic and N. Konjevic, *Fizika* **18**, pp 327–335 (1986).
3. I. L. Babich, V. F. Boretskij, and A. N. Veklich, "Shapes of Spectral Lines of Nonuniform Plasma of Electric Arc Discharge Between Copper Electrodes", *VI Serbian Conference on Spectral line Shapes in Astrophysics*, edited by L. Č. Popović and M. S. Dimitrievi´c, AIP Conference Proceedings 938, American Institute of Physics, New York, 2007, pp. 252-257.
4. C. H. Corliss and W. R. Bozman, *Experimental Transition Probabilities for Spectral Lines of Seventy Elements* [Russian translation], Moscow: Mir, 1968, pp. 80–81.
5. A. G. Shenstone, *Phil. Trans. Roys. Soc.* **241**, p. 297 (1948), `http://physics.nist.gov/PhysRefData/ASD/lines_form.html`, accessed April 15, 2008.
6. P. L. Smith, C. Heise, J. R. Esmond, R. L. Kurucz, *Atomic spectral line database from CD-ROM 23 of R. L. Kurucz.*, `http://cfa-www.harvard.edu/amp/ampdata/kurucz23/sekur.html`, accessed April 15, 2008.

Relativistic calculating the spectral lines hyperfine structure parameters for the heavy atoms and laser spectral detecting the heavy isotopes

O.Yu.Khetselius

Odessa University, P.O.Box 24, Odessa-9, South-East, 65009, Ukraine

Relativistic calculation of the spectra hyperfine structure parameters for heavy elements is carried out. Calculation scheme is based on gauge-invariant QED perturbation theory with using the optimized one-quasiparticle representation at first in the theory of the hyperfine structure for relativistic atomic systems. [1], [2], [3], [4], [5]. Within the new method it is carried out calculating the energies and constants of the hyperfine structure for valent states of cesium 133Cs, cesium-like ion Ba, isotopes of 201Hg, 223Ra, 252Cf are defined. As example, in Table 1 we present the experimental and theoretical data for magnetic dipole constant of the hyperfine structure A (in MHz) for the states: 7s7p $^1P_1$, $^3P_1$, and $^3P_2$ of radium $^{223}_{88}$Ra. We present the results of calculation by other methods, namely: standard uncorrelated Dirac-Fock (DF) method, multi-configuration DF method (MCDF) with accounting for the Breit and QED corrections, relativistic method of configuration interaction with accounting for correlation corrections within the random phase approximation (RCI-RPA) [6], [9], [8]. The contribution due to inter electron correlations to the hyperfine structure constants for considered elements is about 120-1200 MHz for different states, contribution due to the finite size of a nucleus and radiative contribution is till 2 dozens MHz. Obtained data for hyperfine structure parameters are used in further in laser photo-ionization detecting the isotopes in a beam and the buffer gas for systematic studying the short-lived isotopes and nuclear isomers. We propose a new approach to construction of the optimal schemes of the laser photo-ionization method for further applying to problem of the nuclear reactions products detecting. ItŠs studied the reaction of spontaneous 252Cf isotope fission on non-symmetric fragments, one of that is the cesium nucleus. The corresponding experiment on detecting the reactions products is as follows. The heavy fragment of the Cf nucleus fission created in the ionized track 106 electrons which are collected on the collector during 2 mks. The collector is charged negatively 40mks later after nuclear decay and 10mks before the laser pulse action. The photo electrons, arisen due to the selective two-stepped photo-ionization are drafted into the proportional counter for their detecting. Usually a resonant excitation of Cs is realized by the dye laser pulse , the spectrum of which includes the wavelengths of two transitions 62S1/2-72P3/2 (4555A) and 62S1/2-72P1/2 (4593A). This pulse also realizes non-resonant photo-ionization of the Cs excited atoms. The disadvantages of the standard scheme are connected with non-optimality of laser photo-ionization one, effects of impact lines broadening due to the using the buffer gas, the isotopic shift and hyperfine structure masking etc. We proposed new laser photo-ionization scheme, which is based on a selective resonance excitation of the Cs atoms by laser radiation into states near ionization boundary and further autoionization decay of excited states under action of external electric field [7]. The corresponding optimal parameters of laser and electric fields, atomic spectral lines, transitions, states, decay parameters etc are presented.

TABLE 1. Experimental and theoretical data on magnetic dipole constant of the hyperfine structure A (in MHz) for the states: 7s7p $^1P_1$, $^3P_1$, and $^3P_2$ of radium (calculation by different methods: DF, MCDF with accounting for the Breit and QED corrections, relativistic method of configuration interaction with accounting for correlation corrections within the random phase approximation (RCI-RPA) and QED PT method) [5], [9], [8].

Method / State	$^1P_1$	$^3P_1$	$^3P_2$
DF	−226.59	803.97	567.22
MCDF (Breiht+QED)	−330.3	1251.9	737.1
RCI-RPA	−242.4	—	—
QEDPT	−339.1	1209	704.5
Experiment	−344.5 (0.9)	1201.1 (0.6)	699.6 (3.3)

ACKNOWLEDGMENTS

The support of the the Abdus Salam International Centre for Theoretical Physics ICTP (Trieste, Italy) and University of Dresden and Frieburg (Germany) is very much acknowledged.

REFERENCES

1. A. V. Glushkov, and L. N. Ivanov, *Phys. Letters* **A170**, 33–38 (1992).
2. A. V. Glushkov, O. Yu. Khetselius et al., *Nucl. Phys. A* **734**, e21–28 (2004).
3. Á. Glushkov, 'Energy Approach to Resonance states of compound super-heavy nucleus and EPPP in heavy nucleus collisions," in *LEAP'05*, edited by D. Grzonka et al., AIP Series Vol.796, American Institute of Physics, New York, 2005, pp. 206–210.
4. A. Glushkov, O. Khetselius, et al., "QED calculation of heavy multicharged ions with account for the correlation, radiative and nuclear effects," in *Recent Advances in Theor. Phys. and Chem. Systems*, edited by J. Maruani et al., Springer, Paris, 2006, Vol.15, pp. 285–320.
5. O. Yu. Khetselius, *Photoelectronics* **15**, 101-110 (2006).
6. A. Glushkov, O. Khetselius, et al., "Gauge-invariant QED perturbation theory approach to calculating nuclear electric quadrupole moments, hyperfine structure constants for heavy atoms and ions: Superatom package," in *Recent Advances in Theor. Phys. and Chem. Systems*, edited by S. Wilson et al., Springer, London, 2008, Vol.18, pp. 201–224.
7. A. Glushkov, S. Malinovskaya, O. Khetselius, *Europ. Phys. Journ.* **48** (2008).
8. P. Pyykkö and J. Bieron, *Phys. Rev. A* **71**, 012502-1–012502-12 (2005).
9. J. Bieron, and P. Pyykkö, *Phys. Rev. A* **71**, 032502-1–032502-6 (2005).

Monitoring of Trace H_2O in N_2 near Atmospheric Pressure Using Cavity Ring-Down Spectroscopy: Comparison of Integrated Line Intensity and Peak Intensity

Hisashi Abe and Hiroshi Kitano

National Metrology Institute of Japan (NMIJ), AIST, Tsukuba Central 3, Tsukuba 305-8563, Japan

The measurement capability of a trace moisture analyzer based on cavity ring-down spectroscopy was studied using a magnetic suspension balance/diffusion-tube humidity generator (MSB/DTG) in the range between 10 nmol/mol and 1400 nmol/mol. Good linear relationships were observed between the integrated and peak intensities of a line and the amount-of-substance fraction of H_2O in N_2 generated with the MSB/DTG.

INTRODUCTION

The measurement of trace moisture in semiconductor process gases has become increasingly important in the recent decade, because it has been recognized that even the trace level of moisture plays a critical role in the yield and product quality [1]. Various measuring instruments for detecting the trace moisture have been developed [2]. However, the accurate measurement of such a small amount of water in gases is still a challenging issue. A major reason behind this is the lack of suitable humidity standards in the trace moisture region for testing and calibrating the instruments.

Recently, we developed a magnetic suspension balance/diffusion-tube humidity generator (MSB/DTG) [3,4] to realize a primary humidity standard down to 10 nmol/mol (10 ppb). In this work, using the MSB/DTG, we studied the measurement capability of a trace moisture analyzer (MA) based on cavity ring-down spectroscopy (CRDS). The near-infrared spectra of trace moisture in nitrogen gas generated using the DTG were recorded using the MA near atmospheric pressure. The amount-of-substance fraction of the trace moisture was determined by the real-time mass measurement of evaporating water using the MSB and the flow rate measurement of nitrogen gas using a mass flow controller. The integrated line intensity and peak intensity of the $2_{02} \leftarrow 3_{03}$ transition of the $\nu_1+\nu_3$ band of H_2O at 7181.2 cm^{-1} measured from the spectra were compared with the amount-of-substance fraction of the trace moisture generated in the range between 10 nmol/mol and 1400 nmol/mol.

EXPERIMENT

The experimental apparatus used in this work was essentially the same as that described in our previous paper [4]. Dry nitrogen (N_2) gas was introduced into the inlet of a generation chamber and a bypass line using two thermal mass flow controllers (Stec). Total flow rate was maintained at a set value in the range between 1.0 L/min or 20 L/min, and the flow rate for the bypass line was 0.1 L/min; the flow rates in L/min used in this paper correspond to those measured under the standard conditions of 101.325 kPa and 0 °C. Inside the chamber, a diffusion cell [3] was suspended from the measuring load of an MSB (Rubotherm). Water was stored in the diffusion cell, and water vapor that evaporated through the diffusion tube was diluted with dry N_2 gas coming from the inlet. Humid gas generated in this manner was taken from the outlet of the chamber. The line from the outlet was connected to the bypass line, and the humid gas was mixed and diluted with the dry N_2 gas. This mixed flow was divided into two: One was introduced into a pressure regulator (PR) to control the pressure inside the chamber, which was maintained at 150 kPa. The other was led to an MA (Tiger Optics) based on cavity ring-down spectroscopy to record near-infrared spectra of the trace moisture generated. The pressure of the sampling cell of the MA was approximately 140 kPa. The evaporation rate of the water from the diffusion cell was measured as the mass-change rate of the diffusion cell using the MSB. The amount-of-substance fraction of the trace moisture was determined from the evaporation rate and flow rate of the nitrogen gas measured using the mass flow controller.

RESULTS

Fig. 1 shows the infrared spectrum of the trace moisture in nitrogen gas with the amount-of-substance fraction of water x_w=12.1 nmol/mol. The signal-to-noise ratio of the line used for monitoring trace moisture in this work (indicated by arrow) was approximately 35. The spectrum was analyzed with the Voigt function using a non linear least-squares fit procedure. Fig. 2 shows integrated line intensities and peak intensities as a function of x_w. The figure shows good linear relationships between the two intensities and x_w. By a least-squares analysis with linear functions, we obtained R^2=0.99998 for the integrated line intensities and R^2=0.99997 for the peak intensities.

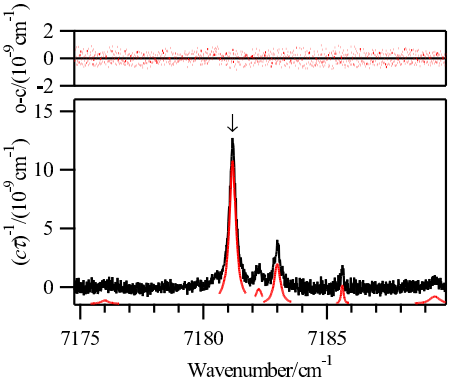

FIGURE 1. Near-infrared spectrum of trace H_2O in N_2.

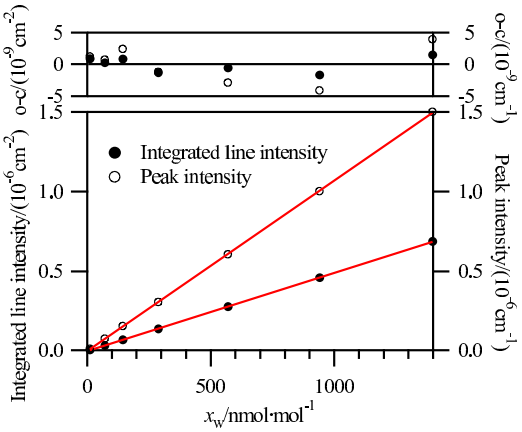

FIGURE 2. Integrated line intensities and peak intensities as a function of x_w.

REFERENCES

1. International Technology Roadmap for Semiconductors (2007), available at http://www.itrs.net/reports.html
2. H.H. Funke, B.L. Grissom, C E. McGrew, and M.W. Raynor, *Rev. Sci. Instrum.* **74**, 3909-3933 (2003).
3. H. Abe and H. Kitano, *Sens. Actuators A:Phys.* **128**, 202-208 (2006).
4. H. Abe and H. Kitano, *Sens. Actuators A:Phys.* **136**, 723-729 (2007).

Separation between Allowed and Forbidden Component of the *He I* 447 *nm* Line in High Electron Density Plasma

M. Ivković*, M. Á. González†, S. Jovićević*, M. A. Gigosos† and N.Konjević*

*Institute of Physics, P.O. Box 68, 11080 Belgrade, Serbia
†Departmento de Optica, Facultad de Ciencias, Universidad de Valladolid, 47071 Valladolid, Spain

The overall complex shape of the *He I* $2p^3\mathrm{P} - 4d^3\mathrm{D}$ and its forbidden component $2p^3\mathrm{P} - 4d^3\mathrm{F}$ was very often used for Stark broadening theory testing. The sensitivity of the overall line shape parameters upon electron density enables the use of these structure of lines for precision diagnostic purposes also. As a consequence of a very low sensitivity upon self-absorption, the separation between forbidden and allowed component - *s*, is most frequently used parameter for plasma diagnostic purposes. Useful empirical formulas relating parameter *s* with electron density N_e at electron densities $< 10^{23} m^{-3}$ were determined [1, 2], but their use at higher electron density plasmas has to be tested. Namely, there are indications that the dependence of *s* parameter upon N_e at higher densities differs from the one at lower N_e [3]. In this paper we report results of $s = f(N_e)$ examination at $N_e > 10^{23} m^{-3}$ performed theoretically by computer simulation [4] and experimentally in a high pressure pulsed discharge.

Linear pulsed discharge is constructed in our laboratory after [5]. The separation between tungsten electrodes (placed inside quartz tube, inner diameter 8 *mm*) was 8 *cm*. Each electrode has 0.6 *mm* diameter openings in order to enable interferometery and spectroscopy measurements along the axis of plasma column. The discharge was driven by the low inductance 15 μF capacitor charged up to 6 *kV*. With 0.17Ω resistor in series and by use of an ignitron switch critically dumped current pulse (up to 10 *kA*, the overall duration of $10\mu s$) is obtained. The reproducibility of the discharge pulsing is enhanced by dc glow preionization. In this discharge the electron densities up to 10^{24} m^{-3} were obtained using continuous flow of helium with a small percentage of oxygen.

The electron density was determined with single wavelength Michelson interferometer at 633 *nm*. Spectral lines shapes were recorded by pulsing discharge, while advancing monochromator in small wavelength steps. For this purpose 1 *m* monochromator (inverse linear dispersion $0.833\ nm/mm$) equipped with a cooled photomultiplier (PMT) is used. Signals from the PMT are led to a digital storage oscilloscope triggered by the signal from the Rogowsky coil set around main current cable. Typical interferogram and shapes of recorded lines are displayed in Figure 1 and Figure 2.

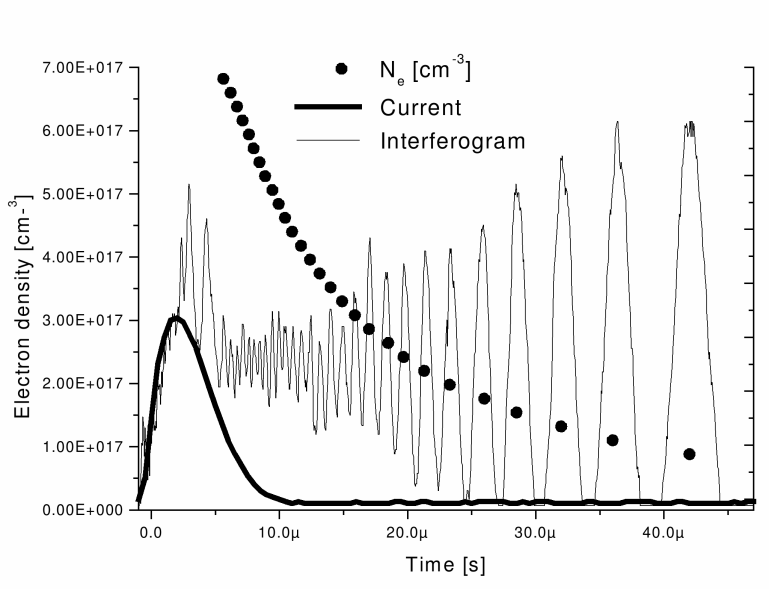

FIGURE 1. The current pulse, interferogram and electron density decay.

The *s* parameter dependence upon electron density evaluated by computer simulation method and experimental results are presented in Figure 3.

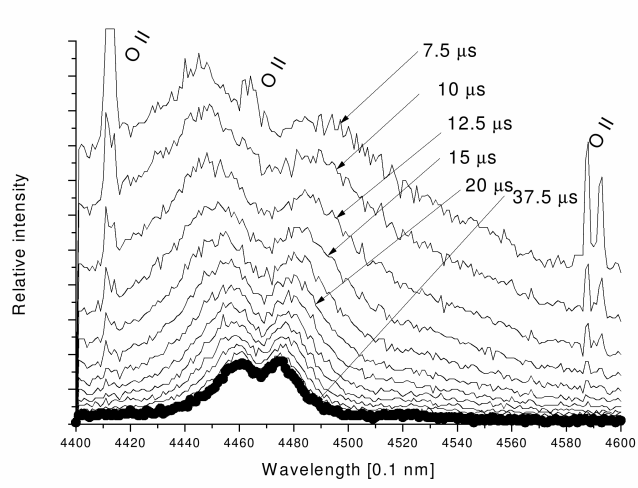

FIGURE 2. The overall shape of the *He I* 447 *nm* lines at different times of plasma decay

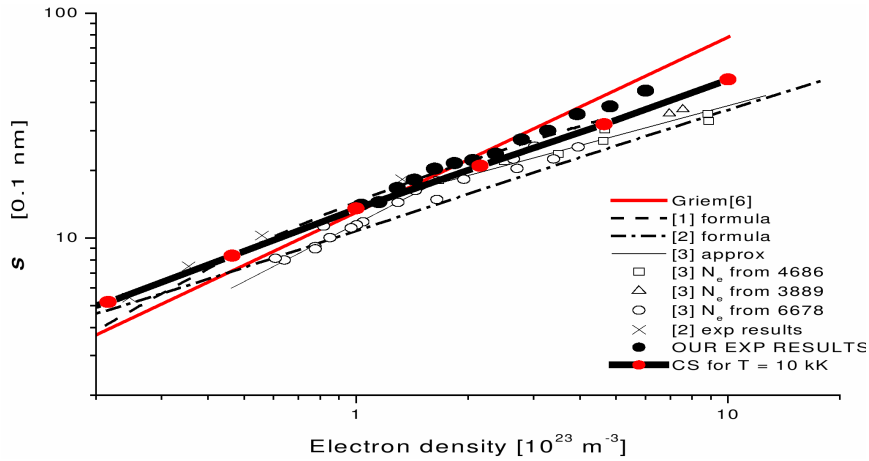

FIGURE 3. The separation - *s* between forbidden and allowed component as a function of N_e.

As evident from Figure 3 our experimental and theoretical results agree reasonably well with earlier calculations by Griem [6]. The deviation of experimental data in Figure 3 reported in [3] was, most likely, caused by the self-absorption of *He* lines used for electron density determination.

ACKNOWLEDGMENTS

This work is partially supported by the Spanish Ministerio de Education y Ciencia under grants ENE2004-05038/FTN and ENE2007-63386/FTN and by the Ministry of Science of the Republic of Serbia under project 141032.

REFERENCES

1. A. Czernichowski and J. Chapell, *JQSRT* **33**, 427-436 (1985).
2. C. Perez, I. de la Rosa, J. A. Aparicio, S. Mar and M. A. Gigosos, *Jpn.J.Appl. Phys.* **35**, 4073-4076 (1996).
3. H. Suemitsu, K. Iwaki, Y. Takemoto and E. Yoshida, *J.Phys.B.* **23**, 1129-1137 (1990).
4. M. A. Gigosos, M. A. González and N. Konjević, *E. Phys. J. D* **40**, 57-63 (2006).
5. K. Grützmacher and U. Johannsen, *Spectral Line Shapes* **7**, Nova Science Publishers Inc, 139-140 (1993).
6. H. R. Griem, *The Astrophysical Journal* **154**, 1111-1122 (1968).

On the Stark Widths and Shifts of Ar II 472.68 nm Spectral Line

Z. Mijatović, T. Gajo, B.Vujičić, S. Djurović and R. Kobilarov

Department of Physics, Faculty of Sciences, Trg Dositeja Obradovića 4, 21000 Novi Sad, Serbia

A. INTRODUCTION AND EXPERIMENTAL

Spectral lines of ionized atoms are used for plasma diagnostics, particularly for dense plasma density determination based on Stark broadening and shifting. Argon plasmas can be found in a number of plasma sources. This paper presents the preliminary results of Stark widths and shifts of Ar II 472.68 nm spectral line measurements using the T-tube plasmas. The obtained results, as well as the results of other experiments are compared with the semi-empirical formula [1].

The T-tube was used as the plasma source. The working gas was a mixture of H_2 and Ar in proportion 90 % to 10 %. This mixture was chosen to provide high enough electron density but also reasonable intensity of the investigated Ar II lines. The pressure of the gas mixture, in a flowing regime, was 90 Pa. The discharge capacitor bank of 4 μF was fired to 23 kV. The plasma was observed in the reflected wave at a distance of 4 mm from the reflector. Plasma radiation was focused on the entrance slit of 1-m monochromator equipped with 1200 g/mm grating. A photomultiplier, placed at the exit slit, was used for spectral intensity measurements. Slit widths were about 10 μm. Output signals from the photomultiplier were led to a digital oscilloscope and shot-to-shot technique was applied for spectral intensity measurements. Plasma temperatures were deduced from the Doppler widths of recorded profiles while electron densities were measured by applying laser interferometer using He-Ne laser radiation at 632.8 nm. Measured plasma electron density ranged $1.8 - 2.2 \cdot 10^{17}$ cm^{-3} while plasma temperature ranged 20000 - 43000 K.

B. RESULTS AND DISCUSSION

Stark widths of the experimental profiles were determined after deconvoluting the Voigt function. The results of the Stark widths obtained in this work and other experimental results compared to the results of semiempirical formula [1]are presented in Fig. 1. In order to compare experimental widths from various experiments, the values predicted by Dimitrijevic and Konjevic [1] were scaled to the reported electron densities and temperatures in Refs. [2-8].

Table 1. Plasma parameters and measured widths w_m obtained in this and other experiments.

N_e 10^{17} (cm^{-3})	T (K)	w_m (Å)	Ref.	N_e 10^{17} (cm^{-3})	T (K)	w_m (Å)	Ref.
0.69	12000	0.82	[2]	1	22000	0.393	[8]
1.2	13800	0.48	[3]	2.19	43300	0.67	This work
1	8500-16500	0.42-0.36	[4]	2.13	39000	0.615	
1	16500	0.36	[5]	2.07	34900	0.59	
1	12800	0.298	[6]	2.0	31400	0.55	
2.03	10880	0.741	[7]	1.94	28600	0.55	
1.79	11520	0.594	[7]	1.89	25760	0.536	
0.74	12200	0.184	[7]	1.83	22400	0.53	
1.1	13030	0.356	[7]	1.77	20260	0.516	

The Stark shifts of the Ar II 472.68 nm line at different times of the plasma evolution were determined from the fitting procedure. Because of the lack of information about the position of the line at null electron density (the unshifted wavelength), the relative shifts were calculated. The line position for the electron density of $2 \cdot 10^{17}$ cm^{-3} and plasma temperature of 31400 K was taken to be the one with zero shift, while the others were compared relative to it. The experimental shifts were then compared to theoretical values obtained from the semi-empirical formula [1] using the plasma parameters determined in this work. This comparison for different electron densities is presented in Fig. 2.

The average w_m/w_{th} for all experimental results (exluding that from Ref. 2) is 0.92 with standard deviation of 0.17. The average for this work is 1.00 with standard deviation of 0.11. Conclusion is that fairly good agreement between

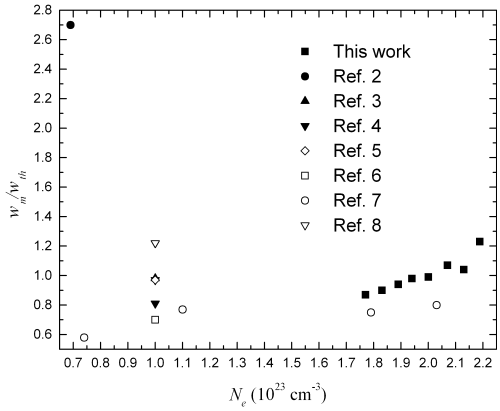

FIGURE 1. Comparison of measured and theoretical widths.

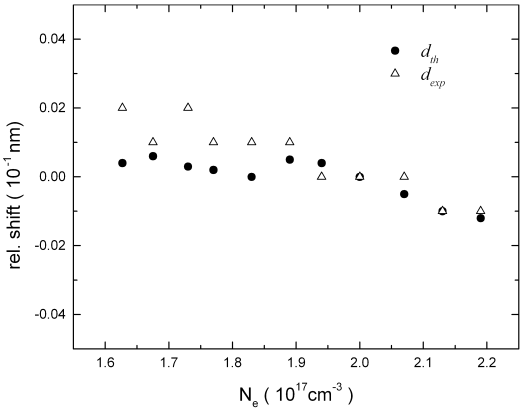

FIGURE 2. Theoretical and measured shifts.

semiepirical formula [1] and experimental results are found. Similar conclusion can be drawn for shifts also. As it is seen from Fig.2 agreement between sempirical formula [1] and experimental results of this work is well inside experimental error (± 0.05 Å).

ACKNOWLEDGMENTS

This work is suported by Ministry of Science and Tecnology, Republic of Serbia, under the project No. 141024

REFERENCES

1. M. S. Dimitrijević and N. Konjević, *J. Quant. Spectrosc. Radiat. Transfer* **24**, 451 (1980).
2. A. Abbas, T. S. Basha and Z. A. Abdel-Aal, *Jap. J. Appl. Phys.* **27**, 804 (1988).
3. J. Sy. A. Chapelle, F. Cabannes and J. Blandin, *J. Quant. Spectrosc. Radiat. Transfer* **8**, 1201 (1968); J. Sy. A. Chapelle, F. Cabannes and J. Blandin, *C.R.H. Academ. Sci., Ser.* **B264**, 853 (1967).
4. N. Konjević, J. Labat, Lj. Ćirković and J. Purić, *Z. Phys.* **235**, 35 (1970).
5. J. Labat, S. Djeniže, Lj. Ćirović and J. Purić, *J. Phys. B* **7**, 1174 (1974).
6. K. P.Nick and V. Helbig, *Phys. Scr.* **33**, 55 (1986).
7. K. Dzierzega and K. Musiol, *J. Quant. Spectrosc. Radiat. Transfer* **52**, 747 (1994).
8. S. Pellerin, K.Musiol and J. Chapelle, *J. Quant. Spectrosc. Radiat. Transfer* **57**, 377 (1997).

Anomalous broadening of Balmer H_α line in aluminum and copper hollow cathode glow discharges

N. M. Šišović*, G. Lj. Majstorović† and N. Konjević*

*Faculty of Physics, University of Belgrade, 11001 Belgrade, P.O. Box 368, Serbia
†Military Academy, 11105 Belgrade, Pavla Jurišića - Šturma 33, Serbia

The presented results are concerned with the shape of Balmer alpha line emitted from a low pressure DC glow discharge with aluminum (Al) and copper (Cu) hollow cathode (HC) in Ar-H_2 gas mixture. The analysis indicates that the line profile represents a convolution of Gaussian profiles resulting from different collision excitation processes.

INTRODUCTION

The present explanation of the phenomena of anomalous Doppler broadening (ADB) of hydrogen Balmer lines is based on a "sheath-collision model" [1-3]. This model, among other processes, takes into account the influence of gas composition and cathode material on ADB.

Recently recorded Balmer line shapes along the axis of a hollow cathode discharge and side-on from the Grimm discharge are found to be symmetric in H_2 or hydrogen-inert gases mixtures [4,5]. These profiles exhibit multicomponent behaviour that can be analyzed using Gaussians with great precision. The narrowest part of profile with the Doppler temperature not exceeding 1 eV, and of the middle part of line profile, with Doppler temperature smaller then 10 eV, are related to excited H^* atoms generated in collisions of high-energy electron with H_2 molecule. The pedestal of line profile is anomalous broad, indicating the presence of energetic H^* atoms, which may have energies larger than a hundred eV.

In argon-hydrogen mixtures, the ADB Balmer line profile looks different from those in pure hydrogen isotopes, see [6] and the references therein. The line shape with strong line wings, see below, fig. 1, is the result of dominant role of H_3^+ ion that is efficiently produced in Ar-H_2 mixture. The excited H atoms after fragmentation of H_3^+ ion in collision with H_2 or back-scattered H atoms from cathode have smaller energy (total ion energy is shared between three particles) than in the case of H^+.

EXPERIMENTAL

In this experiment, the H line shapes were observed in aluminum and copper hollow cathode discharges operated in an inert gas-hydrogen mixture (Ar + 0.8% vol. H_2) and pure hydrogen at a pressure of 2 mbar. The HC tubes were 100 mm long with 6 mm internal diameter. The discharge source is described in [4]. Here, we shall mention only few important details related to the optical setup for line shape recordings. The light along the axis of hollow cathode glow discharge is focused by an achromat quartz lens onto the entrance slit of spectrometer (2 m focal length; reciprocal dispersion of 0.74 nm/mm in the first order with a 651 grooves/mm reflection grating). Spectral line shape measurements are performed with an instrumental profile having Gaussian shape with 0.018 nm full half-width. Signals from CCD detector are collected and processed by PC. During the discharge operation, cathode was air cooled while HC wall temperature is controlled with a K-type thermocouple.

RESULTS AND DISCUSSION

Typical examples of the H_α line shape recording from the central region of aluminum and copper hollow cathode operated in low-voltage glow discharge regime are given in fig. 1. For the fitting of experimental profiles three Gaussian (Gauss 1, 2 and 3) are usually successfully utilized. Here, it should be noticed that an exception occurs when the extremely large contribution of the ADB part masks the middle component. An illustrative example is the shape of H_α line recorded from the copper HC discharge in Ar-H_2 mixture, see fig. 1b. The discharge conditions, relative contributions of Gaussian components to the total line fit and full half-widths of Gaussian components in energy unit scale for both hollow cathode discharges are given in table 1.

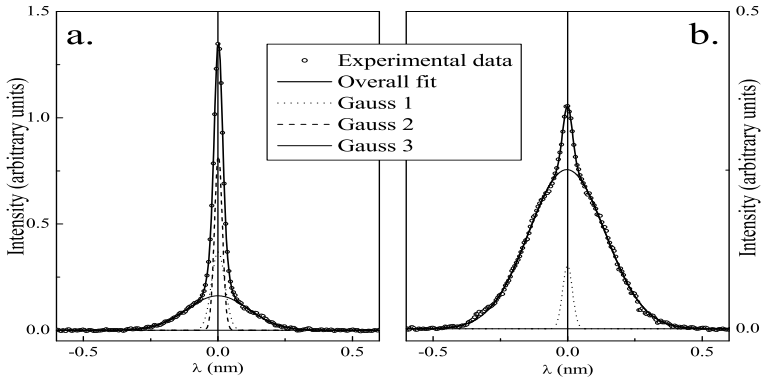

FIGURE 1. The H_α profiles recorded along the axis of hollow cathode glow discharge in Ar-H_2 and their best fits: (a) Aluminum, U=324V; I=90 mA and p=2 mbar; and (b) Copper, U=326V; I=90 mA and p=2 mbar.

TABLE 1. Experimental conditions, relative contributions G_i/G_{total} $(i = 1,2,3)$ and energies E_i $(i = 2,3)$ of excited hydrogen atoms obtained by applying multi Gaussian fits to the H_α profiles. Discharge conditions: gas mixture Ar+0.8%H_2; p=2 mbar; and I=90mA.

Cathode	**Voltage (V)**	G_1/G_{total} (%)	G_2/G_{total} (%)	G_3/G_{total} (%)	E_1 **(eV)**	E_2 **(eV)**	E_3 **(eV)**
Al	324	29.9	23.2	46.9	0.4	2	29
Cu	326	4.9	-	95.1	0.4	-	44

The results for energies of fast excited hydrogen atoms derived from the width of Gauss 3, see table 1, show that the anomalous H_α line broadening is present in both discharges under the studied experimental conditions. The Gauss 3 contribution to the overall profile is considerably lower for aluminum than in case of copper. In an another experiment, this difference is detected also for pure hydrogen matrix gas. The latter can be explained qualitatively by lower number reflection coefficient R_N of H^+ ions on aluminum [7]. Here, it should be pointed out that the reflection coefficients of H and H^+ are of marginal importance in argon gas mixtures with H_2 where the dominant interacting ion with cathode is H_3^+. Unfortunately, the reflection coefficients for the interaction of this ion with polycrystalline metals are not available.

The results in fig.1 indicate that the concentration and energy of fast excited hydrogen atoms depend upon cathode material through its back scattering coefficient, which may be related also to the surface composition in relation to the presence of metal hydrides at cathode surface, see [8].

ACKNOWLEDGMENTS

This work is supported by the Ministry of Science of the Republic of Serbia (Project # 141029B).

REFERENCES

1. Z. Lj. Petrović, B. M. Jelenković and A. V. Phelps, *Phys.Rev.Lett.* **68**, 325-328 (1992).
2. S. B. Radovanov, K. Dzierzega, J. R. Roberts and J. K. Olthoff, *Appl.Phys.Lett.* **66**, 2637-2639 (1995).
3. M.R. Gemišić-Adamov, B. M. Obradović, M. M. Kuraica and N. Konjević, *IEEE Trans.Plasma Sci.* **31**, 444-454 (2003).
4. N. M. Šišović, G. Lj. Majstorović and N. Konjević, *Eur. Phys. J. D* **32**, 347-354 (2005).
5. N. Cvetanović, M. M. Kuraica and N. Konjević, *J. Appl. Phys.* **97**, 033302-9 (2005).
6. G. Lj. Majstorović, N. M. Šišović, N. Konjević, *Phys.Plasmas* **14**, 043504-9 (2007).
7. T. Tabata, R. Ito, Y. Itikawa, N. Itoh and K. Morita, *At. Data Nucl. Data Tables* **28**, 493-530 (1983).
8. N. M. Šišović, G. Lj. Majstorović and N. Konjević, *Eur. Phys. J. D* **41**, 143-150 (2007).

Path integral formalism for the spectral line shape in plasmas: Lyman-α with fine structure

N. Bedida *, D. Boland†, M.T. Meftah * and R. Stamm †

*Laboratoire Lenreza Faculté des Sciences et Sciences de l'ingénieur, Université de Ouargla 30000 Algerie
†Laboratoire de Physique des Interactions Ioniques et Moléculaires 13397 Marseille France

We examine in this work the expression of the dipolar autocorrelation function for an emitter in the plasma using the path integrals formalism. The results for Lyman alpha lines with fine structure are retrieved in a compact formula. The expression of the dipolar autocorrelation function takes into account the ions dynamics and the fine structure effects.

INTRODUCTION

In this work we have retrieved the formula of the dipolar auto-correlation function common in the line broadening theory. Our derivation uses the Feynman path integral formalism [1]. Since the mean time of the electron-emitter collision is negligible compared with the ion-emitter one, we shall replace the electron-emitter collision effects by a standard collision operator [2], whereas the ion-emitter collisions effects, via the dipole approximation, will be treated in the perturbative approach using the path integral formalism. Section 2 is concerned by the formulation of the dipolar auto-correlation function in the formalism of the path integrals and in section 3, we apply earlier results to the Lyman alpha line with fine structure in time-dependent electric microfield. Conclusion and perspectives are given in section 4.

THE SPECTRAL LINE SHAPE IN THE PATH INTEGRALS THEORY

In this work we present a new expression of the evolution operator [2-3] using the path integral formalism based on the quantum-mechanical Dirac representation and the amplitude concept. The usual start of spectral line shape theory is the general formula giving the radiation power [3]:

$$I(\omega) = \frac{1}{\pi}\Re \int_0^\infty C(t)\exp(-i\omega t)dt \tag{1}$$

in this formula C(t) is the auto-correlation function of the dipolar momentum of the emitter given by:

$$C(t) = \sum_{\alpha\alpha'}\sum_{\beta\beta'} \vec{d}_{\alpha\beta}\left\{\left\langle\beta\left|T_b(t,0)\right|\beta'\right\rangle\left\langle\alpha\left|T_a(t,0)\right|\alpha'\right\rangle\right\}\vec{d}^{\,*}_{\alpha'\beta'} \tag{2}$$

where $\alpha\alpha'$ and $\beta\beta'$ are the upper and lower states respectively of the emitter including the spin states, and $\{...\}$ stands for a statistical average over the perturbers. As we are concerned in this work by the Lyman structure, we have in this case that the lower state β,β' is degenerate, and we can, after using the selection rule and the impact approximation for the electrons, transform C(t) as:

$$C(t) = exp(-it\varepsilon_{1,1/2}/\hbar).\sum_{jm_j}\left[\begin{array}{l}\frac{1}{4}\left|\left\langle 2\frac{3}{2}\right|d^1\left|1\frac{1}{2}\right\rangle\right|^2\exp\left(\Phi_e^1 t\right)\sum\limits_{m=\frac{-3}{2}}^{+\frac{3}{2}}\left\{\left\langle 2\frac{3}{2}m_j\right|T_a\left|2\frac{3}{2}m_j\right\rangle\right\}+ \\ +\frac{1}{2}\left|\left\langle 2\frac{1}{2}\right|d^1\left|1\frac{1}{2}\right\rangle\right|^2\exp\left(\Phi_e^2 t\right)\sum\limits_{m=-\frac{1}{2}}^{+\frac{1}{2}}\left\{\left\langle 2\frac{1}{2}m_j\right|T_a\left|2\frac{1}{2}m_j\right\rangle\right\}\end{array}\right] \tag{3}$$

where Φ_e is the collision operator, d^1 is the reduced matrix element, $\varepsilon_{1,1/2}$ the energy corresponding to $(n=1, j=1/2)$ and the matrix element of the evolution operator T in upper state a is:

$$\left\langle\alpha\left|T_a(t,0)\right|\alpha'\right\rangle = \int d\vec{r}\,d\vec{r'}\,\phi_\alpha^*(\vec{r})K_a(\vec{r'},t/\vec{r},0)\phi_{\alpha'}(\vec{r'}) \tag{4}$$

where $K(\overrightarrow{r_2},t_2/\overrightarrow{r_1},t_1)$ is the Feynman propagator describing the emitter evolution in the surrounding ion plasma . $\varphi_\alpha(\overrightarrow{r})$ are the eigen functions of the Dirac operator relative to the free hydrogen atom. Then, to calculate the dipolar auto-correlation function $C(t)$, it is useful to evaluate the Feynman propagator $K_a(\overrightarrow{r'},t/\overrightarrow{r},0)$ as follows:

$$K_a\left(r',t;r,0\right)=\int_{\overrightarrow{r}(0)=\overrightarrow{r}}^{\overrightarrow{r}(t)=\overrightarrow{r}'} D[\overrightarrow{r}(\tau)]\exp\left\{\frac{i}{\hbar}\int_0^t\left(L_0^D+e\overrightarrow{r}\overrightarrow{E}(\tau)\right)d\tau\right\} \tag{5}$$

where L_0^D is the Dirac Lagrangian for the free hydrogen atom, and $(e\overrightarrow{y}\overrightarrow{E}(\tau))$ is the interaction between the hydrogen atom and the surrounding plasma in the dipole approximation. It is possible to develop the propagator $K_a(r',t;r,0)$ as a perturbation series knowing the free propagator K_0 relative to the free hydrogen atom:

$$\begin{aligned}K_a(x)=\sum_{\alpha_1\ldots\alpha_{k+1}}\sum_{k=0}^{\infty}(\frac{i}{\hbar})^k\frac{1}{k!}\int_0^t d\tau_1\ldots\int_0^t d\tau_k\int d\overrightarrow{r}_1.....\int d\overrightarrow{r}_k(\overrightarrow{E}_1\overrightarrow{r}_1)....(\overrightarrow{E}_k\overrightarrow{r}_k)\\ \varphi^*_{\alpha_{k+1}}(\overrightarrow{r})\varphi_{\alpha_{k+1}}(\overrightarrow{r}_k)\exp\frac{i}{\hbar}\varepsilon_{\alpha_{k+1}}(t-\tau_k).\varphi_{\alpha_k}(\overrightarrow{r})\varphi^*_{\alpha_{k-1}}(\overrightarrow{r}_{k-1})\\ \exp\frac{i}{\hbar}\varepsilon_{\alpha_k}(\tau_k-\tau_{k-1})\ldots\varphi_{\alpha_2}(\overrightarrow{r}_2)\varphi^*_{\alpha_2}(\overrightarrow{r}_1)\exp\frac{i}{\hbar}\varepsilon_{\alpha_2}(\tau_2-\tau_1).\varphi_{\alpha_1}(\overrightarrow{r}_1)\varphi^*_{\alpha_1}(\overrightarrow{r}')\exp\frac{i}{\hbar}\varepsilon_{\alpha_1}(\tau_1-0)\end{aligned} \tag{6}$$

where $\{\alpha_i\}=\{n,j,l,m_j\}$, $l=j\pm\frac{1}{2}$, $l'=2j-l$ and ε_{nj} is the spectra of the free atom including the fine structure.

APPLICATION TO LYMAN-ALPHA BROADENING

Summarizing (3-4) and (6) we calculate both $\left\langle 2\frac{3}{2}m_j\right|T\left|2\frac{3}{2}m_j\right\rangle$ and $\left\langle 2\frac{1}{2}m_j\right|T\left|2\frac{1}{2}m_j\right\rangle$ and use the weak coupling approximation ($\langle E_1E_2E_3E_4\rangle\approx\langle E_1E_2\rangle\langle E_3E_4\rangle$), we can write the formula (3) for the dipolar auto-correlation function C(t) as:

$$\begin{aligned}C(t)=\frac{1}{4}|\langle 2,\frac{3}{2}|d^1|1,\frac{1}{2}\rangle|^2.exp(\Phi_e^1t+\frac{i}{\hbar}(\varepsilon_{2,3/2}-\varepsilon_{1,1/2})t).(2+\cos(\frac{D_+}{\hbar}\sqrt{h(t)})+\cos(\frac{D_-}{\hbar}\sqrt{h(t)}))\\ +\frac{1}{2}|\langle 2,\frac{1}{2}|d^1|1,\frac{1}{2}\rangle|^2.exp(\Phi_e^2t+\frac{i}{\hbar}(\varepsilon_{2,1/2}-\varepsilon_{1,1/2})t).(cos(\frac{D_+}{\hbar}\sqrt{h(t)})+cos(\frac{D_-}{\hbar}\sqrt{h(t)}))\end{aligned} \tag{7}$$

where:

$$h(t)=\int_0^t d\tau\int_0^t d\tau'\left\{E(\tau)E(\tau')\right\},D_\pm=\left|\int d\overrightarrow{r}\varphi_{2,3/2,\pm1/2}(\overrightarrow{r})\overrightarrow{r}\varphi^*_{2,1/2,\pm1/2}(\overrightarrow{r})\right| \tag{8}$$

Φ_e^1 and Φ_e^2 are the electronic collision operators relative to $(2p_{3/2}\longrightarrow 1s_{1/2})$ and $(2p_{1/2}\longrightarrow 1s_{1/2})$ transitions respectively, and the symbol $\{\ldots\}$ means as said earlier the statistical average over the ionic perturbers.

CONCLUSION

We have applied the formalism of path integrals to the spectral line shape in plasmas providing an alternative treatment of Stark broadening. This formalism is suitable for keeping the ionic dynamics in the calculation of the evolution operator and in the auto-correlation function C(t).

REFERENCES

1. R.P. Feynman and A.R. Hibbs: "Quantum Mechanics and Path-Integral" (McGraw-Hill, New York, 1965)
2. H. Griem: Plasma Spectroscopy. (McGraw Hill N.Y. 1964)
3. M. Baranger: Phys. Rev. 111. 481 (1958)

Electronic Broadening operator for relativistic plasmas

M.T. Meftah* and A. Naam†

*Laboratoire Lenreza, Département de Physique, Faculté des Sciences et Sciences de l'ingénieur, Université de Ouargla 30000 Algerie
†Département de Physique, Faculté des Sciences et Sciences de l'ingénieur, Université de Ouargla 30000 Algerie

In this work we review some aspects of the semiclassical dipole impact approximation for isolated ion lines in relativistic plasma. Mainly we focuss our work on the collision operator for relativistic electrons. In this case, the electron trajectory around a positive charge in the plasma differs dragistically from those known earlier as hyperbolic. The effect of this difference on the collision operator is discussed with respect the various plasma conditions. Some theoretical and practical aspects of lines –shape calculations are discussed. Detailed calculations are performed for the collision operator in the semiclassical (dipole) impact approximation.

INTRODUCTION

Our task consist to present the electronic collision operator ϕ where the unbounded electrons are subjected to move at high velocity in relativistic plasma. We have developed exactly the collision operator for the relativistic impact electrons in the case where the inelasticity parameter is zero (without fine structure) and in the semi-classical theory keeping only the dipole interaction.

RESULTS

We have discussed the effect of the different plasma parameters (temperature, electronic density N, Z charge and the principal quantum number) on the difference between Spiros operator (hyperbolic trajectory of the impact electrons)[1] and our operator calculated within the unbounded relativistic electrons. Evoking the direct term $\phi_d^* \equiv \phi^*$(relativistic), we have concluded that depends slowly on the principal quantum number n and on the electronic plasma density N. Whereas the rate $\frac{\Delta\phi(0)}{\phi(0)}(\%)$ is a increasing function of the electronic temperature T. This rate reaches 60% for $T = 5.93 \times 10^9$ °K corresponding to the case where the electronic mean velocity v reaches the light velocity c ($v = \sqrt{2kT_e/m_e}$). The relativistic effect increases with the energy separation ω about 1% which is negligible effect.

REFERENCES

1. S. Alexiou, Phys. Rev. A 49, 106 (1994)

On the electric micro-field in plasmas: statistics of the spatial derivatives

S. Guerricha *, S. Chihi† and M.T. Meftah †

*Laboratoire Lenreza Faculté des Sciences et Sciences de l'ingénieur, Université de Ouargla 30000 Algerie
†Laboratoire Lenreza, Département de Physique, Faculté des Sciences et Sciences de l'ingénieur, Université de Ouargla 30000 Algerie

Using the Monte-Carlo simulation we calculated for some specific plasmas, the distribution functions of the derivatives of the micro-field components. Some of them are compared to those calculated earlier by other authors.

INTRODUCTION

The micro-field effect plays a significant role in the broadening of spectral line shape. This effect is represented by the distribution function of the ionic micro-field when the interaction between the radiator and the plasma is treated in the dipole approximation. The latter is well justified at lower densities, where the assumption of a uniform micro-field at the radiator is usually admitted. Conversely, at high temperatures and densities, the dipole approximation becomes severe, and it is important to consider the effects of higher-order of micro-field on spectral line shape. As the densities increases, the distances between particles decrease and then the micro-field gradients (the non-uniformity) appear in the vicinity of the radiator nucleus. Therefore it becomes necessary to study the contribution of the non-uniformity on the spectral line shape. This requires knowledge of the statistic of the field spatial derivatives in such plasmas. In this work, we calculate the conditional statistic of the micro-field spatial derivatives for a given value of the micro-field and compared it to those found in the literature [1, 2, 3]. Strictly speaking, we have only needed two distributions which we have calculated in this work: one is relative to the derivative towards the micro-field $P(\partial E_z/\partial z)_\varepsilon$ the second is relative to the perpendicular derivative $P(\partial E_z/\partial x)_\varepsilon$. In section (2), we outline some basic theory for the calculation of the constrained distribution function of the spatial derivative towards the micro-field in the independent particles model(Holtsmark model). The particles interact with the radiator via Debye potential. In section (3), using Monte-Carlo simulation(MCs), we calculate $P(\partial E_z/\partial z)_\varepsilon$ and $P(\partial E_z/\partial x)_\varepsilon$. In section (4) we present our theoretical results (both analytical and simulation) and compare them to others found in the literature. We conclude this contribution with a discussion.

SUMMARY OF THEORETICAL APPROACH

Analytical approximation

We can write

$$Q(f,\varepsilon) = P(\partial E_z/\partial z)_\varepsilon = <\delta(f-\partial E_z/\partial z)\delta(\varepsilon - E)> \tag{1}$$

where the brackets <...> denote the statistical average over the ions with respect to the canonical ensemble. In the model of the independent particles, the formula (1)can be simplified as:

$$Q(f,\varepsilon) = \int_{-\infty}^{+\infty}\int_{-\infty}^{+\infty} du d\omega . e^{i(\omega f+u\varepsilon)} [\frac{\int_{r_i}^{R} r^2 dr . exp(-i(\omega \partial E_z/\partial z + uE) - U(r)/kT)}{\int_{r_i}^{R} r^2 dr . exp(-U(r)/kT)}]^{N_i} \tag{2}$$

where $4\pi r_i^3 n_i/3 = 1$, $(n_i = N_i/V)$, $4\pi R^3/3 = V$, $U(r)$ is the Debye potential energy between a particle and the radiator, k is the Boltzmann constant and T is the temperature of the system. N_i is the total number of ions, V is the volume of the system and r_i is the ion sphere radius. In the case of weak coupling limit, the formula (2) transforms as:

$$Q(f,\varepsilon) = \int_{-\infty}^{+\infty}\int_{-\infty}^{+\infty} du d\omega . e^{i(\omega f+u\varepsilon)} [\frac{4\pi}{V}\int_{r_i}^{R} r^2 dr . exp(-i(\omega \partial E_z/\partial z + uE))]^{N_i} \tag{3}$$

A simple computation gives the distribution $Q(f,\varepsilon)$ as a normalized gaussian form:

$$Q(f,\varepsilon) = \frac{1}{\sqrt{4\pi\alpha}} exp(-\frac{(f-(B-\frac{\varepsilon-A}{2C}G))^2}{4\alpha}) \tag{4}$$

where:

$$A = 4\pi Zen_i(2\lambda + r_i)e^{-s}, B = 4\pi Zen_i(E_i(s) + e^{-s}), C = \pi(Ze)^2 n_i(\frac{2\lambda + r_i}{\lambda r_i}), \alpha = -(D + \frac{G^2}{4C}) \tag{5}$$

and

$$D = \frac{2\pi(Ze)^2}{3\lambda^3} n_i[-2E_i(2s) + e^{-2s}(\frac{1}{s} - \frac{2}{s^2} - \frac{1}{s^3})], G = \frac{4\pi(Ze)^2}{\lambda^2} n_i[-E_i(2s) + e^{-2s}(\frac{1}{s} + \frac{1}{2s^2})] \tag{6}$$

here s is the screening parameter defined as $s = r_i/\lambda$,λ is the Debye length and $E_i(x)$ is the exponential integral function. We can see in formula (4) that the distribution shifts to the left when the common micro-field ε increases. Although, our theoretical calculation (4) is based on the independent particles model, it agrees(in the sense of the shifting to the left) with Kilcrease results (MDS) and our (MCs) where the interactions between the particles are taken into account.

MCs approach

As MCs method has given a good results for the distribution of the electric micro-field in the plasmas [4], we have in this work used this method to compute the distribution of its spatial derivatives. We have taken at all a plasma of hydrogenic Argon ($Z = 17^+, T = 800eV$ and a density $n_i = 10^{24} cm^{-3}$ which are the Kilcrease [3] conditions for different values of the common electric field ε.

RESULTS AND COMPARISON

As the theoretical results are done in more ideal situation (independent particles model and zero coupling between the ions and the radiator), we have only reported in the figures the results relative to the MC simulation, and compared them with Kilcrease ones. We have taken the the common micro-field $\varepsilon = 0.5$ in (e/r_e^2) unit and referred the spatial micro-field derivative to (e/r_e^3) where $4\pi r_e^3 n_e/3 = 1$ $(n_e = Zn_i)$. Our distributions agree in general aspect: semi Gaussian, decrease in height, increase in width and shift to the left, when the common micro-field ε increases. The little difference between the results is possible due to the idea of model: the MD simulation solves the differential equations describing the actual movement of each particle, whereas MC treats them as static particles, randomly distributed in space.

DISCUSSION

In this communication, we have interested in the statistic of the spatial derivatives of the electric micro-field in plasmas. We have used the MCs method to compute the distribution functions $Q(f,\varepsilon)$ both towards the micro-field and in the perpendicular direction.

REFERENCES

1. Holtsmark J. Ann Phys (Leipzig) 1919;58:577.
2. S. Chandrasekhar and J. Von Neumann ApJ. 1943, pp489
3. D. P. Kilcrease and M. S. Murillo, J. Quant. Spectrosc. Radiat. Transfer, 65, 343 (2000).
4. A. Y. Potekhin, G. Chabrier and D. Gilles: Phys.Rev. E65 (2002) 036412

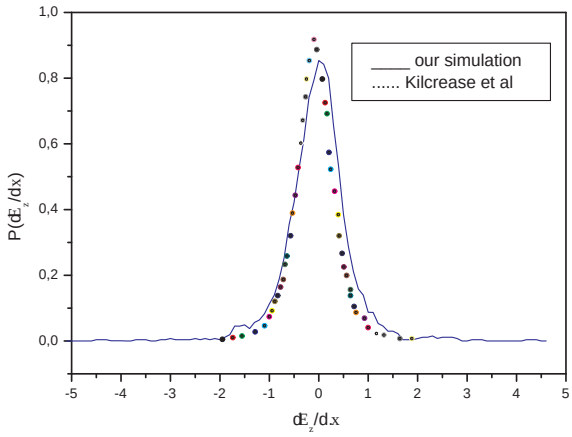

FIGURE 1. perpendicular distribution

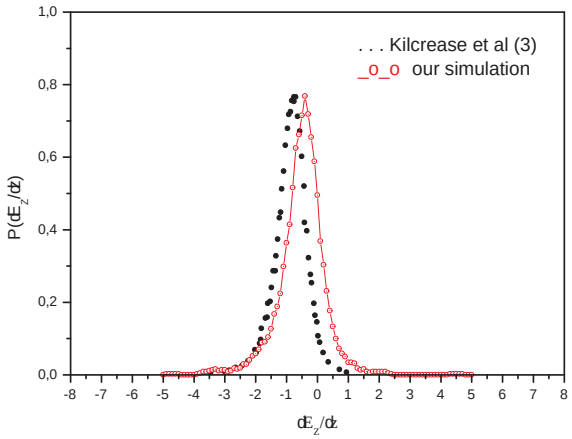

FIGURE 2. parallel distribution

Characterization of the Three Phase Plasma Arc and its Applications in Analyzing Environmental Samples

Mina Zekry Fahmy

Faculty of Science, Alexandria University, Egypt
163 Horrya Avenue, P.O. 832 Shatby, Alexandria, EGYPT

ABSTRACT

The paper describes the some spectrophysical characteristics of a home made three phase plasma spectrometer and its application in analyzing airborne samples. The excitation temperature of plasma is calculated using Boltzmann plot from the iron lines in the spectral range between 370 nm and 377 nm. The excitation temperature measurements along the central vertical axis of the plasma for iron are plotted as function of the electric current (15A, 27A, 35A and 45A, respectively) for different heights above the quartz tube. Under the assumption of local thermal equilibrium (LTE), the electron number density obtained from the Saha-Eggert equation is about 5×10^{14} cm^{-3}. Ionization interference effects on Ca (II) emission produced by an easily ionized element (EIE) are in general agreement with inductively coupled plasma (ICP). Analytical calibration curves and detection limits data are shown for Al, Ca, Cd, Cr, Cu, Fe, Mg, Mn, Ni, Pb, V, and Zn. The present technique is applied for the analysis of airborne samples and compared with ICP.

Quantum calculations of Stark broadening of Li-like ions; T and Z-scaling

Haykel Elabidi*, Nébil Ben Nessib† and Sylvie Sahal-Bréchot**

*Groupe de Recherche en Physique Atomique et Astrophysique, faculté des Sciencs de Bizerte, Zarzouna, Tunisia
†Groupe de recherche en Physique Atomique et Astrophysique, Institut National des Sciences Appliquées et de Technologie, B.P. 676, 1080 Tunis Cedex, Tunisia.
**LERMA, UMR 8112 CNRS, Observatoire de Paris-Meudon, F-92195 Meudon Cedex, France

Diagnostic of stellar and laboratory plasmas, atomic abundances, opacity calculations, particle densities can be determined through knowledge of Stark broadening of isolated spectral lines of multicharged ions in plasmas. This broadening is due to a complex interaction between electrons and radiating ions [1, 2]. We note that Stark broadening diagnostics generally require quite elaborate calculations. Comparison of theoretical with experimental Stark widths measured for well determined plasmas conditions is therefore very important for the improvement of theoretical methods and techniques.

The study of plasmas broadening of analogous spectral lines along isoelectronic sequences gives good opportunity for testing the theory under conditions of gradual change of energy levels structure of the emitter with gradual increase of ionic charge. These studies also enable determination of the Stark width dependence upon the effective charge $Z = z+1$ "seen" by the optical electron, where z is the charge of the ion. This is important for the estimation of broadening parameters of ions with no available data.

Several methods and techniques were used for the evaluation of broadening parameters, we can cite semi-classical [1, 2, 3, 4], modified [5, 6, 7] semi-empirical [8] and quantum-mechanical calculations [9, 10, 11, 12, 13, 14]. The most theoretical efforts were directed toward elaboration of the two first methods which showed a good accuracy for neutral elements and low-charge ions. For the last method, it makes use of the **T** matrix elements or cross sections. While this method was established a long time ago [9], such calculations become possible only when atomic collision codes were available. Calculations are still very limited. Quantum-mechanical calculations cited above showed that they underestimate the majority of experimental widths. They have the greatest difference from the experimental results compared to other types of theoretical calculations. Recently, a disagreement was found for the 2s3s−2s3p singlet and triplet linewidths in Be-like ions: N IV, O V and Ne VII [13], and for 3s−3p linewidths in Li-like ions from C to Ne [14]. Again most of the quantum-mechanical calculations (in Be-like or Li-like ions) are lower than the experimental results.

In [15], Elabidi *et al.* have obtained the new following quantum-mechanical expression calculating electron impact linewidth for intermediate coupling. Here, N_e is the electron density, v the velocity of the scattered electron and $f(v)$ the Maxwellian electron velocity distribution.

$$
\begin{aligned}
w &= \pi\left(\frac{\hbar}{m}\right)^2 N_e \sum_{J_i^T J_f^T l l' K_i K_f K_{i'} K_{f'}} (-1)^{2J_i+K_i+K_{i'}+K_f+K_{f'}+2J_f^T+l+l'+1} \\
&\times \left[K_i,K_f,K_{i'},K_{f'}\right]^{\frac{1}{2}} \frac{\left[J_f^T,J_i^T\right]}{2} \left\{ \begin{array}{cc} J_i & K_i \; l \\ K_f & J_f \; 1 \end{array} \right\} \left\{ \begin{array}{cc} J_i & K_{i'} \; l' \\ K_{f'} & J_f \; 1 \end{array} \right\} \\
&\times \left\{ \begin{array}{cc} K_i & J_i^T \; s \\ J_f^T & K_f \; 1 \end{array} \right\} \left\{ \begin{array}{cc} K_{i'} & J_i^T \; s \\ J_f^T & K_{f'} \; 1 \end{array} \right\} \int_0^\infty \frac{f(v)}{v} dv \Big\{ \delta_{l'l} \delta_{K_{i'}K_i} \delta_{K_{f'}K_f} \\
&- Re\left[S_F^{*IC}(\Delta_{f'} J_f l' K_{f'} s J_f^T; \Delta_f J_f l K_f s J_f^T)\right. \\
&\times \left. S_I^{IC}(\Delta_{i'} J_i l' K_{i'} s J_i^T; \Delta_i J_i l K_i s J_i^T)\right] \Big\} \qquad (1)
\end{aligned}
$$

L and S represent the atomic orbital angular momentum and spin of the target, l and l' are the electron orbital momentum before and after collision, the superscript T denote the quantum numbers of the total electron+ion system. $S_I^{IC}(\Delta_{i'} J_i l' K_{i'} s J_i^T; \Delta_i J_i l K_i s J_i^T)$ is the scattering matrix element for the initial level, denotes as I, expressed in the intermediate coupling approximation, the same definition as for the complex conjugate $S_F^{*IC}(\Delta_{f'} J_f l' K_{f'} s J_f^T; \Delta_f J_f l K_f s J_f^T)$ of **S** for the final level, denoted as F, $Re(....)$ is the real part of (...),

In an earlier paper [16], Elabidi *et al.* have applied this method for Be-like ions and good agreement between experiments has been found. We have used the UCL atomic code package SUPERSTRUCTURE/DW/JAJOM. This

package has been used for many years and provides fine structure wavefunctions, energy levels, wavelengths, radiative probability rates and electron impact collision strengths [17, 18, 19]. We extend the use of these codes to electron impact linewidths calculations.

We present in this work, quantum calculations of electron impact linewidths for five Li-like ions (C IV, N V, O VI, F VII and Ne VIII). The Comparisons with experiment show a good agreement. We study the behavior of linewidths versus electron temperature and ionic charge Z.

ACKNOWLEDGMENTS

We are grateful to Jacques Dubau from LUTH/LIXAM and Marguerite Cornille from LUTH (France) for their valuable discussions and help to achieve the present work.

REFERENCES

1. H. R. Griem, *Spectral line broadening by plasmas*, New York: New York Academic Press 1974.
2. H. R. Griem, *Principles of plasma spectroscopy*, Cambridge: Cambridge University press 1997.
3. S, Sahal-Bréchot, *Astron. Astrophys.* **1**, 91–123 (1969).
4. S, Sahal-Bréchot, *Astron. Astrophys.* **2**, 322–354 (1969).
5. M. S. Dimitrijević, and N. Konjević, *J. Quant. Spectrosc. Radiat. Transfer* **24**, 451–459 (1980).
6. M. S. Dimitrijević, and N. Konjević, *Proc. Int. Conf. on Spectral line broadening by plasmas* edited by B. Wende and W. de Gruyter, Berlin, 1981, p. 211.
7. H. Elabidi, N. Ben Nessib, and M. S. Dimitrijević, *New Astronomy* **12**, 64–70 (2006)
8. H. R. Griem, *Phys. Rev.* **165**, 258–266 (1968).
9. M. Baranger, *Phys. Rev.* **112**, 855–865 (1958).
10. M. J. Seaton, *J. Phys. B.: At. Mol. Phys.* **21**, 3033–3053 (1988).
11. H. R. Griem, Yu. V. Ralchenko, and I. Bray, *Phys. Rev.* E **56**, 7186–7192 (1997).
12. Yu. V. Ralchenko, H. R. Griem, I. Bray, and D. V. Fursa, *Phys. Rev.* A **59**, 1890–1895 (1999).
13. Yu. V. Ralchenko, H. R. Griem, I. Bray, and D. V. Fursa *J. Quant. Spectrosc. Radiat. Transfer* **71**, 595–607 (2001).
14. Yu. V. Ralchenko, H. R. Griem, and I. Bray, *J. Quant. Spectrosc. Radiat. Transfer* **81**, 371–384 (2003).
15. H. Elabidi, N. Ben Nessib, and S. Sahal-Bréchot, *J. Phys. B.: At. Mol. Opt. Phys.* **37**, 63–71 (2004)
16. H. Elabidi, N. Ben Nessib, J. Dubau, M. cornille, and S. Sahal-Bréchot, *J. Phys. B.: At. Mol. Opt. Phys.* **41**, n 025702 (2008)
17. N. Ben Nessib, H. Elabidi, M. Cornille, and J. Dubau, *Physica Scipta* **72**, 23–30 (2005)
18. C. Blancard, M. Cornille, and J. Dubau, *Physica Scipta* **64**, 452–454 (2001)
19. M. Cornille, J. Dubau, and S. Jacquemot, *At. Data Nucl. Data Tables* **58**, 1–66 (1994)

Gas Temperature Determination in Argon-Helium Plasma at Atmospheric Pressure using van der Waals Broadening

Jose Muñoz*, Milan S. Dimitrijević†, Cristina Yubero* and Maria Dolores Calzada*

*Grupo de Espectroscopia de Plasmas, Edificio A. Einstein (C-2), Campus Rabanales, Universidad de Córdoba, Spain
†Astronomical Observatory, Volgina 7, 11060 Belgrade, Serbia

INTRODUCTION

In the last years, a common characteristic of most of the technological applications of plasmas is that they are a gas mixture. When more than one kind of gas is present in the discharge, the complexity of experimental determination of plasma parameters by spectroscopic techniques increases. It is due to the existence of different types of perturbers in the plasma gas, which have influence on the spectral line profiles and van der Waals broadening is a function of the reduced mass of colliding atoms. Studies of such influences are important for the application of spectroscopic techniques in the diagnostics of plasmas generated with gas mixtures.

In this work, the use of the van der Waals broadening of the atomic lines to determine the gas temperature in Ar-He plasmas, taking into account both argon and helium atoms as perturbers, has been analyzed. The values of the gas temperature inferred from this broadening have been compared with the ones obtained from the spectra emitted by the OH molecular species in the discharges.

Theoretically, any spectral line could be used for the determination of the plasma gas temperature from its van der Waals broadening. However, experimental studies carried out by several authors (see Refs. cited in [1]) have stated that only a few lines can be used for this purpose. First of all, the separation of the van der Waals broadening from the whole width of the spectral profile, needs a deconvolution process. Also, the theory does not describe equally good the van der Waals broadening for each spectral line and for each kind of perturbers, so that the corresponding investigations in order to find the most convenient lines for this purpose are of interest.

In a surface wave plasma generated with pure Ar, in [2] is studied the contribution of the Stark broadening to the Lorentzian width for Ar lines belonging to the $nd - 4p$ transitions ($4 \leq n \leq 7$). The procedure used to separate both Lorentzian and Gaussian parts by these authors was the same as one used in the present work. Their results showed that Stark broadening can be considered negligible for the 737.2 nm ($n = 4$) line and very small for the 603.2 nm ($n = 5$). Consequently, they considered that the Lorentzian width of these lines was mainly due to the van der Waals effect and the gas temperature obtained from 603.2 nm was approximately equal to the one obtained from OH radical band (approximately 1500 K) in this case.

In [3] is proposed a method to measure the gas temperature T_g from atomic lines whose Stark broadening is comparable with the van der Waals one. T_g was obtained from the origin ordinate corresponding to the Lorentzian width for zero electron density which could be considered approximately equal to van de Waals line width. For this study the best argon atomic lines for the gas temperature T_g calculation in an argon microwave plasma at atmospheric pressure were 603.2 nm, 549.6 nm and 522.1 nm. The values obtained from this method were between 1100 and 1200 K. On the other hand, in [4] was studied the Stark broadening of the 425.9 nm line. By extrapolating the results in [4] to their experimental conditions, Yubero *et al.* [3] obtained that the van der Waals width value of the above mentioned line was about 90% of the total Lorentzian width and the gas temperature from the van der Waals broadening of this line was equal to 1380 K. Consequently with all these results, the use of 425.9, 603.2, 549.6 and 522.1 nm lines to measure the gas temperature in plasmas generated with Ar-He mixtures was considered in the present work.

GAS TEMPERATURE DETERMINATION IN AR-HE MIXTURE DISCHARGE

The experimental procedure is described in detail in [1]. The spectra for these lines were registered in different conditions of Ar-He mixtures, observing a significant decrease of the intensities of the Ar atomic lines when He is added to the plasma gas. An analysis of the profiles of these lines was carried out in the more extreme condition which corresponded, in our case, to a 30% of He in the mixture. We found that with the increase of the upper level of the transition a high dispersion in the fit of the 549.6 nm ($4p - 6d$ transition) and 522.1 nm ($4p - 7d$ transition)

line profiles to a Voigt function appears. Thus, only the 425.9 nm ($4s-5p$) and 603.2 nm ($4p-5d$) lines have been considered for this study.

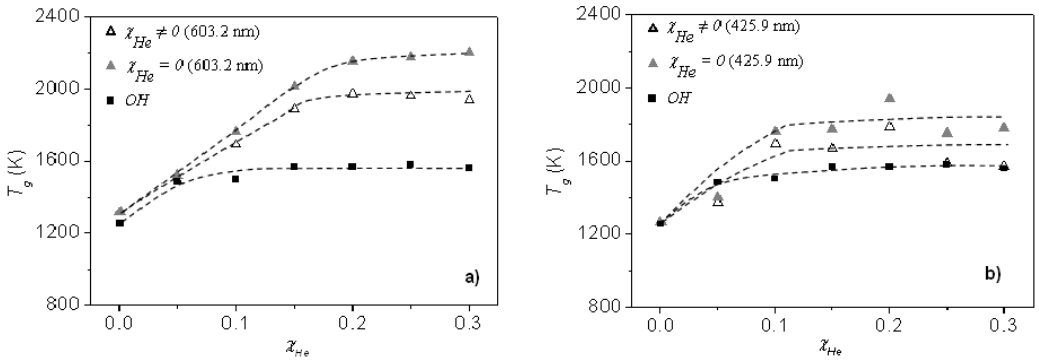

FIGURE 1. Gas temperature calculated using the (0 – 0) 309 nm rovibrational band of the OH radical and the 603.2 nm (a) and 425.9 nm (b) atomic argon lines taking into account (hollow triangle) and neglecting (full triangle) the contribution of He to the van der Waals broadening

The T_g values obtained from the van der Waals of the 603.2 and 425.9 nm lines appear depicted in Figs.1a and 1b, respectively. These temperature values have been calculated by using equations derived in [1]. In the case of an Ar-He mixed gas discharge, full width at half maximum (FWHM) provoked by van der Waals broadening (w_W) is given by the following equations

$$w_W(425.9\,\text{nm}) = \chi_{Ar}\frac{1.479}{T_g^{0.7}} + \chi_{He}\frac{1.059}{T_g^{0.7}} \tag{1}$$

$$w_W(603.2\,\text{nm}) = \chi_{Ar}\frac{4.217}{T_g^{0.7}} + \chi_{He}\frac{3.019}{T_g^{0.7}} \tag{2}$$

where χ_{Ar} and χ_{He} are molar fractions of the constituting gases, argon and helium. Also, the values obtained from OH radical band have been represented. In Fig. 1 one observes that the T_g calculated from w_W are a slightly higher that those obtained from OH radical. It is also observed a bigger dispersion in T_g values from w_W of 425.9 nm line than 603.2 nm line because of its smaller Lorentzian width value w_L, which results in higher error in the deconvolution process.

Moreover, to point up that T_g values obtained from OH radical is lower than those obtained from the Lorentzian width of Ar lines for He concentrations obove 5%. This can be due to a lack of sensitivity of the OH radical for temperatures higher than 1600 – 1800 K. This result seems to indicate that for the lines used in this work and under our experimental conditions the lorentzian width of the atomic lines can be considered almost equal to their van der Waals broadenings without inducing large errors in T_g determination. The most important result found in this study is the necessity to taking to account He contribution to the van der Waals broadening for lines used in Ar-He mixtures. This allows us to conclude that the above equations may be used when the van der Waals broadening of the considered argon lines is utilized for measuring the gas temperature in an Ar-He plasma.

ACKNOWLEDGMENT

This work was supported by the Ministry of Science and Technology (Spain) within the framework of the project no. ENE2005-00314, and by the Ministry of Science of Serbia through the project 146001.

REFERENCES

1. J. Muñoz, M. S. Dimitrijević, C. Yubero, M. D. Calzada,to be published
2. M. Christova, E. Castaños-Martínez, M. D. Calzada, Y. Kabouzi, J. M. Luque, M. Moisan, *Appl. Spectrosc.* **58**, 1032 (2004).
3. C. Yubero, M. S. Dimitrijević, M. C. Garcia, M. D. Calzada, *Spectrochim. Acta B* **62**, 169 (2007).
4. S. Djurović, Z. Mijatović, R Kobilarov, N. Konjević, *J. Quant. Spectrosc. Radiat. Transfer*, **57**, 695 (1996).

Self-absorption effects in experimental methods used to determine electronic density and gas temperature in an argon microwave plasma (SWD) generated at atmospheric pressure

I. Santiago, J. Muñoz and M. D. Calzada

Grupo de Espectroscopia de Plasmas, Dpto. de Física. Edificio C-2. Campus de Rabanales. Universidad de Córdoba 14071 Córdoba (Spain). E-mail: fa1cazal@uco.es

INTRODUCTION

Emission spectroscopy is a passive (non-perturbative) technique used to perform the physics diagnosis of surface wave discharges (microwave discharges) at atmospheric pressure. The radiation emitted by plasma is collected and analyzed to obtain information about the values of the plasma parameters and the discharge kinetics. The correct study of the intensity distribution of the spectral lines around their central wavelength (broadenings and total intensity) allows for the determination of plasma macroscopic parameters such as temperatures, electron density and atom and ion populations.

At atmospheric pressure line profiles are adequately fitted by a Voigt function, which is the convolution of a Gaussian function (Doppler and instrumental broadenings) and a Lorentzian one (natural, van der Waals and Stark broadenings). However there are some phenomena, such as self-absorption, which affect some spectral lines emitted by plasmas [1], which could distort their real spectral distribution. The radiation emitted by the discharge has to traverse it before emerging outside. During its passage it is at risk of being absorbed by the atoms or molecules of the same kind as those that cause the emission. Thus, the light observed outside the source could be less intense than the radiation originally emitted inside it, and the profiles of the spectral lines would present an anomalous broadening (a greater decrease in the intensity at the centre of the spectral lines) produced by this phenomenon [2]. When these self-absorbed spectral lines are used for the plasma diagnosis they can cause erroneous results. It is well known that for high populations of absorbing atoms and f (oscillator strength) values of the spectral line, the self-absorption and the variation of the Voigt full width at half-maximum is higher. Each spectral line can be absorbed differently, therefore an study of the experimental line shapes is needed in order to obtain plasma magnitudes properly. In this work a procedure is applied to determine if self-absorption affects the spectral lines used in the determination of electron density (n_e) and the gas temperature (T_{gas}) in these plasmas at atmospheric pressure, assuring that the results obtained are not perturbed by this phenomenon.

EXPERIMENTAL PROCEDURE AND RESULTS

The plasma was generated in a quartz tube opened to the atmosphere with an inner diameter of 1 mm. A surfatron was used as excitation device. The gas used was pure argon (99.99%) with a flow of 0.250 slm. Microwave power (100 W) at 2.45 GHz was supplied in continuous mode by a Microtron 200 E.M.S. generator. Radiation is collected by an optical fibre in two directions, transversal and longitudinal to the plasma tube [1] (figure 1). The radiation collected transversally from the discharge tube (2 cm near Surfatron) can be considered to show negligible self-absorption since that direction of observation is sufficiently small (1 mm). The spectral lines collected longitudinally, as opposed to the plasma column, could be affected by the phenomenon of self-absorption since in this case the radiation has to pass right through the whole length of the discharge (7.5 cm long). In this case the whole width of the Voigt line could increase (self-absorption broadening).

The half-maximum Voigt width of H_α and H_β hydrogen lines, lines used to determine n_e, are compared in longitudinal and transversal directions and it can be confirmed that there is not an additional broadening in the longitudinal measurements (Table 1). Therefore neither of the two lines are affected by this phenomenon in their path along the 7.5 cm of the discharge. So for these plasma conditions, the H_α line (more affected by this phenomenon in the literature [3]) could be used to measure electron density in plasmas created in tubes with a bigger diameter without being affected by self-absorption. Another line used to measured n_e (549.6 nm, $6d - 4p$ argon transition) [4] is not affected either, due to the low value of its f parameter and the small population in the absorbing level of this transition, nearer the ionization threshold.

TABLE 1. Half-maximum Voigt width for transversal and longitudinal measurements

	$\Delta\lambda_V$ Transversal ($l = 1$ mm)	$\Delta\lambda_V$ Longitudinal ($l = 750$ mm)
H_β (486 nm)	0.149 ± 0.019 nm	0.149 ± 0.015 nm
H_α (656 nm)	0.1213 ± 0.0006 nm	0.1209 ± 0.0010 nm

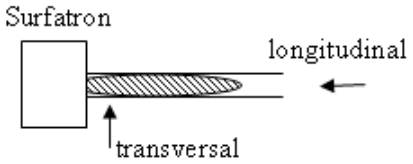

FIGURE 1. Positions of the optical fibre

T_{gas} is determined by considering it equal to the rotational temperature obtained from the ro-vibrational spectra of the OH species, present in the plasma as impurities [5]. The results obtained from transversal and longitudinal measurements are the same (figure 2), so these lines belonging to the OH rotational band are not affected by this phenomenon. Other authors also use argon spectral lines (such as 603.2 nm, $5d - 4p$ transition) to determine T_{gas} [4], also unaffected either by self-absorption. In the same manner these magnitude can also be measured in directions with greater dimensions (flames or plasma columns in a tube with a diameter > 1 mm) without being distorted by this phenomenon.

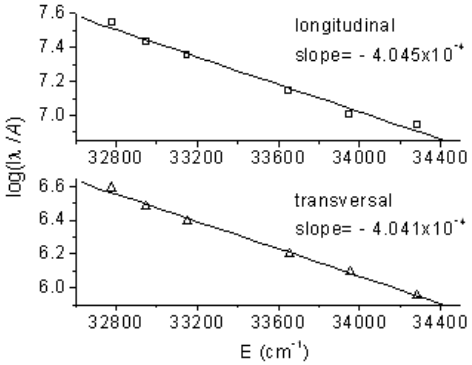

FIGURE 2. Linear fit of the longitudinal and transversal intensity of the OH species

ACKNOWLEDGEMENT

This work was subsidised by the Ministry of Science and Technology (Spain) in the framework of the project no. ENE2005-00314.

REFERENCES

1. I. Santiago, M.D. Calzada, *Appl. Spectrosc.* **61**, (2007) 725-733
2. N. Konjevic, *Phys. Rep.* **316** (1999) 339-401
3. J. M. Luque, M. D. Calzada, M. Saez, *J. Phys. B: At. Mol.Opt. Phys.* **36** (2003) 1573-1584
4. M. Christova, E. Castaños-Martínez, M.D. Calzada, Y. Kabouzi, J.M. Luque, M. Moisan, *Appl. Spectrosc.* **58**, 9 (2004), 1032-1037.
5. M. D. Calzada, M. Moisan, A. Gamero, A. Sola. *J. Appl. Phys.* **80**, 1, (1996). 46-55

WEDNESDAY, 18 JUNE

Surface interactions in Matter Wave Optics: Towards a Schlieren-type Atomic Nanoscope?

J. Grucker, M. Hamamda, V. Bocvarski, F. Perales, G. Dutier, J. Baudon and M. Ducloy

Laboratoire de Physique des Lasers (CNRS-UMR 7538), Université Paris 13, 99 Av. J.B. Clément, 93430 Villetaneuse, France
e-mail: martial.ducloy@univ-paris13.fr

The interaction at mean distance (z ~1-100nm) between an atom and a surface is of the van der Waals type in $1/z^3$ (see *e.g.* [1]). It has been known for sometime that surface attraction has a noteworthy influence in atom interferometry using material gratings as beam splitters [2]. However as soon as the atom has a non-zero internal angular momentum, such as rare-gas metastable atoms like $Ar^*(^3P_2)$, the surface interaction potential is not purely scalar, but rather contains an additional quadrupolar part. This quadrupolar part breaks the atomic state symmetry and is able to induce inelastic transitions between fine structure levels [3]. When an external magnetic field **B**, the direction of which is different from that of the normal **n** to the surface, is applied, transitions between Zeeman states (M→M') are also induced [4], provided that the distance of closest approach (or impact parameter ρ) is small enough (ρ < 2 or 3 nm). When such transitions, called "van der Waals - Zeeman" (vdW-Z) transitions, are exo-energetic (M'-M = ΔM < 0), the atom experiences a repulsive deflection, by an angle $\gamma \approx |g\ \mu_B B\ \Delta M / E_0|^{1/2}$, where g is the Landé factor, μ_B the Bohr magneton and E_0 the initial kinetic energy (deflection observed on metastable $Ne^*(^3P_2)$, [4]). The fact that the atom diffraction originates from a small volume located near the surface, and occurs in a different internal state (allowing for an easy discrimination from the incident atomic wave) reminds one of the well-known methods of Schlieren photography.

Those vdW-Z transitions act as tuneable (*via* **B**) beam splitters, usable in atomic interferometers. The simplest configuration of such an interferometer is the atomic counterpart of the bi-prism Fresnel's interferometer. It consists of two opposite surfaces, *e.g.* the two opposite edges of a few μm wide slit. Using a nozzle beam of $Ar^*(^3P_2)$ atoms [2] slowed down to a velocity of a few tens of m/s by a standard Zeeman slower [5], one easily gets transverse coherence lengths larger than the slit width. Under such conditions, a single atomic wave packet can be inelastically scattered by both edges, generating two coherent wave packets deflected at opposite angles. Because of the very narrow range of impact parameters where the vdW-Z transitions occur (2-3 nm), these packets strongly spread out and overlap beyond a distance of few cm from the slit, leading to a Young-slit interference pattern [6]. For instance, with a velocity of 56 m/s, a slit width of 10 μm, one gets at a distance of 30 cm, a fringe spacing of 5 μm. It is worthwhile to note that this device realises a textbook measurement of coherences in the atomic beam: longitudinal coherence *via* the number of visible fringes, transverse coherence *via* the contrast at the centre of the interference pattern. Because of the velocity spread (a few %) the beam longitudinal coherence length is finite, and only a limited number of fringes (about 50) is observable; but the most interesting thing here is the *envelope* of these fringes. Indeed this envelope is the Fourier transform of the vdW transition-probability profile at the vicinity of the surface [6]. By this way this profile can be explored with a sub-nanometric resolution.

The group "Interferometry and Optics with Atoms" is a member of the *Institut Francilien des Atomes Froids* (IFRAF)

References

[1] D. Bloch and M. Ducloy, Adv. At. Mol. Opt. Phys., **50**, 91 (2005)
[2] J.-C. Karam *et al.*, J. Phys. B: At. Mol. Opt. Phys, **38**, 2691 (2005), and references therein.
[3] M. Boustimi *et al.*, Phys. Rev. Lett., **86**, 2766 (2001)
[4] J.-C. Karam *et al.*, Europhysics Letters **74**, 36 (2006)
[5] J. Grucker *et al.*, J. Phys. B: At. Mol. Opt. Phys, **41**, 021001 (2008)
[6] J. Grucker *et al.*, Eur. Phys. Journal D, **47**, 427 (2008)

Spectroscopy of alkali-helium exciplexes in condensed helium

P. Moroshkin, V. Lebedev, A. Hofer, A. Weis

Department of Physics, University of Fribourg, Chemin du Musée 3, 1700 Fribourg, Switzerland

ALKALI-HELIUM EXCIPLEXES

While alkali-metal atoms and helium atoms in their ground states strongly repel each other, an alkali-metal atom excited to one of its P states can exert an attractive force on nearby helium atoms and form bound states, known as exciplexes. The interatomic interaction in such quasimolecules is dominated by the Pauli repulsion between the valence electron of the alkali atom and the closed electronic shell of the He atom. Only when the helium atom approaches the alkali atom along a nodal line or a nodal plane of the latter's electron-density distribution, it experiences a van der Waals attraction, which is responsible for the formation of a bound state. The structure of the quasimolecule thus is determined by the shape of the electronic orbital of the excited alkali atom. In the light alkalis Li, Na, K, in which the spin-orbit interaction is negligible compared to the van der Waals interaction, dumbbell-like P orbitals lead to an exciplex in which the He atoms form a ring around the dumbbell's waist. The maximal number N of bound He atoms in those complexes is limited by the repulsive interaction between the neighboring He atoms. In the heavier alkali atoms Rb and Cs one has to take into account the spin-orbit interaction and consider nP_J orbitals. In that case mostly linear diatomic and triatomic exciplexes are formed with the He atoms located in the dimples of the apple-shaped $nP_{3/2}, M_J = 3/2$ orbital [1]. However, when several He atoms approach at a close enough distance, a spin-orbit uncoupling may occur. This results in the formation of the ring-shaped exciplex with up to 7 He atoms [2].

Exciplexes are usually observed via their laser-induced fluorescence which is strongly red-shifted with respect to the corresponding transition in the free alkali atom and which has a very large spectral width. The red-shift and the broadening are a consequence of the strongly repulsive interaction in the ground state and increase with the number of bound He atoms. The spectra and the exciplex structure are well reproduced by a simple model [3] that assumes that the interatomic interaction is pairwise additive and that uses theoretical L-dependent anisotropic pair potentials existing in the literature. It is usually assumed that the electronic wavefunction of the alkali atom in the exciplex is not affected by the presence of the He atoms and that the radiative transition to the ground state has the same dipole moment d as in the free atom. The radiative lifetime τ of the exciplex, given by

$$\frac{1}{\tau} = \frac{\omega_0^3 d^2}{3\pi\varepsilon_0 \hbar c^3}, \tag{1}$$

is significantly longer than that of the corresponding excited state of a free atom, due to the strong redshift of the transition frequency ω_0.

EXPERIMENTS IN CONDENSED HELIUM

Alkali-helium exciplexes have been observed in liquid [4] and solid [2] He, in cold He gas [4], and in He nano-droplets [5]. In the present contribution we concentrate on experiments in solid ^{4}He. Due to the very low temperature and the high density of He atoms, this environment is very well suited for studies of weakly bound short-lived complexes. Alkali (Rb or Cs) atoms are introduced into solid He by means of laser ablation from a metallic target located at the bottom of the experimental cell. The experiments are carried out at a temperature of 1.5 K and a He pressure in the range of 25 - 40 bar. Under those conditions impurity atoms can be trapped in the He matrix for many hours. We excite the dopants with a tunable pulsed or cw laser and study their spectrally and time-resolved fluorescence.

In gaseous helium the attachment of He atoms to the exciplex occurs via binary collisions, so that the formation of a polyatomic exciplex requires a large sequence of such collisions to occur within the radiative lifetime of the excited alkali state. It has been shown that in a doped He droplet the alkali atoms are loosely bound at the droplet surface, and the energy released by the attachment of a single He atom usually leads to the desorption of the excimer from the droplet. In condensed (liquid or solid) helium, on the other hand, the alkali atoms reside in small spherical cavities, called atomic bubbles. The characteristic diameter of the bubble is about 1 nm and is determined by a balance between the repulsive alkali-helium interaction and the surface tension at the bubble interface acting together with the bulk

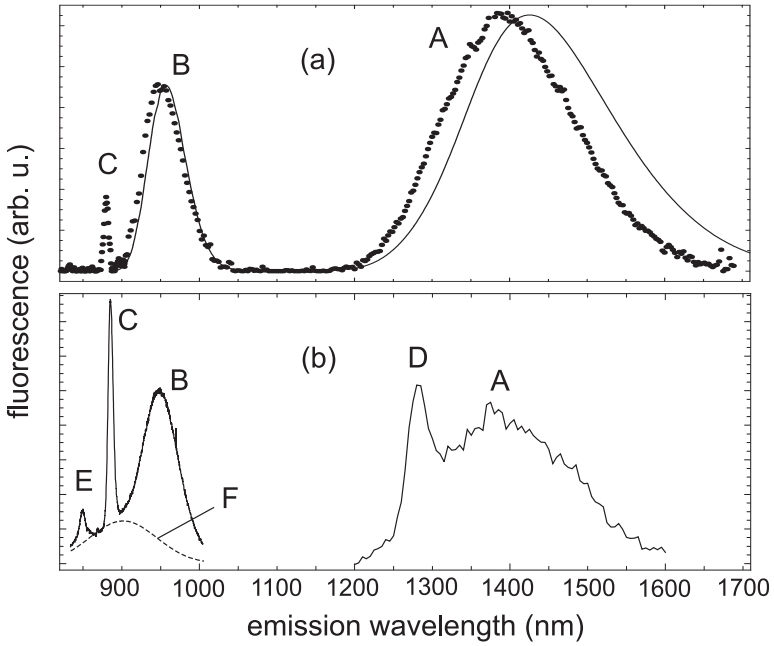

FIGURE 1. Fluorescence spectrum of Cs-doped solid He excited at the $6S_{1/2} - 6P_{3/2}$ transition of Cs (a), and at the $(2)^3\Pi_g \leftarrow a^3\Sigma_u$ band of the Cs_2 molecule (b). In (a) the experimental data (points) are compared to a theoretical calculation (solid lines). The bands are labeled as follows: A - ring-shaped Cs*He_7 exciplex, B - linear Cs*He_2 exciplex, C - atomic $6S_{1/2} - 6P_{1/2}$ (D_1) line, D - $(1)^3\Pi_u \rightarrow X^1\Sigma_g$ band of Cs_2, E - atomic $6S_{1/2} - 6P_{3/2}$ (D_2) line, F - unidentified band, probably $Cs^*_2He_N$ exciplex.

pressure. The laser excitation of the atom in the bubble is immediately followed by the exciplex formation. In that case only fluorescence from the largest exciplex is observed. All smaller complexes exist only as a transient products and have no time to emit fluorescence.

The excited *nP* states of the light alkali elements in condensed He are completely quenched by exciplex formation. The stronger spin-orbit coupling makes that, in Rb and Cs, the excited $nP_{1/2}$ states (n=5 and 6, respectively) in liquid He preserves their spherical shapes and form bubbles which is larger than those of ground state atoms. When the liquid He is pressurized, the atomic bubbles shrink and perturb the trapped atoms more strongly. At He pressures above 15 bar Rb behaves as the light alkalis and only excited Cs($6P_{1/2}$) atoms retain their bubble-state up to the solidification point and even in solid He. At the same time the $nP_{3/2}$ states of Rb and Cs are quenched both in liquid and solid He to form linear and ring-shaped exciplexes. Their experimentally observed spectra agree well with theory (Fig. 1(a)). The existing small discrepancy is attributed to the interaction of the exciplex with the solid He matrix, not included in the model.

We have studied the lifetimes of Cs*He_2 and Cs*He_7 exciplexes by measuring the decay times of the corresponding fluorescence following pulsed excitation. The comparison of the experimental results with the predictions from Eq. 1 shows that Cs*He_2 is quenched by a radiationless process, most likely by its transformation into a larger exciplex. On the other hand, the ring-shaped complex has a lifetime of 95 ns, much longer than that of the excited Cs atom (36 ns). This result cannot be explained by the spectral shift (ω_0^3 term in Eq. 1) only. It is therefore reasonable to assume that the transition dipole moment is significantly increased by the strong perturbation of the Cs ground state by the interaction with the He-ring.

DIALKALI-HELIUM EXCIPLEXES

In addition to the direct exciplex formation processes discussed above there exist other formation mechanisms involving intermediate atomic or molecular electronic states. The laser ablation applied for the doping produces alkali atoms, dimers, and larger clusters. The electronic structure and spectra of the alkali-metal dimer molecules are well known. In solid He we could identify a number of absorption bands of Rb_2, Cs_2, and RbCs. The laser-

induced fluorescence of all those molecules comes only from the lowest excited state $^3\Pi$, which is metastable (in the free molecule) and which is populated by radiationless transitions from the laser-excited states. We have also observed the photodissociation of dimer molecules into one ground-state and one excited atom. The latter either emits fluorescence, or produces an exciplex. A detailed comparison of the fluorescence spectra of the dissociation products (figure 1(b)) with those obtained under the direct laser-excitation of nP_J states of Rb and Cs reveals a small redshift, which we attribute to the interaction of the excited atom or of the exciplex with the nearby ground-state alkali atom. This observation suggests that the dissociation products do not separate completely, but stay in close proximity in the matrix, residing probably within the same diatomic bubble.

We have also discovered two very broad spectral features, which can be excited at some absorption bands of Cs_2 and Rb_2 respectively and overlap with the spectra of their dissociation products (Fig. 1(b)). We suggest that they come from two new quasimolecular complexes (exciplexes), consisting of an excited Rb_2 or Cs_2 dimer in a Π state and of several ground-state He atoms, arranged around a waist of the dumbbell-like Π orbital. The fluorescence spectrum of such a molecular exciplex is strongly broadened and redshifted with respect to the corresponding band of the free molecule due to the strongly repulsive interaction of the helium belt with the Σ ground state. A quantitative modeling of such complexes will require the knowledge of the anisotropic alkali dimer–helium interaction potentials.

REFERENCES

1. J. Dupont-Roc, *Z. Phys. B* **98**, 383–386 (1995).
2. D. Nettels, A. Hofer, P. Moroshkin, S. Ulzega, A. Weis, *Phys. Rev. Lett.* **94**, 063001 (2005).
3. P. Moroshkin, A. Hofer, D. Nettels, S. Ulzega, A. Weis, *J. Chem. Phys.* **124**, 024511 (2006).
4. K. Hirano, K. Enomoto, M. Kumakura, Y. Takahashi, T. Yabuzaki, *Phys. Rev. A* **68**, 012722 (2003).
5. J. Reho, C. Callegari, J. Higgins, W. E. Ernst, K. K. Lehman, G. Scoles, *Faraday Discuss.* **108**, 161–174 (1997).

Near-resonant femtosecond laser induced cone emission from rubidium vapor

S. Vdović, H. Skenderović, G. Školnik, T. Ban, N. Vujičić, D. Aumiler and G. Pichler

Institut za fiziku, Zagreb, Croatia

INTRODUCTION

The phenomenon known in the literature as cone or connical emission has been widely investigated since the early 1970s. As the intense light beam interacting with a nonlinear medium has a very complex interpretation it is natural to suspect that cone emission (CE) appears due to different physical mechanisms in different experimental conditions.

The CE is usually observed as a diffuse ring of light appearing around a central laser spot emerging from a dense metallic vapor, when the laser beam that propagates through a vapor is blue detuned with respect to the atomic transition. In most cases, the CE spectrum is red detuned from the resonance. This complex phenomenon provoked researchers to propose various models of description. One of the popular models is based on four-wave mixing (FWM) of Rabi sidebands and the efects of diffractive spreading during propagation [1]. This model gives good results when applied to CE from glasses or liquids, i.e. when the laser frequency is far from resonances. The red-detuned and blue-detuned sidebands emerge at the cone angles according to FWM phase matching conditions.

In measurements in which the laser beam is tuned near atomic resonance the situation is more complicated. The experiment of Harter and Boyd in sodium showed that the red detuned light was emitted in the cone whereas no blue sideband was present. They argued that simultaneously with FWM, self-focusing occurs resulting in formation of the stable filaments. The blue sideband remains trapped inside the filament by total internal reflection. However, there are observations indicating that FWM and boundary refraction propagation are more complicated than predicted by the simple model. In order to solve this inconsistency, several other models were proposed like Cherenkov-type process, superfluorescence and self-phase modulation. Time-dependent theory including full propagation for the laser and frequency sidebands could not account for the high levels of optical gain in CE. In our previous work [2], we obtained CE with 100-fs pulses in dense Cs vapor.The laser was tuned far from the Cs atomic resonance but in the range of the cesium dimer absorption. The largest cone angle was observed at about 755 nm, far away from the closest D2 cesium resonance line at 852 nm. We established that this emission originates from the nonlinear behavior of index of the refraction connected with the presence of Cs_2 X-B molecular transition with the maximum of the absorption at about 760 nm. This was further supported with a direct correlation between observed cone angle and the dimer density. We established the molecular origin of the CE with spatial self-phase modulation as a dominant mechanism of the CE generation.

In this work [4] we report the CE from the dense rubidium vapor excited by the output from the mode-locked, 100 fs laser oscillator. The cone emission was observed only when the laser beam propagated through the high-density vapor ($N>5x10^{16}$ cm^{-3}) and for the smaller densities no CE was observed. The laser central wavelength was changed in the wide interval, from the far blue wing of the D2 line to the far red wing of the D1 line. The observed CE in the far blue wing of the D2 line is interpreted as a consequence of the self-focusing and self-phase modulation according to the adiabatic following limit. The emission in the red wing of the D2 line shows defocusing of the propagating beam.In contrast to the CE reported so far, the bright central spot was not observed in the far blue wing. In the near blue wing the central spot appears due to the two- photon resonance at 778 nm. The temporal shape of the CE, measured by cross-correlation in the SHG crystal shows pulse breaking and extreme lengthening.

EXPERIMENTAL TECHNIQUE: FREQUENCY-RESOLVED OPTICAL GATING

One of the best techniques of obtaining information about ultrashort (fs) pulses is probably the frequency resolved optical gating (FROG) in some of its subvariants. We used it in order to retrieve pulse field using the autocorrelation and the crosscorrelation setup. The beams were intersected in the nonlinear BBO crystal with 100μm thickness and the second harmonic signal was collected and spectrally resolved in the computer controlled compact spectrometer. A 12 cm long all-sapphire cell containing pure rubidium was installed in the specially designed oven and heated to the desired temperatures/densities.

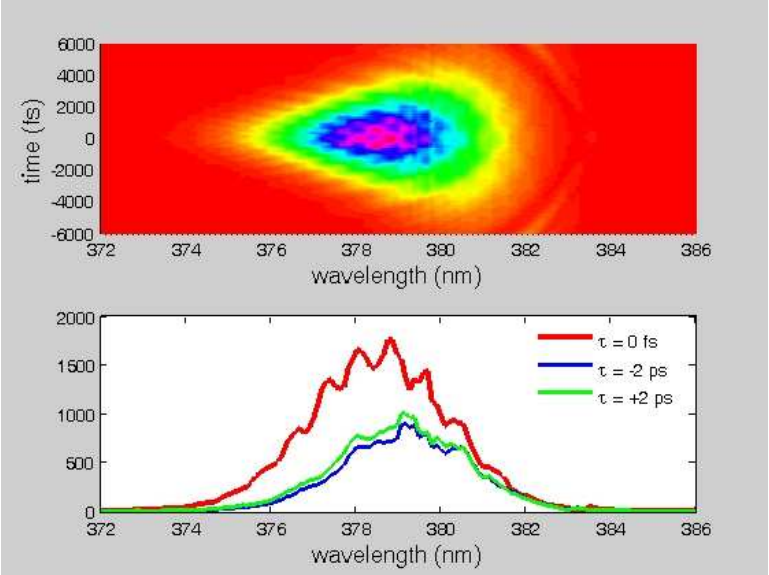

FIGURE 1. Up: FROG signal for the temperature of 347°C corresponding to atomic concentration of 6.7x10^{16} cm^{-3}. Down: signal spectrum at different delay times

FIGURE 2. photos of the cone emission at distance of approximately 3 m from the Rb cell at pulse central wavelengths of 760, 780 and 820 nm, from left to right

A typical SHG FROG measurement of the cone effect pulse is shown in fig.1 together with the signal spectrum at different delay times. For higher densities corresponding to lager cone angles autocorrelation setup becomes unreliable and the crosscorrelation SHG FROG was performed. Using the 'Frog3' [3] software we were able to extract pulse electric field and phase together with the pulse spectral and temporal length.

ACKNOWLEDGMENTS

We acknowledge the support from the Ministry of Science Education and Sports of Republic of Croatia (Project No. 035-0352851-2857), European Commission Research Training Network (FW-5) and Alexander von Humboldt Foundation.

REFERENCES

1. D. Harter and R. Boyd, *Phys. Rev. A* **29**, 739 (1984).
2. D. Aumiler, T. Ban, and G. Pichler, *Phys. Rev. A* **71**, 063803 (2005).
3. `http://www.swampoptics.com/products_femtosoft.htm`.
4. to be published in *Phys. Rev. A* (2008).

Importance of linewidth data for thermometry using CARS spectroscopy

P.-E. Bengtsson

Combustion Physics, Faculty of Engineering, Lund University
per-erik.bengtsson@forbrf.lth.se, www.forbrf.lth.se

Coherent anti-Stokes Raman Spectroscopy (CARS) is a technique based on a non-linear optical process, and this technique can be used mainly for temperature measurements in combustion but sometimes also for concentration measurements [1,2]. In CARS normally three laser beams are focused to a common intersection point. If the frequency difference between two of the laser beams is in resonance with a molecule (either rotational or vibrational), an oscillating polarization will be induced. The third beam is scattered off this resonance frequency and a CARS signal emerges as a laserlike beam in a direction given by the phase-matching condition. The signal is after spectral isolation directed to a spectrometer, and the detected spectrum contains temperature and concentration information mainly related to its shape and the widths of the lines. A rotational CARS setup is shown in Fig. 1, and an experimental rotational CARS spectrum is shown in Fig. 2.

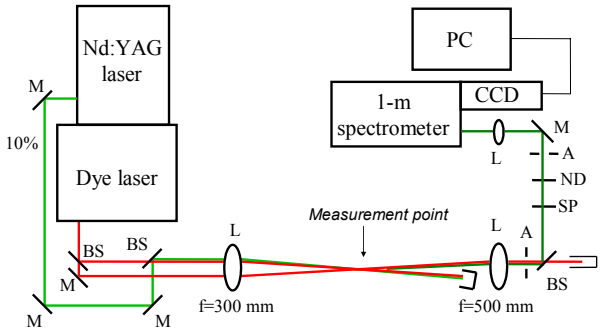

Figure 1. Experimental pure rotational CARS setup. M=Mirror, BS=Beam splitter, L=Lens, A=Aperture, SP=Short-pass filter, ND=Neutral density filter, CCD=CCD-camera.

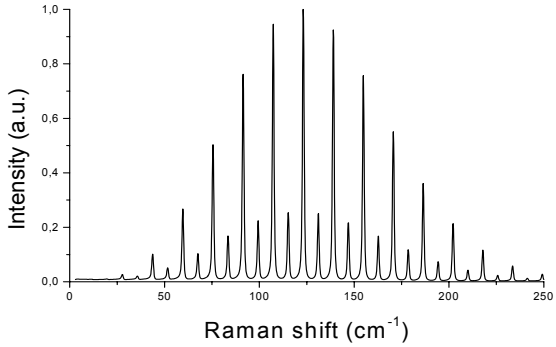

Figure 2. Experimental rotational CARS spectrum from nitrogen recorded at 295 K. The lines at higher Raman shifts correspond to faster molecular rotations and thereby populations on higher rotational energy levels.

The CARS spectrum has a complex dependence on molecular structure (equilibrium distance, moment of inertia, rotational energy levels, centrifugal distortion) and its interaction with the radiation (resonant and non-resonant susceptibility, rotational Raman linewidths), the Boltzmann distribution, the experimental equipment (laser line profiles), and measurement conditions (pressure, instrument function, dispersion of spectrograph).

The CARS signal strength, S, has the following dependence on different parameters, for which the definitions can be found in [3]:

$$S \propto \omega_{as}^2 \; I_1 I_2 I_3 \left|\chi_{CARS}\right|^2 l^2 \left(\frac{sin(\Delta k\, l/2)}{\Delta k\, l/2}\right)^2 \qquad \text{(Eq.1)}$$

The spectral information in Eq. 1 is attributed to χ_{CARS}, which is the coupling between the third power of the applied electric fields and the induced molecular polarization. The factor χ_{CARS} can further be divided into a resonant contribution from rotational or vibrational Raman resonances in the molecule, and a non-resonant term due to electronic response, i.e.

$$\chi_{CARS} = \chi_{NR} + \chi_R \qquad \text{(Eq.2)}$$

The resonant susceptibility, χ_R, can be expressed as

$$\chi_R = \sum_J \frac{a_{J,J+2}}{\omega_{J,J+2} - \omega_1 + \omega_2 - ip\Gamma_{J,J+2}(T,J)/2} \qquad \text{(Eq.3)}$$

The line strength factor $a_{J,J+2}$ in Eq.3 can be written as

$$a_{J,J+2} = \frac{4}{45}\frac{N}{\hbar} b_J^{J+2}\ F(J,J+2)\,\varsigma_e^2 \Delta\rho_{J,J+2} \qquad \text{(Eq.4)}$$

In Eq.4 the population difference factor, $\Delta\rho_{J,J+2}$, can be expressed as

$$\Delta\rho_{J,J+2} = \frac{g_I(2J+1)}{Q_J}\left\{\exp\left[-\frac{E(v,J)}{kT}\right] - \exp\left[-\frac{E(v,J+2)}{kT}\right]\right\} \qquad \text{(Eq.5)}$$

The spectral sensitivity to temperature is present in the population difference factor (Eq.5), and the rotational Raman linewidths, $\Gamma_{J,J+2}(T,J)$ (Eq.3). Since, however, the population distribution as a function of temperature is known, the main uncertainty in the temperature determination is in the Raman linewidths (apart from the experimental uncertainties). Accurate linewidth data is thus important for the accuracy of temperature measurements. The temperature and species concentrations are evaluated by fitting of experimental spectra using a library of theoretical spectra, which are calculated with input from molecular data and experimental parameters.

CARS was developed as a useful laser-based technique for combustion diagnostics during the 1970´s, and it has since then been developed through fundamental laboratory studies and has the last decades been used for applied measurements in practical devices such as internal combustion engines [4], see Fig. 3.

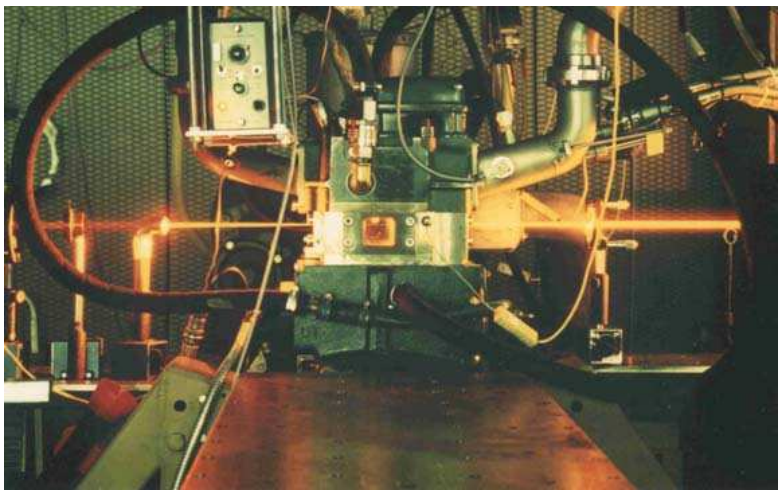

Figure 3.
Photo from rotational CARS measurements of temperature inside an optical engine.

Research on CARS spectroscopy deals with improvement of accuracy and precision in the measurements of temperatures and concentrations by investigations of experimental approaches, evaluation strategies, and theoretical models [5].

The invited talk will show examples of the importance of accurate linewidth models for accurate temperature measurements using CARS spectroscopy.

REFERENCES

1. A. C. Eckbreth, *Laser diagnostics for combustion temperature and species,* 2nd ed., Combustion science and technology book series (Gordon & Breach, Amsterdam, 1996), Vol. 3.
2. D. A. Greenhalgh, *Quantitative CARS spectroscopy*, Advances in non-linear spectroscopy (Wiley and Sons, New York, 1988), pp. 193-251.
3. L. Martinsson, P.-E. Bengtsson, M. Aldén, S. Kroll, and J. Bonamy, "A Test of Different Rotational Raman Linewidth Models - Accuracy of Rotational Coherent Anti-Stokes-Raman Scattering Thermometry in Nitrogen from 295-K to 1850-K," Journal of Chemical Physics **99**(4), 2466-2477 (1993).
4. C. Brackmann, J. Bood, M. Afzelius, and P. E. Bengtsson, "Thermometry in internal combustion engines via dual-broadband rotational coherent anti-Stokes Raman spectroscopy," Measurement Science & Technology **15**(3), R13-R25 (2004).
5. F. Vestin, M. Afzelius, C. Brackmann, and P. E. Bengtsson, "Dual-broadband rotational CARS thermometry in the product gas of hydrocarbon flames," Proceedings of the Combustion Institute **30**, 1673-1680 (2005).

THURSDAY, 19 JUNE

High accuracy line profile study of transitions in the 30012 ← 00001 and 30013 ← 00001 bands of carbon dioxide

A.R.W. McKellar[1], Daniel R. Hurtmans[2], Adriana Predoi-Cross[3]

[1]*Steacie Institute for Molecular Sciences, National Research Council of Canada, Ottawa, ON K1A 0R6 Canada*
[2]*Service de Chimie Quantique et Photophysique, Université Libre de Bruxelles, 50 Av F.D. Roosevelt, cp160/09, B-1050 Bruxelles, Belgium*
[3]*Physics Department, University of Lethbridge, 4401 University Drive, Lethbridge, AB, T1K 3M4 Canada*

INTRODUCTION

The global carbon cycle is influenced by the anthropogenic emission of carbon dioxide with significant implications to climate change. Uncertainties in our understanding of the global budget of atmospheric carbon dioxide are limiting our ability to predict the changes in climate. Estimates indicate that about half of the carbon dioxide emitted anthropogenically remains in the atmosphere. The remaining half, often called the "*missing carbon*" is absorbed by the oceans and the terrestrial biosphere, the biosphere being the main sink. Without a good understanding of the fate of the "*missing carbon*", predictions of future climate change will remain suspect. The spectral parameters reported here are relevant for the mixed air conditions of Earth's atmosphere and could be used, for example, to validate the measurements of the OCO mission that intends to obtain total column CO_2 measurements with a precision of ~0.3%. Future remote sensing of planetary bodies, such as Mars and Venus that have atmospheres with a high content of CO_2 gas will benefit from our spectroscopic pure CO_2 results.

EXPERIMENTAL DETAILS

Fifteen room temperature CO_2-air and eighteen pure carbon dioxide spectra [1,2] were recorded at the Steacie Institute for Molecular Sciences at the National Research Council in Ottawa using a Bomem DA3.002 Fourier Transform Spectrometer. The gas pressures ranged from a few Torr to one atmosphere. Thirty-two scans were co-added to each measurement to achieve a strong signal to noise ratio at resolutions of 0.008 or 0.009 cm^{-1}. A White-type cell with a base length of 500 cm was used to obtain pathlengths between 40.15 and 80.15 m. The output from the cell was recorded with a germanium detector operated at room temperature. The pressure was measured with two Baratron 127 capacitance manometers and a Wallace and Tiernan precision Bourdon tube gauge. Lakeshore PT-103 platinum resistance thermometers and Lakshore Model 91C and Model 211 read out units were used to record temperature with an accuracy of ±0.4 K. The line positions of the recorded spectra were calibrated internally with respect to the carbon dioxide positions listed in HITRAN 2004 [3].

SPECTROSCOPIC ANALYSIS AND DISCUSSION

The individual batches of pure CO_2 and CO_2+air spectra were analyzed using a multi-spectrum non-linear least-square curve fitting program [4] that models the spectral lines using the line shape model of choice convolved with the instrumental line shape function appropriate for the Bomem instrument. The program makes corrections for interferogram truncation and field of view effects. The spectral backgrounds and zero transmission levels were appropriately modeled. The differences between the experimental and the calculated spectra were minimized by adjusting various line parameters through non-linear least-squares fitting. The band was analyzed on a line by line basis by selecting the same interval ranging from 1.5 to 3 cm^{-1} within every spectrum. Voigt and Speed Dependent Voigt profiles with an asymmetric line mixing component were used in the analysis. As shown in Fig.1, the Speed Dependent Voigt profile with line mixing reproduces best our results.

The line mixing effects have been measured directly from the spectra using our line by line fitting method and the weak mixing expression of Rosenkranz [5]. We use the relaxation matrix formalism [6] to treat the CO_2 bands as a whole and relate the band's behavior over a range of pressures to the elements of the relaxation matrix. This formalism incorporates the impact approximation and the approximation that the density matrix can be factored. The impact approximation assumes that the collisions are binary and their duration is negligible compared with the time between consecutive collisions. The density matrix is factorized by dividing the gas sample into a large number of identical cells and considering one cell as the system while the remaining cells are referred to as thermal bath gas. Line mixing coefficients can be quantified by the off diagonal elements of the relaxation matrix along with the dipole transition moments [6] the diagonal elements of which represent the broadening and shift coefficients. The collisional transfer rates can be calculated using energy scaling laws that characterize the off-diagonal matrix elements of the relaxation matrix for any rotational state using a set of fitting parameters. We have used Exponential Power Gap (EPG) and the Energy Corrected Sudden (ECS) fitting laws to predict the line mixing coefficients. The results are presented in Fig. 2.

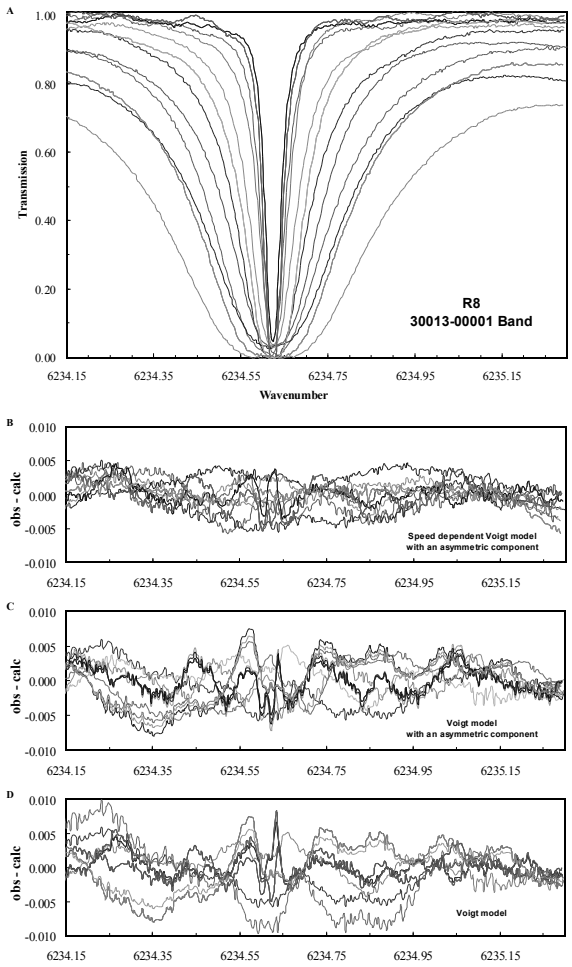

Figure 1. a) Overlaid spectra. b) Fit using the Speed Dependent Voigt profile with an asymmetric line mixing component, c) Fit with Voigt profile and an asymmetric line mixing component. d) Fit with Voigt profile.

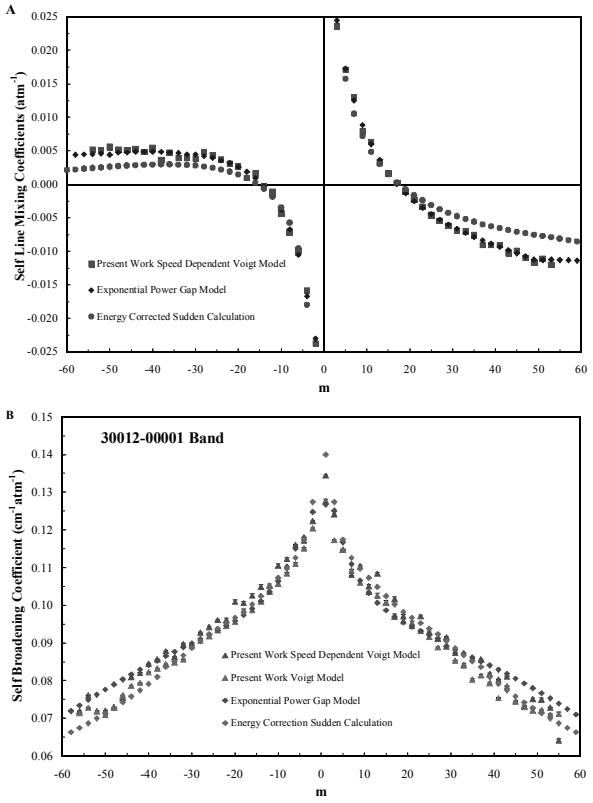

Figure 2. A) Overlaid measured and calculated line mixing results in the 30013←00001 band obtained using the Exponential Power Gap law (EPG) and Energy Corrected Sudden (ECS) law, respectively. B) Overlaid measured and calculated broadening parameters in the 30012←00001 band plotted against m.

ACKNWOLEDGEMENTS

The research presented here was funded by the Strategic and Discovery Grant programs of the Natural Sciences and Engineering Research Council of Canada (NSERC). We thank W. Liu, A.V. Unni, I. Schofield and C. Holladay of University of Lethbridge for their participation and contributions to this project.

REFERENCES

1. A. Predoi-Cross, W. Liu, C. Holladay, A.V. Unni, I. Schofield, A.R.W. McKellar, D. Hurtmans, *J. Mol. Spectrosc.* **246**, 98-112 (2007).
2. A. Predoi-Cross, A.V. Unni, W. Liu, I. Schofield, C. Holladay, A.R.W. McKellar, D. Hurtmans, *J. Mol. Spectrosc.* **245**, 34–51 (2007).
3. L.S. Rothman, D. Jacquemart, A. Barbe, D.C. Benner, M. Birk, L.R.Brown, M.R. Carleer, C. Chackerian Jr., K. Chance, V. Dana, V.M.Devi, J.-M. Flaud, R.R. Gamache, J.-M. Hartmann, K.W. Jucks,A.G. Maki, J.-Y. Mandin, S. Massie, J. Orphal, A. Perrin, C.P.Rinsland, M.A.H. Smith, R.A. Toth, J. Vander Auwera, P. Varanasi and G. Wagner, *J. Quant. Spectrosc. Radiat. Transfer* **96**, 139–204 (2005).
4. D. Hurtmans, G. Dufour, W. Bell, A. Henry, A. Valentin and C.Camy-Peyret, *J. Mol. Spectrosc.* **215**, 128–133 (2002).
5. P.W. Rosenkranz, *IEEE Trans. Antenn. Propag.* **23** 498–506 (1975).
6. A. Levy, N. Lacome, C. Chackerian Jr., in: K. Narahari Rao, A. Weber Eds., *Spectroscopy of the Earth's Atmosphere and of the Interstellar Medium*, Academic Press, New York, 1992, pp. 261–337.

Semi-classical line shape models of rovibrational H_2O spectra tested using frequency-stabilized cavity ring-down spectroscopy

R. Ciuryło*, D. Lisak* and J. T. Hodges†

*Instytut Fizyki, Uniwersytet Mikołaja Kopernika, ul. Grudziadzka 5/7, 87-100 Toruń, Poland
†Process Measurements Division, National Institute of Standards and Technology, 100 Bureau Drive, Gaithersburg, Maryland 20899, USA

The need for high-accuracy spectroscopic data motivates advances in experimental methods and first-principles models required for data analysis. In order to get fundamental spectroscopic parameters of spectral lines (such as intensities, pressure broadening and shifting coefficients) with an accuracy of 1% or better, one must use more sophisticated profiles than the commonly used Voigt line shape. To this end, we will briefly describe well-known mechanisms that influence the shape of spectral lines including Dicke narrowing and speed-dependence of collisional broadening and shifting.

Experimental methods which are sensitive, accurate and as free as possible from instrumental distortion have to be used to provide accurate spectroscopic data for a large variety of molecular lines, with intensities ranging from the relatively strong to very weak. As such a method, we present frequency-stabilized cavity ring-down spectroscopy (FS-CRDS). This new technique incorporates a ring-down spectrometer with a stabilized and tuneable comb of resonant frequencies and a continuous-wave external-cavity diode probe laser. The FS-CRDS experimental setup is characterized by a high frequency resolution of 50 kHz and a high sensitivity with a noise-equivalent absorption coefficient of $1.2 \times 10^{-10}\mathrm{cm}^{-1}\mathrm{Hz}^{-1/2}$. This spectrometer provides line shape measurements with signal-to-noise ratios in excess of a few thousand to one.

We present several experiments intended to demonstrate the suitability of the FS-CRDS technique for precise and accurate line shape measurements. As an example, we investigated the shapes of near-ir rovibrational absorption lines of water vapor. We discuss the results of these tests and the applicability of different models for the description of the measured water vapor line shapes. We identify the need for realistic quantum-mechanical calculations of the speed-dependence of the collisional broadening and shifting: models which are crucial for interpreting and analyzing line shape measurements. Finally we discuss the potential impact on spectral line lists (such as those incorporated in the HITRAN database) of this new experimental technique when combined with more refined models of line shape.

Exact low-order classical moments in collision-induced bands by linear rotors: $CO_2 - CO_2$

M. Chrysos[1]*, A. P. Kouzov[2+], N. I. Egorova[1,2] and F. Rachet[2]

[1]*Laboratoire des Propriétés Optiques des Matériaux et Applications, UMR CNRS 6136, Université d'Angers, 2 boulevard Lavoisier, 49045 Angers, France ; *E-mail: michel.chrysos@univ-angers.fr*

[2]*Institute of Physics, Saint Petersburg State University, Ulyanovskaya str. 1, Peterhof, Saint Petersburg 195904, Russia; +E-mail: alex@ak1197.spb.edu*

Carbon dioxide is directly concerned with debates over the role of greenhouse gases and the opacity of planetary atmospheres. Because of this, its collision-induced absorption (CIA) and scattering (CIS) spectra were the subject of several experimental [1,2] and theoretical [3-5] investigations. There are two primary integrated characteristics necessary for the quantitative interpretation of a collision-induced band, zero moment M_0, and the square-rooted reduced second moment, $\bar{M}_2^{1/2} = (2\pi c)^{-1}\sqrt{M_2 / M_0}$, respectively. We report new exact analytic $M_0^{(r)}$ and $M_2^{(r)}$ exp- ressions for classically treated linear rotor - linear rotor collisions which are applicable for whatever type of the spectroscopy, i.e. CIA *(r=1)* and CIS (*r=0,2*). The expressions are used to CO_2- CO_2, focusing on those regions of the CIA and CIS spectra that correspond to the forbidden pure-rotational and asymmetric-stretching ν_3 vibrational transitions, respectively. Accordingly, we here provide compelling evidence that the quadrupole induction is sufficient for the meaningful description of the published CIA rototranslational band characteristics of CO_2- CO_2 [1] and so is the dipole-quadrupole interaction with respect to the ones of the ν_3 CIS band. This finding is manifestly opposite to the belief that, for CO_2- CO_2, short-range exchange interactions are indispensable [4]. The proper account of a novel mechanism of polarization, the hitherto neglected vibrational polarizability corrections, the anisotropy of the interaction potential, as well as a refined CO_2- CO_2 potential energy surface (PES) [6] were critical to the success of our enterprise.

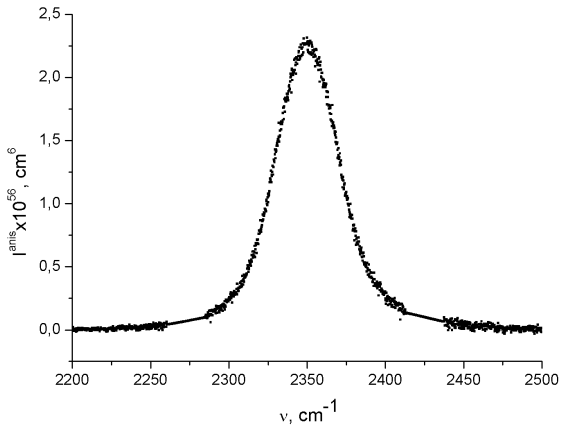

Figure 1. Anisotropic CIS ν_3 band of CO_2 - CO_2.

For $\Delta\mu^{(1)}$, conventional quadrupole induction was the only relevant mechanism of polarization, thereby involving the CO_2 permanent quadrupole moment Q and the dipole-dipole polarizability tensor $\acute{\alpha}$. For $\Delta\alpha^{(2)}$, Amos, Buckingham and Williams introduced two long-range polarization mechanisms, namely the dipole-induced quadrupole (DIQ) interaction and a nonlinear quadrupole (NLQ) polarization [5]. The first brings into play the CO_2 dipole-quadrupole polarizability tensor $\hat{A}_a$ along with the dipole-dipole polarizability tensor $\acute{\alpha}_b$. The second

involves Q_b of the buffer particle along with the dipole-dipole-dipole polarizability tensor $\hat{\beta}_a$ of the active molecule. However, while these authors found NLQ to contribute only little in comparison with DIQ [5] (a conclusion also confirmed by our own computations), they missed the coupling between the dipole matrix-elements $(\mu_a^{(1)})_{fàia}$ of the vibrating active molecule and the dipole-dipole-quadrupole polarizability tensor $\hat{B}_b$ of the perturber. The formal structure of the nonlinear dipole (NLD) term was recently revealed by us using the Feynman diagram approach [7]. Pronounced, destructive DIQ - NLD interference was found for CIS by CO_2 - CO_2 resulting in a spectacular decrease of the $M_0^{(2)}$ value of the ν_3 band (see below) and in excellent agreement with the measurement. However, neither trustful data for the electronic polarizabilities and $(\mu_{Za}^{(1)})_{fàia}$ nor the exhaustive description of the PES anisotropy were sufficient to ensure a reliable description of the CIA moments. For the latter process, it was necessary to supplement the electronic term $\alpha \approx \alpha^{(el)}$ by the vibrational correction $\alpha^{(vib)}$, after which the calculated moments fit the measurement. Besides, on strictly quantitative grounds, solely the state-of-the art PESs obtained on the basis of *ab initio* calculation [6] were unambiguously compatible with the observation for both M_0 and M_2, and for both CIA and CIS. The theoretical values of M_0 and $\bar{M}_2^{1/2}$ calculated at T=294.5 K with the PES [6] are gathered in Table 1. Entries supplied with stars and with filled circles and crosses represent values obtained upon turning off the PES anisotropy, the vibrational polarizabilities, and the (solely in CIS) NLD polarization, respectively. According to Table I, zero moments are greatly affected by the PES anisotropy. By switching it on properly, the M_0 value is lowered by more than 30% for CIA and to a somewhat lesser extent for CIS. What is even more impressive, however, is the huge effect ($\approx$ 25%) of $\alpha^{(vib)}$ on the CIA M_0 values and, as anticipated above, an even huger contribution ($\approx$ 60%) of NLD to the CIS ones. Far lesser is the impact of all three effects on the width of the bands.

TABLE 1. M_0 (in a.u.) and $\bar{M}_2^{1/2}$.
Measurements: (*a*) CIA [1], (*b*) CIS , this study

M_0 $(e^2a_0^5)$	**CIA**	$\bar{M}_2^{1/2}$ (cm^{-1})
12.4* 6.8• 9.9*•		40.0*
8.5		43.4
Exper. [a]: 10±2		Exper. [a]: 40±4
M_0 (a_0^9)	**CIS**	$\bar{M}_2^{1/2}$ (cm^{-1})
30.4* 54.8 68.6*		31.2* 32.9 31.2*
24.6		32.4
Exper. [b]: 24.6±2		Exper. [b]: 32±4

REFERENCES

1. W. Ho *et al*, J. Chem. Phys. **55**, 1028 (1971); I. R. Dagg *et al*, Can. J. Phys. **64**, 1475 (1986).
2. W. Holzer and R. Ouillon, Mol. Phys. **36**, 817-826 (1978).
3. T. I. Cox and P. A. Madden, Mol. Phys. **39**, 1487-1506 (1980); A. Borysow and M. Moraldi, Phys. Rev. Lett. **68**, 3686-3689 (1992).
4. M. Gruszka and A. Borysow, Mol. Phys. **88**, 1173 (1996).
5. R. D. Amos, A.D. Buckingham, and J.H. Williams, Mol. Phys. **39**, 1519-1526 (1980).
6. R. Bukowski *et al*, J. Chem. Phys. **110**, 3785-3803 (1999).
7. A.P. Kouzov, M. Chrysos, F. Rachet, N. Egorova, Phys. Rev A **74**, 012723 :1-8 (2006).

Speed Dependence in the Collision Process

François Rohart

Laboratoire de Physique des Lasers, Atomes et Molécules,
Université de Lille 1,
F-59655 Villeneuve d'Ascq cedex, France

INTRODUCTION

Remote sensing detection of molecular species is widely used for atmospheric or chemical studies. This technique is based on the analysis of observed line shapes and, in addition to information about absorption line frequencies, it requires preliminary studies of molecular relaxation.

With the advent of quite sensitive spectrometers, it is now well known that actual line shapes exhibit clear deviations from the time-honored Voigt profile [1]. More recently, such deviations have also been observed on some atmospheric spectra. These departures, generally denoted as "line narrowings", are characteristic of line shapes which are higher and narrower than expected from the Voigt model. They result from the approximated nature of the Voigt model which neglects the correlations induced by molecular displacements between the collisional processes and the Doppler effect.

1. On the one hand, relaxation rates depend on the relative speed of absorbing and perturbing molecules. Fast molecules relax more rapidly than slow molecules that interact a longer time with the electromagnetic field. Thus, line shapes get higher and narrower than expected from the Voigt model. They are modeled by the so-called Speed Dependent Voigt (SDV) profiles.
2. On the other hand, molecular collisions induce velocity changes of absorbing molecules. This process leads to a diffusion process, that is to a reduction of mean molecular velocities. This effect, generally referred to "Dicke effect" or optical diffusion, entails a reduction of the Doppler contribution and then a line narrowing. In this context, widely used models are Galatry and Rautian profiles that consider soft and hard collision processes, respectively.

Of course, these effects have very different physical origins and can occur simultaneously. However, they both lead to similar line shapes that are narrower than predicted by the Voigt model. Thus, an important problem is the interpretation of observed departures from the Voigt profile, namely: is it possible to obtain from experimental results a clear discrimination between these two processes?

Although the speed dependence of relaxation rates was considered theoretically by Voigt as far back as 1912, first experimental evidences of departures from the Voigt profile were performed on H_2 by Herzberg in 1950 and clearly attributed to the Dicke effect.

Since the 1980s, a lot of experimental works performed on molecular species of atmospheric interest - such as OCS, HCN, N_2O, C_2H_2, CO, CO_2, O_3, ... - have clearly shown that departures from the Voigt profile are a general phenomenon, more pronounced as perturbing molecules are more massive than absorbing ones. Without going into the details, the Dicke effect was generally retained for the interpretation of experiments involving a large Doppler effect, as the infrared domain, whereas the speed dependence of relaxation rates was rather considered in the millimeter range. However in the late 1990s, strong difficulties were reported by consideration of the Dicke narrowing, namely optical diffusion rates that evolve non linearly with the gas pressure and get larger than kinetic diffusion rates.

EXPERIMENTAL RESULTS

Since several years, numerous experiments have been performed in Lille for the determination of line broadening parameters of atmospheric molecules and a great attention was given to line shape analysis. These experiments were performed mainly on isolated lines, either by a time domain coherent transient technique in the millimeter range [2, 3] or by frequency domain steady state experiments in the millimeter range [4, 5] or in the infrared range [6].

As a general result, observed line shapes are narrower than expected from the Voigt profile, discrepancies being larger as mass ratios of perturber and absorber are larger. Clear asymmetries were also observed with molecular pairs

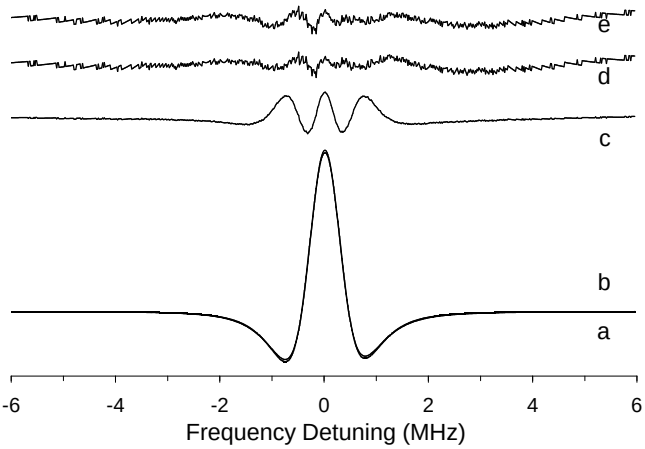

FIGURE 1. Recorded shape of the 172 GHz line of $HC^{15}N$ in collision with N_2. The signal (a) was observed by a frequency modulation technique and fitted by using a Voigt profile (b). Residua (obs.-calc.): Voigt (c, enlarged by a factor of 10), Galatry (d, factor 50), SD-Voigt (e, factor 50). $HC^{15}N$ pressure (enriched sample): 0.2 mTorr, N_2 pressure: 100 mTorr, temperature: 296 K.

involving large pressure induced frequency line shifts [3]. Finally, these departures are clearer by using a frequency modulation technique [5].

For the purpose of comparison of optical diffusion and speed dependence effects, two basic profiles have been considered [1]:

1. The Galatry profile which considers a relaxation rate Γ related to the line broadening and a diffusion rate β related to velocity changing collisions.
2. The speed dependent Voigt profile: a well known model considers the relaxation rate follows a power law versus the relative speed v_r, such as $\Gamma(v_r) \propto (v_r)^{\mu}$, where μ is a parameter. An other model considers a quadratic dependence of the relaxation rate on the absorber speed v_a [2]

$$\Gamma(v_a) = \Gamma_0 + \Gamma_2 \left[\left(\frac{v_a}{v_{a0}} \right)^2 - \frac{3}{2} \right] \tag{1}$$

where Γ_0 is the mean relaxation rate over molecular speeds, Γ_2 a rate describing speed dependence effects and v_{a0} the most probable absorber speed. The main advantage of this second model is that speed dependent effects are described by a pressure dependent rate Γ_2 which has a role similar to that of the Galatry diffusion rate β in linefits.

As a matter of fact, these two profiles generally lead to similar agreement for the fitting of a line shape obtained at a given pressure (see Fig. 1, taken from [5]). However, a better insight for the discrimination of these profiles is obtained from the analysis of the pressure dependence of narrowing relaxation rates. Three different regimes are observed (see Fig. 2, taken from [5]):

1. At low pressure, *i.e.* in the Doppler regime, both diffusion rate β and speed dependence rate Γ_2 behave linearly versus the pressure with $\beta \simeq 3\Gamma_2$.
2. For higher pressures, the diffusion rate β behaves non linearly versus the pressure, in contradiction with the binary collisional regime approximation. Moreover, β gets much larger than than the kinetic diffusion parameter β_{kin} which can be deduced from the Lennard-Jones potential used for the description of collisional trajectories.
3. For still higher pressures, the β value diverges and not fit can be performed by using the Galatry profile. Let us note that quite similar results are obtained from the Rautian profile. On the other hand, the speed dependent Voigt profile remains appropriate with a linear pressure dependence of the Γ_2 rate.

Such observations have been done with molecules of atmospheric interest such as HCN, N_2O, CO or O_3, but similar difficulties were previously reported in literature for C_2H_2, CO_2, CH_3F or CO. In any cases, these features are more pronounced as colliding molecules are more massive and as relaxation rates are larger. Finally, they are well explained by a mathematical analysis of the correlation existing between Galatry and speed dependent Voigt profiles [6].

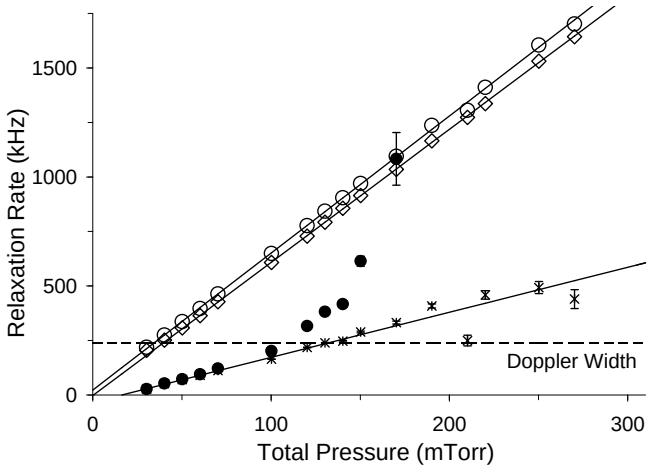

FIGURE 2. Relaxation of the 172 GHz line of $HC^{15}N$ in collision with N_2. For different considered line profiles, relaxation rates are displayed versus the total pressure and the straight lines are derived from weighted least squares fits: Γ^{Voigt} ($\diamond$), Γ_0^{SDV} ($\circ$), $3\Gamma_2^{\text{SDV}}$ ($*$), β^{Galatry} ($\bullet$). No fit is possible by using the Galatry profile for pressures larger than 180 mTorr.

As a consequence of these experimental results, it can be inferred that:

- The Galatry profile must be disregarded for a realistic modeling of observed line shapes. This means that velocity changing collisions have nearly a negligible role on the line shape.
- The speed dependent Voigt profile could be used for the whole pressure range explored.

SPEED DEPENDENCE AND OPTICAL DIFFUSION EFFECTS

From a theoretical point of view, speed dependence effects can be modeled from a simple extension of Anderson-type collision theories. Thus, calculations performed with the Robert-Bonamy formalism allow accurate predictions of speed dependent Voigt profile parameters that are in good agreement with observed ones.

However, a remaining problem is: why do velocity changing collisions play nearly a negligible role on observed line shapes? To our knowledge, no theoretical predictions of the optical diffusion rate β_{opt} seem presently available but it can be argued that optical diffusion is a consequence of collisions which alter molecular velocities while preserving molecular coherences [7]. Such a condition requires that velocity changing collisions be sufficiently soft from the point of view of relaxation, which means that impact parameters leading to significant velocity changes are much larger than those leading to collisional dephasing. This implies that the collisional relaxation rate Γ_0 must be small enough by comparison with the kinetic diffusion rate β_{kin}.

For aforementioned molecules in collision with N_2 or O_2, relaxation rates Γ_0 are at least 3-4 times larger than kinetic diffusion rates β_{kin}. Thus, velocity changes should have a negligible role on line shapes actually observed. For the sake of completeness, tentative determinations of optical diffusion rates β_{opt} have been made. By using a speed dependent Galatry profile [1, 8] and the theoretical results obtained for speed dependence relaxation rates, optical diffusion rates β_{opt} are estimated smaller than kinetic diffusion ones β_{kin} by at least a factor 3-4. Then, observed failures of the Galatry profile are easily understood from such results and it can be claimed that line shapes are actually mainly governed by speed dependence effects.

However, previous results are rather specific to molecules that exhibit relaxation rates much larger than kinetic diffusion rates. The situation is completely different for some molecules such as H_2 or HF that present small relaxation rates as well as large pressure induced frequency line shifts. As discussed in details in the literature [1], the Dicke effect is then the leading process and is accompanied by strong line shape asymmetries.

CONCLUSION

From the experimental studies that have been performed in Lille in the millimeter and infrared domains, using either steady state or transient experiments, following conclusions can be given, at least for molecules involving relaxation rates clearly larger than kinetic diffusion rates:

- Line shapes present clear departures from the Voigt profile. Even if these departures are weak, an accurate determination of line broadening parameters requires a correct modeling of actual line shapes.
- Two main process are simultaneously involved:
  - The speed dependence of relaxation rates: as it results from an obvious generalization of any collisional theory, it must be included in any line shape model, whichever the pressure is.
  - The optical diffusion due to velocity changing collisions: this effect cannot be considered alone but occur in addition to relaxation speed dependence effects. As this effect is tightly connected to the Doppler effect, it is occurs only in the low pressure regime.
- From an experimental point of view, a careful analysis of the pressure dependence of relaxation rates is required in order to check the appropriateness of considered profiles. In this way:
  - A clear failure of the Galatry profile has been demonstrated, the behavior of the retrieved diffusion rate β being in contradiction with the binary collisional approximation. This allows to claim that the Dicke effect is not the main process involved and the Galatry profile cannot be used, even as an effective line shape model.
  - The speed dependent Voigt profile looks as appropriate, which demonstrates the predominant influence of speed dependence effects on observed line shapes. Thus, this profile could be safely used as an effective line shape model.
- Velocity changing collisions can lead to effective consequences on line shapes only if molecular coherences are preserved during the collisional process, that is if the collisional relaxation rate is small enough by comparison with the kinetic diffusion rate.

These conclusions should apply to a number of molecules of atmospheric interest and could be considered for the extension of data bases to line shape properties. However, they do not apply to some particular cases, such as H_2O, for which some very narrow infrared lines have been observed, leading to a clear Dicke effect. Finally, whereas speed dependence effects can be accurately modeled via *ab initio* or semi-classical calculations, further theoretical works are still required for the modeling of optical diffusion effects.

ACKNOWLEDGMENTS

This work has benefited of grants from Programme National de Planétologie and Programme National de Chimie Atmosphérique from CNRS-INSU, and from European Space Agency. The Laboratoire de Physique des Lasers, Atomes et Molécules is Unité Mixte de Recherches CNRS-Université de Lille 1 and belongs to the Centre d'Etudes et Recherches Lasers et Applications which is supported by the Ministère chargé de la Recherche, the Région Nord-Pas de Calais, and the Fonds Européen de Développement Economique des Régions.

REFERENCES

1. J.-M. Hartmann, C. Boulet, D. Robert, *Collisional Effects on Molecular Spectra: Laboratory Experiments and Models, Consequences for Applications*, Elsevier, to be published, 2008.
2. F. Rohart, H. Mäder, H.-W. Nicolaisen, *J. Chem. Phys.*, **101**, 6475-6486 (1994).
3. F. Rohart, F. Kaghat, A. Ellendt, H. Mäder, *J. Mol. Spectrosc.*, **185**, 222-233 (1997).
4. D. Priem, F. Rohart, J.-M. Colmont, G. Wlodarczak, J.-P. Bouanich, *J. Mol. Structure*, **517-518**, 435-454 (2000).
5. F. Rohart, L. Nguyen, J. Buldyreva, J.-M. Colmont, G. Wlodarczak., *J. Mol. Spectrosc.*, **246**, 213-227 (2007).
6. J.-F. D'Eu, B. Lemoine, F. Rohart, *J. Mol. Spectrosc.*, **212**, 96-110 (2002).
7. J.P. Looney, *Ph.D. Thesis*, Pennsylvania State University, Philadelphia, 1987.
8. R. Ciuryło, J. Szudy, *J. Quant. Spectrosc. Radiat. Transfer*, **57**, 411-423 (1997).

Characteristics of Quasi-Molecular State Interaction

A.Devdariani[1], E.Dalimier[2] , P.Sauvan[3] , T.Kereselidze[4], I. L.Noselidze[4] and F.Rebentrost[5]

[1]*Dept.Optics&Spectroscopy, St.Petersburg University, Ulianovskaya 1, 198904 St.Petersburg, Russia*
[2]*Physique Atomique dans les Plasmas Denses, LULI UMR 7605, CNRS-CEA-Ecole Polytechnique, Université Paris 6, Case 128, 4 Place Jussieu, 75252 Paris Cedex 05, France*
[3]*UNED, Dpto Ingeneria Energetica, 12 Juan del Rosal, 28040 Madrid, Spain*
[4] *Department of Exact and Natural Sciences, Tbilisi State University, Chavchavadze Avenue 3, 0128 Tbilisi, Georgia*
[5]*Max-Planck-Institut für Quantenoptik,D-85748 Garching, Germany*

INTRODUCTION

The work reports on the radiative characteristics of the one-electron quasi-molecules Z1eZ2 (Z1, Z2 are for the nuclear charges), such as dipole optical transition moments and spectral profiles produced by interacting states. Although the problem has been discussed earlier mostly for neutral species, e.g., [1-3] there are three reasons to revert to the discussion of the influence of the interaction on the radiative characteristics:

- New general properties of the dipole moments of arbitrary interacting states [4], that had not been taken into account in earlier works, were obtained recently;
- The energy terms and the dipole moments for the Z1eZ2 quasi-molecules can be calculated exactly on the basis of the Schrödinger equation depending on the distance between nucleus;
- Potential applications to current experimental data in hot plasma physics and astrophysics are in progress.

DIPOLE MOMENTS OF INTERACTING STATES

The input data for spectral profile calculations include potential energy surfaces (energy terms) of the initial and final states and dipole transition moments. In contrast to potential energy surfaces, very little appears to be known about the general features of the dipole moments. Of particular interest are the roots (or zeros) of dipole transition moments, which can lead to the formation of dips in the far wing spectral profiles [5]. Generally, the prediction of the position of such a root does not appear to be possible a priori. But it is well known, especially from atomic collision theory, that the two-state approximation can be applied in many situations to describe quasi-molecules in excited states. For this last case, the question of roots can be solved directly under rather general assumptions. It has been shown that the intersection of the diabatic transition energy terms is neither a necessary nor a sufficient condition for the occurrence of an adiabatic dipole moment root. For example, counter-intuitively, the existence of a root for non-intersecting diabatic terms is possible. The underlying reason for the occurrence of a root is rather fundamental and related to the orthogonality of the adiabatic states. The conclusions obtained are confirmed by specific calculations of dipole moments.

ADIABATIC CASE

In order to reveal the physical picture, two limiting cases in the situation known as avoided crossings of quasi-molecular terms are discussed. In the first adiabatic case, particles follow mainly adiabatic terms. In terms of Z1eZ2 quasi-molecules, this case is typical for the region of small distances where quasi-molecular wave functions are transformed into ones of the combined ions. The occurrence of a root produces inevitably a distinctive structure in the spectral profile which can be described qualitatively as a sum of a maximum and a dip broken up by the term splitting. The qualitative discussion is supported by analytical considerations and computations of the spectral structures.

DIABATIC CASE AND CHARGE EXCHANGE

In the second limiting case the particles follow mainly diabatic terms. This case is typical for the region of large distances where the wave functions of separated ions are transformed into quasi-molecular ones. Special attention is given to the case of slightly different Z1,Z2 that is called "swapping" in the physics of collision with inner-shell vacancy production [6]. The qualitative discussion confirmed by computational results leads to the conclusion that the dipole moments of the quasi-molecular states, the optical transitions of which are forbidden for large distances, will undergo a strong changing in the vicinity of the interionic distances about $V/\Delta F$ (V is the splitting of terms, ΔF is the force difference between diabatic terms). According to the discussion in [1] the interaction between quasi-molecular states produces not only spectral structures but leads to non-adiabatic transitions, governed by the same Massey parameter. In the case of Z1eZ2 quasi-molecules it leads to the connection between the spectral features and the cross sections of charge exchange. The specific results for spectral profiles and cross-sections are discussed in the context of recent experimental results [7].

ACKNWOLEDGEMENTS

This work was supported by INTAS under grant 06-1000017-9041.

REFERENCES

1. A.Z.Devdariani and Yu.N.Sebyakin, *Sov.Phys. JETP* 1127-1133 (1989).
2. Rebentrost, "Thermally averaged coupled-channels calculations of collisional redistribution", in *Spectral Line Shapes*, **5**, 249-274 (1989).
3. A.Gallagher, "Line Shapes and Radiation Transfer" in *Atomic, Molecular, & Optical Physics Handbook*, edited by G.W.F.Drake, Springer, 2006, pp. 220-232.
4. A.Devdariani and E.Dalimier (to be published).
5. A.Devdariani, T. M. Kereselidze, I. L. Noselidze, E.Dalimier, P.Sauvan, P.Angelo, and R.Schot, *Phys.Rev.A*, **71,** 022512 (2005).
6. R. Anholt, *Rev. Mod. Phys*. **57**, 995 (1985).
7. E.Dalimier , E.Oks, O.Renner, and R.Schott, *J.Phys.B : At. Mol. Opt. Phys.* **40**, 909-919 (2007).

A Statistical Model for Scalar Collision–Sequence Interference

John Courtenay Lewis* and Roger M. Herman†

*Department of Physics and Physical Oceanography
Memorial University of Newfoundland
St. John's NL
Canada A1B 3X7
†104 Davey Laboratory
Department of Physics
Pennsylvania State University
University Park, PA 16802
U.S.A.

Scalar collision–sequence interference has received considerable theoretical and experimental attention, for which refs. [1, 2, 3] and references therein may be consulted.

The present work is a continuation of ref. [4], in which a class of statistical–mechanical models for collision-sequence interference is studied. The key features of these models are:

1. the collisions are treated as instantaneous, as is appropriate for the study of collision–sequence interference effects at low densities;
2. for vector interference the dipole moment $\boldsymbol{\mu}(t)$ induced in a single particle (molecule) is followed, as a time series; for scalar interference the scalar modulation $\mu(t)$ of the dipole moment is followed;
3. the dipole moment is taken to be proportional to the force; hence the integrated induced dipole moment $\boldsymbol{\mu}_k$ induced in a collision k of a collision sequence is proportional to the impulse $\boldsymbol{f}_k$ imparted to the molecule in that collision; for scalar interference the integrated scalar modulation μ_k of the dipole moment is taken to be proportional to the impulse f_k for collision k;
4. the velocity of the particle is Maxwellian and is completely randomised in each collision: the persistence of velocity is zero.

In addition, in [4] the times between successive collisions were all equal. This allowed the use of discrete Fourier transforms. Because of the close relationship between the impulse and the velocity the various quantities which enter the final expressions for the spectra can be expressed as integrals over Gaussians and, in most instances, can be evaluated analytically. This analytical tractability is an important feature of the models.

These models were first introduced in [5]. Their purpose is not for detailed comparison with experiment, which indeed is not attempted, but rather to gain insight into the processes underlying the collision–sequence interference effects.

In ref. [4] a previously unknown correlation among induced dipole amplitudes present in the scalar interference effect was identified.

In the present work the final assumption of ref. [4], that of equal intervals between collisions, is replaced by the much more realistic assumption that the collision times form a Poisson process. In a real gas the collision times are not exactly Poisson–distributed [6] but deviations from a Poisson process are small.

We find that assumptions 1 to 4 above, with Poisson–distributed collision times, lead (as for the simpler models of ref. [4]) to expressions for the parameters are expressible as integrals over Gaussians.

A principal result is that the correlation described above leads to a Lorentzian line shape with HWHH equal to the collision frequency.

The inclusion of a line shifting mechanism in the model is also discussed.

ACKNOWLEDGMENTS

One of us (JCL) acknowledges support from the Natural Sciences and Engineering Research Council of Canada.

REFERENCES

1. J. D. Poll, 'The infrared spectrum of HD," in *Phenomena Induced by Intermolecular Interactions*, edited by G. Birnbaum, Plenum Press, New York, 1985.
2. R. M. Herman, "Scalar and Vector Collisional Interference in the Vibration–Rotation Absorption Spectra of H_2 and HD," in *Proceedings of the 8th ICSLS*, edited by R. J. Sexton, A . Deepak Publishing, Hampton, Virginia, USA, 1987.
3. J. C. Lewis and R. M. Herman, *Phys. Rev. A* **68**, 032703 (2003).
4. J. C. Lewis, *Phys. Rev. A* , accepted for publication (2008).
5. J. C. Lewis, "Lattice Gas Models for Intercollisional Interference," in *Proceedings of the 15th ICSLS*, edited by J. Seidel, AIP Conference Proceedings 559, American Institute of Physics, New York, 2001.
6. S. Chapman and T. G. Cowling, *The Mathematical Theory of Non–Uniform Gases 2nd ed.*, Cambridge University Press, 1964.

Collision-induced hyperpolarizability and hyper-Rayleigh spectra in the H_2-Ar supermolecule

W. Głaz and T. Bancewicz*, J-L. Godet† and G. Maroulis**

* *Nonlinear Optics Division, Faculty of Physics,*
Adam Mickiewicz University, Poznań, Poland
† *Laboratoire POMA*
Université d'Angers, 2 Angers, France
** *Department of Chemistry, University of Patras, Patras, Greece*

INTRODUCTORY REMARKS

The report that is to be presented at the Conference refers to recent results in the work devoted to theoretical and numerical analyses of the so-called collision-induced hyper-Rayleigh scattering (CHRS) of light by media composed of supermolecular systems of atoms interacting with linear molecules. The project is a step forward towards more complex geometries then those previously considered in our work, i.e. atomic noble gas pairs [1].

BRIEF OUTLINE OF THE RESEARCH

The Phenomenon

The effect studied within the framework of the project presented is a nonlinear process in which a gaseous molecular system is excited with two photons of laser frequency ω and spontaneously emits another one at a frequency of about 2ω. The main quantity which makes this possible is the first hyperpolarizability described by β_{ijk} tensor (or its spherical counterpart). The number of its non-zeroth independent components chiefly depends upon the geometry of the scattering system: for molecules with a center of symmetry they all vanish identically and no hyper-Rayleigh scattering is possible unless, due to the interaction between them, the symmetry is broken and CHRS may occur. The simplest supermolecule where it becomes possible consists of two unlike atoms for which there are two independent spherical components of tensor β, whereas for the situation of interest in this study their number grows to six.

The mechanism considered can be a source of a rather weak signal of much lower intensity then these of non-collisional HRS (not even mentioning much more powerful occurrences of the linear light scattering) [5]. Hopefully though, in view of the tremendous development of experimental methods of molecular spectroscopy, measurements subtle enough to detect it can be supposedly available in the foreseeable future— an incentive for theoretical and numerical work [6].

The method

As far as the theoretical approach is concerned, the problem of choosing a method by means of which the molecular properties needed are obtained is a key question. Fortunately, advances in numerical procedures in quantum chemistry of recent decades have provided us with proper tools. In this study the hyperpolarizability tensor dependence on the intermolecular distance R between Ar atoms and H_2, obtained by Maroulis and coworkers, was used. The calculation of the data sets were based on the well-tested Boys-Bernardi counterpoise method [2]. Subsequently these values were applied in order to calculate significant spherical components of β; there are in fact two of them: β_1 ('dipolar', of rank 1) and β_3 ('octopolar'), each additionally expanded in terms of more elementary, 'symmetry allowed' tensorial quantities, $\beta_{\lambda L}$ [3]. As a consequence, there are two types of translational correlation functions defining the resulting intensity of CHRS. They were numerically determined by means of two methods of computation, whose results are then compared: the former was based on solving the equations of motion of the system classically, whereas the latter treated the problem quantum-mechanically by having recourse to the Schrödinger equation [4]. The rotational part of the spectra was obtained by means of an independent procedure so that the two parts could be convoluted into actual intensities.

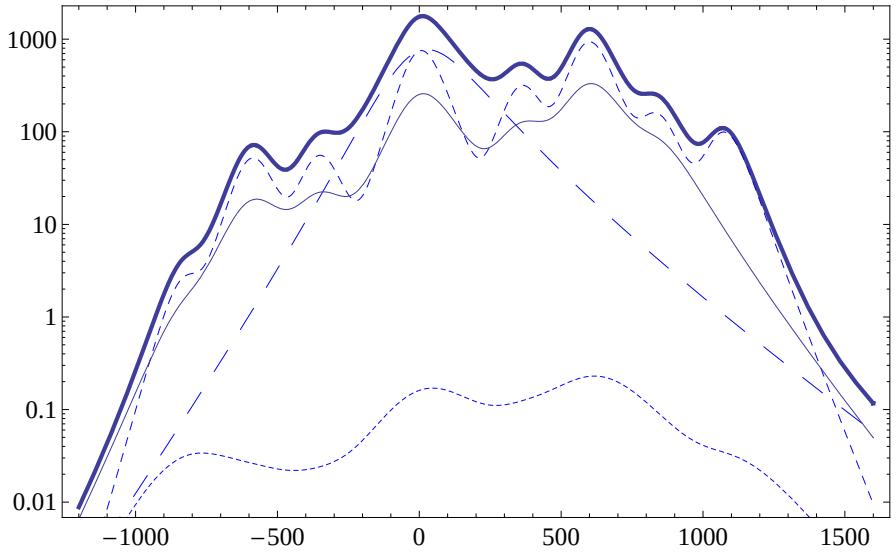

FIGURE 1. Dipolar part of the hyper-Rayleigh spectrum. Intensity (in a.u.) versus wavenumber (in cm^{-1}). From top to bottom at zero frequency: total intensity (solid line), **01**-contribution (long-dashed line), **21**-contribution (short-dashed line), **23**-contribution (thin solid line), **45**-contribution (thin dashed line).

A result

The resulting profiles for different components of the dipolar part of the hyperpolarizability tensor, $\beta_{\lambda L}$ (λL= **01**,**21**, **23** and **45**, respectively) are presented in Fig. 1 as an example, as well as to enable an assessment of their relative contribution in shaping the total spectrum. It is noteworthy that the characteristic rotational 'multi-peak' structure of the features in the figure is typical of all the lines except for the purely translational, **01** contribution. Moreover, the very low value of **45** relative to other parts indicates satisfactory convergence of the series applied even for relatively small number of the the terms.

REFERENCES

1. W. Głaz, T. Bancewicz, J.-L. Godet, G. Maroulis and A. Haskopoulos, *Phys. Rev.* **A 73**, 042708 (2006).
2. G. Maroulis, *J. Phys. Chem.* **104**, 4772 (2000).
3. T. Bancewicz, 'Induced Rayleigh and hyper-Rayleigh spectra. Pair hyperpolarizability," in Computation in Moder Sciences and Engineering *International Conference in Science and Engineering* , edited by T. E. Simons and G. Maroulis, AIP Conference Proceedings 963, Vol. 1 Part A, American Institute of Physics, New York, 2007, pp. 250-256.
4. L. Frommhold, in *Collision-induced Absorption in Gases*, Cambridge University Press, Cambridge, 1993.
5. R. D. Pyatt and D. P. Shelton, *J. Chem. Phys* **114**, 9938 (2001).
6. F. Rachet, M. Chrysos, C. Guillot-Noël and Y. Le Duff, *Phys. Rev. Lett.* **84**, 2120 (2000).

The Keilson and Storer 3-dimensional (KS-3D) line shape model : application to optical diagnostic in combustion media

P. Joubert

Institut UTINAM, UMR CNRS 6213, Université de Franche-Comté,
16 route de Gray, 25030 Besançon Cedex, France

High-resolution infrared [1] and Raman [2] spectroscopies require refine spectral line shape model to account for all observed features. For instance, for gaseous mixtures of light molecules with heavy perturbers, drastic changes arise particularly in the collision regime [3, 4], resulting from the inhomogeneous effects due to the radiator speed-dependence of the collisional line broadening and line shifting parameters. High temperature enhances such spectral lineshape changes, so that a specific interest lies in their study for diagnostics in combusting media [5].

Efficient models based on the hard collision approximation have been proposed to fit accurately such inhomogeneous profiles. In these models, the crucial parameter is the frequency of speed-changing collisions which governs the speed class exchanges. This parameter has been found to be typically one order of magnitude lower than the velocity changing collision frequency for H_2 in heavy perturbers mixtures [3, 4]. This was recently confirmed by molecular dynamics calculations [6, 7]. In order to understand the physical mechanism underlying such a drastic change from the velocity- to the speed-changing collision frequency, a kinetic model based on a realistic speed memory function characterized by a unique parameter γ has been already studied [8]. It has been demonstrated that this kinetic model well accounts for the observed speed inhomogeneous spectral effects in the collision regime (i.e. in the absence of confinement narrowing [9]). It allows one to calculate the speed dependent spectral lineshapes at high density from the hard (H) collision approximation (i.e. when each collision thermalizes the radiator speed) up to the opposite soft (S) collision one (i.e. when a significant speed change requires a large number of collisions).

This work is devoted to generalize this kinetic model to lower densities [10], when the Doppler contribution, and the concomitant collisional confinement narrowing, can be no longer neglected. Such an intermediate density range between the pure Doppler and the collision regimes is relevant for many applications, not only in combustion but also in atmospheric sciences where the existing models are frequently not enough accurate. The main objective is thus the rigorous study of both the collisional confinement narrowing of the Doppler distribution and the inhomogeneous effects due to the radiator speed-dependence of the collisional half width and shift on the lineshape, within the framework of the impact kinetic equation using the Keilson-Storer (KS) expression [11] for the translational velocity-memory function.

We present then applications of this new model called KS-3D line shape model concerning optical diagnostics, particularly for H_2-N_2 mixtures with high pressure and high temperature [12]. The effects of collisional relaxation on the spectral line shapes are discussed and the determination of collisional parameters using recent development of femtosecond time resolved spectroscopy are presented. Using the KS-3D line shape model, we present consequences for optical diagnostic of temperature and concentrations in combustion media.

REFERENCES

1. P. Duggand, P. M. Sinclair, R. Berman and J. R. Drummond, *J. Mol. Spectrosc.* **186**, 90 (1997).
2. F. Chaussard, X. Michaut, R. Saint-Loup, H. Berger, P. Joubert, B. Lance, J. Bonamy and D. Robert, *J. Chem. Phys.* **112**, 158 (2000).
3. R. L. Farrow, L. A. Rahn, G. O. Sitz and G. J. Rosasco, *Phys. Rev. Lett.* **63**, 746 (1989).
4. J. Ph. Berger, R. Saint-Loup, H. Berger, J. bonamy and D. Robert, *Phys. Rev. A* **49**, 3396 (1994).
5. J. Hussong, W. Stricker, X. Bruet, P. Joubert, J. Bonamy, D. Robert, X. Michaut, T. Gabard and H. Berger, *Appl. Phys. B* **70**, 447 (2000).
6. P. N. M. Hoang, P. Joubert and D. Robert, *Phys. Rev. A* **89**, 012507 (2002).
7. P. Joubert, P. N. M. Hoang, L. Bonamy and D. Robert, *Phys. Rev. A* **66**, 042508 (2002).
8. D. Robert and L. Bonamy, *Eur. Phys. J. D* **2**, 245 (1998).
9. R. H. Dicke, *Phys. Rev.* **89**, 472 (1953).
10. L. Bonamy, H. Tran, P. Joubert and D. Robert, *Eur. Phys. J. D* **31**, 459 (2004).
11. J. Keilson and J. E. Storer, *Quaterly Appl. Math.* **10**, 243 (1952),
12. H. Tran, P. Joubert; L. Bonamy, B. Lavorel, V. Renard, F. Chaussard, O. Faucher and B. Sinardet, *J. Chem. Phys.* **122**, 194317 (2005).

STUDIES OF NEW DIFFUSION SIGNATURES IN THE IR COLLISION-INDUCED SPECTRA OF MOLECULAR HYDROGENS IN LIQUID NEON

W. A. Herrebout[1], B. J. van der Veken[1] and A.P. Kouzov[2*]

[1]*Department of Chemistry, University of Antwerp, Antwerp, Belgium*
[2]*Institute of Physics, Saint Petersburg State University, Peterhof, Saint Petersburg 198504, Russia*
**E-mail: alex@ak1197.spb.edu*

The first spectroscopic observation of the relative (solute-solute) diffusion in a fluid environment is reported. New, unusually sharp $Q_1^q(J)$ lines developing against the diffuse background in the collision-induced fundamental IR bands of hydrogen isotopomers (H_2, D_2 and HD) dissolved in liquid Ne (T ≈ 25 K) are studied as functions of the solute concentration x (Fig. 1). In all cases, the Q_1^q intensity parabolically scales with x accompanied by a stri-king narrowing of the line shapes (Fig. 2). Accurate fittings of the *para*-H_2 solution band shapes allowed to separate the single $Q_1^q(0)$ line into the guest-host and guest-guest components. The observed narrowing is due to a faster growth of the sharper guest-guest line with x. The latter as well as other observed guest-guest lines are strongly narrowed by fast velocity de-correlations and are signatures of microscopic-scale diffusion. Also, a first observation of the $U_1(J)$ transitions (with $J = 4$) induced by the guest-host interactions is reported.

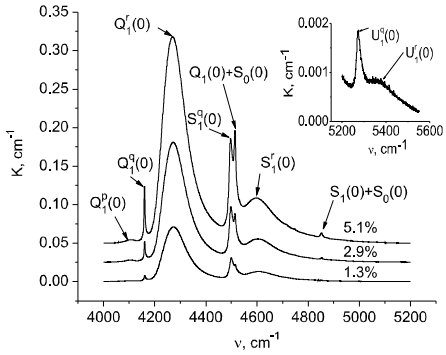

FIGURE 1. Absorption coeficient $K(\nu)$ of p-H_2 solution in liquid neon (T=25.0 K) at different concentrations (molar per cent). Curves are shifted by 0.025. Inset shows the spectrum near the $U_1(0)$ transition.

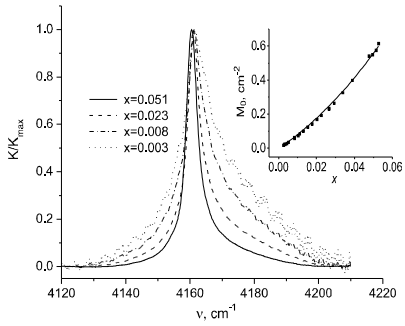

FIGURE 2. Normalized $Q_1^q(0)$ shapes of p-H_2 solution (T=25.0 K) at different concentrations x. Integrated $Q_1^q(0)$ absorption coefficient M_0 vs x is plotted in inset: squares – experimental M_0 values, solid line - parabolic fit.

ACKNOWLEDGMENTS

Useful discussions with M.O. Bulanin are appreciated. We thank the Special Research Fund of the University of Antwerp and the FWO-Vlaanderen for financial support.

Linewidths of C_2H_2 perturbed by H_2: calculations from an ab initio potential and comparison with experimental results

Franck Thibault*, Benoît Corretja*, Alexandra Viel*, Dionisio Bermejo†, Raúl Z. Martínez† and Béatrice Bussery-Honvault**

*Institut de Physique de Rennes, UMR CNRS 6251, Université de Rennes I, F-35042 Rennes, France
†Instituto de Estructura de la Materia, CSIC, Serrano 123, ES-28006 Madrid, Spain
**Institut UTINAM, UMR CNRS 6213, Université de Franche-Comté, F-25030 Besançon, France

ABSTRACT

In this work we present a theoretical and experimental study of the acetylene - hydrogen system. An *ab initio* potential surface has been obtained by *ab initio* quantum chemistry methods. This 4-dimensional potential is further used to compute pressure broadening coefficients of C_2H_2 isotropic Raman Q lines on a large scale of temperatures within both the close-clouping approach and the coupled-states approximation. Experimental data for the acetylene ν_2 Raman lines broadened by molecular hydrogen are obtained using stimulated Raman spectroscopy. Comparisons of theoretical values with experimental data measured at 143 K are promising.

EXPERIMENT

The stimulated Raman spectra recorded and analyzed for this work have been obtained with the spectrometer of Instituto de Estructura de la Materia, already described in previous works [1, 2]. The samples consisted of diluted mixtures of $^{12}C_2H_2$ (5% in volume) in H_2 at different pressures (20, 40, 60, 80 and 100 mb approximately). Raman spectra of the Q-branch of the ν_2 band of $^{12}C_2H_2$ at 143 K have been recorded up to $j = 17$ for all pressures. The spectral lines have been analyzed by fitting them to Voigt profiles. The Gaussian part of the Voigt profile, resulting from the convolution of the Gaussian Doppler width at 143 K and the Gaussian apparatus function, can be pre-calculated and fixed during the fit of the profiles. In this way the Lorentzian contribution to the Voigt profile of each spectral line can be extracted, and from its variation with sample pressure an experimental value of the broadening coefficient for each line has been obtained. Other details can be found in [3].

INTERMOLECULAR POTENTIAL

To perform the calculations, we have used the Molpro package which proposes a large variety of *ab initio* levels. We choose the coupled cluster method at a level of single and double excitations with the triple excitations included perturbatively, i.e. CCSD(T), and performed a few additional calculations with the symmetry adapted perturbation method based on monomer orbitals built up with the density functional theory (DFT-SAPT). We have conducted potential energy calculations for specific conformations (R, θ_A, θ_B, ϕ) of the C_2H_2-H_2 dimer where (R, θ_A, θ_B, ϕ) are the four angular Jacobi coordinates which describe the relative orientation of the two monomers (the "A "index refers to C_2H_2 while "B "refers to H_2). Computations are performed for a large number of geometries located on a (R, θ_A, θ_B, ϕ) grid. The product grid includes 20 values of R from R=5. to 20 bohr, 9 values of θ_A and θ_B between 0 and 90 degrees and 17 values of ϕ between 0 and 180 degrees resulting in 27540 geometries. In order to perform the quantum dynamical study of the collision the interaction potential is developed onto 30 bispherical harmonics [4]:

$$V(R,\theta_A,\theta_B,\phi) = \sum_{L_A,L_B,L} V_{L_A,L_B,L}(R) A_{L_A,L_B,L}(\theta_A,\theta_B,\phi), \tag{1}$$

with

$$A_{L_A,L_B,L}(\theta_A,\theta_B,\phi=\phi_A-\phi_B) = \left(\frac{2L+1}{4\pi}\right)^{1/2} \sum_m \langle L_A m L_B m | L0\rangle Y_{L_A}^m(\theta_A,\phi_A) Y_{L_B}^{-m}(\theta_B,\phi_B) \tag{2}$$

CALCULATIONS OF PRESSURE BROADENING CROSS SECTIONS

The way of performing the calculations with the MOLSCAT package is very similar to the one used for our N_2-H_2 study [4] and thus details are not given here. For isotropic Raman lines, pressure broadening (PB) cross sections are derived from rotational 2-state to 2-state cross sections. Defining [4] a partial PB cross section as:

$$\sigma(j_A, j_B, E_{kin}) = \sum_{j_A', j_B'} \sigma\left(j_A j_B \rightarrow j_A' j_B'; E_{kin}\right) \tag{3}$$

with $j_A' \neq j_A$, and using the Maxwell Boltzmann thermal average based on the kinetic energies, the PB cross section at temperature T of a $Q(j_A)$ line is a sum of two contributions due to the para and ortho species of H_2:

$$\sigma(j_A, T) = \frac{1}{4}\sigma_{\mathrm{pH_2}}(j_A, T) + \frac{3}{4}\sigma_{\mathrm{oH_2}}(j_A, T) \tag{4}$$

with

$$\sigma_{\mathrm{pH_2}}(j_A, T) = \sum_{j_B \text{ even}} \rho_{j_B}\sigma(j_A, j_B, T) \tag{5}$$

and

$$\sigma_{\mathrm{oH_2}}(j_A, T) = \sum_{j_B \text{ odd}} \rho_{j_B}\sigma(j_A, j_B, T). \tag{6}$$

Finally, the PB coefficient is given by

$$\gamma(j_A) = \frac{n_{H_2}\bar{v}}{2\pi c}\sigma(j_A, T). \tag{7}$$

This quantity can be compared with measurements performed at a given temperature T with natural H_2 and C_2H_2.

RESULTS

Details of the calculations [3] show that: i) the partial PB cross sections for $j_B = 0$ are the smallest, ii) at room T and above cross sections for $j_B > 0$ are very close to each other, and iii) at high T it is not useful to compute both ortho and para cross sections but simply set $\sigma_{\mathrm{pH_2}} = \sigma_{\mathrm{oH_2}}$. This allows to save CPU time. Experimental and theoretical PB coefficients of isotropic Raman lines, at 143 K are displayed in Fig. 1. Taken into account the experimental error bars, a good agreement between the current experimental data and our calculations is observed. Moreover, there is no substantial disagreement even using eq. (7) without performing the thermal average over the relative kinetic energies.

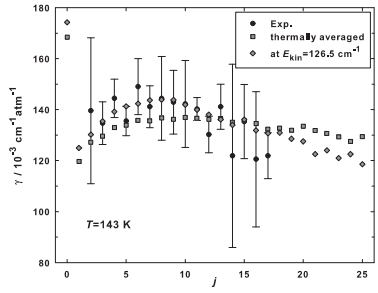

FIGURE 1. HWHM of acetylene lines broadened by H_2

REFERENCES

1. J. Santos, P. Cancio, J. L. Domenech, J. Rodriguez and D. Bermejo, *Laser Chem.* **12**, 53-63 (1992).
2. J. L. Domenech, F. Thibault, D. Bermejo and J.-P. Bouanich, *J. Mol. Spectrosc.* **225**, 48-54 (2004).
3. F. Thibault, B. Corretja, A. Viel, D. Bermejo, R. Z. Martínez, B. Bussery, *Phys. Chem. Chem. Phys.* submited (2008).
4. L. Gomez, R. Z. Martínez, D. Bermejo, F. Thibault, P. Joubert, B. Bussery-Honvault and J. Bonamy, *J. Chem. Phys.* **126**, 204302-8 (2007).

Molecular Dynamics Simulations of Collision–Induced Absorpion in Lennard–Jonesium at High Densities

John Courtenay Lewis

Department of Physics and Physical Oceanography
Memorial University of Newfoundland, St. John's NL, Canada A1B 3X7

We have previously reported[1, 2] on simulations of collision–induced absorption in Lennard–Jonesium. These simulations described a mixture of two species *A*, *B*, where the intermolecular potential was a pairwise additive sum of Lennard–Jones terms of the form

$$U(r;\sigma,\varepsilon) = 4\varepsilon\left[\left(\frac{\sigma}{r}\right)^{12} - \left(\frac{\sigma}{r}\right)^{6}\right]$$

with different ranges for *AA*, *AB*, and *BB* pairs. In these simulations particles of species *A* had the mass of H_2 while each *B* particle had the mass of an Ar atom. Furthermore the ranges σ_{AA}, σ_{AB}, and σ_{BB} were approximately those of $H_2 - H_2$, $H_2 - Ar$, and $Ar - Ar$. However, all interactions were spherically symmetric.

Furthermore, the total induced dipole moment was pairwise additive over *AB* pairs, with each pair dipole $\boldsymbol{\mu}\left(r;\sigma_\mu,\varepsilon_\mu\right)$ being parallel to the pair force and of magnitude

$$\mu\left(r;\sigma_\mu,\varepsilon_\mu\right) = -\frac{\partial}{\partial r}U\left(r;\sigma_\mu,\varepsilon_\mu\right).$$

Hence each pair dipole moment is of the form of a Lennard–Jones force. However, the range σ_μ of the dipole moment is, in these simulations, treated as a free parameter, and effects of its variation have been studied for $0.90 \leq \sigma_\mu/\sigma_{AB} \leq 1.3$.

The effects of varying σ_μ, and varying concentration and temperature, were studied at relatively low densities [1, 2], with one set of studies [2] near the critical point for pure *A*.

In the present work we will discuss the simulations at high densities and approximately room temperature. The essential feature is that the simulation line shapes are unlike observed line shapes at high densities. Furthermore, there is little tendency for the interference dip to fill in, which is expected on the basis of an argument quoted by Birnbaum and Mountain.

The differences between simulation and observation are discussed in the light of the known behaviour of the irreducible three–body induced dipole moment[3, 4, 5], and also the Deryagin approximation[6] for taking into account irreducible contributions of all orders.

ACKNOWLEDGMENTS

We thank Milton W. Cole for many useful discussions on many–body interactions in fluids, and in particular for bringing the work of Deryagin in this area to our attention. We thank Roger M. Herman for useful discussions on collision–sequence interference and other aspects of spectroscopy. We acknowledge support from the Natural Sciences and Engineering Research Council of Canada.

REFERENCES

1. J. C. Lewis, in *Spectral Line Shapes Volume 12*, edited by C. A. Back (American Institute of Physics, 2002), no. 645 in AIP Conference Proceedings, pp. 394–400, proceedings of the 16th ICSLS.
2. J. C. Lewis, in *Proceedings of the 17th International Conference on Spectral Line Shapes*, edited by E. Dalimier (Frontier Group, 2004), pp. 358–360, proceedings of the 17th ICSLS.
3. L. W. Bruch, C. T. Corcoran, and F. Weingold, Mol. Phys. **35**, 1205 (1978).
4. L. W. Bruch and T. Osawa, Mol. Phys. **40**, 491 (1980).
5. B. Guillot, R. D. Mountain, and G. Birnbaum, Mol. Phys. **64**, 747 (1988).
6. A. Stone, *The Theory of Intermolecular Forces* (Clarendon Press, Oxford, 1996).

Level energies, oscillator strengths, and lifetimes for transitions in Pb IV

C. Colón*, A. Alonso-Medina*, A. Zanón† and J. Albeniz**

*Departamento de Física Aplicada. EUITI. Universidad Politécnica de Madrid (UPM)
†Departamento de Matemática Aplicada. EUITI. (UPM)
**Departamento de Química Industrialy Polímeros. EUITI. (UPM)

Data on atomic properties are relevant not only to spectroscopy, as these values are also of interest in a variety of other fields in physics and technology. The presence of Pb IV in stellar spectra has been reported in a few different type of stars. As an example the Pb IV resonance lines has been detected in Far Ultraviolet Spectroscopic Explorer (FUSE) spectra of hot subdwarf B (sdB) stars [1] and [2].

In this work we present oscillator strengths for lines arisinf from of $5d^{10}ns$ (n=6,7,8), $5d^{10}np$ (n=6,7), $5d^{10}nsd$ (n=6,7,8), $5d^96s^2$ and $5d^96s6p$ configurations of Pb IV and some level radiative lifetimes of Pb IV. We have obtained theoretical values of oscillator strenths in intermediate coupling (IC) ad using ab initio relativistic Hartree-Fock(HFR)calculations.

For the IC calculations we used the standard method of least-square fitting of experimental energy levels by means of computer codes from Cowan (1981)[3]. In this way we obtained the LS composition of each level and the degree of configuration mixing, when we consider their interaction. For the HFR calculations the Cowan computer code provide with us the radial parts for determination of transition probabilities and initial estimated of the parameters for the IC fittings. The radial integrals for calculations of transition probabilities were obtained from the HFR wavefunctions.

The system considered is complex, since at high Z both relativistic and correlation effects are important. In this case east square fitting of experimental energy levels partially accounts for correlations effects not explicitly calculated in this work. A most detailed description of this method can be seen in others works of these authors [4], [5], [6] and [7].

Several of the values calculated in this work are the first presented in the bibliography. Levels no designed by Moore (1958) have been assigned.

In Table 1 we present as example the results obtained for two lifetimes orresponding to resonance lines of Pb IV of high astrophysical interest . There is a good agreement between our results and the experimental values.

TABLE 1. Radiative lifetimes of Pb IV levels

Transition levels	**Wavelength (nm)***		**Lifetimes (ns)** **This wort**	**Other expt.†**
$6s\ ^2S_{1/2}$–$6p\ ^2P_{1/2}$	131.3	0.95		1.11 ± 0.10
$6s\ ^2S_{1/2}$–$6p\ ^2P_{3/2}$	102.9	0.48		0.52 ± 0.04

* Moore 1958
† Ansbacher et al 1988

ACKNOWLEDGMENTS

This work has been supported by the project CCG07-UPM/ESP-1632 of the TECHNICAL UNIVERSITY OF MADRID (UPM). Support to the lines of UPM investigation groups included in the IV PRICIT of the CAM (Comunidad Autónoma de Madrid), SPAIN .

REFERENCES

1. P. Chayer et al, *Baltic Astronomy* **15**, 131–137 (2006).
2. S. J. O' Toole, *A&A* **423**, L25–L28 (2006).
3. R. D. Cowan, in *Theory of Atomic Structure and Spectra*, edited by University Press, Los Angeles, (1981).
4. C. Colon, and A. Alonso-Medina, *Physica Scripta* **62**, 132–136 (2000).

5. C. Colon, and A. Alonso-Medina, *A&A* **422**, 1109–1112 (2004).
6. A. Alonso-Medina et al, *Physica Scripta* **71**, 154–158 (2005).
7. A. Alonso-Medina et al, *MNRAS* in revision
8. C. E. Moore, in *Atomic Energy Levels*, edited by NBS 467, Washington D. C., (1958).
9. W. Ansbacher et al, *Canadian Journal of Physics* **66**, 402–404 (1988).

Theoretical Study of several oscillator strengths and lifetimes od Germanium, Thallium and Bismuth. Measures of somme relative transition probabilities

A. Alonso-Medina*, C. Colón*, A. Zanón†, J. L. Montero**, F. Fernández Martínez** and C.Rivero‡

*Departamento de Física Aplicada. EUITI. Universidad Politécnica de Madrid (UPM)
†Departamento de Matemática Aplicada. EUITI. (UPM)
**Departamento de Química Industrial y Polímeros. EUITI. (UPM)
‡Departamento de TAT. ETSIT. (UPM)

The presence of Thallium, Bismuth and Germanium in stellar spectra has been reported in a few different type of stars. (see e. g. [1], [2], [3] and [4]). Data on atomic properties are relevant not only to spectroscopy, as these values are also of interest in a variety of other fields in physics and technology.

Calculations of oscillator strength for different transitions in Thallium, Bismuth and Germanium has been the subject of numerous theoretical studies see e. g. [5], [6], [7], [8] and [9]).

In this work a complete study of atomic parameters of different species of these elements has been made. We have obtained theoretical values of oscillator strenths in intermediate coupling (IC) ad using ab initio relativistic Hartree-Fock(HFR)calculations. The system considered is complex, since at high Z both relativistic and correlation effects are important. In this case east square fitting of experimental energy levels partially accounts for correlations effects not explicitly calculated in this work.

For the IC calculations we used the standard method of least-square fitting of experimental energy levels by means of computer codes from Cowan (1981) [10]. In this way we obtained the LS composition of each level and the degree of configuration mixing, when we consider their interaction.

For the HFR calculations the Cowan computer code provide with us the radial parts for determination of transition probabilities and initial estimated of the parameters for the IC fittings. The radial integrals for calculations of transition probabilities were obtained from the HFR wavefunctions.

To provide level energy for our calculation we have used the Tables of Moore [13].

Also in this work we present experimental values for several lines corresponding to different transitions of Tl I, Tl II, Ge I, Ge II, Bi I and Bi II. Relative values have been obtained from measures of emission line intensities in hollow cathode lamp discharges operating with a tipically current of 10 mA.

The wavelengths of the measured transitions are the UV, Visible and IR. The infrared spectra was obtained using a Czerny-Turner monochromator (Digikrom CVI). A IHR55 Jobin-Ibon monochromator was used to obtain the visible and UV spectrum. We used in both cases a CCD to detected the optical signal.

We have used two different methods in order to place data on an absolute scale.We have use the experimental lifetimes present in the bibliography and usiung line-strength sum rules applied to our relativistic calculations.

Our results have been compared with the values presents in the literature. As exampñle there is a relatively good agreement between our results and the values by the Tl I [11] and [12]

ACKNOWLEDGMENTS

This work has been supported by the project CCG07-UPM/ESP-1632 of the TECHNICAL UNIVERSITY OF MADRID (UPM). Support to the lines of UPM investigation groups included in the IV PRICIT of the CAM (Comunidad Autónoma de Madrid), SPAIN .

REFERENCES

1. N. C. Sterling et al, *ApJ* **578**, L55–L58 (2002).
2. G. M. Wahlgren, *Proccedings IAU Symposium* **224**, 291–299 (2004).
3. S. Goriely, and L. Siess, *A&A* **378**, L25–L28 (2001).
4. D. S Leckrone et al, *ApJ* **117**, 1454–1470 (1999).
5. L. J. Curtis, *Physica Scripta* **62**, 31–35 (2000).
6. P. Palmeri et al, *Physica Scripta* **63**, 468–475 (2001).

7. U.I. Safranova et al, *Physical Review A* **71**, 052506–18 (2005).
8. E. Biemont, *J. Phys. B:At. Mol. Opt. Phys.* **38**, 3547–3556 (2005).
9. A. Alonso-Medina, *An. Phys.* **92**, 71–84 (1996).
10. R. D. Cowan, in *Theory of Atomic Structure and Spectra*, edited by University Press, Los Angeles, (1981).
11. A. alonso-Medina *JQSRT* **56**, 557–562 (1996).
12. A. alonso-Medina *J. Phys. B:At. Mol. Opt. Phys.* **30**, 1377–1384 (1997).
13. C. E. Moore, in *Atomic Energy Levels*, edited by NBS 467, Washington D. C., (1958).

Spectral Broadening of excitation induced by ultralong-range interaction in a cold gas of Rydberg atoms

A.V.Glushkov*,†, O.Yu.Khetselius* and A.V.Loboda*

*Odessa University, P.O.Box 24, Odessa-9, South-East, 65009, Ukraine
†Institute for Spectroscopy of Russian Academy of Sciences, Troitsk, Moscow reg., 142090, Russia

With the advances in a laser cooling and trapping techniques, new important perspectives for studying Rydberg atoms have been opening. When cooled to very low temperatures, the core motion can be neglected for timescales of Rydberg excitation. One could wait for realization of the unusual effects, such as the spontaneous formation and recombination of ultracold plasma, spectral broadening of excitation induced by long-range interactions in a cold gas of Rydberg atoms etc. Here we present new precise theory (based on the relativistic perturbation theory [1], [2], [3], [5], [4], [6],[7]) to calculating the spectral broadening and suppression of excitation induced by ultralong- range (100 Bohr radii) interactions in a cold gas of Rb atoms, hyperfine structure, collision shift. Precise ab initio van-der-Waals interaction potential is used. The theory describes the density dependence of these effects for S-,P,-D Rydberg states with main quantum numbers n=60-80 in an excellent agreement with the precise Freiburg (K. Singer, M.R. Lamour, T. Amthor, et al, 2004) experiment.

REFERENCES

1. A. V. Glushkov, and L. N. Ivanov, *Phys. Letters* **A170**, 33–38 (1992).
2. A. V. Glushkov, O. Yu. Khetselius et al., *Nucl. Phys. A* **734**, e21–28 (2004).
3. Á. Glushkov, 'Energy Approach to Resonance states of compound super-heavy nucleus and EPPP in heavy nucleus collisions," in *LEAP'05*, edited by D. Grzonka et al., AIP Series Vol.796, American Institute of Physics, New York, 2005, pp. 206–210.
4. A. V. Glushkov, O. Yu. Khetselius et al., *J. Phys. CS* **11**, 188-198 (2005).
5. A. Glushkov, O. Khetselius, et al., "QED calculation of heavy multicharged ions with account for the correlation, radiative and nuclear effects," in *Recent Advances in Theor. Phys. and Chem. Systems*, edited by J. Maruani et al., Springer, Paris, 2006, Vol.15, pp. 285–320.
6. A. V. Glushkov, O. Yu. Khetselius et al., *J. Phys. CS* **35**, 420-425 (2006).
7. O. Yu. Khetselius, *Photoelectronics* **15**, 101-110 (2006).
8. A. Glushkov, O. Khetselius, et al., "Gauge-invariant QED perturbation theory approach to calculating nuclear electric quadrupole moments, hyperfine structure constants for heavy atoms and ions: Superatom package," in *Recent Advances in Theor. Phys. and Chem. Systems*, edited by S. Wilson et al., Springer, London, 2008, Vol.18, pp. 201–224.
9. A. Glushkov, S. Malinovskaya, O. Khetselius, *Europ. Phys. Journ.* **48** (2008).

Collisional shift of the Tl hyperfine lines in atmosphere of inert gases

O.Yu. Khetselius*, A.V.Glushkov*,†, E.P.Gurnitskaya*, A.V.Loboda*, E.V.Mischenko* and T.A.Florko*

*Odessa University, P.O.Box 24, Odessa-9, South-East, 65009, Ukraine
†Institute for Spectroscopy of Russian Academy of Sciences, Troitsk, Moscow reg., 142090, Russia

We propose a new relativistic approach to calculation of the inter atomic potentials, spectra, hyperfine structure (hfs) collision shift for heavy atoms in atmosphere of inert gases and diatomic quasi molecules. Am approach is based on the gauge-invariant perturbation theory [1],[2], [3], [4] with using the optimized relativistic wave functions basis's, generated in the perturbation theory zeroth order. We have carried out the detailed studying and calculation of the inter atomic potentials, collision shifts of the hyperfine transition lines for Tl atom in atmosphere of the inert gases (for systems Tl-He, Tl-Ar etc.).

METHOD OF CALCULATION

To calculate the spectral lines hyperfine structure collision shift we have used the following known expression from kinetical theory of spectral lines form:

$$f_p = D/p = (4\pi w_0/kT)\cdot\int dw(R)\exp[-U(R)/kT]R^2dR, \quad (1)$$

where $U(R)$ is an effective potential of the inter atomic interaction, which has a central symmetry in a case of the systems $Tl-B$ ($B=He,Ar$); T is temperature, w_0 is a frequency of the hyperfine transition in the isolated active atom; $dw(R)=Dw(R)/w_0$ is the relative local shift of the hyperfine structure lines, which is arisen due to the disposition of atoms of the Tl and B on a distance R. To calculate an effective potential of the inter atomic interaction we used a method of the exchange perturbation theory [4]. To calculate a local shift one uses a method of exchange perturbation theory (we use version $EL-HAV$). With exactness to second order terms on potential of Coulomb interaction of the valent electrons and atomic cores one can write as follows:

$$dw(R) = [S_0/(1-S_0)] + \Omega_1 + \Omega_2 - [C_6/R^6][2/E_a + 1/(E_a+E_b)], \quad (2)$$

where C_6 is the van der Waals constant for interaction $A-B$ (for example $Tl-He$); S_0 is the overlapping integral; Ω_1 and Ω_2 are the non-exchange and exchange non-perturbation sums of the first order. The value $E_{a,b}$ is defined as follows:

$$E_{a,b} = (I_{a,b} + E_{1a,b})/2. \quad (3)$$

where I and $E_{1a,b}$ are the ionization potential and excitation energy on the first level for atoms of A and B correspondingly. For atom of Tl authors [6] have used the relativistic Dirac-Fock wave functions (first variant). Another variant is using relativistic functions, solutions of the Dirac equations with the Green model potential. Let us note that these basis's are not optimized. We have used the gauge invariant optimized basis of relativistic functions, generated by the QED perturbation theory method [1], [7], [8].

RESULTS AND DISCUSSION

We present the results of calculations (in atomic units) for the local $dw(R)$ and observed f_p shifts for systems: $Tl-He$, $Tl-Ar$ and others. The experimental (observed) and calculated values of the f (Gz/Torr) shifts for system $Tl-He$ are presented in table 1 (see table 1) and compared with calculation results [6], which are obtained within the non-gauge-invariant perturbation theory with Hartree-Fock like orbital basis's. The important feature of our scheme is a correct account of the correlation and polarization effects with using special effective potentials from [4]. Analysis shows that our data for system $Tl-He$ are in good agreement with the known experimental data by Charou-Scheps-Galakher and theoretical data [6]. For other $Tl-Ne,Ar,Kr,Xe$ systems there are no quite precise data. It is provided first of all

TABLE 1. Observed and calculated f_p (Gz/Torr) shifts for the system $Tl - He$

	T (K^o)	Theory Our data	Theory Ref.[6]	Experiment
1	700	139	155	130±30
2	750	137	153	-
3	800	135	151	-
4	850	133	149	-
5	900	131	-	-
6	950	129	-	-
7	1000	126	-	-

by worse description of these systems within exchange perturbation theory. The mistake of data, that are available in the literature, is about 70-80 percents for observed shift for pair $Tl - Kr$ and 40-50 percents for systems $Tl - Xe$.

REFERENCES

1. A. V. Glushkov, and L. N. Ivanov, *Phys. Letters* **A170**, 33–38 (1992).
2. L.-N. Ivanov et al., *Phys. Rev. A* **48**, 4365–4380 (1993).
3. A. V. Glushkov et al., *Int. Journ. Quant. Chem.* **104**, 512–522 (2005).
4. Á. Glushkov, E. Gurnitskaya, and A. Loboda 'Advanced quantum mechanical calculation of superheavy ions: energy levels, Radiation and Finite Nuclear size effects," in *LEAP'05*, edited by D. Grzonka et al., AIP Conference Proceedings 796, American Institute of Physics, New York, 2005, pp. 211–215.
5. A. Glushkov et al., "QED calculation of heavy multicharged ions with account for the correlation, radiative and nuclear effects," in *Recent Advances in Theor. Phys. and Chem. Systems*, edited by J. Maruani et al., Springer, Paris, 2006, Vol.15, pp. 285–320.
6. V.-V. Batygin, and I. M. Sokolov, *Optics Spectr.* **55**, 30–38 (1983).
7. E. P. Ivanova, L. N. Ivanov, A. V. Glushkov, and A. E. Kramida, *Phys. Scripta* **32**, 513–524 (1985).
8. A. V. Glushkov, and E. P. Ivanova, *J. Quant. Spectr. Rad. Transfer* **36**, 125–148 (1986).

Unification of the Impact and One-Perturber Theories of Line Shapes

G. Peach*, D.F.T. Mullamphy† and I.B. Whittingham†

*Department of Physics and Astronomy, University College London, Gower Street, London WC1E 6BT, UK
†School of Mathematics, Physics and Information Technology, James Cook University, Townsville 4811, Australia

ABSTRACT

It has long been known that in the far wings of a spectral line the impact approximation can be related to one-perturber theory by replacing the full wave functions for the initial and final states of the emitter+perturber system by their asymptotic forms, see for example [1]. It is shown here that one-perturber theory can be rewritten into a form in which the quantity that should directly correspond to the width of the line as calculated from the impact approximation can be extracted explicitly. This theory has been developed generally for a full quantum mechanical description of the emitter-perturber system in which coupled equations are used to describe the details of the collision, see [2] and [3].

Previous fully quantum-mechanical calculations of line widths and shifts have been extended to consider the line-wing profiles where impact theory is no longer valid. Lorentzian line widths of the lithium, sodium and potassium resonance lines broadened by helium have been calculated using both impact and one-perturber theory for the temperature range $70 \leq T \leq 3000K$. Initial results have been previously reported by Peach [4]. Excellent agreement between these two approximations is obtained, demonstrating that full quantum-mechanical calculations of the line profiles can be made that are accurate over the whole range of frequencies from the line centre to the line wings.

REFERENCES

1. G. Peach, *Adv. Phys.* **30**, 367–474 (1981).
2. P.J. Leo, G. Peach and I.B. Whittingham, *J. Phys. B: At. Mol. Opt. Phys* **33**, 4779–4797 (2000).
3. D.F.T. Mullamphy, G. Peach, V. Venturi, I.B. Whittingham and S.J. Gibson, *J. Phys. B: At. Mol. Opt. Phys* **40**, 1141–1152 (2007).
4. G. Peach, D.F.T. Mullamphy and I.B. Whittingham, 'Recent work on line shapes for the spectra of cool stars, ' in *VI Serbian Conference on Spectral Line Shapes in Astrophysics*, edited by L.Č. Popović and M.S. Dimitrijević, AIP Conference Proceedings 938, American Institute of Physics, New York, 2007, pp. 142–147.

Influence of temperature on line shape parameters of the self-broadened 748,8 nm Ne line

A. Urbanowicz*, C. Sajna*, A. Bielski*, S. Brym and R. S. Trawiński*

* *Instytut Fizyki, Uniwersytet Mikołaja Kopernika, ul. Grudziadzka 5, 87-100 Torun, Poland*

Katedra Fizyki Relatywistycznej, Uniwersytet Warmińsko-Mazurski, ul. Żołnierska 14, 10-561 Olsztyn, Poland

¨*e-mail: adamu@fizyka.umk.pl*

Shapes of the self-broadened 748.8 nm neon line emitted from a glow discharge in the pressure range between 1.5 and 80 Torr in pure neon have been measured using a pressure-scanned Fabry-Perot interferometer. Our first goal in the present study was to verify theoretical prediction [1] that speed-dependent effects may be important for relatively cold atoms. Our second goal was to verify whether pressure broadening, asymmetry and shift coefficients depend on temperature. Similarly as in Ref. [2] we have used emission lamp which was equipped with three independent heaters which allowed us to work for temperatures equal to 300, 400, 500 and 600 K. We also used another lamp which allowed the line shapes measurements in liquid nitrogen temperature (77 K).

As was shown in previous paper [3] when the mass ratio of the perturbing and emitting atoms is close to one, the correlation between the Doppler and collisional broadening plays an important role. In this case when we fit ordinary Voigt profile (VP) to experimental profiles, the values of the Doppler half-width decrease with neon pressure. This effect was observed for each temperature. As the next step a speed-dependent Voigt profile (SDVP) was fitted to our experimental data. As a result we found the Doppler widths practically independent of the neon pressure. We also used theoretical line-shapes expressions for asymmetric Voigt profile (AVP) and speed-dependent asymmetric Voigt profile (SDAVP) to analyze the influence of temperature on collision-time asymmetry and asymmetry resulting from correlation effects.

REFERENCES

1. P. R. Berman, *J. Quant. Spectr. Radiat. Trasf.* **12**, 1331 (1972).
2. A. Urbanowicz, A. Bielski, R. S. Trawiński, S. Brym, J. Wolnikowski, *European Physical Journal ST* **144**, 247-249 (2007).
3. R. Ciuryło, A. Bielski, S. Brym, J. Domysławska, D. Lisak, J. Szudy, R.S. Trawiński, *Acta Physica Polonica A* **96**, 359-372 (1999).

Line Shape Study of the 326.1 nm ^{113}Cd line perturbed by Ar and Xe

P. Masłowski*, K. Bielska, A. Śliwińska, J. Domysławska, D. Lisak, R. Ciuryło,
J. Szudy and R. S. Trawiński

Instytut Fizyki, Uniwersytet Mikołaja Kopernika, Grudziadzka 5/7, 87–100 Torun, Poland
**pima@fizyka.umk.pl*

We report results of measurements of the shapes of two hyperfine-structure components (F'=1/2–F''=1/2 and F'=3/2–F''=1/2) of the intercombination 326,1 nm line corresponding to the 5^1S_0–5^3P_1 transition for the even-odd ^{113}Cd isotope perturbed by Xe and Ar. Experiments were performed using a laser-induced fluorescence method and the values of the pressure broadening, shift and asymmetry coefficients were determined. In the course of the present study we employed a recently verified isotope structure of the 326.1 nm line [1].

Using the verified data of the isotope structure we re-analysed our previous experimental results for the ^{113}Cd–Ar system [2]. The corrected values of the broadening, shift and asymmetry coefficient for ^{113}Cd–Ar as well as those for ^{113}Cd–Xe system are reported. Both for ^{113}Cd–Xe (the emitter to perturber mass ratio 1.15) and ^{113}Cd–Ar (the mass ratio 0.35) the effects due to correlation between pressure and Doppler broadening of the 326.1 nm line were observed.

Our analysis was performed using a Speed Dependent Asymmetric Voigt Profile (SDAVP). Functions describing speed-dependence of collisional broadening and shifting, incorporated in SDAVP, depend on assumed interaction potential for given emitter-perturber systems. In order to increase the accuracy of line-shape parameters there is a need for more realistic interaction potentials.

REFERENCES

1. P. Masłowski, K. Bielska, A. Śliwińska, J. Domysławska, R. Ciuryło, D. Lisak, A. Bielski, R. S. Trawiński, "Isotope structure and hyperfine splitting of 326.1 nm ^{113}Cd line" in *19th International Conference on Spectral Line Shapes* Valladolid 2008
2. P. Masłowski, J. Domysławska, K. Bielska, R. Ciuryło, D. Lisak, R. S. Trawiński, J. Szudy, Spectral Line Shapes, AIP Conference Proceedings vol. 874, pp. 214, American Institute of Physics, New York 2006

Isotope Structure and Hyperfine Splitting of 326.1 nm ^{113}Cd line

P. Masłowski*, K. Bielska, A. Śliwińska, J. Domysławska, D. Lisak, R. Ciuryło, A. Bielski and R. S. Trawiński

Instytut Fizyki, Uniwersytet Mikołaja Kopernika, Grudziadzka 5/7, 87–100 Torun, Poland
**pima@fizyka.umk.pl*

High resolution measurements of spectral line shapes require the konwledge of frequencies determing the positions of all isotope components of a line under investigation. In the course of this work the influence of the isotope structure of the 326.1 nm ($5^1S_0 - 5^3P_1$) cadmium line on the fitted line shape parameters describing the pressure broadening, shift and collision–time asymmetry was carefully studied.

Measurements for the ^{113}Cd line perturbed by Ne at low pressure (below 2 Torr) were inspired by results of our experimental studies for the ^{114}Cd and ^{113}Cd isotopes perturbed by Ar and Xe at pressures up to 250 Torr [1]. Using these data we were able to determine the hyperfine splitting for ^{113}Cd 326.1 nm line with uncertainity below 10^{-3} cm^{-1}. Relatively small splitting between hyperfine components of the line caused difficulties in data analysis, especially for higher pressures, which are also presented.

REFERENCES

1. P. Masłowski, K. Bielska, A. Śliwińska, J. Domysławska, R. Ciuryło, D. Lisak, J. Szudy, R. S. Trawiński, “Line Shape Study of 326.1 nm ^{113}Cd line perturbed by Ar and Xe” in *19th International Conference on Spectral Line Shapes* Valladolid 2008

Low-Uncertainty CRDS Measurements of O_2 *A*-Band Line Parameters

Piotr Masłowski[1,2], Joseph T. Hodges[2], David J. Robichaud[3] , Laurence Y. Yeung[3], Mitchio Okumura[3], Charles E. Miller[4], and Linda R. Brown[4]

[1]*Instytut Fizyki, Uniwersytet Mikołaja Kopernika, ul. Grudziadzka 5/7, 87-100 Torun, Poland*

[2]*Process Measurements Division, National Institute of Standards and Technology, 100 Bureau Drive, Gaithersburg, MD 20899, USA*

[3]*Division of Chemistry and Chemical Engineering, California Institute of Technology, Pasadena, CA 91125, USA*

[4]*Jet Propulsion Laboratory, California Institute of Technology, 4800 Oak Grove Drive, Pasadena, CA 91109 USA*

There are many applications of molecular spectroscopy which require low relative uncertainty (less than 0.5%) and SI traceability in line parameters such as intensity, transition frequency, pressure-induced frequency shifts and broadening, and other quantities related to line shape and line mixing effects. Notable examples include remote sensing technologies to study the Earth's climate which probe atmospheric gases from ground- and satellite-based instruments. These measurements are rapidly evolving and rely on well-defined line lists that enable highly predictive models of atmospheric spectra valid over a wide range of temperature and pressure. Typically, reference-grade line parameters are derived from laboratory Fourier-transform spectroscopy (FTS) measurements, where the spectrometer instrument function is convolved with relatively simple line shapes (such as the Voigt profile) to model the observed spectra. However, we have recently demonstrated that frequency-stabilized cavity ring-down spectroscopy (FS-CRDS) can provide higher spectral resolution and sensitivity than the FTS, yielding line parameters for relatively weak transitions with lower uncertainty.

To illustrate these capabilities of FS-CRDS, we present line position data for 32 *P*-branch transitions of the O_2 *A*-band. Absolute positions were calibrated in terms of hyperfine components of ^{39}K D_1 (12985.19 cm^{-1}) and D_2 (13042.90 cm^{-1}) atomic transitions. A continuous-wave external cavity diode laser synchronously probed the ring-down cavity and ^{39}K absorption cell. The latter system was arranged in a double-pass configuration and yielded Doppler-free saturation spectra of ^{39}K with a resolution of 300 kHz. Using this calibration, the ring-down cavity's free-spectral range (used for interpolation and extrapolation from the ^{39}K transition reference points) was determined to within 80 Hz. The combined uncertainty in the O_2 *A*-band transition frequencies was < 1 MHz, which is more than 20 times lower than previously reported uncertainties for the O_2 *A*-band. Finally, we measured eight O_2 *A*-band transitions measured over the pressure range 20 – 700 torr in order to investigate line shape effects. We conclude that the Voigt profile can not model the data with accuracy at the sub-1% level or better. Moreover, we see evidence of Dicke narrowing and speed-dependence of collisional broadening and shifting, indicating that relatively sophisticated line shape models must be used to minimize systematic biases in fit-derived line parameters.

Spectrally Resolved Intensities of Ultra-Dense Hot Aluminum Plasmas

J.M.Gil[#], R.Rodríguez[#], R. Florido[#], J.G.Rubiano[#], P.Martel[#], E.Mínguez*, P.Sauvan , P.Angelo[‡], R.Schott [‡], E. Dalimier [‡] and R.Mancini[§]

[#] *Departamento de Física, Universidad de Las Palmas de Gran Canaria, 35017 Las Palmas de Gran Canaria, Spain*
**Instituto de Fusión Nuclear, E.T.S. de Ingeniros Industriales, U.P.M., 28006 Madrid, Spain*
Departamento de Ingeniería Energética, UNED, Madrid, Spain
[‡] *Physique Atomique dans les Plasmas Denses-LULI, CNRS-CEA-Ecole Polytecnique-Université Paris 6, 75252 Paris cedex 05 and 91128 Palaiseau cedex.*
[§] *Physics Department University of Nevada, Reno, NV 89557, USA*

ABSTRACT

Radiative properties of hot dense plasmas remain a subject of current interest [1, 2] since they play an important role in the inertial fusion confinement (ICF) research as well as studies in stellar physics. In particular, the understanding of ICF plasmas requires emissivities and opacities both for hydro-simulations and diagnostics [3]. The first step on the calculation of plasma radiative properties is the computation of the required atomic data. However, this is a complex task since the number of the atomic levels involved, and therefore the amount of atomic data to obtain is huge and approximations must be made in order to include. Due to this fact, the calculation of plasma ion populations and radiative properties is still an open question and continuous efforts are made to develop new models and numerical codes that improve the currently available ones.

Recently, it has been developed at the University of Las Palmas de Gran Canaria a computation package composed by two codes called ABAKO [4] and RAPCAL [5] that calculate atomic data and plasma level populations (ABAKO) and radiative properties such as opacities, emisivities, intensities or radiative power losses (RAPCAL) for optically thin and thick plasmas, both under LTE and NLTE conditions. In particular, plasmas of elements such as carbon, aluminum, argon, iron, krypton, xenon and gold have been studied in several plasma situations (Corona, NLTE or LTE, optically thin and thick,…) and density and temperature conditions, obtaining accurate results.

In this work both codes are used to analyse the spectrally resolved intensities of ultra-dense and hot aluminum plasma experimentally obtained at the 80J LULI laser facility. In these experiments, the 600 ps laser operating with a quadrupled frequency have been focalized onto the edge of a 30-80 μm thickness aluminum foils. The emission spectra of the plasma have been analysed with a progressivly curved KAP spectrograph in the range of 3.8 to 8.7 Angstroms. The spatial resolution of the spectrograph along the laser axis allows to access regions of the plasma with different conditions of density and temperature.

REFERENCES

1. S. Alexiou, et al. *JQSRT*, **58**, 399 (1997).
2. G. Csanak, and W. Daughton *JQSRT,* **83**, 83, (2004).
3. O. Peyrusse, *Nucl. Fus.,* **44**, S202, (2004).
4. J.M. Gil, et al. *Laser Part. Beams* **26**, (2008).
5. R. Rodríguez, et al. *J. Phys. IV* **133**, 981, (2006).

On "Averaged" Diffusion of Radiation in Spectral Lines intra Interjacent Plasma - Gas Layer

A.V. Demura and G.V. Demchenko

HEPTI, RRC "Kurchatov institute". Kurchatov Square 1. Moscow 123182, Russia

The modeling of gas divertors for ITER and other tokamak devices requests to perform large scale computations of atomic kinetics with radiation transfer for rather high density, nonuniform and nonequilibrium peripheral interjacent plasma - gas layer [1]. In these systems the influence of radiation transfer on plasma equilibrium and atomic kinetics is quite essential, and thus its correct description plays significant role although represents itself quite a complicated task. In these conditions the spectral lines of the main species are severely trapped due to the surrounding plasma peripheral layer of relatively dense neutral gas [1]. In this work we present a model of "averaged" diffusion of radiation in spectral lines applied for the approximate description of radiation transfer in [1] that enables to decrease substantially computer time consumption and at the same time to preserve affordable accuracy for such type of problems with important role of the radiation transfer processes. In this model the essential spectral interval of each line is divided into two regions of strong and weak absorption (compare with [2]). The latter region corresponds to the wings, where photons easily escape the medium [2]. So, in the case of strongly trapped spectral lines we reduce the radiation transfer equations in the center to the diffusion-like equations and introduce the "effective photons" by averaging over frequency [1]. Thus the present model of "averaged" radiation diffusion describes the radiation transfer in terms of the "effective photons". The description of radiation transfer in the line wings, where formally the diffusion-like equations are not valid, in fact could be achieved in the frames of the same equations by introduction of corresponding sink terms [1], that could be evidently expressed through escape factors.

REFERENCES

1. N.V. Antonov, A.V. Demura, G.V. Demchenko, V.B. Petrov, B.I. Khripunov, G.V. Sholin, *Kinetics of Atomic Excited States Population with Account of Resonance Radiation Transfer in Interajacent Region Plasma-Gas*, Preprint IAE-6409/6, RRC "Kurchatov institute", Moscow, 2006, 1–46 (in Russian).
2. V. A. Abramov, V.I. Kogan, V.S. Lisitsa, *Radiation Transfer in Plasma*, in Plasma Theory Reviews v. 12, ed. M.A. Leontovich, B.B. Kadomtsev, Moscow, Energoizdat, 1982, pp. 114–155 (in Russian).

Spectral Line Calculation Model in no Optically Thin Plasma

K. Chenini , F. Khelfaoui and M.T. Meftah

Laboratoire Lenreza, Département de Physique, Faculté des Sciences et Sciences de l'ingénieur, Université de Ouargla 30000 Algerie

INTRODUCTION

Plasma produced by Laser generally involves temperature and density gradients. It is useful to study the thick plasma in which the radiation transport becomes important. The total broadening of optically thick lines will be affected by a combination of opacity effects and broadening mechanisms inherent to the plasma (Stark and Doppler). Klisnick et al [1] studied the experimental radiation transfer and showed from their experimental results how the plasma radiative transfer investigation can be used in the soft X-rays, for the diagnostic of population inversions and for the related amplification of spontaneous emission. In A. Klisnick et al experiment, the plasma is produced by focusing a powerful laser pulse into a dense medium with a fast recombination stage appears at the end of the pulse.

THEORETICAL MODEL

This work present opacity calculations performed on high density and thick plasma. A simplified transfer equation can be written as [2]:

$$\mu \frac{\partial}{\partial x} I_{\upsilon\mu j}(x) = -K_{\upsilon j}(x) I_{\upsilon\mu j}(x) + J_{\upsilon j}(x) \tag{1}$$

where $J_{\upsilon j}(x)$, $K_{\upsilon j}(x)$ are the emissivity and opacity of the plasma respectively. We study a plasma of aluminium lithium-like with electronic density N_e, of temperature T, and of a length(thickness) L. We consider that the plasma consists of several elementary layers of thickness dx. We treat the transfer equation taking, as hypothesis, that each layer emit and absorb a photon. The emitted photon is reabsorbed by the next nearest neighboring layers. It results that the radiation emitted by the thick (thickness L), is the sum of the radiation emitted and absorbed by the several layers of plasma.

A pencil of radiation of intensity I_ω enters on face; the radiation in the outgoing pencil of intensiy $I_\omega + dI_\omega$ leaves. We get the transfert equation as:

$$n_r^2 \frac{d}{dx}\left(\frac{I_\omega}{n_r^2}\right) = J_\omega - K_\omega I_\omega \tag{2}$$

wich n_r is the refractive index. J_ω and K_ω are the emission and the absorption coefficient [3]. For an homogeneous medium the solution of the equation gives the radiance as:

$$I_\omega(L) = I_\omega(0)\,(\exp -K_\omega L) + \frac{J_\omega}{K_\omega}(1 - \exp -K_\omega L) \tag{3}$$

where $I_\omega(0)$ is the incident intensity of the radiance (at x=0) on the element of volume. This equation is applied for every radiative transition and the final profil is the sum on all cases.

DISCUSSION AND RESULTS

We present results corresponding to a plasma of Al^{+10} at density $N_e = 4.4.10^{16} cm^{-3}$, temperature $T = 75eV$ and length $L = 8mm$. We have used the populations proposed by Klisnick et al [1]. The profiles used in expressions of J_ω and K_ω are the profiles calculated by a model where medium is considered optically thin. In these cases we have used calculation of PPP model [4].

The comparison between the experimental results [1] and our model shows that for the 2s-3p line that in a medium optically thin the FWHM of the line is $0.14A^\circ$ whereas our model gives a broadening $\Delta\lambda = 0.25A^\circ$. The experimental

width is $\Delta\lambda = 0.25A^{\circ}$, it means that our model is quite close to the experimental results. For the 2p-3d line, we find a good agreement in FWHM between our model and the experience ($\Delta\lambda_{th} = 0.29A^{\circ}$, $\Delta\lambda_{\exp} = 0.34A^{\circ}$). The comparison of ratio between the picks R shows a good agreement with experimental results.

We have calculated the Ly_α spectral line shape of Ar^{+17} for plasma of different thickness. The choosen conditions are $T = 3.10^{6}K^{\circ}$ and $N_e = 10^{24}cm^{-3}$. The lines show that the absorption of the radiation depends on the length of plasma and also depends on the properties of the medium.

REFERENCES

1. Annie Klisnick, Pierre Jeaglé, Gérard Jamelot and Antoine Carillon; " Spectral Spectral line Shapes"; **3**, 157 (1985).
2. I. E. Golovkin and R. C. Mancini; JQRST **65**, 273 (2000).
3. Alin. Corney," Atomic and Laser Spectroscopy" Clarendon press. Oxford, (1977).
4. A. Calisti, F. Khelfaoui, R. Stamm, B. Talin and R. W. Lee; Phy. Rev. **A 42**, 5433 (1990).

Experimental Stark widths for Zn II

Rafael Mayo[*,†] and Montserrat Ortiz[†]

[*]*Centro de Investigaciones Energéticas, Medioambientales y Tecnológicas (CIEMAT), E-28040 Madrid, SPAIN*
[†]*Facultad de Ciencias Físicas, Universidad Complutense de Madrid (UCM), E-28040 Madrid, SPAIN*

In the present work, we have studied experimentally the Stark widths from several lines of Zn II, some of them not measured before. For doing this, the LIBS technique has been used on an Cd-Zn alloy with a lower content of Zinc in a controlled atmosphere. The final results are compared with the ones already published. A study of the plasma conditions has been also made.

INTRODUCTION

In the present work, we have studied experimentally the Stark widths from several lines of Zn II, some of them not measured before. The interest in Zn II resides not only on the knowledge of its atomic structure to check the adequacy of theoretical models, but also on its astrophysical importance because the observations of trace metals like Nickel or Zinc provide an opportunity to study the chemical and dust evolution of galaxies [1]. Besides, the Stark parameters are useful for the determination of plasma characteristics [2].

For the case of Zn II, there are scarce publications related to the broadening parameters. In addition, there is also a difference between the experimental and theoretical results published to the date related to Stark parameters, so the aim of this work is to try to throw some light on that.

THE EXPERIMENT

The plasma source of Zn II spectrum was produced by laser ablation on an Cd-Zn alloy with a lower content of Zinc in order to avoid the effects of self-absorption. The neutral atom and other higher ions from Zinc and Cadmium were present in the plasma. The experimental work was performed in the facility provided by UCM and employed the Laser Induced Breakdown Spectroscopy (LIBS) technique.

A Nd:YAG laser beam, the characteristics of which are 200 mJ pulses of 7 ns of duration at a frequency of 20 Hz and 10640 Å wavelength, was focused on the surface of the target in order to generate the plasma in a controlled Argon atmosphere. The necessary measurements and verifications for checking the homogeneity of the plasma as well as the satisfaction of the Local Thermodynamic Equilibrium condition were done.

In order to avoid spectral blending, the same experiments, but with pure Cd and Zn as targets and using Ne as buffer gas were also made.

The light emitted by the laser-produced plasma was focused on the input slit of a grating monochromator (1-m Czerny-Turner, 0.32 Å resolution in first order), which was coupled with a time-resolved optical multichannel analyzer system (OMA III, EG&G). The spectra were stored in a computer for their further analysis by a software which is able to do the convolution for Voigt profiles, the ones that are used to fit the lines, as well as the subtraction of the background.

The experimental plasma conditions (plasma temperature, electronic density, composition) were obtained from a Boltzmann plot of the temperature, the available results for the Stark broadening of some Cd II lines [3] and by means of the Saha equation. Experimental branching ratios and already published data for transition probabilities were used for this purpose too [4].

RESULTS

The experimental results obtained in this work will be presented during the Conference as well as their comparison with previous theoretical [3, 5] and experimental [5, 6] results available in the literature.

The lines of singly ionised Zinc that have been studied are those in 2025.48, 2062.00, 2064.23, 2099.94, 2501.99 and 2557.95 Å. These lines arise from the $4p$, $4d$ and $5s$ electron configurations of Zn II.

For the sake of comparison, the contribution from other broadening mechanisms than Stark have been taken into account. In this way, an estimation of the quasistatic ion, Van der Waals, natural and resonance broadenings has been calculated.

ACKNOWLEDGMENTS

The present work was supported by Spanish DGICYT (project FIS2006-10117)

REFERENCES

1. J. Zsargo, and S. R. Federman, *Astrophys. J.* **498**, 256–260 (1998).
2. J. A. Aguilera, and C. Aragón, *Spect. Acta. B: Atomic Spec* **59**, 1861–1876 (2004).
3. L. C. Popovic, I. Vince, and M. S. Dimitrijevic, *Astron. Astrophys. Suppl. Ser.* **102**, 17–23 (1993).
4. R. Mayo, M. Ortiz, and J. Campos, *Eur. Phys. J. D* **37**, 181–186 (2006).
5. S. Djenize, A. Sreckovic, J. Labat, R. Konjevic, and L. Popovic, *Phys. Rev. A* **44**, 410–416 (1991).
6. H. J. Kusch, and E. Oberschelp, *Z. Astrophys.* **67**, 77 (1967).

AXMon (HD 45910) kinematical parameters in the Fe II spectral lines as a function of the excitation potential

Antoniou, A.*, Danezis, E.*, Lyratzi, E.*,†, Popović, L., Č.**, Dimitrijević, M., S.**, Theodosiou, E.* and Stathopoulos, D.*

*University of Athens, Faculty of Physics Department of Astrophysics, Astronomy and Mechanics, Panepistimioupoli, Zographou 157 84, Athens, Greece
†Eugenides Foundation, 387 Sygrou Av., 17564, Athens, Greece
**Astronomical Observatory of Belgrade, Volgina 7, 11160 Belgrade, Serbia

INTRODUCTION

AX Monocerotis (HD 45910=BD+5°, 1267=SAO 13974, a=6^h 27^m 52^s, δ=+5°, 54′,1 (1950), V=6,59-6,88 mag) is a binary system [1], consisting of a B2e III star and a some what fainter K0 III star, with an orbital period of 232.5 days [2, 3] and a variable spectrum [4, 5].

Danezis et al. [6, 7, 8] studied the UV spectrum of the system at phase 0.568 and detected the existence of two satellite components at the violet side and one at the red side of the main absorption lines, indicating that the envelope consists of four independent layers of matter. In the Fe II region they found three levels of values of radial velocities. The first level has values about -10 km/s, the second level has values about -72 km/s and the third level has values about -250 km/s.

Danezis et al. [9, 10] proposed the so called Gaussian-Rotational (GR) model. By applying this model we calculate the apparent rotational and radial velocities, the random velocities of the ions, as well as the Full Width at Half Maximum (FWHM) and the column density of the independent density regions of matter which produce the main and the satellite components of the studied spectral lines.

In this paper we apply the above mentioned model and calculate the radial, rotational and random velocities for a group of Fe II lines with values of excitation potential between 0.35 to 3.75 eV.

RESULTS AND DISCUSSION

In Figure 1, we give as an example the fit of the λ 2607.086 Å Fe II spectral line. We can see that the observed complex structure can be explained with SACs phenomenon.

In Figure 2 we present the variation of the radial, rotational and the random velocities of the studied group of Fe II lines as a function of the excitation potential. As we can see we detected three levels of radial velocities (up-left). The first level has values about -260 km/s (circle), the second one has values about -125 km/s (open square) and the third one has values about -18 km/s (triangle). These values are in agreement with the respective values found by Danezis et al. [8]. The values of the rotational velocities (Figure 2 up-right) for all SAC are between 20 and 60 km/s. Finally we detected three levels of the random velocities of the ions (Figure 2 down). The first level has values about 115 km/s (open circle), the second one has values about 70 km/s (square) and the third one has values of 35 km/s (triangle).

ACKNOWLEDGMENTS

This research project is progressing at the University of Athens, Department of Astrophysics, Astronomy and Mechanics, under the financial support of the Special Account for Research Grants, which we thank very much. This work also was supported by Ministry of Science of Serbia, through the projects “Influence of collisional processes on astrophysical plasma line shapes” and “Astrophysical spectroscopy of extragalactic objects”.

REFERENCES

1. P. W. Merrill, *ApJ*, **115**, 145 (1952).
2. N. L. Magalashvili, and Ya. I. Kumsishvili, *Bull. Abastumani Astrophys. Obs.*, **37**, 3 (1969).

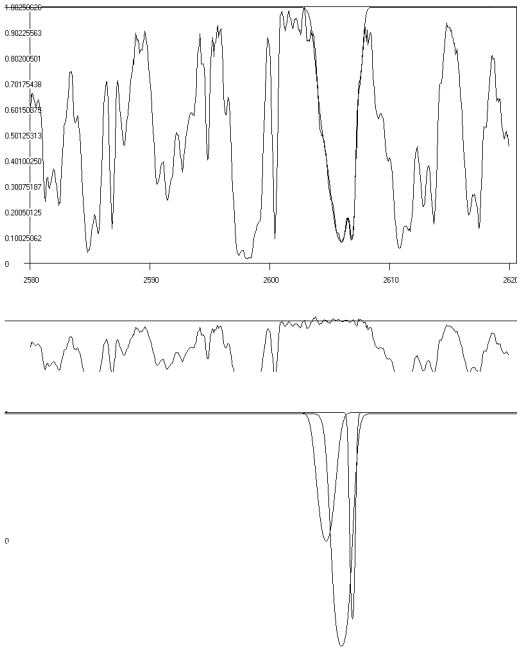

FIGURE 1. Best fit of the λ 2607.086 Å Fe II spectral line. We can explain the complex structure of these lines as a DACs or SACs phenomenon. Below the fit one can see the analysis (GR model) of the observed profile to its SACs.

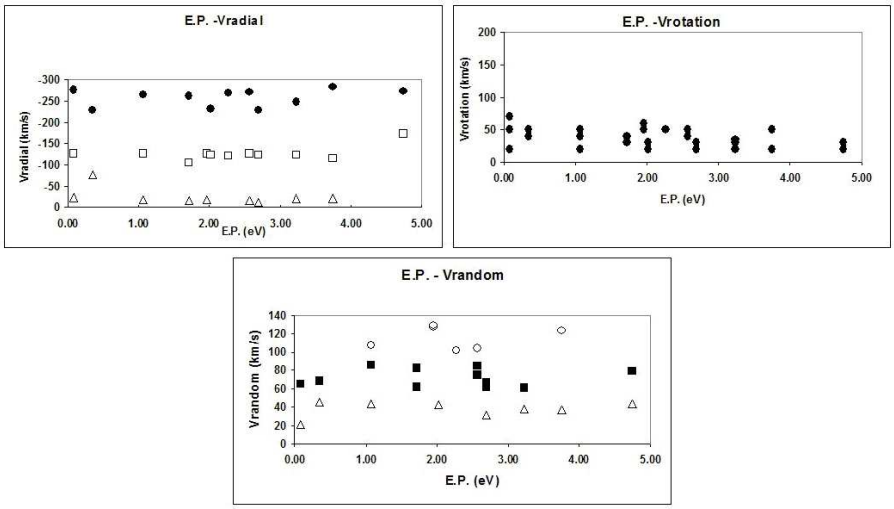

FIGURE 2. Radial (up, left), rotational (up, right) and random velocities (down) of the studied group of Fe II spectral line as a function of the excitation potential.

3. J. Papousek, *Scripta Fac. Sci. Nat. Purkyne Yniv. Brunensis, Physica 2*, **9**, 75 (1979).
4. P. W. Merrill, *PASP*, **35**, 303 (1923).
5. J. S. Plaskett, *PASP*, **35**, 145 (1923).
6. E. Danezis, *The nature of Be stars*, PhD Thesis, University of Athens, 1983.
7. E. Danezis, "The Far UV Spectrum of Binary System AX MON" in *IAU Colloq. 92, Physics of Be Stars*, edited by A. Slettebak and T. P. Snow, Cambridge University Press, 1987, p. 149.
8. E. Danezis, E. Theodossiou and P. Laskarides, *Ap&SS*, **179**, 111 (1991).
9. E. Danezis, D. Nikolaidis, E. Lyratzi, A. Antoniou, L. Č. Popović, and M. S. Dimitrijević, *Mem. Soc. It. Suppl.*, **7**, 107 (2005).
10. E. Danezis, D. Nikolaidis, E. Lyratzi, L. Č. Popović, M. S. Dimitrijević, A. Antoniou and E. Theodossiou, *PASJ*, **59**, 827 (2007).

A study of the structure of different ionization potential regions in the atmosphere of AX Mon (HD 45910)

Antoniou, A.*, Danezis, E.*, Lyratzi, E.*,†, Popović, L., Č.**, Dimitrijević, M., S.**, Theodosiou, E.* and Katsavrias, G.*

*University of Athens, Faculty of Physics Department of Astrophysics, Astronomy and Mechanics, Panepistimioupoli, Zographou 157 84, Athens, Greece
†Eugenides Foundation, 387 Sygrou Av., 17564, Athens, Greece
**Astronomical Observatory of Belgrade, Volgina 7, 11160 Belgrade, Serbia

INTRODUCTION

AX Monocerotis (HD 45910) is a binary system [1], consisting of a B2e III star and a some what fainter K0 III star, with an orbital period of 232.5 days [2, 3] and a variable spectrum [4, 5].

Danezis et al. [6] presented a study of the variation of radial velocities and of the blue edge width. In this paper, using the Gaussian-Rotational (GR) model [7, 8] we calculate the radial, rotational and random velocities in the Al II (λ 1670.81 Å), Al III ($\lambda\lambda$ 1854.722, 1867.782 Å), Mg II ($\lambda\lambda$ 2795.523, 2802.698 Å), Fe II (λ 2586.876 Å), C II ($\lambda\lambda$ 1334.515, 1335.684 Å) and Si IV ($\lambda\lambda$ 1393.73, 1402.73 Å) spectral lines of AX Mon, as a function of the ionization potential.

RESULTS AND DISCUSSION

In Figure 1 using the GR model we can see that the complex structure of the $\lambda\lambda$ 1854.722, 1862.782 Å Al III (left) and $\lambda\lambda$ 2795.523, 2802.698 Å absorption and emission Mg II (right) resonance spectral lines can be explained with SACs and DACs phenomenon.

In Figure 2 we present the variation of the radial, rotational and the random velocities in the Al II (λ 1670.81 Å), Al III ($\lambda\lambda$) 1854.722, 1867.782 Å), Mg II ($\lambda\lambda$ 2795.523, 2802.698 Å), Fe II (λ 2586.876 Å) C II ($\lambda\lambda$ 1334.515, 1335.684 Å) and Si IV ($\lambda\lambda$ 1393.73, 1402.73 Å) spectral lines as a function of the ionization potential.

As we can see, we detected four levels of radial velocities (up-left). The first level has values about -260 km/s and corresponds to ionization potential larger than 20 eV. The second level has values about -140 km/s, the third one has values about -35 km/s and the fourth one has values about 119 km/s. All these values correspond to ionization potential with values between 0 and 10 eV. The values of the rotational velocities (Figure 2 up-right) are between 150 and 450 km/s and correspond to ionization potential larger than 10 eV. The low values of the rotational velocities (10-50 km/s) correspond to ionization potential with values between 0 and 10 eV. Finally, we also detected four levels of the random velocities of the ions (Figure 2 down). The first level has values about 108 km/s and corresponds to ionization potential larger than 18 eV. The second level has values about 80 km/s, the third one has values about 47 km/s and the fourth one has values about 22 km/s. All these values correspond to ionization potential with values between 0 and 10 eV.

ACKNOWLEDGMENTS

This research project is progressing at the University of Athens, Department of Astrophysics, Astronomy and Mechanics, under the financial support of the Special Account for Research Grants, which we thank very much. This work also was supported by Ministry of Science of Serbia, through the projects “Influence of collisional processes on astrophysical plasma line shapes” and “Astrophysical spectroscopy of extragalactic objects”.

REFERENCES

1. P. W. Merrill, *ApJ*, **115**, 145 (1952).
2. N. L. Magalashvili, and Ya. I. Kumsishvili, *Bull. Abastumani Astrophys. Obs.*, **37**, 3 (1969).
3. J. Papousek, *Scripta Fac. Sci. Nat. Purkyne Yniv. Brunensis, Physica 2*, **9**, 75 (1979).

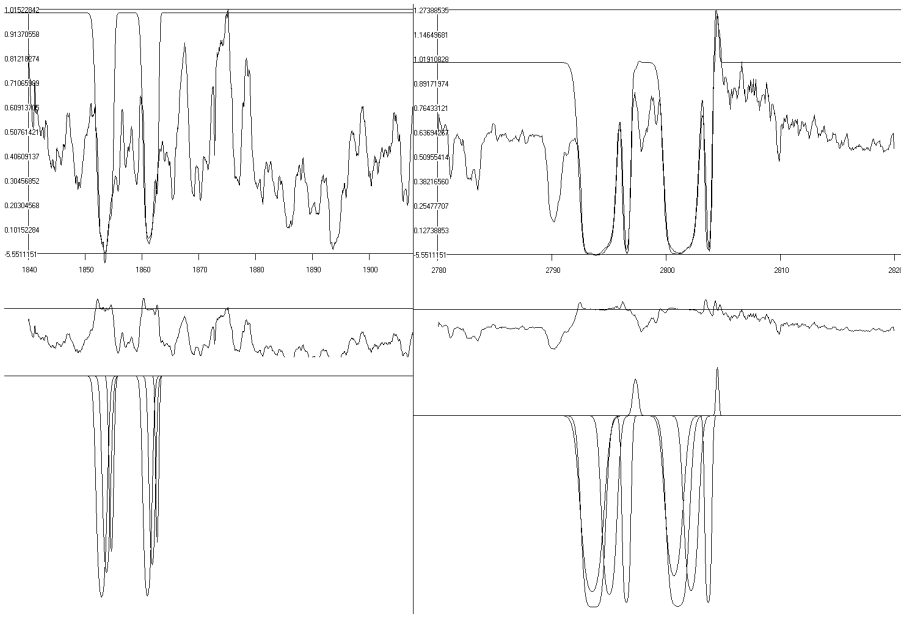

FIGURE 1. Best fit of the $\lambda\lambda$ 1854.722, 1862.782 Å Al III (left) and $\lambda\lambda$ 2795.523, 2802.698 Å absorption and emission Mg II (right) resonance spectral lines. We can explain the complex structure of these lines as a DACs or SACs phenomenon. Below the fit one can see the analysis (GR model) of the observed profile to its SACs or DACs.

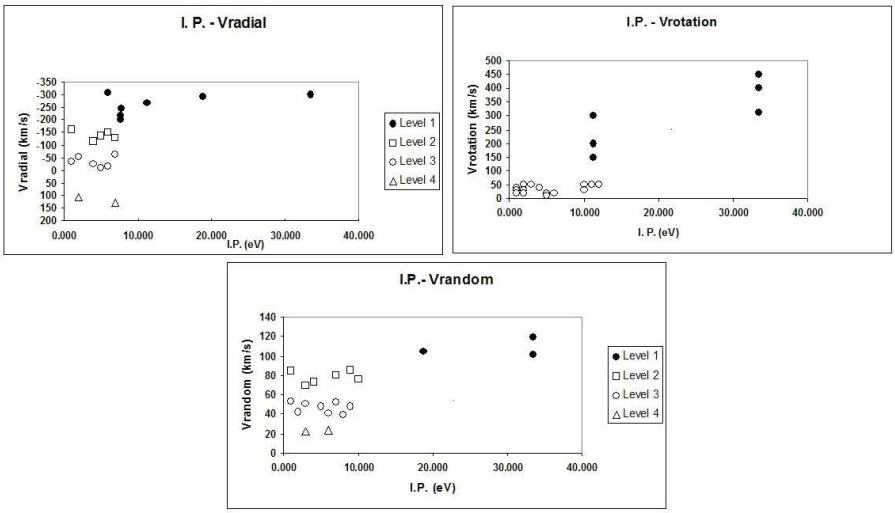

FIGURE 2. Radial (up, left), rotational (up, right) and random velocities (down) in the atmosphere of AXMon (HD 45910) spectral lines as a function of the ionization potential.

4. P. W. Merrill, *PASP*, **35**, 303 (1923).
5. J. S. Plaskett, *PASP*, **35**, 145 (1923).
6. E. Danezis, E. Theodossiou and P. Laskarides, *Ap&SS*, **179**, 111 (1991).
7. E. Danezis, D. Nikolaidis, E. Lyratzi, A. Antoniou, L. Č. Popović, and M. S. Dimitrijević, *MSAIS*, **7**, 107 (2005).
8. E. Danezis, D. Nikolaidis, E. Lyratzi, L. Č. Popović, M. S. Dimitrijević, A. Antoniou and E. Theodossiou, *PASJ*, **59**, 827 (2007).

Kinematics of Broad Absorption Line Regions of PG 1254+047

Lyratzi, E.[*,†], Danezis, E.[*], Popović, L., Č.[**], Dimitrijević, M., S.[**] and Antoniou, A.[*]

[*]*University of Athens, Faculty of Physics Department of Astrophysics, Astronomy and Mechanics, Panepistimioupoli, Zographou 157 84, Athens, Greece*
[†]*Eugenides Foundation, 387 Sygrou Av., 17564, Athens, Greece*
[**]*Astronomical Observatory of Belgrade, Volgina 7, 11160 Belgrade, Serbia*

INTRODUCTION

In a number of quasars (about 10-20%), blue-shifted, broad absorption lines (BALs) are observed in the ultraviolet spectra. These lines are formed in partially ionized outflows with velocities up to 0.1 c. The outflow is likely driven by intensive radiation of the quasar probably along the equatorial directions to the extension at least larger than the broad emission line region (BLR). Disk wind and material evaporating from the putative dust torus are two plausible scenarios for the origin of the gas. In order to understand the nature of outflow in quasars, we need to explore many properties of the outflow such as the global covering factor of BAL region, the column density and velocity fields.

Here we investigate the physical properties of Broad Absorption Line Regions (BALRs) of quasar PG 1254+047 using a model (previously developed for stellar absorption line modelling) proposed by Danezis et al. [1] (GR model). With this model one can accurately fit the observed complex profiles of both emission and absorption spectral lines. With this model we can calculate the apparent rotational and radial velocities, the random velocities of the ions, as well as the Full Width at Half Maximum (FWHM), the column density of the independent density regions of matter which produce the main and the satellite components of the studied spectral lines and the respective absorbed or emitted energy. We are able to explain the observed peculiar profiles of the BALs using the DACs/SACs theory, i.e. the complex profiles of the BALs are composed by a number of DACs or SACs which are created in different regions [2, 3].

In this paper we apply the GR model on the spectrum of the BALQSO PG 1254+047 (Z=1.024), taken with HST (FOS/G160L,G270H), on February 17, 1993. We study the C IV $\lambda\lambda$ 1548.187, 1550.772 Å, Si IV $\lambda\lambda$ 1393.755, 1402.77 Å, N V $\lambda\lambda$ 1238.821, 1242.804 Å and Lyα λ 1215.68 Å lines.

RESULTS AND DISCUSSION

The best fit of the UV spectra with the model is shown in Figure 1. As one can see from Figure 1 there are several absorption components. In Table 1 we presented only the kinematical parameters of the absorption components, i.e. the random velocities of the studied ions as well as the rotational and radial velocities of the BALRs.

As one can see in table 1, the values of the rotational velocities are too large (from 800 km/s to 1500 km/s) indicating that the region of origin of the components is close to the massive black hole. Such large rotational and random velocities are expected near the massive black hole, in difference the large widths observed in stellar spectra (see [4, 5]).

ACKNOWLEDGMENTS

This research project is progressing at the University of Athens, Department of Astrophysics, Astronomy and Mechanics, under the financial support of the Special Account for Research Grants, which we thank very much. This work also was supported by Ministry of Science of Serbia, through the projects “Influence of collisional processes on astrophysical plasma line shapes” and “Astrophysical spectroscopy of extragalactic objects”.

REFERENCES

1. E. Danezis, D. Nikolaidis, E. Lyratzi, L. Č. Popović, M. S. Dimitrijević, A. Antoniou and E. Theodossiou, *PASJ*, **59**, 827 (2007).

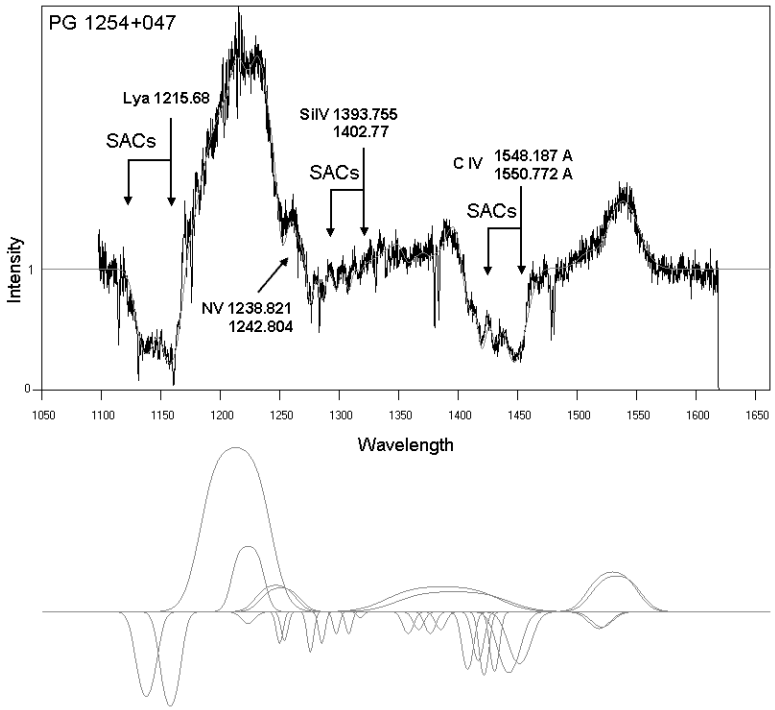

FIGURE 1. Best fit of the C IV, Si IV, N V and Lyα spectral lines. The components obtained from fit are given bottom.

TABLE 1. Random (V_{rand}), Rotational (V_{rot}) and Radial (V_{rad}) velocities (in km/s) of the studied absorption regions.

Ion	Random Velocity	Rotational Velocity	Radial Velocity
Lyα	1162	1500	1973
	1598	1500	-14303
	1598	1500	-19235
	291	800	14895
	2912	800	1726
	291	800	20098
	291	800	22688
	291	800	25154
N V	484	800	2658
Si IV	1768	1200	10442
	707	1000	5960
	581	1200	3002
	505	1000	-3645
	505	1000	-7719
C IV	1596	1000	-5804

2. E. Danezis, L. Č. Popović, E. Lyratzi and M. S. Dimitrijević, *AIP Conference Proceedings*, **876**, 373 (2006).
3. E. Danezis, E. Lyratzi, L. Č. Popović, M. S. Dimitrijević and A. Antoniou, "Similarity between DACs/SACs phenomena in hot emission stars and quasars absorption lines", in *Proceedings of 19th ICSLS, Valladolid, Spain*, 2008a.
4. A. Antoniou, E. Danezis, E. Lyratzi, L. Č. Popović and M. S. Dimitrijević, *PASJ*, submited (2008).
5. E. Danezis, E. Lyratzi, A. Antoniou, L. Č. Popović and M. S. Dimitrijević, "A new idea about the structure of large line broadening in the UV spectra of hot emission stars and quasars", in *Proceedings of 19th ICSLS, Valladolid, Spain*, 2008b.

DACs and SACs in the UV spectrum of the quasar PG 0946+301

Lyratzi, E.[*,†], Danezis, E.[*], Popović, L., Č.[**], Dimitrijević, M., S.[**] and Antoniou, A.[*]

[*]*University of Athens, Faculty of Physics Department of Astrophysics, Astronomy and Mechanics, Panepistimioupoli, Zographou 157 84, Athens, Greece*
[†]*Eugenides Foundation, 387 Sygrou Av., 17564, Athens, Greece*
[**]*Astronomical Observatory of Belgrade, Volgina 7, 11160 Belgrade, Serbia*

INTRODUCTION

In the spectra of many quasars we observe complex profiles of broad absorption lines, mainly in the case of high ionization ions (e.g. C IV, Si IV, N V). These complex profiles are composed of a number of DACs or SACs which are created in the Broad Absorption Line Regions (BALR) that result from dynamical processes such as accretion, jets, ejection of matter etc.

By applying the model proposed by Danezis et al. [1] (GR model) we can accurately fit the observed complex profiles of both emission and absorption spectral lines. With this model we can calculate the apparent rotational and radial velocities, the random velocities of the ions, as well as the Full Width at Half Maximum (FWHM), the column density of the independent density regions of matter which produce the main and the satellite components of the studied spectral lines and the respective absorbed or emitted energy. We are able to explain the observed peculiar profiles using the DACs/SACs theory, i.e. the complex profiles are composed by a number of DACs or SACs which are created in different regions [2, 3].

In this paper we apply the GR model on the spectrum of the BALQSO PG 0946+301 (Z=1.216), taken with HST (FOS/G400,G570), on February 16, 1992. We study the C IV $\lambda\lambda$ 1548.187, 1550.772 Å, and Si IV $\lambda\lambda$ 1393.755, 1402.77 Å lines. We point out that the C IV doublet of this BALQSO is one of the very few lines that present clearly the DACs phenomenon.

RESULTS

With GR model we were able to fit accurately the studied spectral lines (see Figure 1). Here we present only the kinematical parameters of the absorption components, i.e. the random velocities of the studied ions as well as the rotational and radial velocities of the BALRs that create the DACs or SACs of the studied lines. The calculated values are given in table 1. As one can see in table 1, some components of the C IV and Si IV resonance lines, present much larger radial velocities (large shifts). These absorption components are discrete (DACs) and appear on the left side of the main absorption features. On the other hand, the main absorption features are composed by a number of SACs (Figure 1).

TABLE 1. Random (V_{rand}), Rotational (V_{rot}) and Radial (V_{rad}) velocities (in km/s) of the studied regions

Ion	Random Velocity	Rotational Velocity	Radial Velocity
Si IV	505	400	-7611
	204	400	-9005
	204	400	-5617
	204	400	-12071
C IV	615	3000	-5998
	615	1800	-10835
	228	600	-10061
	2	700	-6385

As one can see in table 1, the values of the rotational velocities of the first two C IV components are too large. In order to explain this large broadening, we propose a new idea, based on the theory of SACs phenomenon [4, 5, 6]. The observed very large width is due to the existence of many narrow absorption lines which are created due to micro-

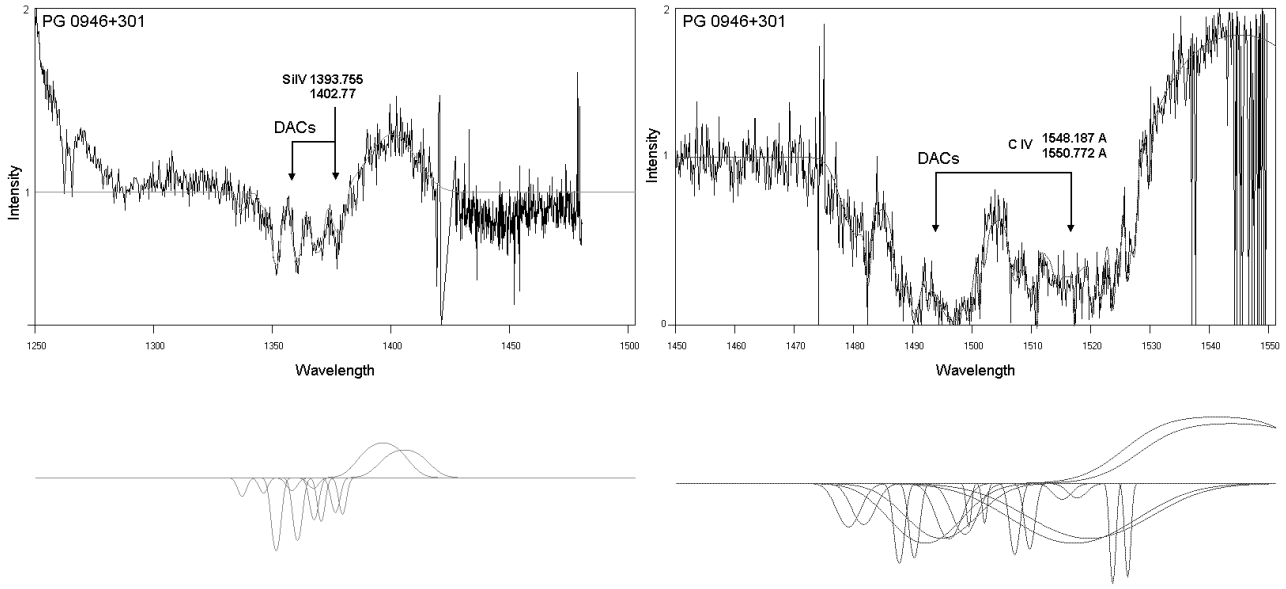

FIGURE 1. Best fit of the Si IV and C IV, resonance lines. We can explain the complex structure of these lines as a DACs or SACs phenomenon. Below the fit one can see the analysis of the observed profile to its DACs/SACs.

turbulence effects. This means that around the main density region where the main spectral line is created, there may exist some micro-turbulent movements that give rise to some narrow absorption components with different shifts, around the main spectral line. If these lines are many and have small differences in their radial velocities, they blend among themselves (SACs phenomenon) and the result may be a very broad absorption line. Thus, the very broad absorption line might result from the composition of many narrow absorption lines that are created by micro-turbulent effects.

ACKNOWLEDGMENTS

This research project is progressing at the University of Athens, Department of Astrophysics, Astronomy and Mechanics, under the financial support of the Special Account for Research Grants, which we thank very much. This work also was supported by Ministry of Science of Serbia, through the projects “Influence of collisional processes on astrophysical plasma line shapes” and “Astrophysical spectroscopy of extragalactic objects”.

REFERENCES

1. E. Danezis, D. Nikolaidis, E. Lyratzi, L. Č. Popović, M. S. Dimitrijević, A. Antoniou and E. Theodossiou, *PASJ*, **59**, 827 (2007).
2. E. Danezis, L. Č. Popović, E. Lyratzi and M. S. Dimitrijević, *AIP Conference Proceedings*, **876**, 373 (2006).
3. E. Danezis, E. Lyratzi, L. Č. Popović, M. S. Dimitrijević and A. Antoniou, “Similarity between DACs/SACs phenomena in hot emission stars and quasars absorption lines”, in *Proceedings of 19th ICSLS, Valladolid, Spain*, 2008a.
4. A. Antoniou, E. Danezis, E. Lyratzi, L. Č. Popović and M. S. Dimitrijević, *PASJ*, submited (2008).
5. E. Danezis, E. Lyratzi, A. Antoniou, L. Č. Popović and M. S. Dimitrijević, “A new idea about the structure of large line broadening in the UV spectra of hot emission stars and quasars”, in *Proceedings of 19th ICSLS, Valladolid, Spain*, 2008b.
6. E. Lyratzi, E. Danezis, L. Č. Popović, M. S. Dimitrijević and A. Antoniou, “Application of the DACs/SACs theory to the Broad Absorption Line Regions of the quasar PG 1254+047”, in *Proceedings of 19th ICSLS, Valladolid, Spain*, 2008.

Multiple perturber effects in the far red wing of Lyman α line

N.F. Allard[*,†] and J.F. Kielkopf[**]

[*]*Institut d'Astrophysique de Paris, CNRS, UMR 7095, UPMC, 98bis boulevard Arago, F-75014 Paris, France*
[†]*Observatoire de Paris-Meudon, GEPI, UMR 8111, CNRS, F-92195 Meudon Principal Cedex, France*
[**]*Department of Physics and Astronomy, University of Louisville, Ky 40292, USA*

ABSTRACT

An accurate determination of the line broadening of the Lyman series of atomic hydrogen has been shown to be fundamental in the interpretation of UV and FUV spectra of DA white dwarfs. The pseudocontinuum due to the $b\,^3\Sigma_u^+ \rightarrow a\,^3\Sigma_g^+$ triplet transition which contributes to the red wing of the Lyman α line perturbed by neutral hydrogen was recently investigated by Kowalski (2006) [1] and Kowalski & Saumon (2006) [2] to improve previous calculations of atmosphere models of white dwarfs.

We will first point out the range of validity of the one-perturber approximation widely used to calculate the line wing. Secondly we will study the relative contribution of the two main transitions which contribute to the far wing of the Lyman α line profile according to the effective temperature and perturber density.

In cool white dwarfs the perturber density is so high that the one perturber approximation breaks down and the collisional effects must be treated by using the autocorrelation formalism in order to take account the simultaneous collisions with more than one perturbing atom.

We will show that at the low temperature of cool white dwarfs the contribution of the singlet $X\,^1\Sigma_g^+ \rightarrow B^1\Sigma_u^+$ transition cannot be neglected in the calculation of Lyman α profile perturbed by neutral hydrogen. The comparison with experimental spectra shows that indeed multiple H-perturbers occurred in the far wing.

A reliable determination of the line profiles in physical conditions of cool white dwarfs requires a unified theory which takes into account both the singlet and triplet transitions contributing to Lyman α using accurate interaction potentials and radiative dipole transition moments. Multiple perturber effects have to be considered using the autocorrelation formalism.

REFERENCES

1. Kowalski, P.M., 2006, ApJ. 651, 1120
2. Kowalski, P.M. & Saumon, D., 2006, ApJ. 651, 137

Collisional line widths of autoperturbed N_2: measurements and quantum calculations

Franck Thibault*, Laura Gómez†, Raúl Z. Martínez† and Dionisio Bermejo†

*Institut de Physique de Rennes, UMR CNRS 6251, Université de Rennes I, F-35042 Rennes, France
†Instituto de Estructura de la Materia, CSIC, Serrano 123, ES-28006 Madrid, Spain

ABSTRACT

In this work we present new experimental and theoretical values for the line broadening coefficients of the Q-branch Raman lines of autoperturbed N_2. For the experimental determination of the coefficients, high resolution stimulated Raman loss spectra of the Q-branch of N_2 at different pressures were obtained at 77, 194 and 298 K. Simultaneously, we carried out Close-Coupling calculations at 77, 113, 194 K, and Coupled-states calculations at 298 K rendering a set of theoretical line broadening coefficients that could be directly compared to those obtained from our measurements and from available data in the literature. We observe a good agreement between theoretical and experimental values.

EXPERIMENT

The experimental setup used for our measurements has already been described in a previous paper [1], so only some details will be given here. 0.4 cm^{-1} are approximately recorded in 18 minutes, averaging 10 laser shots and sampling the spectrum every second. We have tested that under these scan conditions distortion of the line profile is negligible. We have measured the spectra at several pressures (5 - 120 mbars) for each considered temperature and for each studied line. The collisional linewidth has been retrieved from Voigt profile fitted to the lineshape (the gaussian part of which is due to the Doppler effect and the apparatus function).

CALCULATIONS OF PRESSURE BROADENING CROSS SECTIONS

Theoretical pressure broadening (PB) cross sections are derived from binary scattering *S*-matrix elements provided by the MOLSCAT quantum dynamical code. Therefore the impact approximation is assumed. For our calculations we have used the N_2-N_2 potential energy surface of Ref. [2]. The particular case studied is natural N_2, a 2:1 mixture of ortho-nitrogen (oN_2) and para-nitrogen (pN_2) with even and odd j's, respectively. We have considered the two colliding molecules as distinguishable [3]. Pressure broadening cross sections are given by weighted sums of partial pressure broadening cross sections. The latters, depending on the kinetic energy, E_{kin}, are obtained as the sum of two-body rotational state to state cross sections for the specific case of isotropic Raman lines in the rigid rotor approximation:

$$\sigma(j_A, j_B, E_{kin}) = \sum_{j'_A \neq j_A, j'_B} \sigma\left(j_A j_B \rightarrow j'_A j'_B; E_{kin}\right). \tag{1}$$

Due to the fact that natural nitrogen is composed of two noninterconverting species we can speed up our calculations by dealing with these two species separetly. One can can define, for instance, an ortho PB cross sections as:

$$\sigma_{oN_2}(j_A, T) = \sum_{j_B \text{ even}} \rho_{j_B} \sigma(j_A, j_B, T), \tag{2}$$

and a similar quantity for odd j_B's. The line broadening parameter of a Q(j_A) is obained as follows:

$$\gamma(j_A) = \frac{n_{N_2} \overline{v}}{2\pi c} \sigma(j_A, T), \tag{3}$$

where

$$\sigma(j_A, T) = \frac{2}{3}\sigma_{oN_2}(j_A, T) + \frac{1}{3}\sigma_{pN_2}(j_A, T) \tag{4}$$

and a temperature dependant quantity is obtained throught the thermal average over the kinetic energies.

RESULTS

Table 1 provides contributions of calculated ortho-ortho (2) and ortho-para cross sections (in $Å^2$) to the total pressure broadening cross sections (4). We see that it is not useful to calculate both set of partial PB cross sections. Such a result has been also found for PB cross sections of C_2H_2 - H_2 [4]. Figure 1 allows a comparison between our calculated HWHM with measured values. The agreement is rather good.

TABLE 1. ortho and para pressure broadening contributions to the total PB cross section.

T/K	j_A	o-o /$Å^2$	o-p /$Å^2$	total /$Å^2$
77	0	96.46	100.08	97.62
77	2	65.80	65.62	65.71
77	4	64.11	64.28	64.14
77	6	69.59	68.75	69.28
77	8	67.58	67.14	67.41
113	6	66.25	66.16	66.21
194	6	56.86	56.17	56.63
298	0	67.71	67.12	67.36
298	6	45.17	44.80	45.05

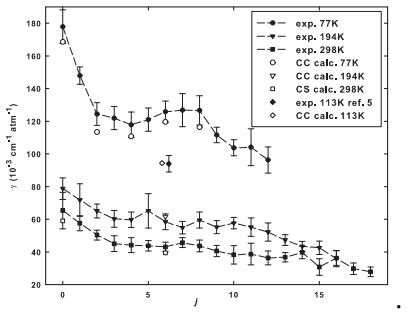

FIGURE 1. Self-broadening parameters of N_2

REFERENCES

1. L. Gomez, R. Z. Martínez, D. Bermejo, F. Thibault, P. Joubert, B. Bussery-Honvault and J. Bonamy, *J. Chem. Phys.* **126**, 204302-8 (2007).
2. D. Cappelletti, F. Vechiocattivi, F. Pirani, E.L. Heck, A.S. Dickinson, *Mol. Phys.* **93**, 485-99 (1998).
3. L. Gomez, R. Z. Martínez, D. Bermejo, F. Thibault, *J. Quant. Spectrosc. Radiat Transfer* submitted (2008).
4. F. Thibault, B. Corretja, A. Viel, D. Bermejo, R. Z. Martínez, B. Bussery, *Phys. Chem. Chem. Phys.* submitted (2008).
5. G.C. Herring, B.W. South, *J. Quant. Spectrosc. Radiat Transfer* **52**, 835-40 (1994).

Theoretical Infrared Line shapes of H-bonds Within The Strong Anharmonic Coupling Theory. Fermi Resonances Effects.

Noureddine Issaoui*, Najeh Rekik*, Brahim Oujia* and Marek J. W†

*Laboratoire de Physique Quantique, Faculté des Sciences de Monastir, Route de Kairouan, 5000 Monastir, Tunisia.
†Laboratory of Molecular Spectroscopy, Faculty of Chemistry, Jagiellonian University, Ingardena 3, 30-060 Kraków, Poland.

The IR bandshape of the high frequency stretching mode of H-bonded complexes involving combined effects of Fermi resonances and intrinsic anharmonicities of the fast and the slow modes is studied within the linear response theory. We propose a generalisation of a previous model [Rekik et al. J. Mol. Struct (Theochem) 821 (2007) 9] by introducing Fermi resonances by the aid of an anharmonic coupling between the fast mode and one or several harmonic bending modes. The quadratic modulation of both the angular frequency and the equilibrium position of the $X-\overrightarrow{H}...Y$ stretching mode on the intermonomer $\overleftarrow{X}-H...\overrightarrow{Y}$ motions is taken into account within the strong anharmonic coupling theory. The direct damping of the fast and bending modes is introduced by assuming that the autocorrelation function disappears exponentially in time as in the fundamental model of Rösch and Ratner. The IR spectral density is obtained by Fourier transform of the autocorrelation function of the transition dipole moment operator of the $X-H$ bond. The numerical calculation shows that Fermi resonances generate very complicated profiles with multi-substructure and also provide a direct evidence of Fermi resonances which were predicted to be a major feature of H-bonds.

Keywords: Hydrogen bond; anharmonicity; Morse potential; Fermi resonances ; Infrared line shape; Temperature and isotopic effects, Direct relaxation; Linear response theory; Autocorrelation function.

Theoretical Modeling of Infrared Line Shapes of Centrosymmetric Cyclic Acid Dimers and Their O-D Deuterated Derivatives at 77 K and 300 K.

Najeh Rekik*, Houcine Ghalla*, Mohamed Baazaoui*, Anna Michta†, Brahim Oujia* and Henryk T. Flakus†

*Laboratoire de Physique Quantique, Faculté des Sciences de Monastir, 5000 route de Kairouan, Tunisia.
†Institute of Chemistry, University of Silesia, 9 Szkolna Street, Pl –40-006 Katowice, Poland. des Sciences de Monastir, 5000 route de Kairouan, Tunisia.

You can follow this template to prepare the abstract of your contributions for the 19^{th} International Conference on Spectral Line Shapes.

ABSTRACT

A more general quantum theoretical approach of the υ_{X-H} IR lineshape of cyclic dimers of weakly H-bonded species is proposed. We have extended a previous approach [Rekik et al., Chem. Phys. (submitted)] by accounting for the Fermi resonances in order to reproduce the unpolarized infrared line shapes of some centrosymmetric cyclic acid dimers and their O-D derivative at 77 K and 300 K. In this approach, the adiabatic approximation is performed for each separate H-bond Bridge of the dimer and a strong nonadiabatic correction is introduced into the model via the resonant exchange between the fast mode excited states of the two moieties. Working within the strong anharmonic coupling theory, according to which the $X-\overrightarrow{H}...Y$ high-frequency mode is anharmonically coupled to the H-bond bridge, this model incorporated the Davydov coupling between the excited states of the two moieties, multiple Fermi resonances between the first harmonics of some bending modes and the first excited state of the symmetric combination of the two υ_{X-H} modes, the quantum direct and indirect dampings and the anharmonicity for the H-bond bridge. The spectral density is obtained within the linear response theory by Fourier transform of the damped autocorrelation functions. The evaluated spectra are in fairly good agreement with the experimental ones by using a minimum number of independent parameters. The effect of deuteration has been well reproduced by reducing simply the angular frequency of the fast mode and the anharmonic coupling parameter. It is found that if Fermi resonances derived in this work do not improve the accuracy of the line shape for some acids, it is not so for other acids.

Keywords: H-bond; Infrared line shape; centrosymmetric cyclic acid dimer; Davydov effect; Fermi resonance; Temperature and isotopic effects; Quantum direct and indirect damping; Morse potential.

[1] corresponding authors : rekik.najeh@fsm.rnu.tn, Fax: (+216) 73 500 278; flakus@ich.us.edu.pl, Fax: +48 32 2599 978.

THE VAN DER WAALS POTENTIAL COEFFICIENTS DIFFERENCES ΔC_6^0 AND ΔC_6^1 OF THE INTERCOMBINATION CD LINE 326.1 NM FOR PURE CD AND CD – INERT GAS SYSTEMS

G. D. Roston and M. S. Helm

Department of physics , Faculty of Science - Alexandria University, Alexandria - Egypt

ABSTRACT

The absorption profiles of the Cd 326.1 nm line for pure Cd and Cd - inert gases (Xe, Kr, Ar, Ne and He) have been carefully studied from the line center to 700 cm-1 in the red wing using a high resolution double beam spectrometer. The density of Cd was about 5.108 x 1018 atoms cm-3.The temperature dependences of the red wings of these profiles were analysed in the frame work of the unified Frank Condon (UFC) treatment of pressure broadening of spectral lines developed by Szudy and Baylis. The van der Waals potential coefficient differences ΔC60 and ΔC61 between the ground 10+ state and the two exited states 30+ and 31 were obtained using Kuhn's law . The values of ΔC60 and ΔC61 are presented in the table.

.Keywords: Waals Potential coefficients, pressure broadening, spectral line profile, potential curves
PACS : 32.70.Jz

TABLE . The van der Waals coefficients for the Cd - inert gases systems in eV Å^6

Molecule	ΔC_6^0	ΔC_1^0
Cd - Cd	—	106.8 ± 2.3
Cd - Xe	43.0 ± 3	86.0 ± 4
Cd - Kr	37.8 ± 2	58.5 ± 3
Cd - Ar	28.7 ± 2	48.0 ± 4
Cd - Ne	23.5 ± 2	39.3 ± 3
Cd - He	14.8 ± 2	28.5 ± 3

REFERENCES

1. Helmi M.S, Grycuk T. and Roston G. D, Spectro. Chem. Acta B, 51, 633, 1996.
2. Helmi M. S, Grycuk T. and Roston G.D., Chem. Phys., 209, 53, 1996.
3. Roston G.D., Grycuk T. and Helmi M.S., Chem. Phys. 213, 365, 1996.
4. Roston G.D. and Helmi M.S., Chem. Phys., 258, 55, 2000.
5. Roston G.D., Physica Scripta., 72, 31, 2005.
6. Roston G.D., J. Quant. Spect. Radiat. Transfer. Transfer, 87, 83-94, 2004.
7. Roston G.D. and Helmi M.S, J. Quant. Spect. Radiat. Transfer, 101, 201, 2006.
8. Roston G.D and Ghatass Z.F, J. Quant. Spect. Radiat. Transfer. 101, 205, 2006.
9. Kowalski A., Czajkowski M. and Breckenridge W.H., J. Chem. Phys. Lett., 121, 217, 1985.
10. Szudy J. and Baylis W., J. Quant. Spect. Radiat. Transfer, 15, 641, 1975.
11. Migdalek J and Baylis W. E., J. Phys. B: At. Mol. Phys., 19 (1986) 1.
12. Byron F. W. and McDermott M. N. , Novick. Phys. Rev. A,134 (1964) 615.

The non Markovian Q-branch of polar diatomic molecules in non polar liquids.

A. Padilla and J. Pérez

Departamento de Física Fundamental y Experimental Electrónica y Sistemas. Universidad de La Laguna. 38205 La Laguna. Tenerife Spain

The apparition, together with the usual P and R branches associated to the vibration rotation spectra of the isolated diatomic, of a central Q branch on the infrared absorption bands of heteronuclear diatomics diluted in inert dense solvents has been a problem lengthy studied but not completely resolved yet. Although this Q branch has been associated to the persistence of long lived spatial correlations between the solute and solvent molecules, the characterization of the time scales in which such correlation persist remains an open problem.

In this work this problem has been analyzed for the fundamental absorption band of *HCl* diluted in *Ar* at the liquid-vapor coexistence state of temperature $T = 115K$. The spectra was calculated by means of a quantum non-Markovian spectral theory [1] which depends of the two time correlation function of the anisotropic interaction potential of the diatomic and the solvent, and where the corresponding statistical parameters were calculated by using molecular dynamics simulation.

In the comparison with available experimental data [2] we have found that the theoretical spectra reproduces the central Q branch with a reasonable agreement with the experimental spectral bands. Two remarkable facts were found. At first the interaction correlation times obtained with the simulations are larger than those calculated with a cell model previously reported. At second we have found that the Q branch is absent in the corresponding Markovian spectral profile so we can associate it to a memory or non Markovian effect.

In generals terms it has been also shown how the non-Markovian effects produce a redistribution of the spectral intensity with a decreasing near to the maxima of the P and R branches, and increasing in the PR inter-branch region, where the Q-branch is located. Together with the Q branch the memory effects also produce a narrowing of the rotational resonances in the P and R branches. The effects of the interference between the P and R branches and the lines which gives significant contributions to the rising of the Q branch was also analyzed.

REFERENCES

1. A. Padilla, J. Pérez and A. Calvo Hernández, J. Chem. Phys. **111**, 11015 (1999).
2. J. Pérez, A. Padilla, W. A. Herrebout, B. J. Van der Veken, A. Calvo Hernández and M. O. Bulanin, J. Chem. Phys. **122**, 194507 (2005).

Satellites of Atomic Transitions Induced by IR Active Vibrational Modes in Molecules.

Vadim A. Alekseev

Institute of Physics, St.Petersburg State University, Ul'janovskaja St.1, Peterhof, 198504 Russia

Spectroscopy of Xe/CF_4 mixtures in the Vac UV region was recently studied at the synchrotron radiation facility BESSY II in Berlin. These higher resolution experiments revealed numerous spectrally narrow bands ($\Delta\nu$ ~ 10 cm^{-1}) coinciding with energies of the n*p*- and n*d*-states of the Xe atom increased by the energy of one ν_3 quantum of CF_4 (ν_3=1281 cm^{-1})[1] . The observed photoprocess may be written as follows

$$Xe(GS)..CF_4\ (\nu_3=0) + h\nu \rightarrow Xe\ (DFS)..CF_4\ (\nu_3=1),$$

where *GS* and *DFS* denote respectively the ground and dipole-forbidden states of the Xe atom. The effect has been confirmed for C_2F_6 perturber molecules [1]. Also, it has been shown that only the IR-active vibrational modes of CF_4 and C_2F_6 induce satellites.

A striking feature of these vibrationally induced transitions is their intensity. Satellites are several orders of magnitude stronger than their parent transitions

$$Xe(GS)..CF_4\ (\nu_3=0) + h\nu \rightarrow Xe\ (DFS)..CF_4\ (\nu_3=0),$$

appearing due to collision-induced breakdown of the optical selection rules. Furthermore, the spectral width of the satellites is almost two orders of magnitude less than the width of the pressure-broadened resonance bands. The strength of these bands combined with their small width implies that the transitions occur predominantly at relatively large Xe–CF_4 distances where the *GS* and *DFS* potentials of the complex are nearly parallel. The most intense satellites were observed on the wings of pressure broadened resonance transitions, i.e. when the energy between the resonance state (*RS*) and the lower lying *DFS* is close to the energy of vibrational transition in molecula, E(*RS*)-E(*DFS*)~ $h\nu_{IR}$. Another factor is the optical coupling between *RS* and *DFS*. Satellite is intence when *DFS* and *RS* states are coupled by a strong dipole-allowed transition in the IR region.

Along with the satellites of forbidden transitions, satellites on the far blue wings of the pressure broadened resonance transitions were studied as well. These bands were observed in early studies of Xe/CF_4 and Kr/CF_4 absorption spectra in the region of Rg($^3P_1 \leftarrow {}^1S_0$) resonance transition [2]. In contrast to the satellites of forbidden transitions, these satellite are spectrally broad bands closely resembling in shape the pressure broadened resonance bands (Fig.1) and can be unambiguously assigned to the photoprocess

$$Xe(GS)..CF_4\ (\nu_3=0) + h\nu \rightarrow Xe\ (RS)..CF_4\ (\nu_3=1)$$

The intensity of resonance transition satellites is orders of magnitude weaker in comparison with the strongest satellites of dipole forbidden transitions implying completely different intensity borrowing mechanisms in two cases. Their large spectral width suggests that transitions take place at small internuclear distances where the upper and lower potentials are not parallel.

The vibrational satellite effect was confirmed in studies of LIF spectra of Na /CF_4 mixtures (Fig.2) [3]. It appears very likely that similar transitions may be observed in many other mixtures of atomic and molecular gases. The same mechanism which induces satellite in absorption spectra may induce new emission bands in collisions of metastable state atoms with vibrationally excited molecules. This may be of applied interest. Further experiments may be performed with many atomic gas/molecular gas mixtures, including those which are of interest for astrophysics and atmospheric spectroscopy.

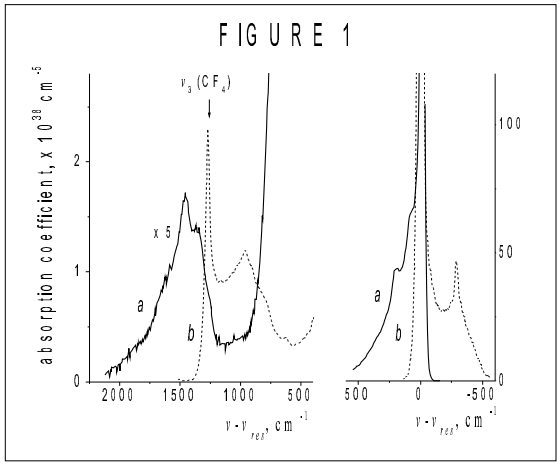

Figure 1. Transitions to ***a*** – Xe 6*s* ($^3P_1$) (ν_{res}=68045.7 cm^{-1}), ***b*** – Xe 7*s* ($^3P_1$) (ν_{res}=85440.5 cm^{-1}) resonance states of the Xe atom in mixture with CF_4 **(right)** and their vibrational satellites **(left).**

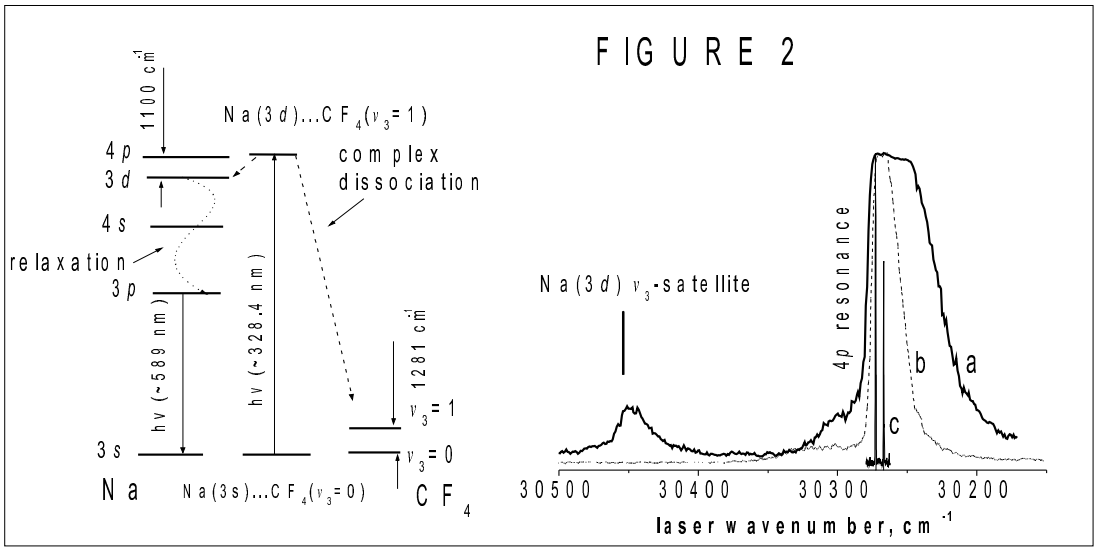

Figure 2. Excitation spectra of Na($3p \rightarrow 3s$) fluorescence: ***a*** – Na/CF_4, ***b*** – Na/Ar. T=350C, [Na] ~ 2 10^{15} cm^{-3}, [CF_4]=[Ar]~2.5 10^{19} cm^{-3}, ***c*** – Na vapor, T=275C. Vertical line indicates the energy of Na(3*d*) increased by the energy of CF_4 ν_3 -quanta (1281 cm^{-1}). The diagram on the right schematically shows energies of Na, CF_4 and Na..CF_4 collision complex.

ACKNOWLEDGMENTS

This work was supported by the Deutsche Forschungsgemeinschaft.

REFERENCES

1. V.A. Alekseev, and N. Schwentner, *Chem.Phys.Lett.* 436, 2007, pp.327–330
2. V.A. Alekseev, *Opt. Spectrosc.* 96, 2004, pp. 547-551, and references cited therein.
3. V.A. Alekseev, and N. Schwentner, submitted to *Chem.Phys.Lett.*

The $^1S_0 \rightarrow ^{3,1}P_1$ Transitions in the Xe and Kr Atoms Perturbed by CF_4 and Model Potentials for the Rg–CF_4 Systems

V. Alekseev*, N. Schwentner†, D. Cappelletti** and F. Pirani‡

*Institute of Physics, St.Petersburg State University, Ul'janovskaja St.1, Peterhof, 198504 Russia
†Institut für Experimentalphysik, Freie Universität Berlin, Arnimallee 14, D-14195, Germany
**Dipartimento di Ingegneria Civile ed Ambientale, Universitá di Perugia, Perugia, I-06125, Italy
‡CNISM Unitá di Perugia and Dipartimento di Chimica, Universitá di Perugia, Perugia, I-06123, Italy

Perfluoromethane is one of the very few polyatomic molecular gases which are transparent in the region of Xe and Kr resonance transitions in the Vac UV. The first studies of absorption spectra of Rg/CF_4 mixtures were performed with use of a low spectral resolution experimental setup [1]. Recently Rg/CF_4 mixtures have been investigated at high resolution and spectra were recorded up to the LiF cutoff wavelength at $\lambda \sim 105$ nm. In this contribution we report experimental spectra of $^1S_0 \rightarrow ^3P_1$ and $^1S_0 \rightarrow ^1P_1$ transitions in Xe and Kr atoms perturbed by collisions with CF_4 and potentials for Rg-CF_4 systems.

EXPERIMENTAL

The experiments were conducted at the synchrotron radiation facility BESSY II in Berlin with use of a 10-m normal incidence monochromator [2] installed at the quasi-periodic undulator. Typical concentrations of Rg and CF_4 in a static gas cell were $\sim 10^{16}$ and 10^{19} cm^{-3} respectively. For comparison a set of spectra under the same experimental conditions (concentrations, spectral resolution, etc) has been recorded for Rg/He mixtures as well. Both absorption and fluorescence excitation spectra were collected. Undispersed Vac UV fluorescence of the resonance state atoms and Rg_2^* dimers was recorded with use of a solar blind photomultiplier tube. Except a narrow region near the line core, the shapes of fluorescence excitation and absorption spectra are nearly identical.

POTENTIAL ENERGY SURFACES

The total potential energy describing the Rg(^{1}S,^{3}P)-CF_4 systems, V_{tot}, is expressed following the atom-bond pairwise additive formalism [3] as,

$$V_{tot}(R,\Theta) = \sum_{i=1}^{4} V_i(r,\theta) \tag{1}$$

where $V_i(r,\theta)$ are the atom-bond (Rg-CF) terms, described by

$$V_i(r,\theta) = \varepsilon(\theta)\left[\frac{6}{n(r,\theta)-6}\left(\frac{r_m(\theta)}{r}\right)^{n(r,\theta)} - \frac{n(r,\theta)}{n(r,\theta)-6}\left(\frac{r_m(\theta)}{r}\right)^{6}\right] \tag{2}$$

For Rg-CF specific interactions r is the distance from Rg to the center of the ellipsoid of polarizability placed on the CF bond and θ is the angle formed by the **r** vector and the CF bond. R and Θ describe the position of the Rg atom in a reference system centered on the center of mass of the CF_4 molecule. The relevant parameters ε and r_m are predicted accordingly to the bond polarizability tensor components of CF_4 and the polarizability of the rare gas atom, both in the ground and in the excited electronic state [3]. The exponent of the repulsive part of the interaction in equation (2) is defined as,

$$n(r,\theta) = \beta + 4\left(\frac{r}{r_m(\theta)}\right)^2 \tag{3}$$

where β is an adjustable parameter within a limited range [3]. In the present case β=9 for the ground state Rg and β=7 for the excited Rg atoms. Some features of the Rg-CF_4 interaction for the main complex configurations are summarized in the Table. Ab-initio results [4] are given in parenthesis for comparison.

TABLE 1. Main features of the interaction potentials (V=vertex, E=edge, F=face)

system		r_0 / **Å**	D_0 / **meV**	**system**		r_0 / **Å**	D_0 / **meV**
Kr(^{1}S)-CF_4	V	4.67 (4.85)	13.2 (14.3)	Kr*(^{3}S)-CF_4	V	6.29	5.51
	E	4.19 (4.25)	20.8 (20.8)		E	6.01	6.53
	F	3.99 (3.90)	25.0 (27.7)		F	5.88	7.05
Xe(^{1}S)-CF_4	V	4.83 (5.05)	15.1 (16.9)	Xe*(^{3}S)-CF_4	V	6.43	5.24
	E	4.38 (4.45)	22.8 (23.8)		E	6.17	6.14
	F	4.19 (4.10)	27.1 (31.2)		F	6.04	6.59

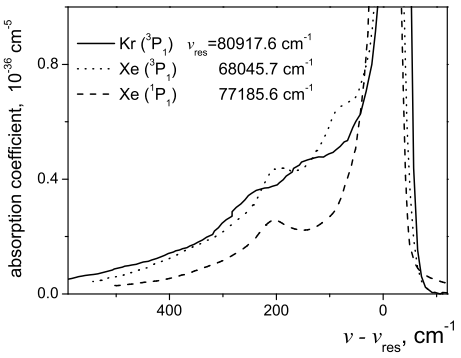

DISCUSSION

The figure shows absorption spectra of Rg/CF_4 mixtures in the region of $^1S_0 \rightarrow ^3P_1$, $^1P_1$ resonance transitions. The spectra for Kr/CF_4 are nearly identical and only $^3P_1$ is shown. The extended absorption on the blue side of the resonance implies that the difference potential is positive in the region of internuclear separations accessible at thermal energies of Rg($^1S_0$)–CF_4 collisions. In contrast to Kr, the spectra of Xe $^1S_0 \rightarrow ^3P_1$ and Xe $^1S_0 \rightarrow ^1P_1$ transitions differ significantly in shape and intensity. This effect have been noted in spectra of Xe/Rg' mixtures. Test line shape simulations showed that the blue wing absorption is mainly due to strong repulsion in the upper Rg($^{3,1}P_1$)-CF_4 state of the transition. At internuclear separations less than r_0 in the lower state, the model overestimates repulsion in the upper state and absorption in calculated spectra extends to the $\nu - \nu_{res} > 500$ cm^{-1} region. The intensity modulations in the 100 - 300 cm^{-1} region is not an interference effect due to contributions from different Rg-CF_4 collision geometries. Experimental studies of Rg/C_2F_6 spectra revealed similar structure on the blue wings of resonance lines. Further work on potentials and line shape modeling for both CF_4 and C_2F_6 gases is currently in progress and results will be reported elsewhere.

ACKNOWLEDGMENTS

Dr. M.Lednev and Dr. A. Zagrebin are acknowledged for test calculations of the line shapes and stimulating discussion. Experimental studies at BESSY were supported by Deutsche Forschungsgemeinschaft.

REFERENCES

1. V. A. Alekseev, *Opt. Spectrosc.* 96, 2004, p. 547, and references cited therein.
2. G. Reichardt, et al, *Nucl. Instr. And Meth. A*, 467-468, 2001, pp. 462-465.
3. F. Pirani, et al., *Chem. Phys. Lett.* 394, 2004, p. 37.
4. W.A.Alexander and D. Troya, *J.Phys.Chem. A* 110, 2006, pp.10834-10843.

Comparative study of RF and DC discharge based Laser Optogalvanic Spectroscopy of Helium Rydberg states

Shahid Hussain, M. Saleem*, and M. A. Baig*

National Tokamak Fusion Program P.O.Box 3329 Islamabad Pakistan
**Atomic and Molecular Physics Laboratory, Department of Physics, Quaid-i-Azam University, Islamabad 45320, Pakistan*
(Hussain et. al., *J. Phys.D: Appl. Phys.* **39**, 3788–3798, 2006)

Abstract

A detailed optogalvanic spectroscopic study of the characteristics of the 1s2s $^1S_o \rightarrow np$ $^1P_1$ Rydberg series of atomic helium using three different discharges, an inductively coupled RF discharge cell operating at 4 MHz, a DC discharge cell and a commercial see-through hollow cathode lamp. We have observed the 2s $^1S_o \rightarrow np$ $^1P_1$ Rydberg series up to $n = 52$ for the first time in RF discharge. In the dc discharge, the series termination of the 1snp $^1P_1$ Rydberg series has been studied as a function of applied voltage at a constant gas pressure, as a function of gas pressure at a constant applied voltage and as a function of radial distance from the electrode centers. The series termination is dependent on the magnitude of the net electric field, which arises from the combination of the isotropic microfield, ambipolar field (radial) and the axial electric field. The contribution of these three types of fields to the net field varies in different regions of the discharge. This net electric field produces shift and broadens the spectral lines especially in the high lying Rydberg transitions. The electric field has been determined from the series termination and also from the observed energy shift. A comparison of the electric field distribution in the three different discharges is presented based on the series termination, Stark shift, line broadening, and relative intensities of the observed spectral lines.

References

1. Barbieri B, Beverini N and Sasso A, *Rev. Mod. Phys.* **62** 6031990
2. Katayama D H, Cook J M, Bondybey V E and Miller T A 1979 *Chem. Phys. Lett.* **62** 542
3. Ganguly B N 1986 *J. Appl. Phys.* **60** 571
4. Ganguly B N and Garscadden A 1985 *Appl. Phys. Lett.* **46** 540
5. Ganguly B N and Garscadden A 1985 *J. Appl. Phys.* **57** 4856
6. Ganguly B N, Shoemaker J R, Preppernau B L and Garscadden A 1987 *J. Appl. Phys.* **61** 2778
7. Shoemaker J R, Ganguly B N, and Garscadden A 1988 *Appl. Phys. Lett.* **52** 2019
8. Ganguly B N and Garscadden A 1985 *Phys. Rev.* A **32** 2544
9. Preppernau B L and Ganguly B N 1993 *Rev. Sci. Instrum.* **64** 1414

2s ^{1}S → *n*p ^{1}P (19 ≤ *n* ≤ limit) Rydberg series of helium, in the same energy range, using three types of discharges.

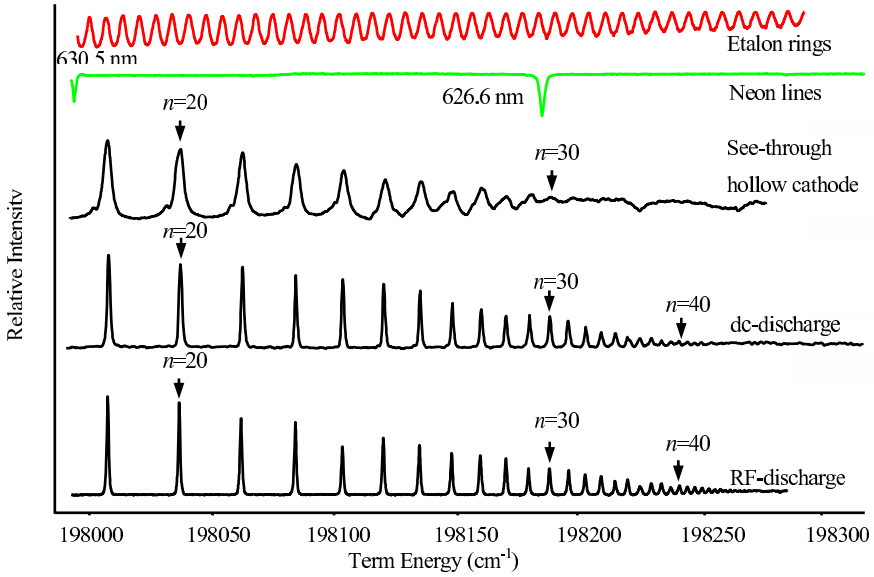

Figure 1

Line shift, line broadening and relative intensity using three discharges

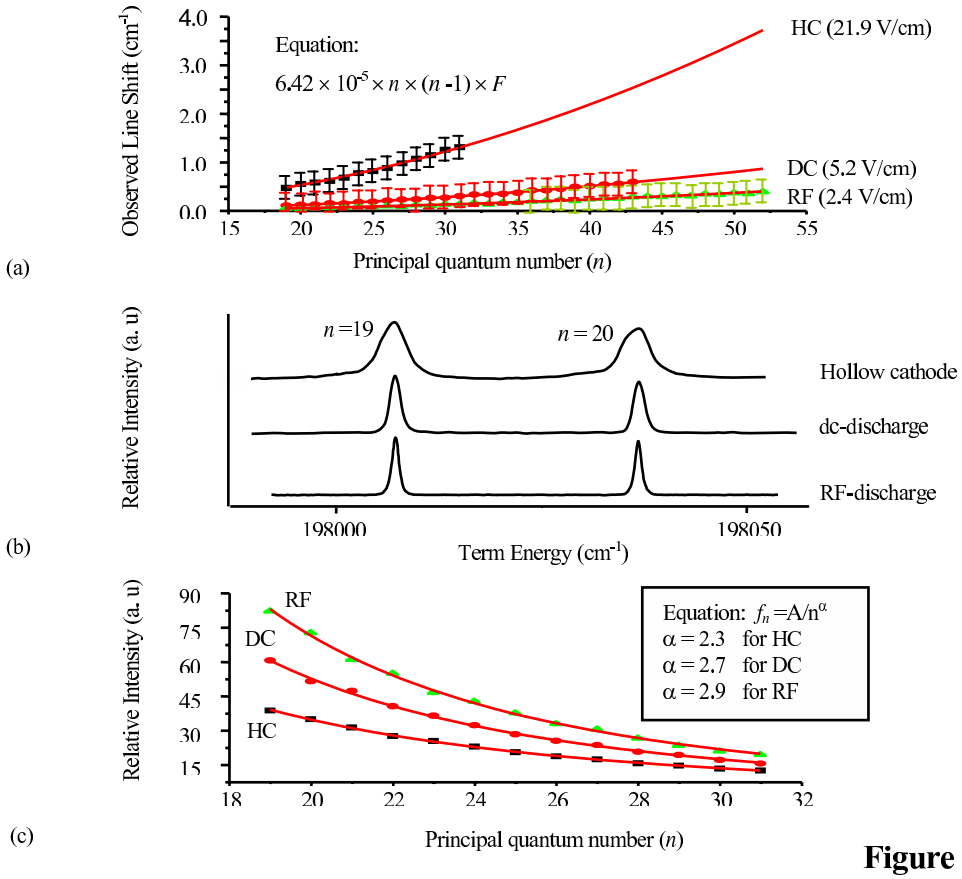

Figure 2

Nonadiabatic Electron Dynamics by Direct Excitation of Collision Pairs

F. Rebentrost[1], O. Hoffmann[2] and J. Grosser[2]

[1] *Max-Planck-Institut für Quantenoptik, 85748 Garching, Germany*

[2] *Institut für Gravitationsphysik, Leibniz Universität Hannover, 30167 Hannover, Germany*

The potential interactions in collisional systems are reflected in the observed spectral line shapes. Optical collisions corresponding to laser excitaion of a collision pairs are the underlying events in the wing of a spectral transition. The study of optical collisions in a molecular beam setup has provided new insights in the collisional process [1]. Excitation of collision pairs with polarized light gives access to the collision geometry ("collision photography") [2, 3]. Control of the collisional process has also been achieved [4]. Accurate tests of the interatomic potentials have been performed using the oscillatory structure seen in the differential cross sections [5]. A direct observation of nonadiabatic transitions in the exit channel of optical collisions is possible by selectively exciting an electronic state and measuring the final populations of *e.g.* the different fine-structure levels after the collision [6]. We here report on nonadiabatic optical collisions of Na atoms with the molecules N_2, CO, C_2H_2, and CO_2. The theoretical analysis of the nonadiabatic electron dynamics on the excited potential surfaces is made within the classical-path formalism using new *ab initio* potential surfaces. The differences between the different collisional systems will be related to the presence and system-specific locations of conical intersections and avoided-crossing seams in the excited potential surfaces.

References

[1] J. Grosser, O. Hoffmann, and F. Rebentrost, in *Atomic and Molecular Beams: The State of the Art 2000*, edited by R. Campargue, Springer 2001, p. 485.

[2] J. Grosser, O. Hoffmann, and F. Rebentrost, Europhys. Lett. **58**, 209 (2002).

[3] R. Goldstein, C. Figl, J. Grosser, O. Hoffmann, M. Jungen, J. Stalder, and F. Rebentrost, J. Chem. Phys. **121**, 8769 (2004).

[4] T. Schmidt, A. Grimpe, J. Grosser, O. Hoffmann, and F. Rebentrost, Phys. Rev. Lett. **92**, 033201 (2004).

[5] A. Grimpe, J. Grosser, O. Hoffmann, and F. Rebentrost, J. Chem. Phys. **122**, 071103 (2005).

[6] C. Figl, R. Goldstein, J. Grosser, O. Hoffmann, and F. Rebentrost, J. Chem. Phys. **121**, 11068 (2004)

QED approach to modelling spectra of the multicharged ions in a laser plasma: Electron-ion collision strengths and rate coefficients

A.V.Glushkov*,†, O.Yu.Khetselius*, A.V.Loboda*, A.V.Ignatenko* and A.A.Svinarenko*

*Odessa University, P.O.Box 24, Odessa-9, South-East, 65009, Ukraine
†Institute for Spectroscopy of Russian Academy of Sciences, Troitsk, Moscow reg., 142090, Russia

Calculation of emission spectra of the plasma ions based in high-precision quantum-electrodynamics (QED) techniques is practical tool, which may be used instead of very expensive sophisticated experiments. Given systematic data about intensities of spectral lines and respective gins, one can establish basic rules of plasma motion in phase space. An important application of the theory of atomic spectra in plasma is search of the optimum plasma excitation condition for lasing and discovery of new pumping approaches. In addition, these investigations are important to understand the plasma processes themselves. Different atomic levels are populated in laboratory plasma by different physical processes. This results in a different dependence of each line intensity on the plasma parameters. In recent years the X-ray laser problem has stimulated a great number of papers devoted to the development of theoretical methods for modelling the elementary processes in collisionally pumped plasma. There is a hope to find lasing effects on the transitions of Li-, Ne-, Ni-like ions. Preliminary investigations of capillary spark discharge were made, which show the possibility of their use as effective plasma sources for the generation of a soft-X-ray or extreme UV amplified spontaneous emission. Two principal theoretical problems must be solved in order to develop a special code adequate to predict the plasma parameters needed to generate a soft-X-ray or extreme ultraviolet amplified spontaneous emission: i). accurate calculation of electron-collisional excitation cross-sections, strengths and rate coefficients for elementary processes in the plasma that are responsible for the formation of emission lines spectra; ii). kinetics calculations to determine level populations, inversions, line intensities and gain coefficients at definite plasma parameters. Under steady-state plasma conditions two dominating elementary processes should be included: i). electron-collisional excitation and de-excitation; ii). radiative relaxation of excited states. In this paper we present the uniform energy approach, formally based on the QED theory with using gauge invariant scheme of generation of the optimal one-electron representation, for the description of spectra of the multicharged ions in a laser plasma, calculation of electron-ion collision strengths, cross-sections and rate coefficients. The electron collision excitation cross-sections, strengths and rate coefficients for some Ne-, Ar-like plasma ions are calculated.

When studying the Stark effect, scattering tasks, the electron-positron pair production in nuclear collisions and elementary processes responsible for emission-lines formation in plasmas, the energy approach has been generalized to cover the problems of scattering theory [1], [2], [3], [4], [5], [6], [7].

Here we briefly outline the main idea using, as an example, the collisional de-excitation of the Ne-like ion: $((2j_{iv})^{-1}3j_{ie}[J_iM_i],\varepsilon_{in}) \to (\Phi_o,\varepsilon_{sc})$. Here Φ_o is the state of the ion with closed shells (ground state of the Ne-like ion); J_i is the total angular moment of the initial target state; indices *iv*, *ie* are related to the initial states of vacancy and electron; indices ε_{in} and ε_{sc} are the incident and scattered energies, respectively to the incident and scattered electrons. Further it is convenient to use the second quantization representation. In particular, the initial state of the system Ş atom plus free electronŤ can be written as

$$|I\rangle = a_{in}^{+}\sum_{m_{iv},m_{ie}} a_{ie}^{+}a_{iv}\Phi_o C_{m_{ie},m_{iv}}^{J_i,M_i} \tag{1}$$

Here $C_{m_{ie},m_{iv}}^{J_i,M_i}$ is the Clebsh-Gordan coefficient. Final state is:

$$|F\rangle = a_{sc}^{+}\Phi_o, \tag{2}$$

where $|I\rangle$ represents three-quasiparticle (3QP) state, and $|F\rangle$ represents the one-quasiparticle (1QP) state. The justification of the energy approach in the scattering problem is in details described in refs. [1], [2], [3], [5], [6]. For the state (1) the scattered part of energy shift ImΔE appears first in the second order of the atomic perturbation theory (fourth order of the QED perturbation theory) in the form of integral over the scattered electron energy ε_{sc} :

$$\int d\varepsilon_{sc} G(\varepsilon_{iv},\varepsilon_{ie},\varepsilon_{in},\varepsilon_{sc})/(\varepsilon_{sc}-\varepsilon_{iv}-\varepsilon_{ie}-\varepsilon_{in}-i0) \tag{3}$$

with

$$\mathrm{Im}\Delta E = \pi G(\varepsilon_{iv},\varepsilon_{ie},\varepsilon_{in},\varepsilon_{sc}). \tag{4}$$

TABLE 1. Comparison of measured and calculated electron-collisional excitation cross-sections (σ) for Ne-like barium for two values of incident electron energy 5.69 keV and 8.20 keV (Units are 10^{-21} cm^2).

Level	J	Measured Marrs et al.	Calculated Ivanov et al.	Calculated Zhang et al.	Calculated Reed	Calculated present paper
			$E_{el} = 5.69$ keV			
Sum	(J=0)	2.50±0.35	2.48	2.58	2.60	2.51
$2p_{3/2}3d_{5/2}$	1	3.98±0.56	3.20	3.44	3.56	3.25
$2p_{1/2}3d_{3/2}$	1	2.12±0.30	1.78	2.42	2.00	1.84
			$E_{el} = 8.20$ keV			
Sum	(J=0)	2.27±0.32	1.83	1.89	1.94	1.86
$2p_{3/2}3d_{5/2}$	1	3.30±0.46	2.87	2.99	3.23	2.93
$2p_{1/2}3d_{3/2}$	1	1.82±0.25	1.64	2.10	1.82	1.64

Here G is a definite squired combination of the two-electron matrix elements (2). The value

$$\sigma = -2\mathrm{Im}\Delta E \tag{5}$$

represents the collisional cross-section if the incident electron eigen-function is normalized by the unit flow condition and the scattered electron eigen-function is normalized by the energy δ function.

The collisional strength $\Omega(I \to F)$ is connected with the collisional cross section σ by expression:

$$\sigma(I \to F) = \Omega(I \to F)\pi / \left((2J_i+1)\varepsilon_{in}\left((\alpha Z)^2\varepsilon_{in}+2\right)\right). \tag{6}$$

Here and below the Coulomb units are used; 1 C.u.$\approx 27.054Z^2$ eV, for energy; 1 C.u.$\approx 0.529\cdot 10^{-8}/Z$ cm, for length; 1 C.u.$\approx 2.419\cdot 10^{-17}/Z^2$ sec for time.

We applied our approach to estimate of the electron collisional excitation cross-sections, strengths and rate coefficients for electron-collisional excitation for Ne-and Ar-like ions. To test our theory we compare our calculations on collisional cross-sections for Ne-like iron with known calculations (c.f. [3], [4], [5]). As example, In table we present measured electron-collisional excitation cross-sections for Ne-like barium for two values of incident electron energy 5.69 keV and 8.20 keV. First of all, no obvious discrepancies for the considered states are found. Our results are at the lower margin of experimental error as the corresponding data with one exception: for the state 2p3=23d5=2(J = 1) our cross-section at collisional energy 5.69 keV is a few percent lower. But one must understand that extraction of the cross section from the experiment is the most ambiguous for this level. It is important to note that inclusion into consideration of Rydberg and autoionization Rydberg states of ions of the previous ionization stage will definitely increase collisional cross-sections. We are calculating the spectra of plasma, containing Ne- and Na-Like Ions, with consistent account for Rydberg and autoionizing Rydberg series in the balance equations. The inclusion of Na-like states, accounting for diffusion-like processes, can increase the population inversion for the 'lasing candidates' by at least a factor of two for a wide range of plasma conditions. This is important for the ionization equilibrium too. Besides, we are calculating the functions, which describe the population distribution within each Rydberg series dependent on the Rydberg electron energy. These functions bear diagnostic information.

REFERENCES

1. A. V. Glushkov, and L. N. Ivanov, *Phys. Letters* **A170**, 33–38 (1992).
2. A. V. Glushkov, and L. N. Ivanov, *J. Phys. B.* **36**, L376–386 (1993).
3. L.-N. Ivanov et al., *Phys. Rev. A* **48**, 4365–4380 (1993).
4. A. V. Glushkov et al., *Int. Journ. Quant. Chem.* **104**, 512-522 (2005).
5. A. V. Glushkov, et al., *J. Phys. CS* **11**, 188–199 (2005).
6. A. V. Glushkov, O. Yu. Khetselius et al., *J. Phys. CS* **35**,420–430 (2006).
7. A. Glushkov, S. Malinovskaya, O. Khetselius, *Europ. Phys. Journ.* **48** (2008).

Line Shape Parameters for ν_3 Transitions of $^{12}CH_4$

Bobby K. Antony, Danielle L. Niles, Sarah B. Wroblewski, Caitlin M. Humphrey, Robert R. Gamache* and Tony Gabard†

*Department of Environmental, Earth, and Atmospheric Sciences, University of Massachusetts School of Marine Sciences, University of Massachusetts Lowell, 265 Riverside Street, Lowell, MA 01854, USA
†Institut Carnot de Bourgogne, UMR 5209 CNRS Univeristé de Bourgogne, Faculté des Sciences Mirande B.P. 47 870, F-21078 DIJON CEDEX, France

INTRODUCTION

Methane, like CO_2, is present in the terrestrial atmosphere in trace amounts, but these two greenhouse gases are thought to be major drivers of climate change and global warming. To understand these processes and predict the future condition of the atmosphere, scientists utilize global climate models, for which the concentrations of the greenhouse gases are part of the input. In this work the focus is on methane, for which the vibration-rotation bands between 9 and 1.6 μm are commonly used to monitor concentrations. A major component in the error budget of atmospheric retrievals for methane in the lower troposphere arise from the poor accuracies of the pressure-broadening coefficients.

The main source of spectroscopic line parameters for methane is the HITRAN database. The 2004 HITRAN database contains some 251 440 methane transitions. Considering vibration-rotation bands of $^{12}CH_4$ between 9 and 1.6 μm with the sum of line intensities greater than 10^{-20} cm^{-1}/(molecule cm^{-1}) yields a list of over one hundred thousand transitions. While it is not practical to measure or calculate the line parameters for all transitions, data are needed for at least the strong vibrational bands. Here, we focus on the region 2726 to 3200 cm^{-1}, which still contains over twenty five thousand transitions for $^{12}CH_4$. The dominant band in this region is the ν_3 band centered at 3018 cm^{-1}. This work presents calculations for 4120 ν_3 transitions in this region.

THEORY AND CALCULATIONS

The complex implimenentation of the Robert-Bonamy formalism [1] has been used to determine the pressure broadened half-width and line shift for methane transitions. Several important features have been incorporated in the present CRB formalism; (i) the imaginary components have been retained, (ii) the elimination of the cut-off procedure, (iii) and the better modeling of close collisions. The current calculations use the mean relative thermal velocity approximation (MRTV) to the CRB formalism. In the present work it is found that convergence of the atom-atom part of the intermolecular potential is obtained at 12th order for transitions involving A- and F-symmetries. However, for E-symmetry transitions the results show that the calculations are not converged even at 14th order of expansion. Since it is the current limit of the codes, results for E-symmetry transitions are not reported here. From the remaining A- and F-symmetry transitions we were able to make calculations for 524 A-symmetry transitions and 3596 F-symmetry transitions with J less than 29 broadened by N_2 and O_2. The calculations are done at 225 and 296 K in order to determine the temperature dependence of the half-width. Air-broadened half-widths of CH_4 are determined from the N_2 and O_2 values.

RESULTS AND DISCUSSION

Therse calculations show that the oxygen-broadened half-widths are similar to the nitrogen-broadened half-widths, in fact the minimum O_2-broadening value is greater than the minimum N_2-broadening value. This fact has also been noted in measurements, for example see Devi *et al.* [2]. Here the half-widths range from small values of 0.017 cm^{-1} atm^{-1} to roughly 0.065 cm^{-1} atm^{-1}. There is not a great amount of variation in the magnitude of the half-width as a function of the perturbing molecules studied here. The large difference in the quadrupole moments of N_2 and O_2 suggests that the CH_4-N_2 and CH_4-O_2 collision systems are not dominated by the electrostatic part of the intermolecular potential. This fact was proved by Neshyba *et al.* [3] in a theoretical study of transitions in the ν_3 band of methane broadened by N_2. In their work they showed that the atom-atom part of the intermolecular potential is dominant, giving results an order of magnitude larger that the electrostatic potential calculation.

The data were analyzed for structure with respect to quantities describing the transitions. The rotational states of methane are described by the rotational quantum number J, the symmetry, and the counting (order) index, N. The results indicate that there does not seem to be a great difference in the half-widths as a function of branch or as a function of the symmetry of the transition. As J increases the number of states increases allowing more transitions for a given J. The spread in the values of the half-width for a given J increases dramatically with J greater than about 10.

Because of the large number of methane transitions, scientists often must attempt to predict half-widths for transitions from half-widths of lines with different symmetry, perturbing species, quantum numbers, etc. Is it possible to predict half-widths for A-/Fspecies transitions from F-/A-species transitions with the same quantum numbers? To address this question the calculated data for N2-broadening were taken and ratios of A-symmetry transition divided by the corresponding F-symmetry transition were calculated. The pairs of lines are chosen such that the upper and lower rotational quantum numbers are the same, the A_1 symmetry is paired with the F_1 symmetry and the A_2 symmetry is paired with the F_2 symmetry, the lower order index values are the same. Because the allowed order index for A- and F-symmetry states are quite different, the pairs were created from the minimum N' and for the maximum N' of each symmetry species. For example the line J'A_1N'$_{min}$ $\leftarrow$ J"A_2N" is paired with J'F_1N'$_{min}$ $\leftarrow$ J"F_2N". The ratios were calculated and for J" less than 10 the ratios are close to one but the spread increases as J" increases. The values range from 0.44 to 2.1, thus one should be cautious applying such an algorithm, especially to intermediate to high J lines. Other approaches were tried with similar results.

The CRB results for the half-widths compared with the measurements of Pine [4], [5] give reasonable percent differences and standard deviations. However, Mondelain *et al.* [6] have demonstrated that retreivals of methane volume mixing rations from balloon spectra made using slightly different line shape parameters show noticeable effects. Some researchers are dismayed at the state of methane broadening parameters with the HITRAN database having measurements for a few thousand transitions and bad estimates (about 20 percent) for the remaining 480 000 transitions. Thus our calculations are not yet at the level desired by all researchers for terrestrial atmospheric applications but certainly an improvement of the estimated values. The accuracies needed for Titan remote sensing are less stringent (5-10 percent) and the CH_4-N_2 calculations presented here meet that criterion.

ACKNOWLEDGMENTS

The authors are pleased to acknowledge support of this research by the National Aeronautics and Space Administration (NASA) through Grant No. NAG5-11064 and by the National Science Foundation (NSF) through Grant No. ATM-0242537. Any opinions, findings, and conclusions or recommendations expressed in this material are those of the author(s) and do not necessarily the views of NASA or NSF.

REFERENCES

1. D. Robert, J. Bonamy, *Journal de Physique* **20** (1979) 923-943.
2. V. M. Devi, D. C. Benner, M. A. H. Smith, C. P. Rinsland, *Appl. Optics* **30** (1991) 287-304.
3. S. P. Neshyba, R. Lynch, R. R. Gamache, T. Gabard, J.-P. Champion, *J. Chem. Phys.* **101** (1994) 9412-9421.
4. A. S. Pine, *J. Chem. Phys.* (1992) 733-785.
5. A. S. Pine, *J. Quant. Spectrosc. Radiative Transfer* (1997) 157-176.
6. D. Mondelain, S. Payan, W. Deng, C. Camy-Peyret, D. Hurtmans, A. W. Mantz, *J. Mol. Spectrosc.* **244** (2007) 130-137.

Effects of Nonlocality in Time of an Interaction Governing the Dynamics of an Atom on Its Spectral Line Profiles

Renat Kh. Gainudinov, Aigul A. Mutygullina

Department of Physics, Kazan State University, 18 Kremlevskaya St, Kazan 420008, Russia

In this talk we will discuss the effects of nonlocality in time of interaction which governs the time evolution of an atom on the broadening of its spectral lines. The effective interaction of an atom with its surroundings whose degrees of freedom are integrated out in describing the evolution of the system is generally nonlocal. The problem consists in the fact that this interaction is nonlocal not only in space but also in time, and hence the dynamics of an atomic system is not governed by the Schrödinger equation with an effective Hamiltonian. This is because this equation is local in time, and the interaction Hamiltonian describes an instantaneous interaction. We will present a novel approach to the theory of the spectral line broadening based on the generalized dynamical equation (GDE) derived in Ref. [1] as a consequence of the first principles of quantum physics. Being equivalent to the Schrödinger equation in the case of instantaneous interactions, this equation allows one to extend quantum dynamics to the case of nonlocal in time interaction. As has been demonstrated in Ref. [2], the effects of such a nonlocality on the broadening of spectral lines of atoms may be very significant: in some cases nonlocality in time of the interaction of an atom with its surroundings can give rise to a spectral line splitting. We will also discuss the effects of nonlocality of the fundamental electrodynamics interaction on the natural broadening of spectral line profiles of atoms. We will show that these effects may be significant in the case of atoms subject to an intensive laser field due to the fact that, in contrast to the bare atoms, some states of laser-dressed atoms with the same values of the total angular momentum J, its projection J_z, and parity may overlap. We will present an equation which determines the natural broadening of spectral line profiles corresponding to transition from overlapping laser-dressed sates. The analysis of the interaction of an atom in such states with its own radiation field gives rise to the surprising finding that in describing the overlapping laser-dressed states QED faces the problem of unrenormalizable ultraviolet divergences. This may be an explicit manifestation of nonlocality of the electromagnetic interaction which in other cases is hidden in the regularization and renormalization procedures. Finally, we will discuss an experimental scheme to measure spectral observables in which the nonlocality of electromagnetic interaction may manifest itself.

REFERENCES

1. R. Kh. Gainutdinov, *J. Phys. A* **3**2, 5657–5677 (1999).
2. R. Kh. Gainutdinov, A. A. Mutygullina and W. Scheid, *Phys. Lett. A* **306**, 1–9 (2002).

Xe-broadened CO line shapes in the fundamental band at 349 K

Adriana Predoi-Cross[1], Jean-Pierre Bouanich[2], Francois Rohart[3], Daniel R. Hurtmans[4]

[1]*Physics Department, University of Lethbridge, 4401 University Drive, Lethbridge, AB, T1K 3M4 Canada*
[2] *Laboratoire de Photophysique Moléculaire, CNRS, Université de Paris-Sud, Bâtiment 350, F-91405 Orsay, France*
[3]*Laboratoire de Physique des Lasers, Atomes et Molécules, Bâtiment P5, Université de Lille 1, 59655 Villeneuve d'Ascq cedex, France*
[4]*Service de Chimie Quantique et Photophysique, Université Libre de Bruxelles, 50 Av F.D. Roosevelt, cp160/09, B-1050 Bruxelles, Belgium*

INTRODUCTION

We present a lineshape analysis on the P(2) and P(7) transitions of CO broadened by Xe in the fundamental band. The spectra were recorded at 349 K using a difference frequency laser spectrometer. We obtained information on the influence of Dicke narrowing and line mixing effects . Several models for implementation of speed-dependent effects are discussed. We have tested the validity of calculating the narrowing parameters using the mass-diffusion or the optical diffusion constants and compared them with experimental narrowing parameters. The line broadening coefficients are modeled using a semiclassical formalism involving successively the atom-atom Lennard-Jones model for the intermolecular potential and a three-term expansion of Legendre polynomials with four adjustable parameters.

EXPERIMENTAL DETAILS

The CO-Xe spectra used in this study were recorded at University of Toronto using a difference-frequency laser spectrometer previously described in [1] and references therein. The tunable infrared radiation was obtained by overlapping and mixing on a nonlinear $LiIO_3$ crystal the visible radiation from an Argon ion laser with tunable radiation from a Coherent 699-29, R6G dye laser. A germanium wedged beamsplitter was used to direct about a third of the infrared power to an InSb reference detector used to normalize the signal and minimize possible problems due to fluctuations in the optical power. The remaining two thirds of infrared power were sent through a 107.1 cm long, heatable absorption cell and then to a second InSb detector. The layout and design of the system allowed is to record spectra with 2 MHz resolution and a signal-to-noise ratio in excess of 1500:1. In our computations the values of self-broadening coefficients were taken from the HITRAN 2004 database [2]. We checked the gas temperature spectroscopically using ratios of intensities at our set temperature and at room temperature (taken from [2]).

SPECTROSCOPIC ANALYSIS

Laser spectrometers such as the one used in this study allow accurate width and shift measurements to be made and can unveil more subtle features of spectral profiles. If we consider the case of isolated spectral lines, these include Dicke narrowing [3] and speed-dependent effects [see for example 4]. For bands of closely spaced spectral lines, line mixing has also been examined and quantified. If collisions cause transitions between the states associated with two different lines, the two lines may interfere such that the intensity in the region between the two lines increases, and it decreases in the outer wings of the two lines. The spectra were fitted successfully using the Rosenkranz [5] first order theory of line mixing. Translational effects were fitted successfully using the hard collision model modified to include an asymmetry component due to line mixing. The spectral profiles were analyzed using a multi-spectrum non-linear least-square curve fitting program [6] that models the spectral lines using several line shape models (Voigt, Galatry, hard collision, speed-dependent Voigt).

Dicke narrowing occurs when the mean free path of the active molecule becomes less than or of the same order of magnitude as the wavelength of absorbed radiation. In this regime the mean translational motion of the active molecules is reduced and the free streaming motion of the molecules becomes diffusive. In the soft collision model (Galatry) [7], the diffusion motion of a molecule is interpreted as consisting of many infinitesimally small (soft) collisions, which eventually result in completely losing the correlation of the molecule's motion with itself. The narrowing parameter is given in this model by $\beta = \frac{1}{2\pi}\frac{k_B T}{cmD}$ where D represents the diffusion constant, m is the mass of the active molecule and k_B and T are the Boltzmann constant and the temperature in K. Since D varies inversely proportional to the pressure, β is in principle proportional to it. An alternative treatment that takes into account the effect of collisions on the translational motion is the *hard collision* model [8,9]. This model assumes that the velocity of the active molecule after the collision is independent of its velocity before the collision. As shown in Fig.2, the beta parameters were found to be strongly non-linear with pressure. Moreover, no fit was possible with these line shape models for pressure larger than 0.14 atm. Thus, the appropriateness of Dicke effect is questionable.

The influence of the velocity of the absorber molecules on the collisional Lorentz half width was investigated in the formalisms developed by Pickett [10], Ward et al. [11] and D'Eu et al. [12] effects known as "speed-dependent effects". As expected, the line profiles are better reproduced when the speed-dependent Voigt profiles are considered.

Xe-broadening coefficients of CO lines in the fundamental band at 297 and 349 K are calculated from a semiclassical formalism involving successively for the intermolecular potential the atom-atom Lennard-Jones model and a second-order expansion of Legendre polynomials with four adjustable parameters. The theoretical results at room temperature are mainly compared to measurements performed by one of the authors nearly forty years ago [13]. The first potential without adjustable parameters leads to underestimated broadening coefficients for low J transitions ($J < 7$) and a reasonable agreement for the other transitions while the second potential gives improved results, in overall agreement with the available experimental data.

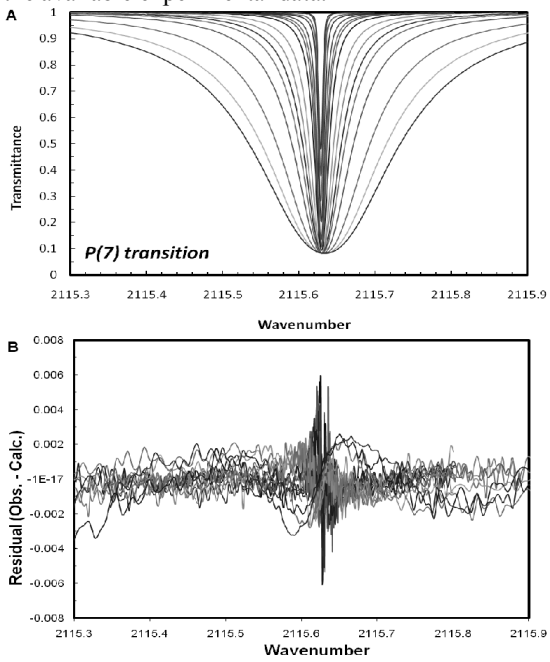

Figure 1. a) Eighteen overlaid spectra for the P(7) transition. b) Fit using the Speed Dependent Voigt profile with an asymmetric line mixing component.

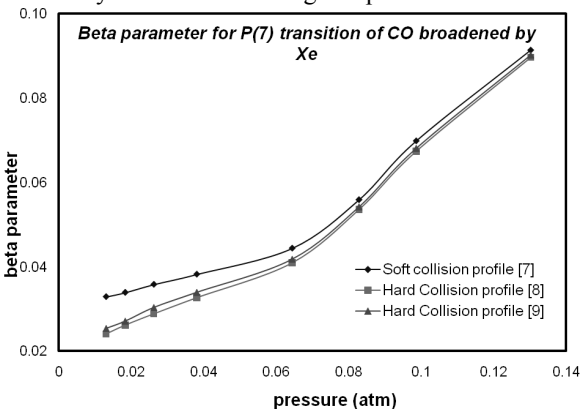

Figure 2. Results for the narrowing parameter ($cm^{-1}atm^{-1}$) for the P(7) transition of CO broadened by Xe at 349 K.

ACKNOWLEDGEMENTS

The research at the University of Lethbridge was performed with funding from the Natural Sciences and Engineering Research Council of Canada (NSERC). A. Predoi-Cross is very grateful to Drs. J.R. Drummond and A.D. May for their guidance, financial support and insightful discussions during her post-doctoral stage at University of Toronto.

REFERENCES

1. A. Predoi-Cross, P.M. Sinclair, C. Luo, J. R. Drummond and A. D. May, *J. Mol. Spectrosc.* **198**, 291-303 (1999).
2. L.S. Rothman, D. Jacquemart, A. Barbe, D.C. Benner, M. Birk, L.R.Brown, M.R. Carleer, C. Chackerian Jr., K. Chance, V. Dana, V.M.Devi, J.-M. Flaud, R.R. Gamache, J.-M. Hartmann, K.W. Jucks,A.G. Maki, J.-Y. Mandin, S. Massie, J. Orphal, A. Perrin, C.P.Rinsland, M.A.H. Smith, R.A. Toth, J. Vander Auwera, P. Varanasi and G. Wagner, *J. Quant. Spectrosc. Radiat. Transfer* **96**, 139–204 (2005).
3. R.H. Dicke, *Phys. Rev*. **89**, 472–473 (1953).
4. P. Duggan, P.M. Sinclair, M.P. Le Flohic, J.W. Forsman, R. Berman, A.D. May and J.R. Drummond, *Phys. Rev. A* **48**, 2077–2083 (1993).
5. P.W. Rosenkranz, *IEEE Trans. Antenn. Propag.* **23** 498–506 (1975).
6. D. Hurtmans, G. Dufour, W. Bell, A. Henry, A. Valentin and C.Camy-Peyret, *J. Mol. Spectrosc.* **215**, 128–133 (2002).
7. L. Galatry, *Phys. Rev*. **122** 1218–1223 (1961).
8. S.G. Rautian and I.I. Sobel'man, *Sov. Phys. Usp* **9**, 701-716 (1967).
9. R. Ciurylo, A. Bielski, S. Brym and J. Jurkowski, *J. Quant. Spectrosc. Radiat. Transfer* **53** 493-500 (1995).
10. H.M. Pickett, *J. Chem. Phys*. **73** 6090–6094 (1980).
11. J. Ward, J. Cooper and E.W. Smith, *J. Quant. Spectrosc. Radiat. Transfer* **14** 555-576 (1995).
12. J.-F. D'Eu, B. Lemoine and F. Rohart, *J. Mol. Spectrosc*. **212** 96-110 (2002).
13. J.P. Bouanich, *J. Quant. Spectrosc. Radiat. Transfer* **12** 1609-1615 (1972).

Two-Photon Frequency Comb Excitation of Rubidium Atoms in External Magnetic Field

N. Vujičić*[1], T. Ban[1], H. Skenderović[1], S. Vdović[1], G. Pichler[1]

*[1]*Institute of Physics, Bijenička 46, Zagreb 10 000-HR, Croatia*
E-mail: natasav@ifs.hr

Mode-locked lasers create short optical pulses with a fixed phase relationship between the laser modes. By transforming a single femtosecond pulse from the time domain into the frequency domain, a broadband continuum is created. But, transforming a modelocked train of femtosecond pulses into the frequency domain one can find dramatically different effect. The repetitive pulses become an optical frequency comb, a set of very sharp and narrow frequency spikes uniformly spaced across the spectral bandwidth of the light source. The comb peaks are continuous-wave, extremely narrow, and separated by the pulse repetition rate. The constant spacing between the frequency peaks makes the comb a natural optical ruler for optical measurements. The higher the repetition frequency, the wider the spacing of comb lines, which in general makes measurements easier. The frequency f_n of each n-th mode can be written as $f_n = f_0 + n \cdot f_r$ where n is the mode number, f_r is the repetition rate (the spacing between modes), and f_0 s a carrier-envelope offset frequency at a frequency between zero and the repetition rate. The offset is proportional to the phase shift between the wave envelopes in successive pulses, which arises because the carrier wave moves at the phase velocity of the pulses but the envelope moves at the group velocity.

The main problem in studying of two-photon transitions is in maximization of the excitation efficiency of the desired state. Frequency comb spectroscopy can be very useful for two-photon transitions. In the context of two-photon transitions, there are two general cases: those with an intermediate resonance and those in which the pulse spectrum is far detuned from an intermediate resonance. In the case where one mode is resonant with the intermediate state, the system can often be understood by considering only two modes. However, when there is no intermediate resonance in the spectrum it should be noted that if one pair of comb modes is two-photon resonant, then all modes will form a resonant pair due to the equal spacing of modes. Here we present the two-photon frequency comb excitation of the rubidium atoms at the room temperature as a result of our previous work on modified direct frequency comb spectroscopy (DFCS) [1,2,3]

Two-photon transitions on cold ^{87}Rb atoms were presented in [4,5]. There, the absolute transition frequencies of several hyperfine levels in the 5D and 7S manifolds were measured, via resonant enhanced transitions through an intermediate 5P hyperfine level. The population of the 5D or 7S states was determined by monitoring the fluorescence at 420 nm resulting from the cascade decay of the 6P state to the 5S state.

In present experiment we investigate the 5*S*-5*D* two-photon transitions in ^{85}Rb and ^{87}Rb atoms as a result of the interaction of the femtosecond frequency comb with atomic levels of both rubidium isotopes. A set of two-photon transitions from the ground-state $5S_{1/2}$ to the excited $5D_{5/2}$, enhanced by the $5P_{3/2}$ intermediate state have been examined. The experiment is preformed with an optical frequency comb emitted from a 200 fs, 80.53 MHz repetition rate, mode-locked femtosecond fiber laser (FFL) centered at 778 nm with a full width at half maximum bandwidth of about 3 nm (1.2 THz). There is ~ 2.4 μW of power in each of the comb lines resonant with the 5S-5P and 5P-5D transitions. The excited 5D state population is determined from the 5D-6P-5S radiative cascades: the atoms relax to the 6P state and then decay down to the ground state, emitting photons at 420 nm. These blue photons are detected with a photomultiplier tube (PMT) (Hamamatsu DM0016), with spectral response range from 280 nm to 630 nm, centered at 350 nm and counted with a multi-channel photon counter. In order to investigate the dependence of the two-photon fluorescence signal as a result of interaction of frequency comb with perturbed energy-level pattern due to the interaction with magnetic field an external magnetic field was applied. Magnetic field was generated by a pair of Helmholtz coils. By scanning the current through the coils from 0 A up to 1.3 A the homogeneous magnetic field from 0-150 Gauss was created. In an external magnetic field the Rb ground- and excited-state levels are not characterized any more by the total angular momentum quantum numbers *Fg* and *Fe*, but they are a mixture of these states created by the external field. The magnetic sublevel energies are dependent on the external magnetic field strength. For very low field strengths each hyperfine level experiences a linear Zeeman effect. As the field strength increases, the Zeeman energy comes close to the hyperfine splitting energy and the energy level pattern becomes

more complex. In our experimental geometry the optical transitions between hyperfine ground- and excited-state levels follow the $M= +1$ or $M= -1$ selection rule. The results for the linear and circular polarizations of the laser beam, as well as for the different mutual orientation of of the $\vec{k}$ and $\vec{B}$ vectors (parallel and antiparallel configurations). Experimental results are shown in Figure 1.

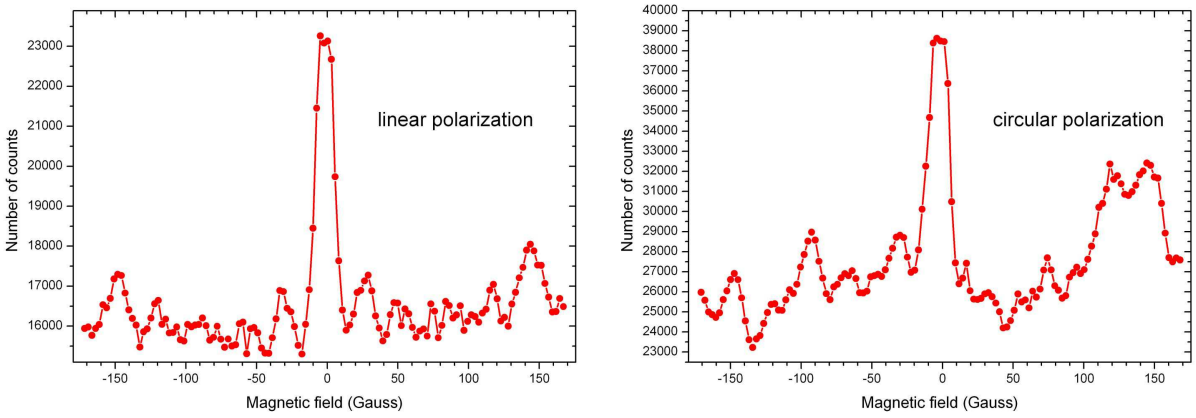

FIGURE 1. Change of two-photon fluorescence signal for different polarization of femtosecond laser beam as a result of interaction with the external magnetic field.

It can be seen that in the absence of magnetic field (B=0 Gauss) we observe maximum signal which decreases as magnetic field increases. This reduction of two-photon fluorescence signal in magnetic field comes as a result of the additionally energy-level splitting due to the Zeeman effect. For the field strength, which leads to favorable energy-level splitting (the frequency separation of different transitions is a multiple of 80 MHz), one would expect amplification of fluorescence signal. We expect that the fluorescence signal should be significantly increased in the condition when the $5S_{1/2}$ atomic Larmor frequency is equal to or a multiple of the pulse repetition rate [6]. We calculated that the first-order ground-state Zeeman coherence is about 110 Gauss. This amplification of fluorescence signal for ~110 Gauss can be observed from our experimental results. Discussion of the present results and future prospects will be given in detailed.

ACKNWOLEDGEMENTS

We acknowledge the support from the Ministry of Science, Education and Sports of Republic of Croatia (Projects 0035002), European Commission Research Training Network on Cold Molecules (FW-5) and Alexander von Humboldt Foundation (Germany).

REFERENCES

1. D. Aumiler, T. Ban, H. Skenderović, G. Pichler, *Phys. Rev. Lett.* **95**. 233001 (2005).
2. T. Ban, D. Aumiler, H. Skenderović, G. Pichler, *Phys. Rev. A* 73. 043407 (2006).
3. T. Ban, D. Aumiler, H. Skenderović, S. Vdović, N. Vujičić, G. Pichler, *Phys. Rev. A*, 76, 043410 (2007).
4. A. Marian, M.C. Stowe, J.R. Lawall, D. Felinto, J. Ye, *Science* **306**, 2063, (2004).
5. A. Marian, M.C. Stowe, J.R. Lawall, D. Felinto, J. Ye, *Science* **306**, 2063, (2004).
6. J. Mlynek, W. Lange, H. Harde, and H. Burggraf, *Phys. Rev. A* **24**, 1099 (1981).

FRIDAY, 20 JUNE

Radio Recombination Lines as Tools for Astronomers and Physicists

M. A. Gordon

National Radio Astronomy Observatory, Tucson, Arizona, USA 85721-0655

GENERAL

Described by simple Bohr theory developed in 1914 [1], spectral lines in the radio range arising from transitions between large principal quantum numbers of atoms have proved to be powerful tools for astronomers. Called radio recombination lines, they are usually easy to observe, give unique information about astronomical objects, and facilitate the study of physical effects in environments that cannot be created in terrestrial laboratories.

NOMENCLATURE AND FREQUENCIES

Transitions between principal quantum numbers $n+1$ and n are called $n\alpha$ lines; between $n+2$ and n, $n\beta$, and so on. Line frequencies vary according to atomic weight (reduced mass of the nucleus) and are designated as H110α [4.874 GHz] for hydrogen lines, He161α [1.562 GHz] for helium lines, and so forth.

For "radio" recombination lines (RRLs) at frequencies less than 100 GHz, principal quantum numbers are large, and simple Bohr hydrogenic models give accurate rest frequencies. For an $n\alpha$ line, the rest frequency ν is

$$\nu_{n+1\rightarrow n} = RcZ^2\left[\frac{1}{(n)^2} - \frac{1}{(n+1)^2}\right], \quad 10\,\mathrm{MHz} < \nu < 100\,\mathrm{GHz}, \tag{1}$$

where R is the Rydberg constant for reduced mass of the nucleus, c the speed of light, and Z the multiple of the electronic charge of the nucleus. But, at small principal quantum numbers where $n < 40$ involving frequencies greater than 100 GHz, the frequencies produced by the classical Bohr model develop small errors because the asymmetric fine-structure components are no longer thermalized and, consequently, shift the monolithic Bohr frequency given by Eq. (1). Here astronomers use a weighted mean of these frequency components to calculate an effective rest frequency.

DETECTION RANGE

First detected in 1964 essentially simultaneously at Lebedev Physical Institute and at Pulkovo Observatory in the Soviet Union, RRLs have now been now detected by astronomers over wavelengths from $\lambda = 20.5$ m (14.6 MHz) to 52.6 μm (5.7 THz)— a range of 5 orders of magnitude.

ASTRONOMICAL RESULTS

The mere detection of RRLs identifies an astronomical object as "thermal," that is, as being an object comprised of ionized gas described by a Maxwell-Boltzmann distribution. The line profiles give the radial velocity of the object, the approximate kinetic temperature of the ionized gas, and information as to the velocity turbulence along the line of sight through the gas.

Observations soon showed the radiation transfer to be more complicated than expected. Often the level populations are out of thermodynamic equilibrium, thereby requiring the calculation of level populations by the statistical equilibrium of all the populating rates associated with a principal quantum level rather than by the detailed balancing of each type of population rate. At some wavelengths the result is a "partial maser" effect in which the intensities of RRLs are slightly amplified; at other wavelengths, the lines are weakened by an under-population of their upper quantum levels.

While detection of RRLs from the hydrogen and helium components of hot ionized gas within emission nebulae are common, there are also detections of carbon recombination lines from much cooler ionized regions of the interstellar medium.

One particularly interesting discovery [2] was the existence of strongly masering, double-peaked RRLs from a peculiar emission star, MWC349A, whose intensities vary by a factor of two on a time-scale of months. The line

profiles imply the lines to arise from a rotating circumstellar disk viewed edge-on. Moreover, a monotonic shift in the central radial velocities of RRLs with frequency suggests an accelerating gas outflow from the star that could be due to photo evaporation of the disk material [3].

RRLs have also been detected from nearby spiral gaseous galaxies and from the Sun.

PHYSICS

Initially surprising, Stark pressure broadening developed for astronomical optical spectra greatly overestimated the line broadening expected for RRLs in the radio range. In fact, many astronomers argued in the early years of radio astronomy that Stark broadening would wash out the RRLs so that they could not be detected.

Griem [4] showed that, in the radio range and unlike the optical range, inelastic electron impacts perturb both upper and lower principal quantum levels in the same energy sense, thereby significantly reducing the effects of Stark broadening on the line widths. Subsequent observations [5] confirmed these calculations.

In the ultra-low densities of the interstellar medium, [carbon] atoms can exist in states with very high principal quantum numbers, that is, with principal quantum numbers of about $n = 1{,}000$ that correspond to classical Bohr atoms with diameters up to 0.1 mm—a dimension comparable to the thickness of this page. Stepkin et al. [6] have recently observed the C1006δ line in absorption against the supernova remnant, Cassiopeia A.

CONCLUSION

Astronomical observations of RRLs not only provide information about thermal objects in the universe but show the Cosmos to be a wonderful laboratory for the study of basic physics phenomena in an environment difficult to create in terrestrial laboratories.

SUPPLEMENTAL READING

A book available in English and in Russian [7, 8] gives the history of the initial detections, derives the detailed physics of RRLs from first principles, develops the transfer process of the emission from source to telescope, and reviews observations through the year 2002. Springer-Verlag will release an updated version in 2008 in both paperback and Ebook formats.

ACKNOWLEDGMENTS

I thank my colleague, R. L. Sorochenko, for suggestions concerning this presentation.

REFERENCES

1. N. Bohr, *Fysisk Tidsskraft* **12**, 97 (1914).
2. J. Martín-Pintado, R. Bachiller, C. Thum and C. .M.Walmsley, *Astron. Astrophys.*, **215**, L13 (1989).
3. M. A. Gordon, *Astrophys. J.*, **589**, 953 (2003).
4. H. R. Griem, *Astrophys. J.*, **148**, 547 (1967).
5. G. T. Smirnov, R. .L. Sorochenko, V. Pankonin, *Astron. Astrophys.*, **135**, 116 (1984).
6. S. V. Stepkin, A. A. Konovalenko, N. G. Kantharia, N. U. Shankar, *Astron. Astrophys.*, **374**, 852 (2006).
7. M. .A. Gordon, R. L. Sorochenko, *Radio Recombination Lines: Their Physics and Astronomical Applications*, Kluwer, Dordrecht, 2002.
8. R. L. Sorochenko, M. A. Gordon, *Rekombinazionnye Radiolinii: Fizika i Astronomiya*, [Recombination Radiolines: Physics and Astronomy], Fismatlit, Moscow, 2003 (in Russian).

Atomic line shapes in stellar spectra

J.F. Kielkopf* and N.F. Allard†,**

*Department of Physics and Astronomy, University of Louisville, Ky 40292, USA
†Institut d'Astrophysique de Paris, CNRS, UMR 7095, UPMC, 98bis boulevard Arago, F-75014 Paris, France
**Observatoire de Paris-Meudon, GEPI, UMR 8111, CNRS, F-92195 Meudon Principal Cedex, France

ABSTRACT

The spectrum emitted by a star is determined by the atmosphere where the photons last scatter. It carries a signature of the presence of atomic species, and of the effects of atomic collisions and motions, on the radiative process. To the astronomer interested in the star, these spectra offer clues to its composition, temperature, surface gravity, magnetic field, rotation and line-of-sight motion. To the atomic physicist, stellar spectra are a probe for collision processes under conditions that are difficult to reproduce in a laboratory. Indeed, an understanding of the underpinning line shape physics is key to exploring a wide range of interesting phenomena – answering questions about the color and composition of brown dwarfs, the temperature, size and age of white dwarfs, and the detection of planets and their atmospheres.

The theory of spectral line shapes, especially the unified approach we have developed, makes possible accurate models of stellar spectra that account both for the centers of spectral lines and their extreme wings in one consistent treatment. Under some circumstances it is possible to test the line shape theories in the laboratory, if not under conditions exactly the same as those in stars, at least under closely similar conditions. For brown dwarf stars, for example, with an atmosphere of molecular hydrogen and the alkali metals, conventional absorption spectroscopy can be used to examine the line wing, to measure the broadening of the line center, and to determine shifts of lines due to collisions. A comparison with theoretical profiles establishes the accuracy of the interaction potentials, which are difficult to compute *a priori*. At the other extreme of temperature, a shock wave in a laser-produced plasma produces for a few nanoseconds the temperature and density of a white dwarf star. We will compare unified line shape calculations with recent experiments to determine the wings of the sodium and potassium resonance lines broadened by hydrogen and helium, and to measure the shift of Balmer α due to electrons at high density.

NONEQUILIBRIUM KINETICS OF RYDBERG ATOMIC STATES

L. A. Bureyeva, M. B. Kadomtsev, M. G. Levashova, and V. S. Lisitsa

"Kurchatov Institute" Russian Research Center, pl. Kurchatova 1, Moscow, 123182 Russia

Broadening of highly excited (Rydberg) hydrogen atomic states is of interest for astrophysical plasmas. The most of the calculations deals with thermodynamically equilibrium populations of atomic states [1-5]. The goal of the present paper is to estimate the non-equilibrium effects in population of hydrogen Rydberg atomic states in astrophysical plasmas.

We developed a two-dimensional quasi-classical model of the radiative-collisional cascade for hydrogen-like systems in plasmas. The structure of the quantum kinetic equation for the radiative-collisional cascade and its iterative solution is as following:

$$\left[\hat{L}_c+\hat{L}_r^q\right]f(nl)+q(nl)=0\ ;\quad \hat{L}_c f_k(n,l)-A(n,l)f_k(n,l)+q_k=0, \tag{1}$$

$$q_k\equiv\sum_{n'=n+1}\ \sum_{l'=l\pm1} f_{k-1}(n',l')A(n',l'\to n,l) \tag{2}$$

where $\hat{L}_c$ is the collisional transition operator, $\hat{L}_r^q$, is the radiative transition operator, $f(nl)$ is the population distribution function in the two-dimensional space of principal, n, and orbital, l, atomic quantum numbers, and $q(nl)$ is the source of atomic state population, $A(n,l)$ is the radiative decay rate. The distribution f is presented in the form of a series $f=f_0+f_1+f_2+\ldots+f_k+\ldots$, that corresponds to a successive emission of quanta. Each term f_k of this series can be determined from the Eqs.(1, 2) using f_{k-1} calculated at the previous step, while f_0 can be found from them with the original source.

The collisional diffusion coefficients in the space of action variables ΔI_k, namely, principal and orbital quantum numbers transfered during a classical collision of the atomic electron with charged plasma particles.

$$\partial f/\partial t=\frac{1}{2}\frac{\partial}{\partial I_k}\langle\Delta I_k\Delta I_j\rangle\frac{\partial f}{\partial I_j}\ ,\quad \langle\Delta E^2\rangle=8E_n\omega\tau\ ,\quad \omega=\frac{4\sqrt{2\pi}}{3}N_e L\sqrt{\frac{1}{T}}\ , \tag{3}$$

where N_e, T are the electron density and temperature, L is the Coulomb logarithm.

We took account of the three-body and photorecombination sources of population in astrophysical plasmas (T= 1 eV and N_e = 10^3-10^4cm^{-3}). Our calculations reveal a noticeable nonequilibrium in the population in orbital quantum number l. Comparison was made with one-dimensional calculations by averaging over the quantum numbers l. The difference in 1D and 2D population models is clear from the equations for atomic states populations $N(n)$:

$$N(n)=\left\langle\frac{q(n,l)}{A(n,l)}\right\rangle_l\neq\frac{\langle q(n,l)\rangle_l}{\langle A(n,l)\rangle_l}=\bar{N}(n) \tag{4}$$

The difference between $N(n)$ and $\bar{N}(n)$ is illustrated in Fig.1.

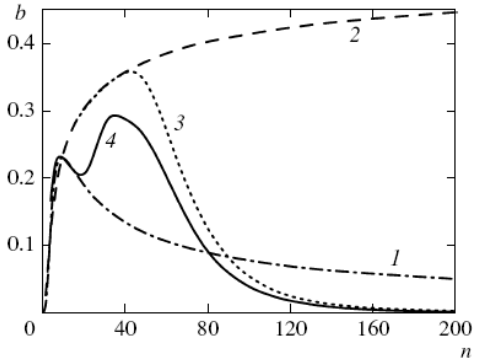

Figure. 1. Populations $b(n)$ (in unit of equilibrium Boltzman population) of atomic levels directly populated by the photorecombination source in astrophysical plasmas (N_e = 2.5 × 10^3 cm^{-3} and T = 1 eV): 1, averaged two-dimensional calculations without collisions; 2, one-dimensional calculations without collisions; 3, one-dimensional calculations with collisions; 4, averaged two-dimensional calculations with collisions.

It is seen that the difference disappeared when the collisional rates dominate over the radiative ones.

The same comparison of 1D and 2D models was made in general case corresponding to both the radiative and the collisional (3 body recombination sources). This comparison reveals a characteristic population minimum attributable to the competition between the collisional and radiative state populations. This minimum in the two-dimensional model is appreciably deeper than that in the one-dimensional models (Fig.2).

Based on the populations found, we calculated the intensities of spectral lines in the range of transition frequencies corresponding to a certain spectral interval of observations (Fig.3). The results allow us to judge the degree of nonequilibrium of the populations of Rydberg atoms in astrophysical plasmas.

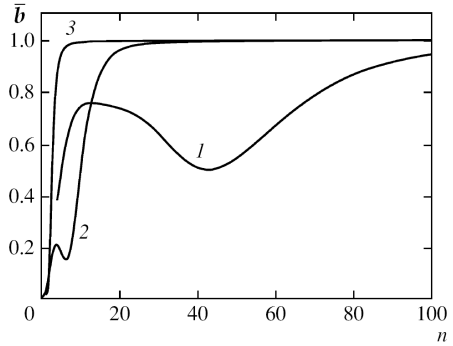

Figure 2. Total (including the photorecombination and three-body sources of population) one- dimensional distribution function obtained by integrating the two-dimensional function over the variable*l*:at T= 1 eV and N_e =2.5x10^3 (1), 10^9 (2), and 10^{13} (3) cm^{-3}.

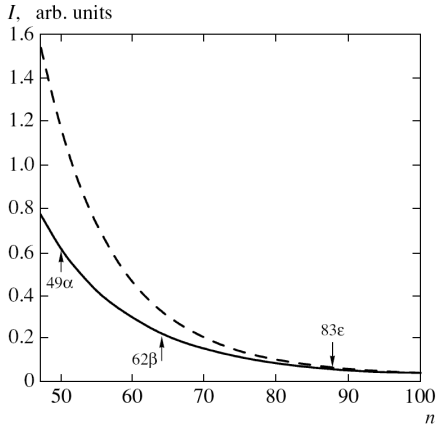

Figure 3. Rydberg line intensities for the transitions from the n = 50-100 levels at fixed observation frequency $\omega = (1/n'^2 - 1/n^2)$ = 8 x 10^{-6} at. units corresponding to the transition with Δn = 1 between the 50 and 49 levels (the population minimum in Fig. 6) at N_e= 2.5x10^{3}cm^{-3} and T= 1 eV; the arrows indicate the positions of some Rydberg lines.

It follows from the consideration above that the nonequilibrium conditions in astrophysical plasma can be realized for principle quantum numbers less then n=100. The 2D kinetics developed can be applied to multicharged ions as well by scaling with Coulomb units.

ACKNWOLEDGEMENTS

This work is supported by the Russian Foundation for Basic Research (project no. 06-02-16614a, 08-02-00294a), a grant from the President of Russia for Support of Leading Russian Schools (no. 2457.2008.2), and the ARCUS program (№ P003-5a).

REFERENCES

1. R. L. Sorochenko and M. A. Gordon, *Radio Recombination Lines: Their Physics and Astronomical Applications*, 2002, Kluwer, Dordrecht.
2. M. B. Bell, L. W. Avery, E. R. Seaquist, and J. P. Valiee, Publ. Astron. Soc. Pac. 112, 1236 (2000).
3. E. Oks, Astrophys. J. 609, L-25 (2004).
4. H. R. Griem, Astrophys. J. 620, L-133 (2005).
5. J. Watson, J. Phys. B. 39, 1889 (2006).

Molecular spectroscopic studies for remote sensing of earth and planetary atmospheres

Adriana Predoi-Cross

Physics Department, University of Lethbridge, 4401 University Drive, Lethbridge, AB, T1K 3M4 Canada

INTRODUCTION

Spectroscopic techniques have the potential to increase our understanding of Earth and planetary atmospheres through spectroscopic studies that will enable more accurate modelling of infrared radiative transfer in the Earth atmosphere and other planetary bodies. There is a need in atmospheric research to accurately model absorption profiles over a wide range of pressures and temperatures. Using a correct understanding of the physics of spectral formation, data may be reliably extrapolated from the laboratory case to the atmosphere. In practice, a full understanding of the physics is hard to obtain, particularly when the numbers of parameters are considered.

This talk will addresses the following objectives: *i)* experimental studies of line shapes and molecular collisional dynamics in molecules of planetary interest, *ii)* theoretical modelling of line mixing effects and broadening parameters.

SELECTED SPECTROSCOPIC STUDIES

At the foundation of all remote sensing activities is basic spectroscopy from laboratory studies. Limitations in the spectroscopic information in turn limit our ability to probe and understand our atmosphere [1] and planetary atmospheres. Recent studies in atmospheric research have focused on areas such as terrestrial carbon cycle and ecosystems, climate change and the composition of planetary atmospheres. 1For spectroscopic remote sensing, the HITRAN database [2] is the most comprehensive and widely used collection of the line parameters needed to characterize atmospheric spectra.

The formation of a spectral line shape is not completely understood. Although Gaussian, Lorentzian and Voigt models have earned their places in the common knowledge of this field, the physics they contain is not enough to explain the details revealed by high-resolution experiments. Complex theories that include line mixing (the effect of collision-induced line interference), speed dependent profiles and statistical correlation between the relaxation of the internal motion and the translational motion of the molecules are needed [3-5]. The main signature of line mixing is the collapse of a multi-line spectrum into a single line at high enough pressures. Thus, the best insight into the physical interactions governing the collisional processes is gained in the weak mixing regime, when the lines are weakly overlapped. If the desired atmospheric measurements are at pressures near 1 bar the subtle effects of non-Voigt line shapes and line mixing are essential for the interpretation of tropospheric spectra, especially near the boundary layer. For this reason, the format of the 2004 edition of HITRAN [2] was expanded so that the line mixing coefficients could be included for CO_2. Such parameters are expected to be included in future updates of the database for CH_4, CO, H_2O, CO_2. Currently, there are satellite instruments that can achieve precisions as high as 1.5 % to 0.3% [6-9]. Such requirements are very challenging for spectroscopists. There are many theoretical and experimental studies of line-mixing effects in the infrared spectral range [for example 10-16 and references therein]. The theoretical models included empirical approaches [16], first principle calculations starting from the intermolecular potential [17], semi-classical models [18], and the use of fitting [19] and scaling laws [16,20,21]. The line shape modelling based on the Energy Corrected Sudden approximation (ECS) has been used successfully in numerous studies [for example 15-16, 22-23 and references therein].

To understand and separate the contributions of each of line shape effects and ultimately to develop new theoretical models, we have studied the spectral signatures of several molecules over a wide range of pressures and temperatures. Typical values of line mixing effects are no more than few tenths of a percent of the peak absorption value of a line and so signal-to-noise ratios in excess of 1500:1 are needed if one looks for an experimental line-mixing signature in a spectrum, with a minimum degree of accuracy. The spacing between spectral lines in crowded Q-branches in CO_2 or N_2O is less than the best resolution that can be offered by a Fourier Transform spectrometer and hence they often cannot be fully resolved in FTIR spectra. Collisional narrowing effects occur at low pressures and they can be studied only with an instrument that offers a resolution below the natural width of the line, a requirement met by laser spectrometers. Remote sensing of trace species is needed to understand the chemistry and composition of planetary atmospheres and interpret the processes therein. This requires accurate determination of small concentrations which in turn requires fundamental understanding of the line broadening and line shifts in the presence of different foreign gases on different planets. For the Earth, we need information on nitrogen and oxygen broadening data. It has been shown that when different line shape models are used, it is difficult to predict the temperature dependence of the broadening coefficients over the range of atmospheric temperatures.

Laboratory spectroscopy of mono-deuterated methane

Monodeuterated methane (CH_3D) is a constituent trace species in planetary atmospheres, and its spectrum is often used to determine the H/D ratios. Its infrared spectrum is continually investigated in order to obtain improved spectroscopic line parameters needed to interpret remote sensing observations. Accurate representation of the positions and intensities of this molecule requires extensive laboratory work. Using a multispectrum fitting technique we have measured for the first time the

line parameters of self-, N_2-, O_2- and air-broadened CH_3D in the ν_2 band. The broadening and shift parameters were modeled using semi-classical theory.

Methane line shapes in the octad spectral range

Methane plays an important role in atmospheric chemistry, and knowledge of the column distribution taken with dynamical data will lead to a better quantitative understanding of its biogeochemical cycles. Methane is increasing in the atmosphere at a rate of 1% per year, but the source of this increase is not certain. Improved knowledge of the source strengths and distributions will help resolve this uncertainty. The objective of this study was to enhance our spectroscopic knowledge of methane in the octad spectral range. This spectral interval contains eight interacting overtone and combination bands.

Near-infrared spectroscopic study of carbon dioxide

We have performed a line profile study of self- and air-broadened carbon dioxide transitions in the 30012←00001 and 30013←00001 vibrational bands. The broadening, shift, and line mixing coefficients were derived using the Voigt and Speed Dependent Voigt line shape models. The results obtained are consistent with other studies in addition to the theoretically calculated values. Two types of scaling laws were used to calculate the broadening and line mixing parameters.

Spectroscopic Line shape Study of the Oxygen A-Band

An adequate knowledge of the physics behind molecular spectral line shapes is necessary to calculate the heating and cooling rates used in climate models. Spectroscopic measurements of transitions in the oxygen A-band are performed by the NASA SAGE III, Orbiting Carbon Observatory (OCO) and ACE-MAESTRO satellite instruments where this band is used to derive atmospheric temperature, pressure, and for the retrieval of aerosol and cloud optical properties using remote sensing techniques. In this study we obtained accurate values for spectral line parameters retrieved from high-quality laboratory Fourier Transform spectra. This is a major step toward a better understanding of self-broadening and self-line mixing mechanisms for transitions in the oxygen A-band. We were able to measure for the first time the line mixing coefficients in self-broadened oxygen. The intensities, self-broadening and self-line mixing coefficients were also modeled and compared with experimental results.

Laboratory Spectroscopy of the ν_4 band of $^{12}CH_4$ and $^{13}CH_4$

This is a collaborative project with researchers from the College of William and Mary and NASA Langley Research Center. Self- and air-broadening, pressure-induced shifts, and line mixing have been quantitatively examined in laboratory infrared absorption spectra of methane in the 7-9 μm region for temperatures from 210 to 314 K.

ACKNWOLEDGEMENTS

The research presented here was funded by the Strategic and Discovery Grant programs of the Natural Sciences and Engineering Research Council of Canada (NSERC) and by the University of Lethbridge research Fund.

REFERENCES

1. L.D. Kaplan, *J. Opt. Soc. Am.* **49** 1004-1007 (1959).
2. L.S. Rothman, D. Jacquemart, A. Barbe, D.C. Benner, M. Birk, L.R.Brown, M.R. Carleer, C. Chackerian Jr., K. Chance, V. Dana, V.M.Devi, J.-M. Flaud, R.R. Gamache, J.-M. Hartmann, K.W. Jucks, et al., *J. Quant. Spectrosc. Radiat. Transfer* **96**, 139–204 (2005).
3. R. Ciurylo R, J. Szudy, *J. Quant. Spectrosc. Rad. Transfer* **57** 411-423 (1997).
4. D. Mondelain, S. Payan, C. Camy-Peyret, D. Hurtmans et al., *J. Mol. Spectrosc.* **244** 130-137 (2007).
5. C.D. Boone, K.A. Walker and P.F. Bernath, *J. Quant. Spectrosc. Rad. Transfer* **105** 525-532 (2007).
6. J.P. Burrows, H. Bovensmann, G. Bergametti, J.M. Flaud et al., *Adv. Space Res.* **34** 682-6 (2004).
7. A. Chedin, R. Saunders, A. Hollingsworth et al., *J. Geo. Res. Atm.* **108** art. no. 4064 (2003).
8. C.E. Miller, D. Crisp, P.L. DeCola, S.C. Olsen et al. *J. Geo. Res. Atmos.* **112** art. no. D10314 (2007).
9. J.M. Flaud, J. Orphal, G. Bergametti, C. Deniel et al. , *Adv. Space Res.* **34** 688-699 (2004).
10. A.S. Pine, T. Gabard, *J. Mol. Spectrosc.* **217** 105-114 (2003).
11. A. Predoi-Cross, A.V. Unni, H. Heung, V.M. Devi et al., et al., *J. Mol. Spectrosc.* **246** 65-76 (2007).
12. A. Predoi-Cross, J.P. Bouanich, D.C. Benner, A.D. May et al., *J. Chem. Phys.* **113** 158-168 (2000).
13. L.R. Brown, D.C. Benner, V. Malathy Devi, R.A. Toth et al., *J. Mol. Struct.* **742** 111-122, (2005).
14. V. M. Devi, D.C. Benner, L.R. Brown, C.E. Miller, R.A. Toth, *J. Mol. Spectrosc.* **245** 52-80 (2007).
15. D. Pieroni, J.M. Hartmann, P. Jeseck et al., *J. Quant. Spectrosc. Rad. Transfer* **68** 117-133 (2001).
16. A. Predoi-Cross, W. Liu, C. Holladay, A.V. Unni et al., *J. Mol. Spectrosc.* **246** 98-112 (2007).
17. S. Green, *J. Chem. Phys.* **90** 3603-3614 (1989).
18. M.V. Tonkov, J. Boissoles et al., *J. Quant. Spectrosc. Radiat. Transfer* **55** 321-334 (1996).
19. B. Gentry and L.L. Strow, *J. Chem. Phys*. **86** 5722-5730 (1987).
20. L. Bonamy, J. Bonamy, S. Temkin et al., *J. Chem. Phys.* **98** 3747-3753 (1993).
21. L. Bonamy and F. Emond, *Phys. Rev*. A **51** 1235-1240 (1995).
22. J.-P. Bouanich, , J.M. Hartmann, Gh. Blanquet et al., *J. Chem. Phys.* **109** 6684-6690 (1998).
23. S. Hadded, F. Thibault, P.M. Flaud et al., *J. Chem. Phys.* **116** 7544-7557 (2002).

Diatom-diatom interactions with light: Applications and line shape theoretical aspects

Magnus Gustafsson

Department of Chemistry, University of Gothenburg, SE 412 96 Gothenburg, Sweden.

Dipoles which are induced when molecules interact with each other give rise to collision-induced absorption. Since the collisions are of short duration they yield quasi-continuous spectral features (due to Heisenberg's uncertainty principle) and for pure rotation and translation transitions they are located in the far infrared. The importance of this absorption in astrophysics has been recognized since about 50 years. In particular it enhances the trapping of infrared radiation in the atmospheres of Jovian planets [1] and cool, low-metallicity stars [2]. The absorption coefficients may be measured in laboratories. However, the measurements often require high gas pressures which introduce unwanted effects due to three body interactions which do not occur in the environments of interest to astronomers. Also, they can only be carried out for certain temperatures, e.g. liquid nitrogen temperature (77 K). Theoretical calculations, on the other hand, can be carried out at arbitrary temperatures and are usually limited to binary collisions.

Simulations of interaction-induced radiative processes involve molecular scattering calculations, which are typically carried out using time-independent quantum dynamics. These calculations require the knowledge of the potential energy surface. The spectral intensities are then obtained with Fermi's golden rule which also requires that the dipole surface is known. I will cover aspects of these computations and present a few research directions involving hydrogen and nitrogen in which we are currently working.

H_2–H_2 ABSORPTION

The atmospheres of the Jovian planets have 80–96% H_2. Most of the remainder is helium and there are only traces of infrared active molecules. Thus much of the infrared absorption in those atmospheres is generated by interacting pairs of molecules. The infrared active trace species also affect the spectra but in certain spectral windows the H_2–H_2 collision-induced absorption dominates as is indicated in Fig. 1.

Uranus: We have computed H_2–H_2 collision-induced absorption [3] on a dense frequency grid from 0.1 to 2400 cm^{-1} and for temperatures from 40 to 400 K. Figure 1 shows a comparison with a previous simulation. The calculated absorption is altered above 800 cm^{-1} and our work resulted in an improved understanding of the atmospheres of Uranus and Neptune. Previously astronomers had to make extraordinary assumptions regarding the composition of those atmospheres to explain the observed spectra. It is worth mentioning that $(H_2)_2$ dimer features around the rotational *S* lines have been carefully investigated before [4]. However, their contribution to the total absorption is small and has been neglected here. I will argue below that this should be different for the nitrogen case.

White Dwarfs: Stars that have run out of fuel explode in supernovae and when the remaining material is pulled together by gravity a white dwarf may be formed. These have no fusion reactions as source of energy and will slowly cool off until they become black. No black dwarf are thought to exist simply because the universe is not old enough. Astronomers are interested in modeling the radiative transfer in white dwarf atmospheres since that could provide a cosmic clock for determination of the age of the universe. Collision-induced absorption is important for certain categories of white dwarfs [2]. To compute spectra at thousands of Kelvins we need the H_2–H_2 potential and collision-induced dipole for large H_2 vibrations and these are currently being developed.

N_2–N_2 ABSORPTION: TITAN

Saturn's largest satellite, Titan, has an atmosphere with 98.4% N_2 and 1.6% CH_4. Collision-induced opacity due to nitrogen pairs is of great importance. A calculation in the isotropic potential approximation [7] is inconsistent with a measured spectrum at 78 K [8]. To resolve this we propose to include photodissociation of dimers, using more accurate dimer states [9] than those used in the previous theory in order to obtain a more realistic spectrum. The N_2 fundamental band collision-induced absorption spectrum has been used for analysis of these dimer states before [10].

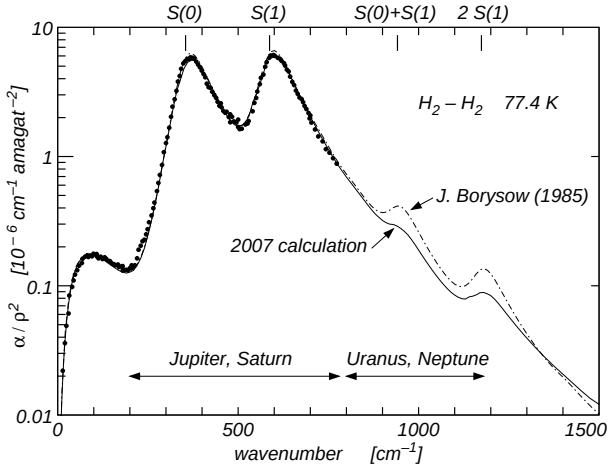

FIGURE 1. The absorption coefficient, α, for equilibrium hydrogen normalized by the square of gas density, ρ, (in units of amagat) as function of frequency at 77 K. The measurement by Birnbaum [5] is shown with dots. The solid line represents the total calculated absorption [3]. The result of Ref. [6] is also shown for comparison (dash-dot).

H_2–H_2 RAMAN SCATTERING

Induced enhancement or depletion of polarizability also occurs when molecules interact [11] and depolarized light scattering is observed even in compressed rare gases. Thus the depolarized Raman spectrum in hydrogen has two components: the (allowed) H_2 spectrum and the (collision-induced) H_2–H_2 spectrum. Rotational level mixing gives rise to interference of the sharp, allowed spectral lines and the quasi-continuous, collision-induced bands. In order to account for the anisotropy of the potential we have modeled the spectrum with a close-coupling scattering calculation [12] and found agreement with a measurement taken at 50 K [13]. The calculation confirms the destructive interference around a Stokes shift of 250 cm^{-1} which was derived before [14]. This effect has much in common with the Fano line shapes observed in the infrared spectrum of compressed HD gas [15]. Those have also been attributed to rotational level mixing and interference between permanent and collision-induced dipoles [16].

ACKNOWLEDGMENTS

This work was supported by the Swedish Research Council.

REFERENCES

1. L. M. Trafton, *Molecular Complexes in Earth's, Planetary, Cometary, and Interstellar Atmospheres* (World Scientific, London, 1998), chap. 6, pp. 177 – 193.
2. A. Borysow, U. G. Jørgensen, and C. Zheng, Astronomy and Astrophysics **324**, 185 (1997).
3. G. S. Orton, M. Gustafsson, M. Burgdorf, and V. Meadows, Icarus **189**, 544 (2007).
4. J. Schäfer and A. R. W. McKellar, Z. Physik D **15**, 51 (1990), erratum: Z. Physik D 17 (1990) 231.
5. G. Birnbaum, J. Quant. Spectroscopy and Rad. Transfer **19**, 51 (1978).
6. J. Borysow, L. Trafton, L. Frommhold, and G. Birnbaum, Astrophys. J. **296**, 644 (1985).
7. A. Borysow and L. Frommhold, Astrophys. J. **311**, 1043 (1986).
8. E. H. Wishnow, H. P. Gush, and I. Ozier, J. Chem. Phys. **104**, 3511 (1996).
9. J. Tennyson and A. van der Avoird, J. Chem. Phys. **77**, 5664 (1982), erratum: *ibid.* vol. 80 (1984) 2986.
10. A. R. W. McKellar, J. Chem. Phys. **88**, 4190 (1988).
11. B. J. Berne and R. Pecora, *Dynamic Light Scattering* (John Wiley & Sons, New York, 1976).
12. M. Gustafsson, L. Frommhold, X. Li, and K. Hunt, to be published (2008).
13. U. Bafile, L. Ulivi, M. Zoppi, F. Barocchi, M. Moraldi, and A. Borysow, Phys. Rev. A **42**, 6916 (1990).
14. A. Borysow and M. Moraldi, Phys. Rev. A **48**, 3036 (1993).
15. R. H. Tipping, J. D. Poll, and A. R. W. McKellar, Can. J. Phys. **56**, 75 (1978).
16. P. G. Drakopoulos and G. C. Tabisz, Phys. Rev. A **36**, 5556 (1987).

Similarity between DACs/SACs phenomena in hot emission stars and quasars absorption lines

Danezis, E.*, Lyratzi, E.*,†, Popović, L., Č.**, Dimitrijević, M., S.** and Antoniou, A.*

*University of Athens, Faculty of Physics Department of Astrophysics, Astronomy and Mechanics, Panepistimioupoli, Zographou 157 84, Athens, Greece
†Eugenides Foundation, 387 Sygrou Av., 17564, Athens, Greece
**Astronomical Observatory of Belgrade, Volgina 7, 11160 Belgrade, Serbia

INTRODUCTION

The spectra of Hot Emission Stars and AGNs present peculiar profiles that result from dynamical processes such as accretion and/or ejection of matter from these objects. In the UV spectra of hot emission stars and AGNs the absorption lines have DACs or SACs that are shifted to the blue. In the case of hot emission stars, DACs or SACs arise from spherical density regions around the star, or from density regions far away from the star that present spherical (or apparent spherical) symmetry around their own center [1, 2, 3].

Similar phenomena can be detected in the spectra of AGNs. Wind (jets, ejection of matter etc.), BLR (Broad Line Regions) and NLR (Narrow Line Regions) are, probably, the density regions that construct these profiles of the spectral lines [3]. In order to study the observed peculiar profiles in the spectra of hot emission stars and AGNs, we use the GR model [4]. With this model we can reproduce the spectral lines complex profiles.

In this paper we indicate that DACs and SACs phenomena, can explain the spectral lines peculiarity in Hot Emission Stars and AGNs [5, 6]. We also try to connect the physical properties of absorption regions around stars and quasars.

RESULTS AND DISCUSSION

Here we applied the GR model [2, 4] in order to fit stellar and quasar absorption lines (see Figures 1-3). In both cases we can find blue-shifted components, which are indicating an outflow (wind) in both objects. Difference is in the velocities, i.e. naturally the outflow velocities in quasars are higher ($\sim$ several 1000 km/s). But, the line profiles (as e.g. P-Cyg profile) in both objects are similar, indicating that natural phenomena are similar, but with different physical properties.

As we can see in Figure 2 (right) we can detect the DACs phenomenon in the spectra of some AGNs constructing complex profiles.

The presence of DACs phenomenon in the spectra of some AGNs lead us to search also for SACs in these spectra.

In Figure 3 (right) using the GR model we can see that the complex structure of many AGNs spectral lines can be explained with SACs phenomenon.

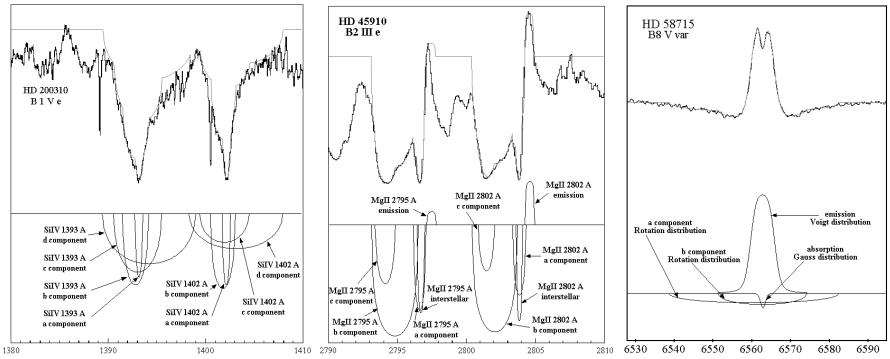

FIGURE 1. Best fit of the Si IV, Mg II and Hα spectral lines. We can explain the complex structure of these lines as a DACs or SACs phenomenon. Below the fit one can see the analysis (GR model) of the observed profile to its SACs.

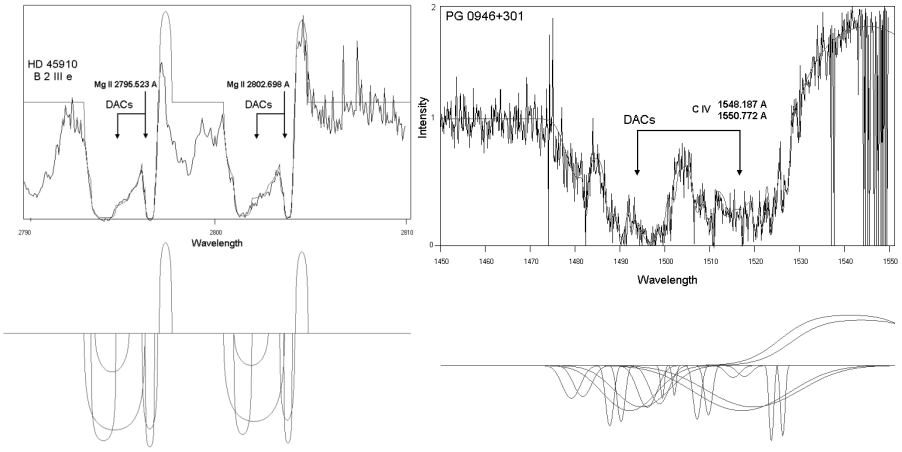

FIGURE 2. DACs in the spectra of Hot Emission Stars (left) and AGNs (right). Below the GR model fit one can see the analysis of the observed profile to its DACs or SACs.

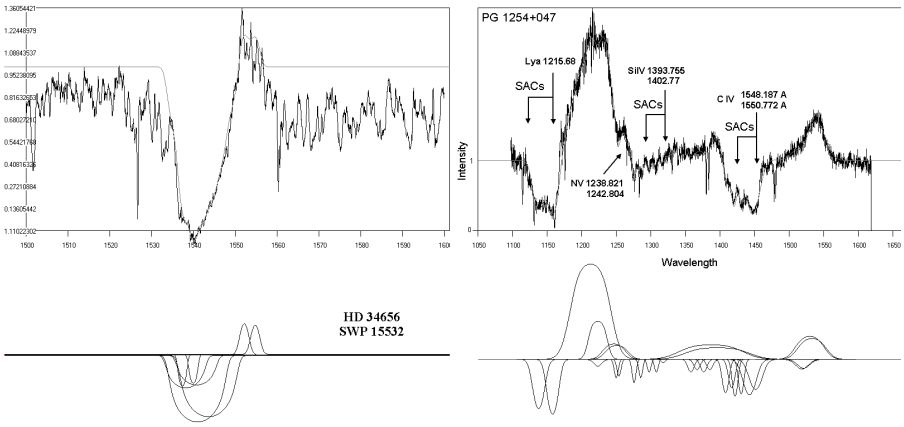

FIGURE 3. SACs in the spectra of Hot Emission Stars (left) and AGNs (right). Below the GR model fit one can see the analysis of the observed profile to its SACs.

ACKNOWLEDGMENTS

This research project is progressing at the University of Athens, Department of Astrophysics, Astronomy and Mechanics, under the financial support of the Special Account for Research Grants, which we thank very much. This work also was supported by Ministry of Science of Serbia, through the projects “Influence of collisional processes on astrophysical plasma line shapes” and “Astrophysical spectroscopy of extragalactic objects”.

REFERENCES

1. B. Bates and D. R. Halliwell, *MNRAS* **223**, 673 (1986).
2. E. Danezis, D. Nikolaidis, E. Lyratzi, A. Antoniou, L. Č. Popović, and M. S. Dimitrijević, *Mem. Soc. It. Suppl.*, **7**, 107 (2005).
3. E. Danezis, L. Č. Popović, E. Lyratzi and M. S. Dimitrijević, *AIP Conference Proceedings*, **876**, 373 (2006a).
4. E. Danezis, D. Nikolaidis, E. Lyratzi, L. Č. Popović, M. S. Dimitrijević, A. Antoniou and E. Theodossiou, *PASJ*, **59**, 827 (2007).
5. E. Danezis, L. Č. Popović, E. Lyratzi and M. S. Dimitrijević, “The SACs broadening” in *SPIG 2006 (Contributed Papers)*, 571 (2006b).
6. E. Danezis, E. Lyratzi, A. Antoniou, L. Č. Popović and M. S. Dimitrijević, “A new idea about the structure of large line broadening in the UV spectra of hot emission stars and quasars”, in *Proceedings of 19th ICSLS, Valladolid, Spain*, 2008.

New line profiles of sodium and potassium perturbed by helium for brown dwarf and very cool white dwarf stars

M. Christova[*], N.F. Allard[†,**] and J.F. Kielkopf[‡]

[*] *Technical University of Sofia, Department of Applied Physics, Sofia, Bulgaria*
[†] *Institut d'Astrophysique de Paris, CNRS, UMR 7095, UPMC, 98bis boulevard Arago, F-75014 Paris, France*
[**] *Observatoire de Paris-Meudon, GEPI, UMR 8111, CNRS, F-92195 Meudon Principal Cedex, France*
[‡] *Department of Physics and Astronomy, University of Louisville, Ky 40292, USA*

ASTROPHYSICAL CONTEXT

Late-type brown dwarfs have atmospheres composed primarily of molecular hydrogen and helium. In earlier phases of the evolution of the brown dwarf, most refractory metals have condensed to grains, which have settled below their now fully radiative photosphere. The alkali elements bind less easily to molecules or grains, and their resonance transitions remain the last sources of optical opacity. The absence of molecular opacities causes theirs to be transparent enough for alkali line broadening to define the "continuum". The optical spectra of L and T-type dwarfs exhibit a continuum dominated by the far wings of the absorption profiles of the Na 3s-3p and K 4s-4p doublet perturbed by molecular hydrogen and helium.

THEORETICAL CALCULATIONS

In previous work Allard et al [1] have presented absorption profiles of Na and K resonance lines perturbed by He and H_2 calculated in a unified line shape semi-classical theory[2] using molecular potentials of [3] to describe the alkali-He interaction and of [4] for the alkali-H_2 interaction. Kirby et al [5] have reported *ab initio* calculations of the potentials of K-H_2 (together with KHe). Babb et al [6] have reported full quantum mechanical calculations in the binary approximation of Na and K perturbed by helium.

We report on our work on new calculations of line profiles of Na and K perturbed by He for the conditions prevailing in brown dwarf atmospheres and very cool white dwarfs. In metal-rich white dwarfs with a helium dominated atmosphere, the perturber density is so high that the one-perturber approximation breaks down, and the collisional effects must be treated by using the autocorrelation formalism in order to take into account simultaneous collisions with more than one perturbing atom. These calculations use the potentials of Theodora et al [7] for Na-He and of Kirby et al [5] for K-He. The calculations take into account the spin-orbit coupling as described by Allard and Spiegelman [8].

REFERENCES

1. Allard, N. F., Allard, F., Hauschildt, P.H., Kielkopf, J. F., Machin, L., A&A. **411**, 473-476 (2003)
2. Allard,N. F., Royer, A., Kielkopf, J. F., Feautrier, N., Phys. Rev. A. **60**, 1021-1033 (1999)
3. Pascale J., Phys. Rev. A, **28**, 632, (1983)
4. Rossi F. and Pascale J., Phys. Rev. A, **32**, 2657, (1985)
5. Santra, R., Kirby, K., J. Chem. Phys., **123**, 214309, (2005)
6. Zhu, C., Babb, J. F., Dalgarno, A., Phys. Rev. A, **73**, 012506, (2006)
7. Theoodorakopoulous, G. and Petsalakis, D., J. Phys. B, **26**, 4367, (1993)
8. Allard, N. F., Spiegelman, F., A&A. **452**, 351, (2006)

Author index

N

O

P

R

S

T

U